Chapter 1

Signals and Signal Spaces

The goal of this chapter is to give a brief overview of methods for characterizing signals and for describing their properties. We will start with a discussion of signal spaces such as Hilbert spaces, normed and metric spaces. Then, the energy density and correlation function of deterministic signals will be discussed. The remainder of this chapter is dedicated to random signals, which are encountered in almost all areas of signal processing. Here, basic concepts such as stationarity, autocorrelation, and power spectral density will be discussed.

1.1 Signal Spaces

1.1.1 Energy and Power Signals

Let us consider a deterministic continuous-time signal $x(t)$, which may be real or complex-valued. If the energy of the signal defined by

$$E_x = \int_{-\infty}^{\infty} |x(t)|^2 \, dt \tag{1.1}$$

is finite, we call it an *energy signal*. If the energy is infinite, but the mean power

$$P_x = \lim_{T \to \infty} \frac{1}{T} \int_{-T/2}^{T/2} |x(t)|^2 \, dt \tag{1.2}$$

is finite, we call $x(t)$ a *power signal*. Most signals encountered in technical applications belong to these two classes.

A second important classification of signals is their assignment to the signal spaces $L_p(a, b)$, where a and b are the interval limits within which the signal is considered. By $L_p(a, b)$ with $1 \leq p < \infty$ we understand that class of signals x for which the integral

$$\int_a^b |x(t)|^p \, dt$$

to be evaluated in the Lebesgue sense is finite. If the interval limits a and b are expanded to infinity, we also write $L_p(\infty)$ or $L_p(\mathbb{R})$. According to this classification, energy signals defined on the real axis are elements of the space $L_2(\mathbb{R})$.

1.1.2 Normed Spaces

When considering normed signal spaces, we understand signals as vectors that are elements of a linear vector space X. The norm of a vector x can somehow be understood as the length of x. The notation of the norm is $\|x\|$.

Norms must satisfy the following three axioms, where α is an arbitrary real or complex-valued scalar, and $\mathbf{0}$ is the null vector:

$$\text{(i)} \qquad \|x\| \geq 0, \quad \|x\| = 0 \ \text{ if and only if } \ x = \mathbf{0}, \qquad (1.3)$$

$$\text{(ii)} \qquad \|x + y\| \leq \|x\| + \|y\|, \qquad (1.4)$$

$$\text{(iii)} \qquad \|\alpha x\| = |\alpha| \, \|x\|. \qquad (1.5)$$

Norms for Continuous-Time Signals. The most common norms for continuous-time signals are the L_p norms:

$$\|x\|_{L_p} = \left[\int_a^b |x(t)|^p \, dt \right]^{1/p} , \ 1 \leq p < \infty \qquad (1.6)$$

For $p \to \infty$, the norm (1.6) becomes $\|x\|_{L_\infty} = \operatorname*{ess\,sup}_{a \leq t \leq b} |x(t)|$.

For $p = 2$ we obtain the well-known *Euclidean norm*:

$$\|x\|_{L_2} = \sqrt{\int_a^b |x(t)|^2 \, dt} , \qquad x \in L_2(a, b). \qquad (1.7)$$

Thus, the signal energy according to (1.1) can also be expressed in the form

$$E_x = \int_{-\infty}^{\infty} |x(t)|^2 \, dt = \|x\|_{L_2}^2 , \qquad x \in L_2(\mathbb{R}). \qquad (1.8)$$

Norms for Discrete-Time Signals. The spaces $\ell_p(n_1, n_2)$ are the discrete-time equivalent to the spaces $L_p(a, b)$. They are normed as follows:

$$\|x\|_{\ell_p} = \left[\sum_{n=n_1}^{n_2} |x(n)|^p \right]^{1/p} \quad , \quad 1 \le p < \infty. \tag{1.9}$$

For $p \to \infty$, (1.9) becomes $\|x\|_{\ell_\infty} = \sup_{n=n_1}^{n_2} |x(n)|$.

For $p = 2$ we obtain

$$\|x\|_{\ell_2} = \sqrt{ \sum_{n=n_1}^{n_2} |x(n)|^2 }, \qquad x \in \ell_2(n_1, n_2). \tag{1.10}$$

Thus, the energy of a discrete-time signal $x(n)$, $n \in \mathbb{Z}$ can be expressed as:

$$E_x = \sum_{n=-\infty}^{\infty} |x(n)|^2 = \|x\|_{\ell_2}^2, \qquad x \in \ell_2(-\infty, \infty). \tag{1.11}$$

1.1.3   Metric Spaces

A function that assigns a real number to two elements x and y of a non-empty set X is called a metric on X if it satisfies the following axioms:

$$\begin{align}
&\text{(i)} && d(x,y) \ge 0, \quad d(x,y) = 0 \ \text{ if and only if } \ x = y, && \text{(1.12)} \\
&\text{(ii)} && d(x,y) = d(y,x), && \text{(1.13)} \\
&\text{(iii)} && d(x,z) \le d(x,y) + d(y,z). && \text{(1.14)}
\end{align}$$

The metric $d(x, y)$ can be understood as the distance between x and y.

A normed space is also a metric space. Here, the metric induced by the norm is the norm of the difference vector:

$$d(x, y) = \|x - y\|. \tag{1.15}$$

Proof (norm $\to$ metric). For $d(x, y) = \|x - y\|$ the validity of (1.12) immediately follows from (1.3). With $\alpha = -1$, (1.5) leads to $\|x - y\| = \|y - x\|$, and (1.13) is also satisfied. For two vectors $x = a - b$ and $y = b - c$ the following holds according to (1.4):

$$\|a - c\| = \|x + y\| \le \|x\| + \|y\| = \|a - b\| + \|b - c\|.$$

Thus, $d(a, c) \le d(a, b) + d(b, c)$, which means that also (1.14) is satisfied. $\square$

An example is the *Euclidean metric* induced by the Euclidean norm:

$$d(\boldsymbol{x}, \boldsymbol{y}) = \left[\int_a^b |x(t) - y(t)|^2 dt \right]^{1/2}, \qquad \boldsymbol{x}, \boldsymbol{y} \in L_2(a, b). \qquad (1.16)$$

Accordingly, the following distance between discrete-time signals can be stated:

$$d(\boldsymbol{x}, \boldsymbol{y}) = \left[\sum_{n=n_1}^{n_2} |x(n) - y(n)|^2 \right]^{1/2}, \qquad \boldsymbol{x}, \boldsymbol{y} \in \ell_2(n_1, n_2). \qquad (1.17)$$

Nevertheless, we also find metrics which are not associated with a norm. An example is the Hamming distance

$$d(\boldsymbol{x}, \boldsymbol{y}) = \sum_{k=1}^n [(x_k + y_k) \bmod 2],$$

which states the number of positions where two binary code words $\boldsymbol{x} = [x_1, x_2, \ldots, x_n]$ and $\boldsymbol{y} = [y_1, y_2, \ldots, y_n]$ with $x_i, y_i \in \{0, 1\}$ differ (the space of the code words is not a linear vector space).

Note. The normed spaces L_p and ℓ_p are so-called *Banach spaces*, which means that they are normed linear spaces which are complete with regard to their metric $d(\boldsymbol{x}, \boldsymbol{y}) = \|\boldsymbol{x} - \boldsymbol{y}\|$. A space is complete if any Cauchy sequence of the elements of the space converges within the space. That is, if $\|\boldsymbol{x}_n - \boldsymbol{x}_m\| \to 0$ as n and $m \to \infty$, while the limit of $\boldsymbol{x}_n$ for $n \to \infty$ lies in the space.

1.1.4   Inner Product Spaces

The signal spaces most frequently considered are the spaces $L_2(a, b)$ and $\ell_2(n_1, n_2)$; for these spaces inner products can be stated. An inner product assigns a complex number to two signals $x(t)$ and $y(t)$, or $x(n)$ and $y(n)$, respectively. The notation is $\langle \boldsymbol{x}, \boldsymbol{y} \rangle$. An inner product must satisfy the following axioms:

$$\text{(i)} \qquad \langle \boldsymbol{x}, \boldsymbol{y} \rangle = \langle \boldsymbol{y}, \boldsymbol{x} \rangle^* \qquad (1.18)$$

$$\text{(ii)} \qquad \langle \alpha \boldsymbol{x} + \beta \boldsymbol{y}, \boldsymbol{z} \rangle = \alpha \langle \boldsymbol{x}, \boldsymbol{z} \rangle + \beta \langle \boldsymbol{y}, \boldsymbol{z} \rangle \qquad (1.19)$$

$$\text{(iii)} \qquad \langle \boldsymbol{x}, \boldsymbol{x} \rangle \geq 0, \qquad \langle \boldsymbol{x}, \boldsymbol{x} \rangle = 0 \ \text{ if and only if } \ \boldsymbol{x} = \boldsymbol{0}. \qquad (1.20)$$

Here, α and β are scalars with $\alpha, \beta \in \mathbb{C}$, and $\boldsymbol{0}$ is the null vector.

Examples of inner products are

$$\langle \boldsymbol{x}, \boldsymbol{y} \rangle = \int_a^b x(t) \, y^*(t) \, dt, \quad \boldsymbol{x}, \boldsymbol{y} \in L_2(a, b) \qquad (1.21)$$

and

$$\langle \boldsymbol{x}, \boldsymbol{y} \rangle = \sum_{n=n_1}^{n_2} x(n)\, y^*(n), \quad \boldsymbol{x}, \boldsymbol{y} \in \ell_2(n_1, n_2). \tag{1.22}$$

The inner product (1.22) may also be written as

$$\langle \boldsymbol{x}, \boldsymbol{y} \rangle = \boldsymbol{y}^H \boldsymbol{x}, \quad \boldsymbol{x}, \boldsymbol{y} \in \ell_2(n_1, n_2), \tag{1.23}$$

where the vectors are understood as column vectors:[1]

$$\begin{aligned}
\boldsymbol{x} &= [x(n_1), x(n_1 + 1), \ldots, x(n_2)]^T, \\
\boldsymbol{y} &= [y(n_1), y(n_1 + 1), \ldots, y(n_2)]^T.
\end{aligned} \tag{1.24}$$

More general definitions of inner products include weighting functions or weighting matrices. An inner product of two continuous-time signals $x(t)$ and $y(t)$ including weighting can be defined as

$$\langle \boldsymbol{x}, \boldsymbol{y} \rangle = \int_a^b g(t)\, x(t)\, y^*(t)\, dt, \tag{1.25}$$

where $g(t)$ is a real weighting function with $g(t) > 0$, $a \le t \le b$.

The general definition of inner products of discrete-time signals is

$$\langle \boldsymbol{x}, \boldsymbol{y} \rangle = \boldsymbol{y}^H \boldsymbol{G}\, \boldsymbol{x}, \quad \boldsymbol{x}, \boldsymbol{y} \in \mathbb{C}^N, \tag{1.26}$$

where $\boldsymbol{G}$ is a real-valued, Hermitian, positive definite weighting matrix. This means that $\boldsymbol{G}^H = \boldsymbol{G}^T = \boldsymbol{G}$, and all eigenvalues λ_i of $\boldsymbol{G}$ must be larger than zero. As can easily be verified, the inner products (1.25) and (1.26) meet conditions (1.18) – (1.20).

The mathematical rules for inner products basically correspond to those for ordinary products of scalars. However, the order in which the vectors occur must be observed: (1.18) shows that changing the order leads to a conjugation of the result.

As equation (1.19) indicates, a scalar prefactor of the left argument may directly precede the inner product: $\langle \alpha \boldsymbol{x}, \boldsymbol{y} \rangle = \alpha \langle \boldsymbol{x}, \boldsymbol{y} \rangle$. If we want a prefactor

---

[1]The superscript T denotes transposition. The elements of $\boldsymbol{x}$ and $\boldsymbol{y}$ may be real or complex-valued. A superscript H, as in (1.23), means transposition and complex conjugation. A vector $\boldsymbol{x}^H$ is also referred to as the *Hermitian* of $\boldsymbol{x}$. If a vector is to be conjugated but not to be transposed, we write $\boldsymbol{x}^*$ such that $\boldsymbol{x}^H = [\boldsymbol{x}^*]^T$.

of the right argument to precede the inner product, it must be conjugated, since (1.18) and (1.19) lead to

$$\langle x, \alpha y \rangle = \langle \alpha y, x \rangle^* = [\alpha \langle y, x \rangle]^* = \alpha^* \langle x, y \rangle . \tag{1.27}$$

Due to (1.18), an inner product $\langle x, x \rangle$ is always real: $\langle x, x \rangle = \Re\{\langle x, x \rangle\}$.

By defining an inner product we obtain a norm and also a metric. The norm induced by the inner product is

$$\|x\| = \langle x, x \rangle^{1/2} . \tag{1.28}$$

We will prove this in the following along with the *Schwarz inequality*, which states

$$| \langle x, y \rangle | \le \|x\| \ \|y\| . \tag{1.29}$$

Equality in (1.29) is given only if x and y are linearly dependent, that is, if one vector is a multiple of the other.

Proof (inner product → norm). From (1.20) it follows immediately that (1.3) is satisfied. For the norm of αx, we conclude from (1.18) and (1.19)

$$\|\alpha x\| = \langle \alpha x, \alpha x \rangle^{1/2} = [\ |\alpha|^2 \langle x, x \rangle \ ]^{1/2} = |\alpha| \ \langle x, x \rangle^{1/2} = |\alpha| \ \|x\| .$$

Thus, (1.5) is also proved.

Now the expression $\|x + y\|^2$ will be considered. We have

$$
\begin{aligned}
\|x + y\|^2 &= \langle x + y, x + y \rangle \\
&= \langle x, x \rangle + \langle x, y \rangle + \langle y, x \rangle + \langle y, y \rangle \\
&= \langle x, x \rangle + 2\Re\{\langle x, y \rangle\} + \langle y, y \rangle \\
&\le \langle x, x \rangle + 2\,| \langle x, y \rangle | + \langle y, y \rangle .
\end{aligned}
$$

Assuming the Schwarz inequality is correct, we conclude

$$\|x + y\|^2 \le \|x\|^2 + 2 \ \|x\| \ \|y\| + \|y\|^2 = (\|x\| + \|y\|)^2.$$

This shows that also (1.4) holds. $\square$

Proof of the Schwarz inequality. The validity of the equality sign in the Schwarz inequality (1.29) for linearly dependent vectors can easily be proved

by substituting $x = \alpha y$ or $y = \alpha x$, $\alpha \in \mathbb{C}$, into (1.29) and rearranging the expression obtained, observing (1.28). For example, for $x = \alpha y$ we have

$$| \langle x, y \rangle | = | \langle \alpha y, y \rangle | = |\alpha| \, \langle y, y \rangle = |\alpha| \, \|y\|^2 = \|\alpha y\| \, \|y\| = \|x\| \, \|y\| .$$

In order to prove the Schwarz inequality for linearly independent vectors, some vector $z = x + \alpha y$ will be considered. On the basis of $(1.18) - (1.20)$ we have

$$
\begin{aligned}
0 \; & \leq \; \langle z, z \rangle \\
& = \; \langle x + \alpha y, x + \alpha y \rangle \\
& = \; \langle x, x + \alpha y \rangle + \langle \alpha y, x + \alpha y \rangle \\
& = \; \langle x, x \rangle + \alpha^* \langle x, y \rangle + \alpha \langle y, x \rangle + \alpha \alpha^* \langle y, y \rangle .
\end{aligned}
\tag{1.30}
$$

This also holds for the special α (assumption: $y \neq 0$)

$$\alpha = - \frac{\langle x, y \rangle}{\langle y, y \rangle},$$

and we get

$$0 \leq \langle x, x \rangle - \frac{\langle x, y \rangle^* \langle x, y \rangle}{\langle y, y \rangle} - \frac{\langle x, y \rangle \langle y, x \rangle}{\langle y, y \rangle} + \frac{\langle x, y \rangle \langle x, y \rangle^* \langle y, y \rangle}{\langle y, y \rangle \cdot \langle y, y \rangle}.$$

The second and the fourth term cancel,

$$0 \leq \langle x, x \rangle - \frac{\langle x, y \rangle \langle y, x \rangle}{\langle y, y \rangle} = \langle x, x \rangle - \frac{| \langle x, y \rangle |^2}{\langle y, y \rangle}, \tag{1.31}$$

and we obtain

$$| \langle x, y \rangle |^2 \leq \langle x, x \rangle \cdot \langle y, y \rangle . \tag{1.32}$$

Comparing (1.32) with (1.28) and (1.29) confirms the Schwarz inequality. $\square$

Equation (1.28) shows that the inner products given in (1.21) and (1.22) lead to the norms (1.7) and (1.10).

Finally, let us remark that a linear space with an inner product which is *complete* with respect to the induced metric is called a *Hilbert space*.

1.2   Energy Density and Correlation

1.2.1   Continuous-Time Signals

Let us reconsider (1.1):

$$E_x = \int_{-\infty}^{\infty} |x(t)|^2 \ dt. \tag{1.33}$$

According to Parseval's theorem, we may also write

$$E_x = \frac{1}{2\pi} \int_{-\infty}^{\infty} |X(\omega)|^2 \ d\omega, \tag{1.34}$$

where $X(\omega)$ is the Fourier transform of $x(t)$.[2] The quantity $|x(t)|^2$ in (1.33) represents the distribution of signal energy with respect to time t; accordingly, $|X(\omega)|^2$ in (1.34) can be viewed as the distribution of energy with respect to frequency ω. Therefore $|X(\omega)|^2$ is called the *energy density spectrum* of $x(t)$. We use the following notation

$$S_{xx}^E(\omega) = |X(\omega)|^2. \tag{1.35}$$

The energy density spectrum $S_{xx}^E(\omega)$ can also be regarded as the Fourier transform of the so-called *autocorrelation function*

$$r_{xx}^E(\tau) = \int_{-\infty}^{\infty} x^*(t) \ x(t+\tau) \ dt = x^*(-\tau) \ * \ x(\tau). \tag{1.36}$$

We have

$$S_{xx}^E(\omega) = \int_{-\infty}^{\infty} r_{xx}^E(\tau) \ e^{-j\omega\tau} \ d\tau. \tag{1.37}$$

The correspondence is denoted as $S_{xx}^E(\omega) \longleftrightarrow r_{xx}^E(\tau)$.

The autocorrelation function is a measure indicating the similarity between an energy signal $x(t)$ and its time-shifted variant $x_\tau(t) = x(t+\tau)$. This can be seen from

$$\begin{aligned} d(\boldsymbol{x},\boldsymbol{x}_\tau)^2 &= \|\boldsymbol{x}-\boldsymbol{x}_\tau\|^2 \\ &= \langle\boldsymbol{x},\boldsymbol{x}\rangle - \langle\boldsymbol{x},\boldsymbol{x}_\tau\rangle - \langle\boldsymbol{x}_\tau,\boldsymbol{x}\rangle + \langle\boldsymbol{x}_\tau,\boldsymbol{x}_\tau\rangle \\ &= 2\|\boldsymbol{x}\|^2 - 2\ \Re\{\langle\boldsymbol{x}_\tau,\boldsymbol{x}\rangle\} \\ &= 2\|\boldsymbol{x}\|^2 - 2\ \Re\{r_{xx}^E(\tau)\}. \end{aligned} \tag{1.38}$$

With increasing correlation the distance decreases.

---

[2]In this section, we freely use the properties of the Fourier transform. For more detail on the Fourier transform and Parseval's theorem, see Section 2.2.

Similarly, the *cross correlation function*

$$r_{xy}^E(\tau) = \int_{-\infty}^{\infty} y(t+\tau)\ x^*(t)\ dt \tag{1.39}$$

and the corresponding *cross energy density spectrum*

$$S_{xy}^E(\omega) = \int_{-\infty}^{\infty} r_{xy}^E(\tau)\ e^{-j\omega\tau}\ d\tau, \tag{1.40}$$

that is

$$S_{xy}^E(\omega) \longleftrightarrow r_{xy}^E(\tau), \tag{1.41}$$

are introduced, where $r_{xy}^E(\tau)$ may be viewed as a measure of the similarity between the two signals $x(t)$ and $y_\tau(t) = y(t+\tau)$.

1.2.2 Discrete-Time Signals

All previous considerations are applicable to discrete-time signals $x(n)$ as well. The signals $x(n)$ may be real or complex-valued. As in the continuous-time case, we start the discussion with the energy of the signal:

$$E_x = \sum_{n=-\infty}^{\infty} |x(n)|^2. \tag{1.42}$$

According to Parseval's relation for the discrete-time Fourier transform, we may alternatively compute E_x from $X(e^{j\omega})$:[3]

$$E_x = \frac{1}{2\pi} \int_{-\pi}^{\pi} |X(e^{j\omega})|^2\ d\omega. \tag{1.43}$$

The term $|X(e^{j\omega})|^2$ in (1.43) is called the *energy density spectrum* of the discrete-time signal. We use the notation

$$S_{xx}^E(e^{j\omega}) = |X(e^{j\omega})|^2. \tag{1.44}$$

The energy density spectrum $S_{xx}^E(e^{j\omega})$ is the discrete-time Fourier transform of the *autocorrelation sequence*

$$r_{xx}^E(m) = \sum_{n=-\infty}^{\infty} x^*(n)\ x(n+m). \tag{1.45}$$

---

[3]See Section 4.2 for more detail on the discrete-time Fourier transform.

We have

$$S_{xx}^E(e^{j\omega}) = \sum_{m=-\infty}^{\infty} r_{xx}^E(m)\, e^{-j\omega m}$$

$$\updownarrow \tag{1.46}$$

$$r_{xx}^E(m) = \frac{1}{2\pi} \int_{-\pi}^{\pi} S_{xx}^E(e^{j\omega})\, e^{j\omega m}\, d\omega.$$

Note that the energy density may also be viewed as the product $\tilde{X}(z)X(z)$, evaluated on the unit circle $(z = e^{j\omega})$, where $X(z)$ is the z-transform of $x(n)$.

The definition of the *cross correlation sequence* is

$$r_{xy}^E(m) = \sum_{n=-\infty}^{\infty} y(n+m)\, x^*(n). \tag{1.47}$$

For the corresponding *cross energy density spectrum* the following holds:

$$S_{xy}^E(e^{j\omega}) = \sum_{m=-\infty}^{\infty} r_{xy}^E(m)\, e^{-j\omega m}, \tag{1.48}$$

that is

$$S_{xy}^E(e^{j\omega}) \longleftrightarrow r_{xy}^E(m). \tag{1.49}$$

1.3   Random Signals

Random signals are encountered in all areas of signal processing. For example, they appear as disturbances in the transmission of signals. Even the transmitted and consequently also the received signals in telecommunications are of random nature, because only random signals carry information. In pattern recognition, the patterns that are to be distinguished are modeled as random processes. In speech, audio, and image coding, the signals to be compressed are modeled as such.

First of all, one distinguishes between *random variables* and *random processes*. A random variable is obtained by assigning a real or complex number to each feature m_i from a feature set M. The features (or events) occur randomly. Note that the features themselves may also be non-numeric.

If one assigns a function ${}^i x(t)$ to each feature m_i, then the totality of all possible functions is called a *stochastic process*. The features occur randomly whereas the assignment $m_i \to {}^i x(t)$ is deterministic. A function ${}^i x(t)$ is called the *realization* of the stochastic process $x(t)$. See Figure 1.1 for an illustration.

(a)

(b)
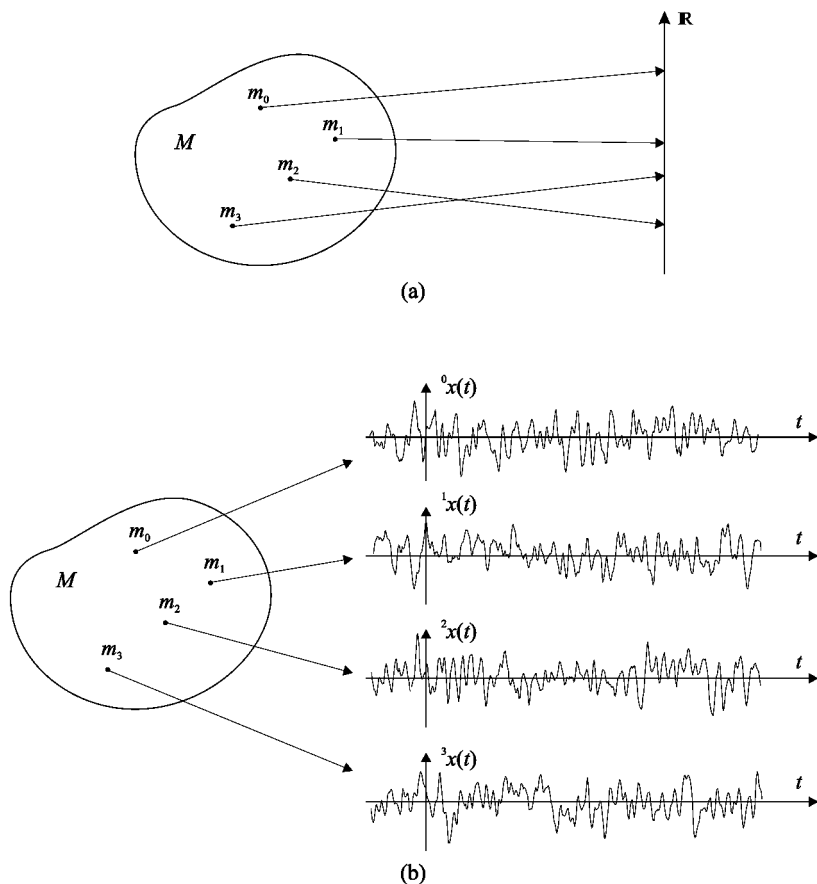
Figure 1.1. Random variables (a) and random processes (b).

1.3.1 Properties of Random Variables

The properties of a real random variable x are thoroughly characterized by its *cumulative distribution function* $F_x(\alpha)$ and also by its *probability density function* (pdf) $p_x(\alpha)$. The distribution states the probability P with which the value of the random variable x is smaller than or equal to a given value α:

$$F_x(\alpha) = P(x \leq \alpha). \tag{1.50}$$

Here, the *axioms of probability* hold, which state that

$$\lim_{\alpha \to -\infty} F_x(\alpha) = 0, \quad \lim_{\alpha \to \infty} F_x(\alpha) = 1, \quad F_x(\alpha_1) \leq F_x(\alpha_2) \quad \text{for} \quad \alpha_1 \leq \alpha_2. \tag{1.51}$$

Given the distribution, we obtain the pdf by differentiation:

$$p_x(\alpha) = \frac{d}{d\alpha} F_x(\alpha). \tag{1.52}$$

Since the distribution is a non-decreasing function, we have

$$p_x(\alpha) \geq 0. \tag{1.53}$$

Joint Probability Density. The joint probability density $p_{x_1,x_2}(\xi_1, \xi_2)$ of two random variables x_1 and x_2 is given by

$$p_{x_1,x_2}(\xi_1, \xi_2) = p_{x_1}(\xi_1)\, p_{x_2|x_1}(\xi_2|\xi_1), \tag{1.54}$$

where $p_{x_2|x_1}(\xi_2|\xi_1)$ is a conditional probability density (density of x_2 provided x_1 has taken on the value ξ_1). If the variables x_1 and x_2 are statistically independent of one another, (1.54) reduces to

$$p_{x_1,x_2}(\xi_1, \xi_2) = p_{x_1}(\xi_1)\, p_{x_2}(\xi_2). \tag{1.55}$$

The pdf of a complex random variable is defined as the joint density of its real and imaginary part:

$$p_x(\xi) = p_u(\xi_1)\, p_{v|u}(\xi_2|\xi_1), \qquad u = \Re\{x\},\ v = \Im\{x\},\ \xi = \xi_1 + j\xi_2. \tag{1.56}$$

Moments. The properties of a random variable are often described by its moments

$$m_x^{(n)} = E\left\{|x|^n\right\}. \tag{1.57}$$

Herein, $E\{\cdot\}$ denotes the *expected value* (statistical average). An expected value $E\{g(x)\}$, where $g(x)$ is an arbitrary function of the random variable x, can be calculated from the density as

$$E\{g(x)\} = \int_{-\infty}^{\infty} g(\xi)\, p_x(\xi)\, d\xi. \tag{1.58}$$

For $g(x) = x$ we obtain the mean value (first moment):

$$m_x = E\{x\} = \int_{-\infty}^{\infty} \xi\, p_x(\xi)\, d\xi. \tag{1.59}$$

For $g(x) = |x|^2$ we obtain the average power (second moment):

$$s_x^2 = E\left\{|x|^2\right\} = \int_{-\infty}^{\infty} |\xi|^2\, p_x(\xi)\, d\xi. \tag{1.60}$$

The *variance* (second central moment) is calculated with $g(x) = |x - m_x|^2$ as

$$\sigma_x^2 = E\left\{|x - m_x|^2\right\} = \int_{-\infty}^{\infty} |\xi - m_x|^2 \; p_x(\xi) \; d\xi. \tag{1.61}$$

The following holds:

$$\sigma_x^2 = s_x^2 - m_x^2. \tag{1.62}$$

Characteristic Function. The characteristic function of a random variable x is defined as

$$\Phi_x(\nu) = \int_{-\infty}^{\infty} e^{j\nu x} \; p_x(\nu) \; d\nu, \tag{1.63}$$

which means that, apart from the sign of the argument, it is the Fourier transform of the pdf. According to the moment theorem of the Fourier transform (see Section 2.2), the moments of the random variable can also be computed from the characteristic function as

$$m_x^{(n)} = (-j)^n \left. \frac{d^n \Phi_x(\nu)}{d\nu^n} \right|_{\nu = 0} \tag{1.64}$$

1.3.2   Random Processes

The starting point for the following considerations is a stochastic process $x(t)$, from which the random variables $x_{t_1}, x_{t_2}, \ldots, x_{t_n}$ with $x_{t_k} = x(t_k)$ are taken at times $t_1 < t_2 < \ldots < t_n$, $n \in \mathbb{Z}$. The properties of these random variables are characterized by their joint pdf $p_{x_{t_1}, x_{t_2}, \ldots, x_{t_n}}(\alpha_1, \alpha_2, \ldots, \alpha_n)$. Then a second set of random variables is taken from the process $x(t)$, applying a time shift τ: $x_{t_1+\tau}, x_{t_2+\tau}, \ldots, x_{t_n+\tau}$ with $x_{t_k+\tau} = x(t_k + \tau)$. If the joint densities of both sets are equal for all time shifts τ and all n, that is, if we have

$$p_{x_{t_1}, x_{t_2}, \ldots, x_{t_n}}(\alpha_1, \alpha_2, \ldots, \alpha_n) = p_{x_{t_1+\tau}, x_{t_2+\tau}, \ldots, x_{t_n+\tau}}(\alpha_1, \alpha_2, \ldots, \alpha_n), \quad \forall \, n, \tau, \tag{1.65}$$

then we speak of a *strictly stationary process*, otherwise we call the process *non-stationary*.

Autocorrelation and Autocovariance Functions of Non-Stationary Processes.   The autocorrelation function of a general random process is defined as a second-order moment:

$$\begin{aligned} r_{xx}(t_1, t_2) &= E\left\{x^*(t_2) \; x(t_1)\right\} \\[2mm] &= \int_{-\infty}^{\infty}\!\!\int_{-\infty}^{\infty} \xi_1 \; \xi_2 \; p_{x_1, x_2}(\xi_1, \xi_2) \; d\xi_1 \; d\xi_2, \end{aligned} \tag{1.66}$$

where $x_1 = x(t_1)$ and $x_2 = x^*(t_2)$.

Basically, the autocorrelation function indicates how similar the process is at times t_1 and t_2, since for the expected Euclidean distance we have

$$E\left\{|x_1 - x_2|^2\right\} = E\left\{|x_1|^2\right\} + E\left\{|x_2|^2\right\} - 2\,\Re\{r_{xx}(t_1, t_2)\}.$$

The *autocovariance function* of a random process is defined as

$$
\begin{aligned}
c_{xx}(t_1, t_2) &= E\left\{[x^*(t_2) - m_{t_2}^*]\,[x(t_1) - m_{t_1}]\right\} \\
&= r_{xx}(t_1, t_2) - m_{t_2}^* m_{t_1},
\end{aligned}
\tag{1.67}
$$

where m_{t_k} denotes the expected value at time t_k; i.e.

$$m_{t_k} = E\left\{x(t_k)\right\}. \tag{1.68}$$

Wide-Sense Stationary Processes. There are processes whose mean value is constant and whose autocorrelation function is a function of $t_1 - t_2$. Such processes are referred to as *"wide-sense stationary"*, even if they are non-stationary according to the above definition.

Cyclo-Stationary Process. If a process is non-stationary according to the definition stated above, but if the properties repeat periodically, then we speak of a *cyclo-stationary process*.

Autocorrelation and Autocovariance Functions of Wide-Sense Stationary Processes. In the following we assume wide-sense stationarity, so that the first and second moments are independent of the respective time. Because of the stationarity we must assume that the process realizations are not absolutely integrable, and that their Fourier transforms do not exist. Since in the field of telecommunications one also encounters complex-valued processes when describing real bandpass processes in the complex baseband, we shall continue by looking at complex-valued processes. For wide-sense stationary processes the *autocorrelation function* (acf) depends only on the time shift between the respective times; it is given by

$$r_{xx}(\tau) = E\left\{x^*(t)\,x(t+\tau)\right\}. \tag{1.69}$$

For $x_1 = x(t + \tau)$ and $x_2 = x^*(t)$, the expected value $E\{\cdot\}$ can be written as

$$r_{xx}(\tau) = E\left\{x_1\,x_2\right\} = \int_{-\infty}^{\infty}\int_{-\infty}^{\infty} \xi_1\,\xi_2\,p_{x_1, x_2}(\xi_1, \xi_2)\,d\xi_1\,d\xi_2. \tag{1.70}$$

The maximum of the autocorrelation function is located at $\tau = 0$, where its value equals the mean square value:

$$r_{xx}(0) = s_x^2 = E\left\{|x|^2\right\} = \int_{-\infty}^{\infty} |\xi|^2 \, p_x(\xi) \, d\xi. \tag{1.71}$$

Furthermore we have $r_{xx}(-\tau) = r_{xx}^*(\tau)$.

When subtracting the mean

$$m_x = E\left\{x(t)\right\} \tag{1.72}$$

prior computing the autocorrelation function, we get the autocovariance function

$$
\begin{aligned}
c_{xx}(\tau) &= E\left\{[x^*(t) - m_x^*]\,[x(t+\tau) - m_x]\right\} \\
&= r_{xx}(\tau) - |m_x|^2.
\end{aligned}
\tag{1.73}
$$

Power Spectral Density. The *power spectral density*, or *power density spectrum*, describes the distribution of power with respect to frequency. It is defined as the Fourier transform of the autocorrelation function:

$$S_{xx}(\omega) = \int_{-\infty}^{\infty} r_{xx}(\tau)\,e^{-j\omega\tau} \, d\tau \tag{1.74}$$

$$\updownarrow$$

$$r_{xx}(\tau) = \frac{1}{2\pi}\int_{-\infty}^{\infty} S_{xx}(\omega)\,e^{j\omega\tau} \, d\omega. \tag{1.75}$$

This definition is based on the *Wiener–Khintchine theorem*, which states that the physically meaningful power spectral density given by

$$S_{xx}(\omega) = \lim_{T\to\infty}\frac{1}{T}\,E\left\{|X_T(\omega)|^2\right\} \tag{1.76}$$

with

$$X_T(\omega) \;\longleftrightarrow\; x(t)\,\mathrm{rect}(\frac{t}{T}),$$

and

$$\mathrm{rect}(t) = \begin{cases} 1, & \text{for } |t| \le 0.5 \\ 0, & \text{otherwise} \end{cases}$$

is identical to the power spectral density given in (1.74).

Taking (1.75) for $\tau = 0$, we obtain

$$s_x^2 = r_{xx}(0) = \frac{1}{2\pi}\int_{-\infty}^{\infty} S_{xx}(\omega)\,d\omega. \tag{1.77}$$

Cross Correlation and Cross Power Spectral Density. The *cross correlation* between two wide-sense stationary random processes $x(t)$ and $y(t)$ is defined as

$$r_{xy}(\tau) = E\left\{x^*(t)\ y(t+\tau)\right\}. \tag{1.78}$$

The Fourier transform of $r_{xy}(\tau)$ is the *cross power spectral density*, denoted as $S_{xy}(\omega)$. Thus, we have the correspondence

$$\begin{aligned}
S_{xy}(\omega) &= \int_{-\infty}^{\infty} r_{xy}(\tau)\ e^{-j\omega\tau}\ d\tau \\
&\updownarrow \\
r_{xy}(\tau) &= \frac{1}{2\pi}\int_{-\infty}^{\infty} S_{xy}(\omega)e^{j\omega\tau}\ d\omega.
\end{aligned} \tag{1.79}$$

Discrete-Time Signals. The following definitions for discrete-time signals basically correspond to those for continuous-time signals; the correlation and covariance functions, however, become correlation and covariance sequences. For the *autocorrelation sequence* we have

$$r_{xx}(m) = E\left\{x^*(n)\ x(n+m)\right\}. \tag{1.80}$$

The *autocovariance sequence* is defined as

$$\begin{aligned}
c_{xx}(m) &= E\left\{[x^*(n) - m_x^*]\ [x(n+m) - m_x]\right\} \\
&= r_{xx}(m) - |m_x|^2,
\end{aligned} \tag{1.81}$$

where

$$m_x = E\left\{x(n)\right\}. \tag{1.82}$$

The discrete-time Fourier transform of the autocorrelation sequence is the *power spectral density* (Wiener–Khintchine theorem). We have

$$S_{xx}(e^{j\omega}) = \sum_{m=-\infty}^{\infty} r_{xx}(m)\ e^{-j\omega m} \tag{1.83}$$

$$\updownarrow$$

$$r_{xx}(m) = \frac{1}{2\pi}\int_{-\pi}^{\pi} S_{xx}(e^{j\omega})\ e^{j\omega m}\ d\omega. \tag{1.84}$$

The definition of the *cross correlation sequence* is

$$r_{xy}(m) = E\left\{x^*(n)\, y(n+m)\right\},\qquad(1.85)$$

where the Fourier transform of $r_{xy}(m)$ is the *cross power spectral density* $S_{xy}(e^{j\omega})$:

$$r_{xy}(m) = \frac{1}{2\pi}\int_{-\pi}^{\pi} S_{xy}(e^{j\omega})\, e^{j\omega m}\, d\omega$$

$$\updownarrow \qquad(1.86)$$

$$S_{xy}(e^{j\omega}) = \sum_{m=-\infty}^{\infty} r_{xy}(m)\, e^{-j\omega m}.$$

A *cross covariance sequence* can be defined as

$$\begin{aligned} c_{xy}(m) &= E\left\{[x^*(n) - m_x^*]\,[y(n+m) - m_y]\right\} \\ &= r_{xy}(m) - m_x^*\, m_y \end{aligned}\qquad(1.87)$$

with

$$m_x = E\left\{x(n)\right\},\qquad m_y = E\left\{y(n)\right\}.\qquad(1.88)$$

Correlation Matrices. *Auto* and *cross correlation matrices* are frequently required. We use the following definitions

$$\begin{aligned} \boldsymbol{R}_{xx} &= E\left\{\boldsymbol{x}\,\boldsymbol{x}^H\right\}, \\ \boldsymbol{R}_{xy} &= E\left\{\boldsymbol{y}\,\boldsymbol{x}^H\right\}, \end{aligned}\qquad(1.89)$$

where

$$\begin{aligned} \boldsymbol{x} &= [x(n), x(n+1), \ldots, x(n+N_x-1)]^T, \\ \boldsymbol{y} &= [y(n), y(n+1), \ldots, y(n+N_y-1)]^T. \end{aligned}\qquad(1.90)$$

The terms $\boldsymbol{x}\boldsymbol{x}^H$ and $\boldsymbol{y}\boldsymbol{x}^H$ are *dyadic products*.

For the sake of completeness it shall be noted that the autocorrelation matrix $\boldsymbol{R}_{xx}$ of a stationary process $x(n)$ has the following *Toeplitz structure*:

$$\boldsymbol{R}_{xx} = \begin{bmatrix} r_{xx}(0) & r_{xx}(-1) & \cdots & r_{xx}(-N_x+1) \\ r_{xx}(1) & r_{xx}(0) & \ddots & \vdots \\ \vdots & \ddots & \ddots & r_{xx}(-1) \\ r_{xx}(N_x-1) & \cdots & r_{xx}(1) & r_{xx}(0) \end{bmatrix}.\qquad(1.91)$$

Here, the property

$$r_{xx}(-i) = r_{xx}^*(i), \tag{1.92}$$

which is concluded from (1.80) by taking stationarity into consideration, has been used.

If two processes $x(n)$ and $y(n)$ are pairwise stationary, we have

$$r_{xy}(-i) = r_{yx}^*(i), \tag{1.93}$$

and the cross correlation matrix $\boldsymbol{R}_{xy} = E\left\{\boldsymbol{y}\,\boldsymbol{x}^H\right\}$ has the following structure:

$$\boldsymbol{R}_{xy} = \begin{bmatrix} r_{xy}(0) & r_{xy}(-1) & \ldots & r_{xy}(-N_x+1) \\ r_{xy}(1) & r_{xy}(0) & \ddots & \vdots \\ \vdots & \ddots & \ddots & r_{xy}(-1) \\ r_{xy}(N_y-1) & \ldots & r_{xy}(1) & r_{xy}(0) \end{bmatrix}. \tag{1.94}$$

Auto and *cross-covariance matrices* can be defined in an analog way by replacing the entries $r_{xy}(m)$ through $c_{xy}(m)$.

Ergodic Processes. Usually, the autocorrelation function is calculated according to (1.70) by taking the ensemble average. An exception to this rule is the *ergodic process*, where the ensemble average can be replaced by a temporal average. For the autocorrelation function of an ergodic continuous-time process we have

$$r_{xx}(\tau) = \lim_{T\to\infty} \frac{1}{2T} \int_{-T}^{T} {}^i x^*(t) \; {}^i x(t+\tau) \, dt, \tag{1.95}$$

where ${}^i x(t)$ is an arbitrary realization of the stochastic process. Accordingly, we get

$$r_{xx}(m) = \lim_{N\to\infty} \frac{1}{2N+1} \sum_{n=-N}^{N} {}^i x^*(n) \; {}^i x(n+m) \tag{1.96}$$

for discrete-time signals.

Continuous-Time White Noise Process. A wide-sense stationary continuous-time noise process $x(t)$ is said to be white if its power spectral density is a constant:

$$S_{xx}(\omega) = \sigma^2. \tag{1.97}$$

The autocorrelation function of the process is a Dirac impulse with weight σ^2:

$$r_{xx}(\tau) = \sigma^2 \, \delta(\tau). \tag{1.98}$$

Since the power of such a process is infinite it is not realizable. However, the white noise process is a convenient model process which is often used for describing properties of real-world systems.

Continuous-Time Gaussian White Noise Process. We consider a real-valued wide-sense stationary stochastic process $x(t)$ and try to represent it on the interval $[-a, a]$ via a series expansion[4] with an arbitrary real-valued orthonormal basis $\varphi_i(t)$ for $L_2(-a, a)$. The basis satisfies

$$\int_{-a}^{a} \varphi_i(t) \, \varphi_j(t) \, dt = \begin{cases} 1 & \text{for } i = j, \\ 0 & \text{otherwise.} \end{cases}$$

If the coefficients of the series expansion given by

$$\alpha_i = \int_{-a}^{a} \varphi_i(t) \, x(t) \, dt$$

are Gaussian random variables with

$$E\left\{\alpha_i^2\right\} = \sigma^2 \qquad \forall \, i$$

we call $x(t)$ a Gaussian white noise process.

Bandlimited White Noise Process. A bandlimited white noise process is a white noise process whose power spectral density is constant within a certain frequency band and zero outside this band. See Figure 1.2 for an illustration.
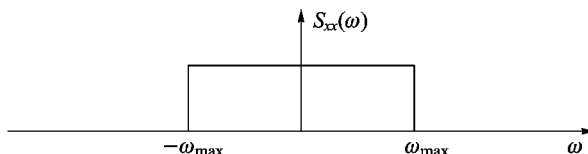
Figure 1.2. Bandlimited white noise process.

Discrete-Time White Noise Process. A discrete-time white noise process has the power spectral density

$$S_{xx}(e^{j\omega}) = \sigma^2 \tag{1.99}$$

[4]Series expansions are discussed in detail in Chapter 3.

and the autocorrelation sequence

$$r_{xx}(m) = \sigma^2 \, \delta_{m0}. \tag{1.100}$$

1.3.3   Transmission of Stochastic Processes through Linear Systems

Continuous-Time Processes. We assume a linear time-invariant system with the impulse response $h(t)$, which is excited by a stationary process $x(t)$. The cross correlation function between the input process $x(t)$ and the output process $y(t)$ is given by

$$
\begin{aligned}
r_{xy}(\tau) &= E\left\{x^*(t)\, y(t+\tau)\right\} \\[2mm]
&= \int_{-\infty}^{\infty} E\left\{x^*(t)\, x(t+\tau-\lambda)\right\} h(\lambda)d\lambda \tag{1.101} \\[2mm]
&= r_{xx}(\tau) * h(\tau).
\end{aligned}
$$

The cross power spectral density is obtained by taking the Fourier transform of (1.101):

$$S_{xy}(\omega) = S_{xx}(\omega)\, H(\omega). \tag{1.102}$$

Calculating the autocorrelation function of the output signal is done as follows:

$$
\begin{aligned}
r_{yy}(\tau) &= E\left\{y^*(t)\, y(t+\tau)\right\} \\[2mm]
&= \iint E\left\{x^*(t-\alpha)\, x(t+\tau-\beta)\right\}\, h^*(\alpha)\, h(\beta)\, d\alpha\, d\beta \\[2mm]
&= \iint r_{xx}(\tau+\alpha-\beta)\, h^*(\alpha)\, h(\beta)\, d\alpha\, d\beta \tag{1.103} \\[2mm]
&= \int r_{xx}(\tau-\lambda) \int h^*(\alpha) h(\alpha+\lambda)\, d\alpha\, d\lambda \\[2mm]
&= \int r_{xx}(\tau-\lambda)\, r_{hh}^E(\lambda)\, d\lambda.
\end{aligned}
$$

Thus, we obtain the following relationship:

$$r_{yy}(\tau) = r_{xx}(\tau) * r_{hh}^{E}(\tau). \tag{1.104}$$

Taking the Fourier transform of (1.104), we obtain the power spectral density of the output signal:

$$S_{yy}(\omega) = S_{xx}(\omega) \; |H(\omega)|^{2}. \tag{1.105}$$

We observe that the phase of $H(\omega)$ has no influence on $S_{yy}(\omega)$. Consequently, only the magnitude frequency response of $H(\omega)$ can be determined from $S_{xx}(\omega)$ and $S_{yy}(\omega)$.

Discrete-Time Processes. The results for continuous-time signals and systems can be directly applied to the discrete-time case, where a system with impulse response $h(n)$ is excited by a process $x(n)$, yielding the output process $y(n)$. The cross correlation sequence between input and output is

$$r_{xy}(m) = r_{xx}(m) * h(m). \tag{1.106}$$

The cross power spectral density becomes

$$S_{xy}(e^{j\omega}) = S_{xx}(e^{j\omega}) \; H(e^{j\omega}). \tag{1.107}$$

For the autocorrelation sequence and the power spectral density at the output we get

$$r_{yy}(m) = r_{xx}(m) * r_{hh}^{E}(m) \tag{1.108}$$

and

$$S_{yy}(e^{j\omega}) = S_{xx}(e^{j\omega}) \; \left| H(e^{j\omega}) \right|^{2}. \tag{1.109}$$

As before, the phase of $H(e^{j\omega})$ has no influence on $S_{yy}(e^{j\omega})$.

Here we cease discussion of the transmission of stochastic processes through linear systems, but we will return to this topic in Section 5 of Chapter 2, where we will study the representation of stationary bandpass processes by means of their complex envelope.

Chapter 2

Integral
Signal Representations

The integral transform is one of the most important tools in signal theory. The best known example is the Fourier transform, but there are many other transforms of interest. In the following, we will first discuss the basic concepts of integral transforms. Then we will study the Fourier, Hartley, and Hilbert transforms. Finally, we will focus on real bandpass processes and their representation by means of their complex envelope.

2.1   Integral Transforms

The basic idea of an integral representation is to describe a signal $x(t)$ via its density $\hat{x}(s)$ with respect to an arbitrary *kernel* $\varphi(t,s)$:

$$x(t) = \int_S \hat{x}(s)\ \varphi(t,s)\ ds, \quad t \in T. \tag{2.1}$$

Analogous to the reciprocal basis in discrete signal representations (see Section 3.3) a *reciprocal kernel* $\theta(s,t)$ may be found such that the density $\hat{x}(s)$ can be calculated in the form

$$\hat{x}(s) = \int_T x(t)\ \theta(s,t)\ dt, \quad s \in S. \tag{2.2}$$

Contrary to discrete representations, we do not demand that the kernels $\varphi(t,s)$ and $\theta(s,t)$ be integrable with respect to t.

From (2.2) and (2.1), we obtain

$$
\begin{aligned}
x(t) &= \int_S \int_T x(\tau)\,\theta(s,\tau)\,d\tau \;\; \varphi(t,s)\,ds \\
&= \int_T x(\tau) \int_S \theta(s,\tau)\,\varphi(t,s)\,ds\,d\tau.
\end{aligned}
\tag{2.3}
$$

In order to state the condition for the validity of (2.3) in a relatively simple form the so-called *Dirac impulse* $\delta(t)$ is required. By this we mean a generalized function with the property

$$
x(t) = \int_{-\infty}^{\infty} \delta(t-\tau)\,x(\tau)\,d\tau, \qquad x \in L_1(\mathbb{R}).
\tag{2.4}
$$

The Dirac impulse can be viewed as the limit of a family of functions $g_\alpha(t)$ that has the following property for all signals $x(t)$ continuous at the origin:

$$
\int_{-\infty}^{\infty} g_\alpha(t)\,dt = 1, \qquad \lim_{\alpha \to 0} \int_{-\infty}^{\infty} g_\alpha(t)\,x(t)\,dt = x(0).
\tag{2.5}
$$

An example is the Gaussian function

$$
g_\alpha(t) = \frac{1}{\sqrt{2\pi\alpha}}\,e^{-\frac{t^2}{2\alpha}}, \qquad \alpha > 0.
\tag{2.6}
$$

Considering the Fourier transform of the Gaussian function, that is

$$
\begin{aligned}
G_\alpha(\omega) &= \int_{-\infty}^{\infty} g_\alpha(t)\,e^{-j\omega t}\,dt \\
&= e^{-\frac{\omega^2}{2\alpha}},
\end{aligned}
\tag{2.7}
$$

we find that it approximates the constant one for $\alpha \to 0$, that is $G_\alpha(\omega) \approx 1$, $\omega \in \mathbb{R}$. For the Dirac impulse the correspondence $\delta(t) \longleftrightarrow 1$ is introduced so that (2.4) can be expressed as $X(\omega) = 1\,X(\omega)$ in the frequency domain.

Equations (2.3) and (2.4) show that the kernel and the reciprocal kernel must satisfy

$$
\int_S \theta(s,\tau)\,\varphi(t,s)\,ds = \delta(t-\tau).
\tag{2.8}
$$

By substituting (2.1) into (2.2) we obtain

$$
\begin{aligned}
\hat{x}(s) &= \int_T \int_S \hat{x}(\sigma)\,\varphi(t,\sigma)\,d\sigma \;\; \theta(s,t)\,dt \\
&= \int_S \hat{x}(\sigma) \int_T \varphi(t,\sigma)\,\theta(s,t)\,dt\,d\sigma,
\end{aligned}
\tag{2.9}
$$

which implies that

$$\int_T \varphi(t,\sigma)\, \theta(s,t)\, dt = \delta(s-\sigma). \tag{2.10}$$

Equations (2.8) and (2.10) correspond to the relationship $\langle \boldsymbol{\varphi}_i, \boldsymbol{\theta}_j \rangle = \delta_{ij}$ for the discrete case (see Chapter 3).

Self-Reciprocal Kernels. A special category is that of self-reciprocal kernels. They correspond to orthonormal bases in the discrete case and satisfy

$$\varphi(t,s) = \theta^*(s,t). \tag{2.11}$$

Transforms that contain a self-reciprocal kernel are also called *unitary*, because they yield $\|\hat{\boldsymbol{x}}\| = \|\boldsymbol{x}\|$.

The Discrete Representation as a Special Case. The discrete representation via series expansion, which is discussed in detail in the next chapter, can be regarded as a special case of the integral representation. In order to explain this relationship, let us consider the discrete set

$$\varphi_i(t) = \varphi(t,s_i), \quad i = 1,2,3,\ldots. \tag{2.12}$$

For signals $x(t) \in \mathrm{span}\,\{\varphi(t,s_i);\ i=1,2,\ldots\}$ we may write

$$x(t) = \sum_i \alpha_i\, \varphi_i(t) = \sum_i \alpha_i\, \varphi(t,s_i). \tag{2.13}$$

Insertion into (2.2) yields

$$\begin{aligned}
\hat{x}(s) &= \int_T x(t)\theta(s,t)\, dt \\
&= \int_T \sum_i \alpha_i \varphi(t,s_i)\theta(s,t)\, dt \\
&= \sum_i \alpha_i \int_T \varphi(t,s_i)\theta(s,t)\, dt.
\end{aligned} \tag{2.14}$$

The comparison with (2.10) shows that in the case of a discrete representation the density $\hat{x}(s)$ concentrates on the values s_i:

$$\hat{x}(s) = \sum_i \alpha_i\, \delta(s-s_i). \tag{2.15}$$

Parseval's Relation. Let the signals $x(t)$ and $y(t)$ be square integrable, $x, y \in L_2(T)$. For the densities let

$$\hat{x}(s) = \int_T x(t)\, \theta(s,t)\, dt,$$

$$\hat{y}(s) = \int_T y(t)\, \theta(s,t)\, dt, \qquad (2.16)$$

where $\theta(s,t)$ is a self-reciprocal kernel satisfying

$$\int_S \theta(s,t)\, \theta^*(s,\tau)\, ds = \int_S \theta(s,t)\, \varphi(\tau,s)\, ds$$

$$= \delta(t-\tau). \qquad (2.17)$$

Now the inner products

$$\langle \hat{x}, \hat{y} \rangle = \int_S \hat{x}(s)\, \hat{y}^*(s)\, ds,$$

$$\langle x, y \rangle = \int_T x(t)\, y^*(t)\, dt \qquad (2.18)$$

are introduced. Substituting (2.16) into (2.18) yields

$$\langle \hat{x}, \hat{y} \rangle = \int_S \int_T \int_T x(\tau)\, \theta(s,\tau)\, y^*(t)\, \theta^*(s,t)\, d\tau\, dt\, ds. \qquad (2.19)$$

Because of (2.17), (2.19) becomes

$$\langle \hat{x}, \hat{y} \rangle = \int_T x(\tau) \int_T y^*(t)\, \delta(t-\tau)\, dt\, d\tau$$

$$= \int_T x(\tau)\, y^*(\tau)\, d\tau. \qquad (2.20)$$

From (2.20) and (2.18) we conclude that

$$\langle \hat{x}, \hat{y} \rangle = \langle x, y \rangle. \qquad (2.21)$$

Equation (2.21) is known as *Parseval's relation*. For $y(t) = x(t)$ we obtain

$$\langle \hat{x}, \hat{x} \rangle = \langle x, x \rangle \qquad \rightarrow \qquad \|\hat{x}\| = \|x\|. \qquad (2.22)$$

2.2   The Fourier Transform

We assume a real or complex-valued, continuous-time signal $x(t)$ which is absolutely integrable ($x \in L_1(\mathbb{R})$). For such signals the Fourier transform

$$X(\omega) = \int_{-\infty}^{\infty} x(t) \; e^{-j\omega t} \; dt \qquad (2.23)$$

exists. Here, $\omega = 2\pi f$, and f is the frequency in Hertz.

The Fourier transform $X(\omega)$ of a signal $x \in L_1(\mathbb{R})$ has the following properties:

1. $X \in L_\infty(\mathbb{R})$ with $\|X\|_\infty \le \|x\|_1$.

2. X is continuous.

3. If the derivative $x'(t)$ exists and if it is absolutely integrable, then

$$\int_{-\infty}^{\infty} x'(t) \; e^{-j\omega t} \; dt = j\omega \; X(\omega). \qquad (2.24)$$

4. For $\omega \to \infty$ and $\omega \to -\infty$ we have $X(\omega) \to 0$.

If $X(\omega)$ is absolutely integrable, $x(t)$ can be reconstructed from $X(\omega)$ via the inverse Fourier transform

$$x(t) = \frac{1}{2\pi} \int_{-\infty}^{\infty} X(\omega) \; e^{j\omega t} \; d\omega \qquad (2.25)$$

for all t where $x(t)$ is continuous.

The kernel used is

$$\varphi(t,\omega) = \frac{1}{2\pi} e^{j\omega t}, \qquad T = (-\infty, \infty), \qquad (2.26)$$

and for the reciprocal kernel we have[1]

$$\theta(\omega, t) = e^{-j\omega t}, \qquad S = (-\infty, \infty). \qquad (2.27)$$

In the following we will use the notation $x(t) \longleftrightarrow X(\omega)$ in order to indicate a Fourier transform pair.

We will now briefly recall the most important properties of the Fourier transform. Most proofs are easily obtained from the definition of the Fourier transform itself. More elaborate discussions can be found in [114, 22].

---

[1]A self-reciprocal kernel is obtained either in the form $\varphi(t,\omega) = \exp(j\omega t)/\sqrt{2\pi}$ or by integrating over frequency f, not over $\omega = 2\pi f$: $\varphi(t, f) = \exp(j2\pi ft)$.

Linearity. It directly follows from (2.23) that

$$\alpha\,x(t) + \beta\,y(t) \longleftrightarrow \alpha\,X(\omega) + \beta\,Y(\omega). \tag{2.28}$$

Symmetry. Let $x(t) \longleftrightarrow X(\omega)$ be a Fourier transform pair. Then

$$X(t) \longleftrightarrow 2\pi\,x(-\omega). \tag{2.29}$$

Scaling. For any real α, we have

$$x(\alpha t) \longleftrightarrow \frac{1}{|\alpha|}X\left(\frac{\omega}{\alpha}\right). \tag{2.30}$$

Shifting. For any real t_0, we have

$$x(t - t_0) \longleftrightarrow e^{-j\omega t_0}\,X(\omega). \tag{2.31}$$

Accordingly,

$$e^{j\omega_0 t}x(t) \longleftrightarrow X(\omega - \omega_0). \tag{2.32}$$

Modulation. For any real ω_0, we have

$$\cos\omega_0 t\; x(t) \longleftrightarrow \frac{1}{2}\,X(\omega - \omega_0) + \frac{1}{2}\,X(\omega + \omega_0). \tag{2.33}$$

Conjugation. The correspondence for conjugate functions is

$$x^*(t) \longleftrightarrow X^*(-\omega). \tag{2.34}$$

Thus, the Fourier transform of real signals $x(t) = x^*(t)$ is symmetric: $X^*(\omega) = X(-\omega)$.

Derivatives. The generalization of (2.24) is

$$\frac{d^n}{dt^n}\,x(t) \longleftrightarrow (j\omega)^n\,X(\omega). \tag{2.35}$$

Accordingly,

$$(-jt)^n\,x(t) \longleftrightarrow \frac{d^n}{d\omega^n}\,X(\omega). \tag{2.36}$$

Convolution. A convolution in the time domain results in a multiplication in the frequency domain.

$$x(t)\;*\;y(t) \longleftrightarrow X(\omega)\,Y(\omega). \tag{2.37}$$

Accordingly,

$$x(t) \, y(t) \longleftrightarrow \frac{1}{2\pi} \, X(\omega) \, * \, Y(\omega). \qquad (2.38)$$

Moments. The nth moment of $x(t)$ given by

$$m_n = \int_{-\infty}^{\infty} t^n \, x(t) \, dt, \quad n = 0, 1, 2 \ldots \qquad (2.39)$$

and the nth derivative of $X(\omega)$ at the origin are related as

$$(-j)^n \, m_n = \frac{d^n}{d\omega^n} \, X(\omega) \bigg|_{\omega \, = \, 0} \qquad (2.40)$$

Parseval's Relation. According to Parseval's relation, inner products of two signals can be calculated in the time as well as the frequency domain. For signals $x(t)$ and $y(t)$ and their Fourier transforms $X(\omega)$ and $Y(\omega)$, respectively, we have

$$\int_{-\infty}^{\infty} x(t) \, y^*(t) \, dt = \frac{1}{2\pi} \int_{-\infty}^{\infty} X(\omega) \, Y^*(\omega) \, d\omega. \qquad (2.41)$$

This property is easily obtained from (2.21) by using the fact that the scaled kernel $(2\pi)^{-\frac{1}{2}} e^{j\omega t}$ is self-reciprocal.

Using the notation of inner products, Parseval's relation may also be written as

$$\langle x, y \rangle = \frac{1}{2\pi} \, \langle \boldsymbol{X}, \boldsymbol{Y} \rangle. \qquad (2.42)$$

From (2.41) with $x(t) = y(t)$ we see that the signal energy can be calculated in the time and frequency domains:

$$\begin{aligned} E_x &= \int_{-\infty}^{\infty} |x(t)|^2 \, dt \\[2mm] &= \frac{1}{2\pi} \int_{-\infty}^{\infty} |X(\omega)|^2 \, d\omega. \end{aligned} \qquad (2.43)$$

This relationship is known as *Parseval's theorem.* In vector notation it can be written as

$$\langle x, x \rangle = \frac{1}{2\pi} \, \langle \boldsymbol{X}, \boldsymbol{X} \rangle. \qquad (2.44)$$

2.3 The Hartley Transform

In 1942 Hartley proposed a real-valued transform closely related to the Fourier transform [67]. It maps a real-valued signal into a real-valued frequency function using only real arithmetic. The kernel of the Hartley transform is the so-called *cosine-and-sine* (cas) function, given by

$$\text{cas}\,\omega t = \cos \omega t + \sin \omega t. \tag{2.45}$$

This kernel can be seen as a real-valued version of $e^{j\omega t} = \cos \omega t + j \sin \omega t$, the kernel of the Fourier transform. The forward and inverse Hartley transforms are given by

$$X_H(\omega) = \int_{-\infty}^{\infty} x(t)\ \text{cas}\,\omega t\ dt \tag{2.46}$$

and

$$x(t) = \frac{1}{2\pi} \int_{-\infty}^{\infty} X_H(\omega)\ \text{cas}\,\omega t\ d\omega, \tag{2.47}$$

where both the signal $x(t)$ and the transform $X_H(\omega)$ are real-valued.

In the literature, one also finds a more symmetric version based on the self-reciprocal kernel $(2\pi)^{-\frac{1}{2}} \text{cas}\,\omega t$. However, we use the non-symmetric form in order to simplify the relationship between the Hartley and Fourier transforms.

The Relationship between the Hartley and Fourier Transforms. Let us consider the even and odd parts of the Hartley transform, given by

$$X_H^e(\omega) = \frac{X_H(\omega) + X_H(-\omega)}{2} = \int_{-\infty}^{\infty} x(t)\ \cos \omega t\ dt \tag{2.48}$$

and

$$X_H^o(\omega) = \frac{X_H(\omega) - X_H(-\omega)}{2} = \int_{-\infty}^{\infty} x(t)\ \sin \omega t\ dt. \tag{2.49}$$

The Fourier transform may be written as

$$
\begin{aligned}
X(\omega) &= \int_{-\infty}^{\infty} x(t)\ e^{-j\omega t}\ dt \\[2mm]
&= \int_{-\infty}^{\infty} x(t)\ \cos \omega t\ dt - j \int_{-\infty}^{\infty} x(t)\ \sin \omega t\ dt \\[2mm]
&= X_H^e(\omega) - j X_H^o(\omega) \\[2mm]
&= \frac{X_H(\omega) + X_H(-\omega)}{2} - j\, \frac{X_H(\omega) - X_H(-\omega)}{2}.
\end{aligned}
\tag{2.50}
$$

Thus,

$$\Re\{X(\omega)\} = X_H^e(\omega),$$

$$\Im\{X(\omega)\} = -X_H^o(\omega).$$

(2.51)

The Hartley transform can be written in terms of the Fourier transform as

$$X_H(\omega) = \Re\{X(\omega)\} - \Im\{X(\omega)\}.$$

(2.52)

Due to their close relationship the Hartley and Fourier transforms share many properties. However, some properties are entirely different. In the following we summarize the most important ones.

Linearity. It directly follows from the definition of the Hartley transform that

$$\alpha\,x(t) + \beta\,y(t) \longleftrightarrow \alpha\,X_H(\omega) + \beta\,Y_H(\omega).$$

(2.53)

Scaling. For any real α, we have

$$x(\alpha t) \longleftrightarrow \frac{1}{|\alpha|} X_H\left(\frac{\omega}{\alpha}\right).$$

(2.54)

Proof.

$$\int_{-\infty}^{\infty} x(\alpha t)\,\operatorname{cas}\omega t\,dt = \frac{1}{|\alpha|}\int_{-\infty}^{\infty} x(\xi)\,\operatorname{cas}\left(\frac{\omega\xi}{\alpha}\right)\,d\xi = \frac{1}{|\alpha|}\,X_H\left(\frac{\omega}{\alpha}\right).$$

Time Inversion. From (2.54) with $\alpha = -1$ we get

$$x(-t) \longleftrightarrow X_H(-\omega).$$

(2.55)

Shifting. For any real t_0, we have

$$x(t - t_0) \longleftrightarrow \cos\omega t_0\,X_H(\omega) + \sin\omega t_0\,X_H(-\omega).$$

(2.56)

Proof. We may write

$$\int_{-\infty}^{\infty} x(t - t_0)\,\operatorname{cas}\omega t\,dt = \int_{-\infty}^{\infty} x(\xi)\,\operatorname{cas}\left(\omega[\xi + t_0]\right)\,d\xi.$$

Expanding the integral on the right-hand side using the property

$$\operatorname{cas}\left(\alpha + \beta\right) = [\cos\alpha\ + \sin\alpha]\ \cos\beta + [\cos\alpha\ - \sin\alpha]\ \sin\beta$$

yields (2.56). $\square$

Modulation. For any real ω_0, we have

$$\cos \omega_0 t \; x(t) \longleftrightarrow \frac{1}{2} X_H(\omega - \omega_0) + \frac{1}{2} X_H(\omega + \omega_0). \qquad (2.57)$$

Proof. Using the property

$$\cos \alpha \; \text{cas} \, \beta = \frac{1}{2} \, \text{cas} \, (\alpha - \beta) \; + \frac{1}{2} \, \text{cas} \, (\alpha + \beta),$$

we get

$$\int_{-\infty}^{\infty} x(t) \; \cos \omega_0 t \; \text{cas} \, \omega t \; dt$$

$$= \frac{1}{2} \int_{-\infty}^{\infty} x(t) \, \text{cas} \, ([\omega - \omega_0]t) \, dt + \frac{1}{2} \int_{-\infty}^{\infty} x(t) \, \text{cas} \, ([\omega + \omega_0]t) \, dt$$

$$= \frac{1}{2} X_H(\omega - \omega_0) + \frac{1}{2} X_H(\omega + \omega_0).$$

$\square$

Derivatives. For the nth derivative of a signal $x(t)$ the correspondence is

$$\frac{d^n}{dt^n} \; x(t) \longleftrightarrow \omega^n \left[\cos \left(\frac{n\pi}{2} \right) X_H(\omega) - \sin \left(\frac{n\pi}{2} \right) X_H(-\omega) \right]. \qquad (2.58)$$

Proof. Let $y(t) = \frac{d^n}{dt^n} \, x(t)$. The Fourier transform is $Y(\omega) = (j\omega)^n \, X(\omega)$. By writing j^n as $j^n = \cos(\frac{n\pi}{2}) + j \, \sin(\frac{n\pi}{2})$, we get

$$Y(\omega) \;\; = \;\; \omega^n \left[\cos \left(\tfrac{n\pi}{2} \right) + j \, \sin \left(\tfrac{n\pi}{2} \right) \right] \; X(\omega)$$

$$= \;\; \omega^n \left[\cos \left(\tfrac{n\pi}{2} \right) \Re\{X(\omega)\} - \sin \left(\tfrac{n\pi}{2} \right) \Im\{X(\omega)\} \right]$$

$$+ j \, \omega^n \left[\cos \left(\tfrac{n\pi}{2} \right) \Im\{X(\omega)\} + \sin \left(\tfrac{n\pi}{2} \right) \Re\{X(\omega)\} \right].$$

For the Hartley transform, this means

$$Y_H(\omega) \;\; = \;\; \omega^n \left[\cos \left(\tfrac{n\pi}{2} \right) X_H^e(\omega) - \sin \left(\tfrac{n\pi}{2} \right) X_H^o(\omega) \right.$$

$$\left. + \; \cos \left(\tfrac{n\pi}{2} \right) X_H^o(\omega) + \sin \left(\tfrac{n\pi}{2} \right) X_H^e(\omega) \right].$$

Rearranging this expression, based on (2.48) and (2.49), yields (2.58). $\square$

Convolution. We consider a convolution in time of two signals $x(t)$ and $y(t)$. The Hartley transforms are $X_H(\omega)$ and $Y_H(\omega)$, respectively. The correspondence is

$$x(t) * y(t) \longleftrightarrow \frac{1}{2}[\, X_H(\omega)Y_H(\omega) + X_H(-\omega)Y_H(\omega)$$
$$+ X_H(\omega)Y_H(-\omega) - X_H(-\omega)Y_H(-\omega)\,]. \tag{2.59}$$

The expression becomes less complex for signals with certain symmetries. For example, if $x(t)$ has even symmetry, then $x(t) * y(t) \longleftrightarrow X_H(\omega)\, Y_H(\omega)$. If $x(t)$ is odd, then $x(t) * y(t) \longleftrightarrow X_H(\omega)\, Y_H(-\omega)$.

Proof.

$$\int_{-\infty}^{\infty} [x(t) * y(t)] \, \text{cas}\,\omega t \; dt = \int_{-\infty}^{\infty} \left[\int_{-\infty}^{\infty} x(\tau)\, y(t-\tau) \; d\tau \right] \, \text{cas}\,\omega t \; dt$$

$$= \int_{-\infty}^{\infty} x(\tau) \left[\int_{-\infty}^{\infty} y(t-\tau) \, \text{cas}\,\omega t \; dt \right] d\tau$$

$$= \int_{-\infty}^{\infty} x(\tau) \, [\, \cos\omega\tau \, Y_H(\omega) + \sin\omega\tau \, Y_H(-\omega) \,] \; d\tau.$$

To derive the last line, we made use of the shift theorem. Using (2.48) and (2.49) we finally get (2.59). $\square$

Multiplication. The correspondence for a multiplication in time is

$$x(t)\, y(t) \longleftrightarrow \frac{1}{4\pi} \, [\, X_H(\omega) * Y_H(\omega) + X_H(-\omega) * Y_H(\omega)$$
$$+ X_H(\omega) * Y_H(-\omega) - X_H(-\omega) * Y_H(-\omega)\,]. \tag{2.60}$$

Proof. In the Fourier domain, we have

$$2\pi \, x(t)\, y(t)$$

$$\updownarrow$$

$$X(\omega) * Y(\omega) \;=\; [\, \Re\{X(\omega)\} * \Re\{Y(\omega)\} - \Im\{X(\omega)\} * \Im\{Y(\omega)\}]$$

$$+ j \; [\, \Im\{X(\omega)\} * \Re\{Y(\omega)\} + \Re\{X(\omega)\} * \Im\{Y(\omega)\} \,].$$

For the Hartley transform this means

$$2\pi\, x(t)\, y(t)$$

$$\updownarrow$$

$$X_H^e(\omega) * Y_H^e(\omega) - X_H^o(\omega) * Y_H^o(\omega) + X_H^o(\omega) * Y_H^e(\omega) + X_H^e(\omega) * Y_H^o(\omega).$$

Writing this expression in terms of $X_H(\omega)$ and $Y_H(\omega)$ yields (2.60). $\square$

Parseval's Relation. For signals $x(t)$ and $y(t)$ and their Hartley transforms $X_H(\omega)$ and $Y_H(\omega)$, respectively, we have

$$\int_{-\infty}^{\infty} x(t)\, y(t)\, dt = \frac{1}{2\pi} \int_{-\infty}^{\infty} X_H(\omega)\, Y_H(\omega)\, d\omega. \tag{2.61}$$

Similarly, the signal energy can be calculated in the time and in the frequency domains:

$$E_x = \int_{-\infty}^{\infty} x^2(t)\, dt$$

$$= \frac{1}{2\pi} \int_{-\infty}^{\infty} X_H^2(\omega)\, d\omega. \tag{2.62}$$

These properties are easily obtained from the results in Section 2.1 by using the fact that the kernel $(2\pi)^{-\frac{1}{2}}\, \text{cas}\,\omega t$ is self-reciprocal.

Energy Density and Phase. In practice, one of the reasons to compute the Fourier transform of a signal $x(t)$ is to derive the energy density $S_{xx}^E(\omega) = |X(\omega)|^2$ and the phase $\angle X(\omega)$. In terms of the Hartley transform the energy density becomes

$$S_{xx}^E(\omega) = |\Re\{X(\omega)\}|^2 + |\Im\{X(\omega)\}|^2$$

$$= [X_H^e(\omega)]^2 + [X_H^o(\omega)]^2 \tag{2.63}$$

$$= \frac{X_H^2(\omega) + X_H^2(-\omega)}{2}.$$

The phase can be written as

$$\angle X(\omega) = \tan^{-1} \frac{\Im\{X(\omega)\}}{\Re\{X(\omega)\}}$$

$$= \tan^{-1} \frac{X_H(-\omega) - X_H(\omega)}{X_H(\omega) + X_H(-\omega)}. \tag{2.64}$$

2.4   The Hilbert Transform

2.4.1   Definition

Choosing the kernel

$$\varphi(t - s) = \frac{-1}{\pi(t - s)}, \tag{2.65}$$

we obtain the Hilbert transform. For the reciprocal kernel $\theta(s - t)$ we use the notation $\hat{h}(s - t)$ throughout the following discussion. It is

$$\hat{h}(s - t) = \frac{1}{\pi(s - t)} = \varphi(t - s). \tag{2.66}$$

With $\hat{x}(s)$ denoting the Hilbert transform of $x(t)$ we obtain the following transform pair:

$$x(t) = \frac{1}{\pi} \int_{-\infty}^{\infty} \hat{x}(s) \frac{-1}{t - s} \, ds$$

$$\updownarrow \tag{2.67}$$

$$\hat{x}(s) = \frac{1}{\pi} \int_{-\infty}^{\infty} x(t) \frac{1}{s - t} \, dt.$$

Here, the integration has to be carried out according to the Cauchy principal value:

$$\int_{-\infty}^{\infty} := \lim_{\varepsilon \to 0} \left(\int_{-\infty}^{s-\varepsilon} + \int_{s+\varepsilon}^{\infty} \right), \quad \varepsilon > 0. \tag{2.68}$$

The Fourier transforms of $\varphi(t)$ and $\hat{h}(t)$ are:

$$\Phi(\omega) = j \ \mathrm{sgn}(\omega) \quad \text{with} \quad \Phi(0) = 0, \tag{2.69}$$

$$\hat{H}(\omega) = -j \ \mathrm{sgn}(\omega) \quad \text{with} \quad \hat{H}(0) = 0. \tag{2.70}$$

In the spectral domain we then have:

$$X(\omega) = \Phi(\omega) \ \hat{X}(\omega) = j \ \mathrm{sgn}(\omega) \ \hat{X}(\omega) \tag{2.71}$$

$$\hat{X}(\omega) = \hat{H}(\omega) \ X(\omega) = -j \ \mathrm{sgn}(\omega) \ X(\omega). \tag{2.72}$$

We observe that the spectrum of the Hilbert transform $\hat{x}(s)$ equals the spectrum of $x(t)$, except for the prefactor $-j \ \mathrm{sgn}(\omega)$. Furthermore, we see that, because of $\Phi(0) = \hat{H}(0) = 0$, the transform pair (2.67) is valid only for signals $x(t)$ with zero mean value. The Hilbert transform of a signal with non-zero mean has zero mean.

2.4.2 Some Properties of the Hilbert Transform

1. Since the kernel of the Hilbert transform is self-reciprocal we have

$$\langle \hat{x}, \hat{y} \rangle = \langle x, y \rangle . \tag{2.73}$$

2. A real-valued signal $x(t)$ is orthogonal to its Hilbert transform $\hat{x}(t)$:

$$\langle x, \hat{x} \rangle = 0. \tag{2.74}$$

We prove this by making use of Parseval's relation:

$$
\begin{aligned}
2\pi \langle x, \hat{x} \rangle &= \langle X, \hat{X} \rangle \\
&= \int_{-\infty}^{\infty} X(\omega) \left[\hat{X}(\omega) \right]^* d\omega \\
&= \int_{-\infty}^{\infty} X(\omega) \left[-j \ \text{sgn}(\omega) \right]^* X^*(\omega) \ d\omega \tag{2.75} \\
&= j \int_{-\infty}^{\infty} |X(\omega)|^2 \ \text{sgn}(\omega) \ d\omega \\
&= 0.
\end{aligned}
$$

3. From (2.67) and (2.70) we conclude that applying the Hilbert transform twice leads to a sign change of the signal, provided that the signal has zero mean value.

2.5 Representation of Bandpass Signals

A bandpass signal is understood as a signal whose spectrum concentrates in a region $\pm[\omega_0 - B, \omega_0 + B]$ where $\omega_0 \geq B > 0$. See Figure 2.1 for an example of a bandpass spectrum.
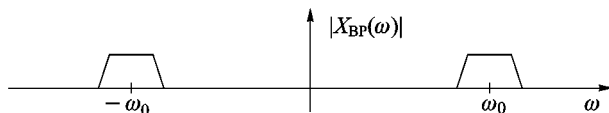
Figure 2.1. Example of a bandpass spectrum.

2.5.1   Analytic Signal and Complex Envelope

The Hilbert transform allows us to transfer a *real bandpass signal* $x_{\mathrm{BP}}(t)$ into a *complex lowpass signal* $x_{\mathrm{LP}}(t)$. For that purpose, we first form the so-called *analytic signal* $x_{\mathrm{BP}}^+(t)$, first introduced in [61]:

$$x_{\mathrm{BP}}^+(t) = x_{\mathrm{BP}}(t) + j\ \hat{x}_{\mathrm{BP}}(t). \qquad (2.76)$$

Here, $\hat{x}_{\mathrm{BP}}(t)$ is the Hilbert transform of $x_{\mathrm{BP}}(t)$.

The Fourier transform of the analytic signal is

$$X_{\mathrm{BP}}^+(\omega) = X_{\mathrm{BP}}(\omega) + j\,\hat{X}_{\mathrm{BP}}(\omega) = \begin{cases} 2\ X_{\mathrm{BP}}(\omega) & \text{for} \quad \omega > 0, \\ X_{\mathrm{BP}}(\omega) & \text{for} \quad \omega = 0, \\ 0 & \text{for} \quad \omega < 0. \end{cases} \qquad (2.77)$$

This means that the analytic signal has spectral components for positive frequencies only.

In a second step, the complex-valued analytic signal can be shifted into the baseband:

$$x_{\mathrm{LP}}(t) = x_{\mathrm{BP}}^+(t)\ e^{-j\omega_0 t}. \qquad (2.78)$$

Here, the frequency ω_0 is assumed to be the center frequency of the bandpass spectrum, as shown in Figure 2.1. Figure 2.2 illustrates the procedure of obtaining the complex envelope. We observe that it is not necessary to realize an ideal Hilbert transform with system function $\hat{H}(\omega) = -j\,\mathrm{sgn}(\omega)$ in order to carry out this transform.

The signal $x_{\mathrm{LP}}(t)$ is called the *complex envelope* of the bandpass signal $x_{\mathrm{BP}}(t)$. The reason for this naming convention is outlined below.

In order to recover a real bandpass signal $x_{\mathrm{BP}}(t)$ from its complex envelope $x_{\mathrm{LP}}(t)$, we make use of the fact that

$$\begin{aligned} x_{\mathrm{BP}}(t) &= \Re\{x^+(t)\} \\ &= \Re\{x_{\mathrm{LP}}(t)\ e^{j\omega_0 t}\} \\ &= u(t)\ \cos\omega_0 t\ -\ v(t)\ \sin\omega_0 t \end{aligned} \qquad (2.79)$$

for

$$\begin{aligned} u(t) &= \Re\{x_{\mathrm{LP}}(t)\}, \\ v(t) &= \Im\{x_{\mathrm{LP}}(t)\}, \\ x_{\mathrm{LP}}(t) &= u(t) + j\,v(t). \end{aligned} \qquad (2.80)$$
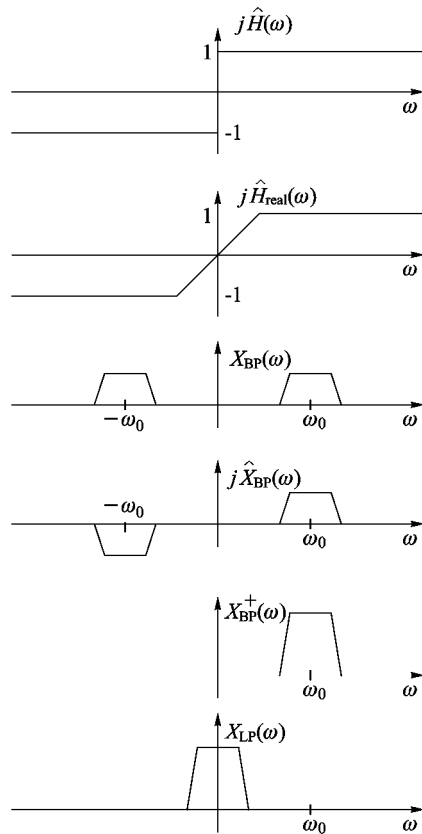
Figure 2.2. Producing the complex envelope of a real bandpass signal.

Another form of representing $x_{\text{BP}}(t)$ is obtained by describing the complex envelope with polar coordinates:

$$x_{\text{LP}}(t) = |x_{\text{LP}}(t)|\, e^{j\theta(t)} \tag{2.81}$$

with

$$|x_{\text{LP}}(t)| = \sqrt{u^2(t) + v^2(t)}, \qquad \tan\theta(t) = \frac{v(t)}{u(t)}. \tag{2.82}$$

From (2.79) we then conclude for the bandpass signal:

$$x_{\text{BP}}(t) = |x_{\text{LP}}(t)|\, \cos(\omega_0 t + \theta(t)). \tag{2.83}$$

We see that $|x_{\text{LP}}(t)|$ can be interpreted as the *envelope of the bandpass signal* (see Figure 2.3). Accordingly, $x_{\text{LP}}(t)$ is called the complex envelope, and the
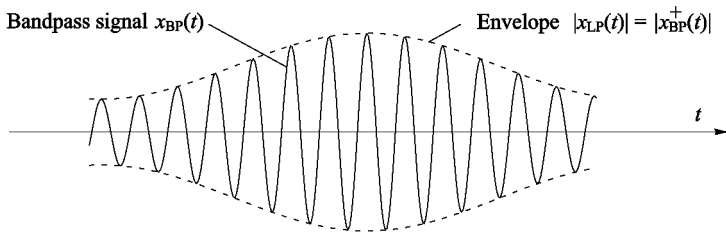
Figure 2.3. Bandpass signal and envelope.

analytic signal is called the *pre-envelope*. The real part $u(t)$ is referred to as the *in-phase component*, and the imaginary part $v(t)$ is called the *quadrature component*.

Equation (2.83) shows that bandpass signals can in general be regarded as amplitude and phase modulated signals. For $\theta(t) = \theta_0$ we have a pure amplitude modulation.

It should be mentioned that the spectrum of a complex envelope is always limited to $-\omega_0$ at the lower bound:

$$X_{\mathrm{LP}}(\omega) \equiv 0 \quad \text{for} \quad \omega < -\omega_0. \tag{2.84}$$

This property immediately results from the fact that an analytic signal contains only positive frequencies.

Application in Communications. In communications we often start with a lowpass complex envelope $x_{\mathrm{LP}}(t)$ and wish to transmit it as a real bandpass signal $x_{\mathrm{BP}}(t)$. Here, the real bandpass signal $x_{\mathrm{BP}}(t)$ is produced from $x_{\mathrm{LP}}(t)$ according to (2.79). In the receiver, $x_{\mathrm{LP}}(t)$ is finally reconstructed as described above. However, one important requirement must be met, which will be discussed below.

The real bandpass signal

$$x_{\mathrm{BP}}(t) = u(t) \, \cos \omega_0 t \tag{2.85}$$

is considered. Here, $u(t)$ is a given real lowpass signal. In order to reconstruct $u(t)$ from $x_{\mathrm{BP}}(t)$, we have to add the imaginary signal $ju(t) \sin \omega_0 t$ to the bandpass signal:

$$x^{(p)}(t) := u(t) \, [\cos \omega_0 t + j \sin \omega_0 t] = u(t) \, e^{j\omega_0 t}. \tag{2.86}$$

Through subsequent modulation we recover the original lowpass signal:

$$u(t) = x^{(p)}(t) \, e^{-j\omega_0 t}. \tag{2.87}$$
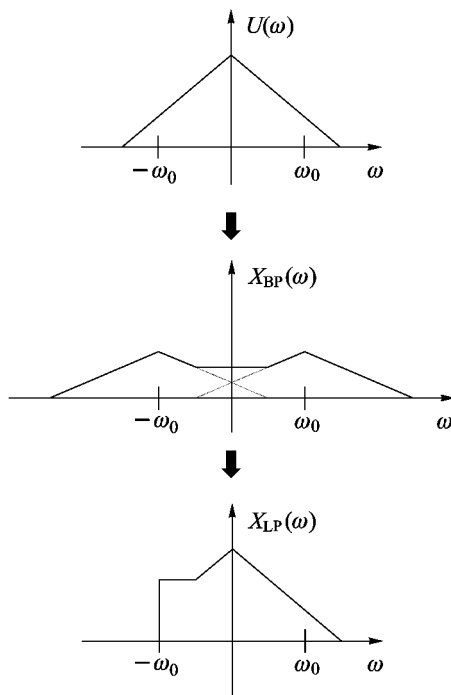
Figure 2.4. Complex envelope for the case that condition (2.88) is violated.

The problem, however, is to generate $u(t) \sin \omega_0 t$ from $u(t) \cos \omega_0 t$ in the receiver. We now assume that $u(t)\, e^{j\omega_0 t}$ is analytic, which means that

$$U(\omega) \equiv 0 \text{ for } \omega < -\omega_0. \tag{2.88}$$

As can easily be verified, under condition (2.88) the Hilbert transform of the bandpass signal is given by

$$\hat{x}(t) = u(t)\ \sin \omega_0 t. \tag{2.89}$$

Thus, under condition (2.88) the required signal $x^{(p)}(t)$ equals the analytic signal $x_{\mathrm{BP}}^{+}(t)$, and the complex envelope $x_{\mathrm{LP}}(t)$ is identical to the given $u(t)$. The complex envelope describes the bandpass signal unambiguously, that is, $x_{\mathrm{BP}}(t)$ can always be reconstructed from $x_{\mathrm{LP}}(t)$; the reverse, however, is only possible if condition (2.88) is met. This is illustrated in Figure 2.4.

Bandpass Filtering and Generating the Complex Envelope. In practice, generating a complex envelope usually involves the task of filtering the real bandpass signal $x_{\mathrm{BP}}(t)$ out of a more broadband signal $x(t)$. This means

that $x_{\text{BP}}(t) = x(t) * g(t)$ has to be computed, where $g(t)$ is the impulse response of a real bandpass.

The analytic bandpass $g^+(t)$ associated with $g(t)$ has the system function

$$G^+(\omega) = G(\omega)\,[1 + j\,\hat{H}(\omega)]. \tag{2.90}$$

Using the analytic bandpass, the analytic signal can be calculated as

$$
\begin{aligned}
x_{\text{BP}}^+(t) &= x(t) * g^+(t) \\
&\updownarrow \\
X_{\text{BP}}^+(\omega) &= X(\omega)\,G^+(\omega).
\end{aligned}
\tag{2.91}
$$

For the complex envelope, we have

$$
\begin{aligned}
x_{\text{LP}}(t) &= [x(t) * g^+(t)]\,e^{-j\omega_0 t} \\
&\updownarrow \\
X_{\text{LP}}(\omega) &= X(\omega + \omega_0)\,G^+(\omega + \omega_0).
\end{aligned}
\tag{2.92}
$$

If we finally describe the analytic bandpass by means of the complex envelope of the real bandpass

$$
\begin{aligned}
g^+(t) &= g_{\text{LP}}(t)\,e^{j\omega_0 t} \\
&\updownarrow \\
G^+(\omega) &= G_{\text{LP}}(\omega - \omega_0),
\end{aligned}
\tag{2.93}
$$

this leads to

$$X_{\text{LP}}(\omega) = X(\omega + \omega_0)\,G_{\text{LP}}(\omega). \tag{2.94}$$

We find that $X_{\text{LP}}(\omega)$ is also obtained by modulating the real bandpass signal with $e^{-j\omega_0 t}$ and by lowpass filtering the resulting signal. See Figure 2.5 for an illustration.

The equivalent lowpass $G_{\text{LP}}(\omega)$ usually has a complex impulse response. Only if the symmetry condition $G_{\text{LP}}(\omega) = G_{\text{LP}}^*(-\omega)$ is satisfied, the result is a real lowpass, and the realization effort is reduced. This requirement means that $|G(\omega)|$ must have even symmetry around ω_0 and the phase response of $G(\omega)$ must be anti-symmetric. In this case we also speak of a *symmetric bandpass*.

Realization of Bandpass Filters by Means of Equivalent Lowpass Filters. We consider a signal $y(t) = x(t) * g(t)$, where $x(t)$, $y(t)$, and $g(t)$ are
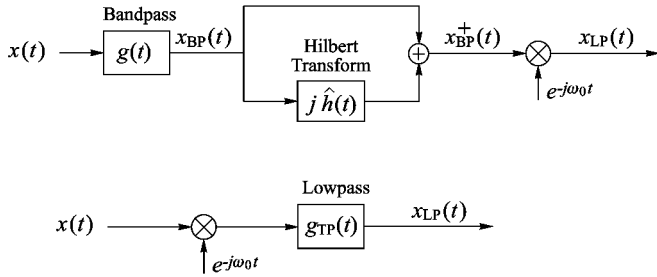
Figure 2.5. Generating the complex envelope of a real bandpass signal.

real-valued. The signal $x(t)$ is now described by means of its complex envelope with respect to an arbitrary positive center frequency ω_0:

$$x(t) = \Re\{x_{\mathrm{LP}}(t)\, e^{j\omega_0 t}\}. \tag{2.95}$$

For the spectrum we have

$$X(\omega) = \frac{1}{2} X_{\mathrm{LP}}(\omega - \omega_0) + \frac{1}{2} X_{\mathrm{LP}}^*(-\omega - \omega_0). \tag{2.96}$$

Correspondingly, the system function of the filter can be written as

$$G(\omega) = \frac{1}{2} G_{\mathrm{LP}}(\omega - \omega_0) + \frac{1}{2} G_{\mathrm{LP}}^*(-\omega - \omega_0). \tag{2.97}$$

For the spectrum of the output signal we have

$$
\begin{aligned}
Y(\omega) &= X(\omega)\, G(\omega) \\[2mm]
&= \tfrac{1}{4} X_{\mathrm{LP}}(\omega - \omega_0)\, G_{\mathrm{LP}}(\omega - \omega_0) \\[2mm]
&\quad + \tfrac{1}{4} X_{\mathrm{LP}}^*(-\omega - \omega_0)\, G_{\mathrm{LP}}^*(-\omega - \omega_0) \\[2mm]
&\quad + \tfrac{1}{4} X_{\mathrm{LP}}(\omega - \omega_0)\, G_{\mathrm{LP}}^*(-\omega - \omega_0) \\[2mm]
&\quad + \tfrac{1}{4} X_{\mathrm{LP}}^*(-\omega - \omega_0)\, G_{\mathrm{LP}}(\omega - \omega_0).
\end{aligned}
\tag{2.98}
$$

The last two terms vanish since $G_{\mathrm{LP}}(\omega) = 0$ for $\omega < -\omega_0$ and $X_{\mathrm{LP}}(\omega) = 0$ for $\omega < -\omega_0$:

$$
\begin{aligned}
Y(\omega) &= \tfrac{1}{4} X_{\mathrm{LP}}(\omega - \omega_0)\, G_{\mathrm{LP}}(\omega - \omega_0) \\[2mm]
&\quad + \tfrac{1}{4} X_{\mathrm{LP}}^*(-\omega - \omega_0)\, G_{\mathrm{LP}}^*(-\omega - \omega_0) \\[2mm]
&= \tfrac{1}{2} Y_{\mathrm{LP}}(\omega - \omega_0) + \tfrac{1}{2} Y_{\mathrm{LP}}^*(-\omega - \omega_0).
\end{aligned}
\tag{2.99}
$$

Altogether this yields

$$Y_{\mathrm{LP}}(\omega) = \frac{1}{2}\, X_{\mathrm{LP}}(\omega)\, G_{\mathrm{LP}}(\omega). \tag{2.100}$$

This means that a real convolution in the bandpass domain can be replaced by a complex convolution in the lowpass domain:

$$y(t) = x(t) * g(t) \qquad \rightarrow \qquad y_{\mathrm{LP}}(t) = \frac{1}{2}\, x_{\mathrm{LP}}(t) * g_{\mathrm{LP}}(t). \tag{2.101}$$

Note that the prefactor $1/2$ must be taken into account. This prefactor did not appear in the combination of bandpass filtering and generating the complex envelope discussed above. As before, a real filter $g_{\mathrm{LP}}(t)$ is obtained if $G(\omega)$ is symmetric with respect to ω_0.

Inner Products. We consider the inner product of two analytic signals

$$x^{+}(t) = x(t) + j\, \hat{x}(t) \qquad \text{and} \qquad y^{+}(t) = y(t) + j\, \hat{y}(t),$$

where $x(t)$ and $y(t)$ are real-valued. We have

$$\langle x^{+}, y^{+}\rangle = \langle x, y\rangle + \langle \hat{x}, \hat{y}\rangle + j\, \langle \hat{x}, y\rangle + j\, \langle x, \hat{y}\rangle. \tag{2.102}$$

Observing (2.73), we get for the real part

$$\Re\{\langle x^{+}, y^{+}\rangle\} = 2\, \langle x, y\rangle. \tag{2.103}$$

If we describe $x(t)$ and $y(t)$ by means of their complex envelope with respect to the same center frequency, we get

$$\langle x, y\rangle = \frac{1}{2}\, \Re\{\langle x_{\mathrm{LP}}, y_{\mathrm{LP}}\rangle\}. \tag{2.104}$$

For the implementation of correlation operations this means that correlations of deterministic bandpass signals can be computed in the bandpass domain as well as in the equivalent lowpass domain.

Group and Phase Delay. The group and phase delay of a system $C(\omega)$ are defined as

$$\tau_g(\omega) = -\frac{d\varphi(\omega)}{d\omega} \tag{2.105}$$

and

$$\tau_p(\omega) = -\frac{\varphi(\omega)}{\omega} \tag{2.106}$$

where

$$C(\omega) = |C(\omega)|\, e^{j\varphi(\omega)}. \tag{2.107}$$

In order to explain this, let us assume that $C(\omega)$ is a narrowband bandpass with $B << \omega_0$. The system function of the associated analytic bandpass may be written as

$$C_{\mathrm{BP}}^+(\omega) = \begin{cases} |C(\omega)|e^{j\varphi(\omega)}, & |\omega - \omega_0| \leq B/2 \\ 0, & \text{otherwise.} \end{cases} \qquad (2.108)$$

Because of $B << \omega_0$, $C_{\mathrm{BP}}^+(\omega)$ may be approximated as

$$C_{\mathrm{BP}}^+(\omega) \approx \begin{cases} |C(\omega_0)|e^{j[\varphi(\omega_0) + (\omega - \omega_0)(\frac{d\varphi(\omega)}{d\omega}|_{\omega=\omega_0})]}, & |\omega - \omega_0| \leq B/2 \\ 0, & \text{otherwise.} \end{cases}$$
$$(2.109)$$

For the complex envelope $C_{\mathrm{LP}}(\omega) = C_{\mathrm{BP}}(\omega + \omega_0)$ it follows that

$$C_{\mathrm{LP}}(\omega) \approx |C(\omega_0)| \; e^{-j\omega_0\tau_p(\omega_0)} \; e^{-j\omega\tau_g(\omega_0)}, \qquad \omega \leq B/2, \qquad (2.110)$$

with τ_g and τ_p according to (2.105) and (2.106). If we now look at the input-output relation (2.100) we get

$$Y_{\mathrm{LP}}(\omega) \approx \frac{1}{2}|C(\omega_0)| \; e^{-j\omega_0\tau_p(\omega_0)} \; e^{-j\omega\tau_g(\omega_0)} \; X_{\mathrm{LP}}(\omega). \qquad (2.111)$$

Hence, in the time domain

$$y_{\mathrm{LP}}(t) \approx \frac{1}{2}|C(\omega_0)|e^{-j\omega_0\tau_p(\omega_0)} \; x_{\mathrm{LP}}(t - \tau_g(\omega_0)), \qquad (2.112)$$

which means that the narrowband system $C(\omega)$ provides a phase shift by $\tau_p(\omega_0)$ and a time delay by $\tau_g(\omega_0)$.

2.5.2 Stationary Bandpass Processes

In communications we must assume that noise interferes with bandpass signals that are to be transmitted. Therefore the question arises of which statistical properties the complex envelope of a stationary bandpass process has. We assume a real-valued, zero mean, wide-sense stationary bandpass process $x(t)$. The autocorrelation function of the process is given by

$$r_{xx}(\tau) = r_{xx}(-\tau) = E\{x(t)\ x(t + \tau)\}. \qquad (2.113)$$

Now we consider the transformed process $\hat{x}(t)$. For the power spectral density of the transformed process, $S_{\hat{x}\hat{x}}(\omega)$, we conclude from (1.105):

$$S_{\hat{x}\hat{x}}(\omega) = \underbrace{|\hat{H}(\omega)|^2}_{\text{1 for } \omega \neq 0} \cdot \underbrace{S_{xx}(\omega)}_{\text{0 for } \omega = 0} = S_{xx}(\omega), \qquad (2.114)$$

where $\hat{h}(t) \longleftrightarrow \hat{H}(\omega)$. Thus, the process $\hat{x}(t)$ has the same power spectral density, and consequently the same autocorrelation function, as the process $x(t)$:

$$r_{\hat{x}\hat{x}}(\tau) = r_{xx}(\tau). \tag{2.115}$$

For the cross power spectral densities $S_{x\hat{x}}(\omega)$ and $S_{\hat{x}x}(\omega)$ we get according to (1.102):

$$S_{x\hat{x}}(\omega) = \hat{H}(\omega)\,S_{xx}(\omega),$$

$$\tag{2.116}$$

$$S_{\hat{x}x}(\omega) = \hat{H}^*(\omega)\,S_{xx}(\omega).$$

Hence, for the cross correlation functions:

$$r_{x\hat{x}}(\tau) = \hat{r}_{xx}(\tau),$$

$$r_{\hat{x}x}(\tau) = r_{x\hat{x}}(-\tau) = \hat{r}_{xx}(-\tau) = -\hat{r}_{xx}(\tau). \tag{2.117}$$

Now we form the analytic process $x^+(t)$:

$$x^+(t) = x(t) + j\,\hat{x}(t). \tag{2.118}$$

For the autocorrelation function we have

$$
\begin{aligned}
r_{x^+x^+}(\tau) &= E\left\{[x(t) + j\,\hat{x}(t)]^*\,[x(t+\tau) + j\,\hat{x}(t+\tau)]\right\} \\
&= r_{xx}(\tau) + j\,r_{x\hat{x}}(\tau) - j\,r_{\hat{x}x}(\tau) + r_{\hat{x}\hat{x}}(\tau) \\
&= 2\,r_{xx}(\tau) + 2j\,\hat{r}_{xx}(\tau).
\end{aligned}
\tag{2.119}
$$

This means that the autocorrelation function of the analytic process is an analytic signal itself. The power spectral density is

$$S_{x^+x^+}(\omega) = \begin{cases} 4\,S_{xx}(\omega) & \text{for } \omega > 0, \\ 0 & \text{for } \omega < 0. \end{cases} \tag{2.120}$$

Finally, we consider the complex process $x_{\text{LP}}(t)$ derived from the analytic process

$$
\begin{aligned}
x_{\text{LP}}(t) &= x^+(t)\,e^{-j\omega_0 t} \\
&= u(t) + j\,v(t).
\end{aligned}
\tag{2.121}
$$

For the real part $u(t)$ we have

$$
\begin{aligned}
u(t) &= \Re\{[x(t) + j\,\hat{x}(t)]\,e^{-j\omega_0 t}\} \\
&= x(t)\,\cos\omega_0 t + \hat{x}(t)\,\sin\omega_0 t \\
&= \tfrac{1}{2}\,[x^+(t)\,e^{-j\omega_0 t} + [x^+(t)]^*\,e^{j\omega_0 t}],
\end{aligned}
\tag{2.122}
$$

and for its autocorrelation function follows

$$
\begin{aligned}
E\left\{u(t)u(t+\tau)\right\} \;=\;& \tfrac{1}{4}\, E\Big\{x^{+}(t)\,x^{+}(t+\tau)\,e^{-j\omega_0(2t+\tau)} \\[4pt]
& + x^{+}(t)\,[x^{+}(t+\tau)]^{*}\,e^{j\omega_0\tau} \\[4pt]
& + [x^{+}(t)]^{*}\,x^{+}(t+\tau)\,e^{-j\omega_0\tau} \\[4pt]
& + [x^{+}(t)]^{*}\,[x^{+}(t+\tau)]^{*}\,e^{j\omega_0(2t+\tau)}\Big\}.
\end{aligned}
\tag{2.123}
$$

In (2.123) two complex exponential functions dependent on t are included whose prefactors reduce to zero:

$$
\begin{aligned}
E\left\{[x^{+}(t)]^{*}\,[x^{+}(t+\tau)]^{*}\right\}^{*} \;=\;& E\left\{x^{+}(t)\,x^{+}(t+\tau)\right\} \\[4pt]
=\;& E\left\{(x(t)+j\,\hat{x}(t))\,(x(t+\tau)+j\,\hat{x}(t+\tau))\right\} \\[4pt]
=\;& \underbrace{r_{xx}(\tau)-r_{\hat{x}\hat{x}}(\tau)}_{0}+\underbrace{jr_{x\hat{x}}(\tau)+jr_{\hat{x}x}(\tau)}_{0} \\[4pt]
=\;& 0.
\end{aligned}
\tag{2.124}
$$

What remains is

$$
\begin{aligned}
r_{uu}(\tau) \;=\;& E\left\{u(t)\,u(t+\tau)\right\} \\[4pt]
=\;& \tfrac{1}{4}\,\left[[r_{x^{+}x^{+}}(\tau)]^{*}\,e^{j\omega_0\tau}+r_{x^{+}x^{+}}(\tau)\,e^{-j\omega_0\tau}\right] \\[4pt]
=\;& r_{xx}(\tau)\,\cos\omega_0\tau+\hat{r}_{xx}(\tau)\,\sin\omega_0\tau.
\end{aligned}
\tag{2.125}
$$

In a similar way we obtain

$$
r_{vv}(\tau)=r_{uu}(\tau)
\tag{2.126}
$$

for the autocorrelation function of the imaginary part of the complex envelope. The cross correlation function between the real and the imaginary part is given by

$$
\begin{aligned}
r_{uv}(\tau) \;=\;& -r_{vu}(\tau) \\[4pt]
=\;& \hat{r}_{xx}(\tau)\,\cos\omega_0\tau-r_{xx}(\tau)\,\sin\omega_0\tau.
\end{aligned}
\tag{2.127}
$$

From (2.125) – (2.127) we conclude that the autocorrelation function of the complex envelope equals the modulated autocorrelation function of the

analytic signal:

$$
\begin{aligned}
r_{x_{\mathrm{LP}} x_{\mathrm{LP}}}(\tau) &= E\left\{[u(t) - j\,v(t)]\,[u(t+\tau) + j\,v(t+\tau)]\right\} \\
&= 2\,r_{uu}(\tau) + 2j\,r_{uv}(\tau) \\
&= 2\left[r_{xx}(\tau) + j\,\hat{r}_{xx}(\tau)\right] e^{-j\omega_0 \tau}.
\end{aligned}
\tag{2.128}
$$

Correspondingly, we get for the power spectral density:

$$
\begin{aligned}
S_{x_{\mathrm{LP}} x_{\mathrm{LP}}}(\omega) &= S_{x_+ x_+}(\omega + \omega_0) \\
&= \begin{cases} 4\,S_{xx}(\omega + \omega_0) & \text{for } \omega + \omega_0 > 0, \\ 0 & \text{for } \omega + \omega_0 < 0. \end{cases}
\end{aligned}
\tag{2.129}
$$

We notice that the complex envelope is a wide-sense stationary process with specific properties:

- The autocorrelation function of the real part equals that of the imaginary part.

- The cross correlation function between the real and imaginary part is antisymmetric with respect to τ. In particular, we have

$$
r_{uv}(0) = r_{vu}(0) = 0.
$$

In the special case of a symmetric bandpass process, we have

$$
S_{x_{\mathrm{LP}} x_{\mathrm{LP}}}(\omega) = S_{x_{\mathrm{LP}} x_{\mathrm{LP}}}(-\omega).
\tag{2.130}
$$

Hence, we see that the autocorrelation function of $x_{\mathrm{LP}}(t)$ is real-valued. It also means that the cross correlation between the real and imaginary part vanishes:

$$
r_{uv}(\tau) = 0, \quad \forall\,\tau.
\tag{2.131}
$$

Chapter 3

Discrete

Signal Representations

In this chapter we discuss the fundamental concepts of discrete signal representations. Such representations are also known as discrete transforms, series expansions, or block transforms. Examples of widely used discrete transforms are given in the next chapter. Moreover, optimal discrete representations will be discussed in Chapter 5. The term "discrete" refers to the fact that the signals are represented by discrete values, whereas the signals themselves may be continuous-time. If the signals that are to be transformed consist of a finite set of values, one also speaks of block transforms. Discrete signal representations are of crucial importance in signal processing. They give a certain insight into the properties of signals, and they allow easy handling of continuous and discrete-time signals on digital signal processors.

3.1   Introduction

We consider a real or complex-valued, continuous or discrete-time signal x, assuming that x can be represented in the form

$$x = \sum_{i=1}^{n} \alpha_i \, \varphi_i.$$

(3.1)

The signal x is an element of the signal space X spanned by $\{\varphi_1, \ldots, \varphi_n\}$. The signal space itself is the set of all vectors which can be represented by linear combination of $\{\varphi_1, \ldots, \varphi_n\}$. For this, the notation

$$X = \mathrm{span}\,\{\varphi_1, \ldots, \varphi_n\} \qquad (3.2)$$

will be used henceforth. The vectors φ_i, $i = 1, \ldots, n$ may be linearly dependent or linearly independent of each other. If they are linearly independent, we call them a *basis* for X.

The coefficients α_i, $i = 1, \ldots, n$ can be arranged as a vector

$$\boldsymbol{\alpha} = [\alpha_1, \ldots, \alpha_n]^T, \qquad (3.3)$$

which is referred to as the *representation* of x with respect to the basis $\{\varphi_1, \ldots, \varphi_n\}$.

One often is interested in finding the best approximation of a given signal x by a signal $\hat{x}$ which has the series expansion

$$\hat{x} = \sum_{i=1}^{m} \beta_i\,\varphi_i \quad \text{with} \quad m < n. \qquad (3.4)$$

This problem will be discussed in Sections 3.2 and 3.3 in greater detail. For the present we will confine ourselves to discussing some general concepts of decomposing signal spaces. We start by assuming a decomposition of x into

$$x = x_1 + x_2, \qquad (3.5)$$

where

$$x_1 \;=\; \sum_{i=1}^{m} \alpha_i \varphi_i, \qquad (3.6)$$

$$x_2 \;=\; \sum_{i=m+1}^{n} \alpha_i \varphi_i. \qquad (3.7)$$

Signal x_1 is an element of the *linear subspace*[1] $X_1 = \mathrm{span}\,\{\varphi_1, \ldots, \varphi_m\}$ and x_2 is an element of the linear subspace $X_2 = \mathrm{span}\,\{\varphi_{m+1}, \ldots, \varphi_n\}$. The space X is called the *sum of the subspaces* X_1 and X_2. If the decomposition of $x \in X$

---

[1]Definition of a linear subspace: *let M be a non-empty set of elements of the vector space X. Then M is a linear subspace of X, if M itself is a linear space.* This means that all linear combinations of the elements of M must be elements of M. Hence, X itself is a linear subspace.

into $\boldsymbol{x}_1 \in X_1$ and $\boldsymbol{x}_2 \in X_2$ is unique,[2] we speak of a *direct decomposition* of X into the subspaces X_1 and X_2, and X is called the *direct sum* of X_1 and X_2. The notation for the direct sum is

$$X = X_1 \oplus X_2. \tag{3.8}$$

A direct sum is obtained if the vectors that span X_1 are linearly independent of the vectors that span X_2.

If a space X is the direct sum of two subspaces X_1 and X_2 and $\boldsymbol{x}_1 \in X_1$ and $\boldsymbol{x}_2 \in X_2$ are orthogonal to one another for all signals $\boldsymbol{x} \in X$, that is if $\langle \boldsymbol{x}_1, \boldsymbol{x}_2 \rangle = 0 \; \forall \, \boldsymbol{x} \in X$, then X is the *orthogonal sum* of the subspaces X_1 and X_2. For this we write

$$X = X_1 \overset{\perp}{\oplus} X_2. \tag{3.9}$$

3.2 Orthogonal Series Expansions

3.2.1 Calculation of Coefficients

We consider a signal $\boldsymbol{x}$ that can be represented in the form

$$\boldsymbol{x} = \sum_{i=1}^{n} \alpha_i \, \boldsymbol{u}_i, \tag{3.10}$$

where the vectors $\boldsymbol{u}_i$ satisfy the *orthonormality condition*

$$\langle \boldsymbol{u}_i, \boldsymbol{u}_j \rangle = \delta_{ij}. \tag{3.11}$$

Here, δ_{ij} is the *Kronecker symbol*

$$\delta_{ij} = \begin{cases} 1 & \text{for } i = j, \\ 0 & \text{otherwise.} \end{cases} \tag{3.12}$$

For all signals $\boldsymbol{x}$ in (3.10) we have $\boldsymbol{x} \in X$ with $X = \operatorname{span} \{\boldsymbol{u}_1, \boldsymbol{u}_2, \ldots, \boldsymbol{u}_n\}$. Because of (3.11), $\boldsymbol{u}_1, \boldsymbol{u}_2, \ldots, \boldsymbol{u}_n$ form an *orthonormal basis* for X. Each vector $\boldsymbol{u}_i, \; i = 1, \ldots, n$ spans a one-dimensional subspace, and X is the orthogonal sum of these subspaces.

The question of how the coefficients α_i can be calculated if $\boldsymbol{x}$ and the orthonormal basis $\{\boldsymbol{u}_1, \ldots, \boldsymbol{u}_n\}$ are given is easily answered. By taking the inner product of (3.10) with $\boldsymbol{u}_j, \; j = 1, \ldots, n$ and using (3.11) we obtain

$$\alpha_j = \langle \boldsymbol{x}, \boldsymbol{u}_j \rangle, \quad j = 1, \ldots, n. \tag{3.13}$$

---

[2]The decomposition is unique if $\boldsymbol{x}_1$ and $\boldsymbol{x}_2$ cannot be represented by means of coefficients $\gamma_i \neq \alpha_i$ as $\boldsymbol{x}_1 = \sum_{i=1}^{m} \gamma_i \boldsymbol{\varphi}_i$ and $\boldsymbol{x}_2 = \sum_{i=m+1}^{n} \gamma_i \boldsymbol{\varphi}_i$.
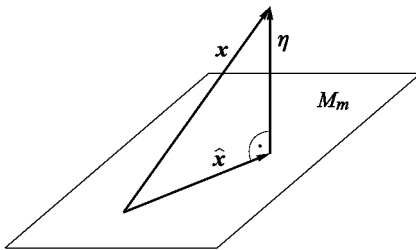
Figure 3.1. Orthogonal projection.

3.2.2   Orthogonal Projection

In (3.10) we assumed that x can be represented by means of n coefficients $\alpha_1, \alpha_1, \ldots, \alpha_n$. Possibly, n is infinitely large, so that for practical applications we are interested in finding the best approximation

$$\hat{x} = \sum_{i=1}^{m} \beta_i \, u_i, \qquad m < n \tag{3.14}$$

in the sense of

$$d(x, \hat{x}) = \|x - \hat{x}\| = \langle x - \hat{x}, x - \hat{x} \rangle^{\frac{1}{2}} \stackrel{!}{=} \min. \tag{3.15}$$

The solution to this problem is[3] $\beta_i = \langle x, u_i \rangle$, which means that

$$\hat{x} = \sum_{i=1}^{m} \langle x, u_i \rangle \, u_i. \tag{3.16}$$

This result has a simple geometrical interpretation in terms of an *orthogonal projection*. Each basis vector u_i spans a subspace that is orthogonal to the subspaces spanned by u_j, $j \neq i$, which means that the signal space X is decomposed as follows:

$$X = M_m \stackrel{\perp}{\oplus} M_m^{\perp} \tag{3.17}$$

with

$$x = \hat{x} + \eta, \qquad x \in X, \quad \hat{x} \in M_m, \quad \eta \in M_m^{\perp}. \tag{3.18}$$

The subspace $M_m^{\perp}$ is orthogonal to M_m, and $\eta = x - \hat{x}$ is orthogonal to $\hat{x}$ (notation: $\eta \perp \hat{x}$). Because of $\eta \perp \hat{x}$ we call $\hat{x}$ the orthogonal projection of x onto M_m. Figure 3.1 gives an illustration.

As can easily be verified, we have the following relationship between the norms of $x, \hat{x}$ and η

$$\|x\|^2 = \|\hat{x}\|^2 + \|\eta\|^2. \tag{3.19}$$

---

[3]The proof is given in Section 3.3.2 for general, non-orthogonal bases.

3.2.3 The Gram–Schmidt Orthonormalization Procedure

Given a basis $\{\varphi_i;\ i = 1,\ldots,n\}$, we can construct an orthonormal basis $\{u_i;\ i = 1,\ldots,n\}$ for the space span $\{\varphi_i;\ i = 1,\ldots,n\}$ by using the following scheme:

$$
\begin{aligned}
w_1 &= \varphi_1 \\
u_1 &= \frac{w_1}{\|w_1\|} \\
w_2 &= \varphi_2 - \langle \varphi_2, u_1 \rangle\, u_1 \\
u_2 &= \frac{w_2}{\|w_2\|} \\
w_3 &= \varphi_3 - \langle \varphi_3, u_1 \rangle\, u_1 - \langle \varphi_3, u_2 \rangle\, u_2 \\
u_3 &= \frac{w_3}{\|w_3\|} \\
&\ \vdots \\
w_i &= \varphi_i - \sum_{k=1}^{i-1} \langle \varphi_i, u_k \rangle\, u_k \\
u_i &= \frac{w_i}{\|w_i\|} \\
&\ \vdots
\end{aligned}
\tag{3.20}
$$

This method is known as the *Gram–Schmidt procedure*. It is easily seen that the result is not unique. A re-ordering of the vectors φ_i before the application of the Gram–Schmidt procedure results in a different basis.

3.2.4 Parseval's Relation

Parseval's relation states that the inner product of two vectors equals the inner product of their representations with respect to an orthonormal basis. Given

$$
x = \sum_{i=1}^{n} \alpha_i\, u_i
\tag{3.21}
$$

and

$$
y = \sum_{i=1}^{n} \beta_i\, u_i
\tag{3.22}
$$

we have

$$
\langle x, y \rangle = \langle \alpha, \beta \rangle
\tag{3.23}
$$

with

$$
\begin{aligned}
\boldsymbol{\alpha} &= [\alpha_1, \ldots, \alpha_n]^T, \\
\boldsymbol{\beta} &= [\beta_1, \ldots, \beta_n]^T.
\end{aligned}
\tag{3.24}
$$

This is verified by substituting (3.21) into (3.23) and by making use of the fact that the basis is orthogonal:

$$
\begin{aligned}
\langle \boldsymbol{x}, \boldsymbol{y} \rangle &= \Big\langle \sum_{i=1}^{n} \alpha_i \boldsymbol{u}_i \, , \, \sum_{j=1}^{n} \beta_j \boldsymbol{u}_j \Big\rangle \\
&= \sum_{i=1}^{n} \sum_{j=1}^{n} \alpha_i \beta_j^* \, \langle \boldsymbol{u}_i, \boldsymbol{u}_j \rangle \\
&= \sum_{i=1}^{n} \alpha_i \beta_i^* \\
&= \langle \boldsymbol{\alpha}, \boldsymbol{\beta} \rangle.
\end{aligned}
\tag{3.25}
$$

For $\boldsymbol{x} = \boldsymbol{y}$ we get from (3.23)

$$
\|\boldsymbol{x}\| = \|\boldsymbol{\alpha}\|.
\tag{3.26}
$$

It is important to notice that the inner product of the representations is defined as $\langle \boldsymbol{\alpha}, \boldsymbol{\beta} \rangle = \boldsymbol{\beta}^H \boldsymbol{\alpha}$, whereas the inner product of the signals may have a different definition. The inner product of the signals may even involve a weighting matrix or weighting function.

3.2.5   Complete Orthonormal Sets

It can be shown that the space $L_2(a, b)$ is complete. Thus, any signal $x(t) \in L_2(a, b)$ can be approximated with arbitrary accuracy by means of an orthogonal projection

$$
\hat{x}(t) = \sum_{i=1}^{n} \langle \boldsymbol{x}, \boldsymbol{\varphi}_i \rangle \, \varphi_i(t),
\tag{3.27}
$$

where n is chosen sufficiently large and the basis vectors $\varphi_i(t)$ are taken from a complete orthonormal set.

According to (3.19) and (3.23) we have for the approximation error:

$$
\begin{aligned}
\|\boldsymbol{x} - \boldsymbol{x}_n\|^2 &= \|\boldsymbol{x}\|^2 - \|\boldsymbol{x}_n\|^2 \\
&= \|\boldsymbol{x}\|^2 - \sum_{i=1}^{n} |\langle \boldsymbol{x}, \boldsymbol{\varphi}_i \rangle|^2.
\end{aligned}
\tag{3.28}
$$

From (3.28) we conclude

$$\sum_{i=1}^{n} |\langle x, \varphi_i \rangle|^2 \leq \|x\|^2 \quad \forall \ n. \tag{3.29}$$

(3.29) is called the *Bessel inequality*. It ensures that the squared sum of the coefficients $\langle x, \varphi_i \rangle$ exists.

An orthonormal set is said to be complete if no additional non-zero orthogonal vector exists which can be added to the set.

When an orthonormal set is complete, the approximation error tends towards zero with $n \to \infty$. The Bessel inequality (3.29) then becomes the *completeness relation*

$$\sum_{i=1}^{\infty} |\langle x, \varphi_i \rangle|^2 = \|x\|^2 \quad \forall \ x \in L_2(a, b). \tag{3.30}$$

Here, Parseval's relation states

$$\langle x, y \rangle = \sum_{i=1}^{\infty} \langle x, \varphi_i \rangle \langle y, \varphi_i \rangle^*, \tag{3.31}$$

and for $x = y$:

$$\|x\|^2 = \sum_{i=1}^{\infty} |\langle x, \varphi_i \rangle|^2. \tag{3.32}$$

3.2.6 Examples of Complete Orthonormal Sets

Fourier Series. One of the best-known discrete transforms is the *Fourier series expansion*. The basis functions are the complex exponentials

$$\varphi_i(t) = \frac{e^{j\pi i t}}{\sqrt{2}}, \quad i = 0, \pm 1, \pm 2, \ldots, \tag{3.33}$$

which form a complete orthonormal set. The interval considered is $T = [-1, 1]$. The weighting function is $g(t) = 1$. Note that any finite interval can be mapped onto the interval $T = [-1, +1]$.

Legendre Polynomials. The *Legendre polynomials $P_n(t)$, $n = 0, 1, \ldots$* are defined as

$$P_n(t) = \frac{1}{2^n n!} \frac{d^n}{dt^n} (t^2 - 1)^n \tag{3.34}$$

and can alternatively be computed according to the recursion formula

$$P_n(t) = \frac{1}{n} [(2n - 1)t \, P_{n-1}(t) - (n - 1) \, P_{n-2}(t)]. \tag{3.35}$$

The first four functions are

$$
\begin{aligned}
P_0(t) &= 1, \\
P_1(t) &= t, \\
P_2(t) &= \tfrac{3}{2}t^2 - \tfrac{1}{2}, \\
P_3(t) &= \tfrac{5}{2}t^3 - \tfrac{3}{2}t.
\end{aligned}
$$

A set $\varphi_n(t)$, $n = 0, 1, 2, \ldots$ which is orthonormal on the interval $[-1, 1]$ with weighting function $g(t) = 1$ is obtained by

$$
\varphi_n(t) = \sqrt{\frac{2n+1}{2}} P_n(t). \tag{3.36}
$$

Chebyshev Polynomials. The *Chebyshev polynomials* are defined as

$$
T_n(t) = \cos(n \arccos t), \quad n \geq 0, \quad -1 \leq t \leq 1, \tag{3.37}
$$

and can be computed according to the recursion

$$
T_n(t) = 2t\, T_{n-1}(t) - T_{n-2}(t). \tag{3.38}
$$

The first four polynomials are

$$
\begin{aligned}
T_0(t) &= 1, \\
T_1(t) &= t, \\
T_2(t) &= 2t^2 - 1, \\
T_3(t) &= 4t^3 - 3t.
\end{aligned}
$$

Using the normalization

$$
\varphi_n(t) = \begin{cases} \sqrt{1/\pi}\; T_0(t) & \text{for } n = 0 \\[2mm] \sqrt{2/\pi}\; T_n(t) & \text{for } n > 0 \end{cases} \tag{3.39}
$$

we get a set which is orthonormal on the interval $[-1, +1]$ with weighting function $g(t) = (1 - t^2)^{-1/2}$.

Laguerre Polynomials. The *Laguerre polynomials*

$$
L_n(t) = e^t \frac{d^n}{dt^n}(t^n e^{-t}), \quad n = 0, 1, 2, \ldots \tag{3.40}
$$

can be calculated by means of the recursion

$$L_n(t) = (2n - 1 - t)\ L_{n-1}(t) - (n - 1)^2\ L_{n-2}(t). \tag{3.41}$$

The normalization

$$\varphi_n(t) = \frac{1}{n!}L_n(t) \quad n = 0, 1, 2, \ldots \tag{3.42}$$

yields a set which is orthonormal on the interval $[0, \infty]$ with weighting function $g(t) = e^{-t}$. The first four basis vectors are

$$
\begin{aligned}
\varphi_0(t) &= 1, \\
\varphi_1(t) &= 1 - t, \\
\varphi_2(t) &= 1 - 2t + \tfrac{1}{2}t^2, \\
\varphi_3(t) &= 1 - 3t + \tfrac{3}{2}t^2 - \tfrac{1}{6}t^3.
\end{aligned}
$$

An alternative is to generate the set

$$\psi_n(t) = \frac{e^{-t/2}}{n!}L_n(t), \qquad n = 0, 1, 2, \ldots, \tag{3.43}$$

which is orthonormal with weight one on the interval $[0, \infty]$. As will be shown below, the polynomials $\psi_n(t),\ n = 0, 1, 2, \ldots$ can be generated by a network. For this, let

$$f_n(t) = \psi_n(2pt) = \frac{e^{-pt}}{n!}L_n(2pt). \tag{3.44}$$

The Laplace transform is given by

$$F_n(s) = L\{f_n(t)\} = \frac{(s - p)^n}{(s + p)^{n+1}}. \tag{3.45}$$

Thus, a function $f_n(t)$ is obtained from a network with the transfer function $F_n(s)$, which is excited by an impulse. The network can be realized as a cascade of a first-order lowpass and n first-order allpass filters.

Hermite Polynomials. The *Hermite polynomials* are defined as

$$H_k(t) = (-1)^k\ e^{t^2}\ \frac{d^k}{dt^k}e^{-t^2}, \qquad k = 0, 1, 2, \ldots \tag{3.46}$$

A recursive computation is possible in the form

$$H_k(t) = 2t\ H_{k-1}(t) - 2(k - 1)\ H_{k-2}(t). \tag{3.47}$$

With the weighting function $g(t) = e^{-t^2}$ the polynomials

$$\phi_k(t) = (2^k \; k! \; \sqrt{\pi})^{-\frac{1}{2}} \; H_k(t), \qquad k = 0, 1, 2, \dots \qquad (3.48)$$

form an orthonormal basis for $L_2(\mathbb{R})$. Correspondingly, the *Hermite functions*

$$\varphi_k(t) = (2^k \; k! \; \sqrt{\pi})^{-\frac{1}{2}} \; e^{-t^2/2} \; H_k(t), \qquad k = 0, 1, 2, \dots, \qquad (3.49)$$

form an orthonormal basis with weight one. The functions $\varphi_k(t)$ are also obtained by applying the Gram–Schmidt procedure to the basis $\{t^k \; e^{-t^2/2}; \; k = 0, 1, \dots\}$ [57].

Walsh Functions. *Walsh functions* take on the values 1 and -1. Orthogonality is achieved by appropriate zero crossings. The first two functions are given by

$$\varphi_0(t) \;\; = \{1 \quad \text{for } 0 \le t \le 1 \,,$$

$$\varphi_1(t) \;\; = \begin{cases} 1 & \text{for } 0 \le t < \frac{1}{2}, \\ -1 & \text{for } \frac{1}{2} < t \le 1. \end{cases} \qquad (3.50)$$

Further functions can be computed by means of the recursion

$$\left.\begin{aligned}
\varphi_{m+1}^{(2k-1)}(t) &= \begin{cases} \varphi_m^{(k)}(2t) & \text{for } 0 \le t < \frac{1}{2} \\ (-1)^{k+1}\varphi_m^{(k)}(2t-1) & \text{for } \frac{1}{2} < t \le 1 \end{cases} \\[2mm]
\varphi_{m+1}^{(2k)}(t) &= \begin{cases} \varphi_m^{(k)}(2t) & \text{for } 0 \le t < \frac{1}{2} \\ (-1)^{k}\varphi_m^{(k)}(2t-1) & \text{for } \frac{1}{2} < t \le 1 \end{cases}
\end{aligned}\right\} \quad \begin{aligned} m &= 1, 2, \dots, \\ k &= 1, \dots, 2^{m-1} \end{aligned}$$

$$(3.51)$$

Figure 3.2 shows the first six Walsh functions; they are named according to their number of zero crossings.

3.3   General Series Expansions

If possible, one would choose an orthonormal basis for signal representation. However, in practice, a given basis is often not orthonormal. For example, in data transmission a transmitted signal may have the form $x(t) = \sum_m d(m) \; s(t - mT)$, where $d(m)$ is the data and $s(t)$ is an impulse response that satisfies $\int s(t)s(t - mT)dt = \delta_{m0}$. If we now assume that $x(t)$ is transmitted through a non-ideal channel with impulse response $h(t)$, then we
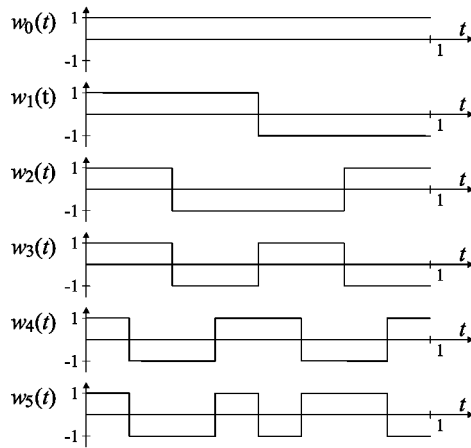
Figure 3.2. Walsh functions.

have a signal $r(t) = \sum_m d(m)g(t - mT)$ with $g(t) = s(t) * h(t)$ on the receiver side. This new basis $\{g(t - mT); m \in \mathbb{Z}\}$ is no longer orthogonal, so that the question arises of how to recover the data if $r(t)$ and $g(t)$ are given.

3.3.1 Calculating the Representation

In the following, signals $x \in X$ with $X = \text{span}\{\varphi_1, \ldots, \varphi_n\}$ will be considered. We assume that the n vectors $\{\varphi_1, \ldots, \varphi_n\}$ are linearly independent so that all $x \in X$ can be represented uniquely as

$$x = \sum_{i=1}^{n} \alpha_i \, \varphi_i \,, \qquad x \in X. \tag{3.52}$$

As will be shown, the representation

$$\alpha = [\alpha_1, \ldots, \alpha_n]^T \tag{3.53}$$

with respect to a given basis $\{\varphi_1, \ldots, \varphi_n\}$ can be computed by solving a linear set of equations and also via the so-called reciprocal basis. The set of equations is obtained by multiplying (inner product) both sides of (3.52) with $\varphi_j, \; j = 1, \ldots, n$:

$$\langle x, \varphi_j \rangle = \sum_{i=1}^{n} \alpha_i \, \langle \varphi_i, \varphi_j \rangle, \qquad j = 1, \ldots, n. \tag{3.54}$$

In matrix notation this is

$$\Phi \, \alpha = \beta \tag{3.55}$$
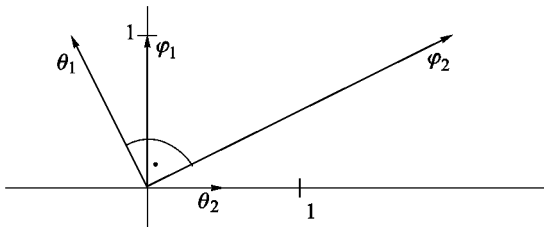
Figure 3.3. Reciprocal basis (The basis is $\varphi_1 = [0, 1]^T$, $\varphi_2 = [2, 1]^T$; the corresponding reciprocal basis is $\theta_1 = [-0.5, 1]^T$, $\theta_2 = [0.5, 0]^T$).

with

$$
\Phi = \begin{bmatrix} \langle \varphi_1, \varphi_1 \rangle & \langle \varphi_2, \varphi_1 \rangle & \cdots & \langle \varphi_n, \varphi_1 \rangle \\ \langle \varphi_1, \varphi_2 \rangle & \langle \varphi_2, \varphi_2 \rangle & \cdots & \langle \varphi_n, \varphi_2 \rangle \\ \vdots & & & \\ \langle \varphi_1, \varphi_n \rangle & \langle \varphi_2, \varphi_n \rangle & \cdots & \langle \varphi_n, \varphi_n \rangle \end{bmatrix},
$$

$$
\beta = \begin{bmatrix} \langle x, \varphi_1 \rangle \\ \langle x, \varphi_2 \rangle \\ \vdots \\ \langle x, \varphi_n \rangle \end{bmatrix}.
\tag{3.56}
$$

Φ is known as the *Grammian matrix*. Due to $\langle \varphi_i, \varphi_k \rangle = \langle \varphi_k, \varphi_i \rangle^*$ it has the property $\Phi = \Phi^H$.

The disadvantage of the method considered above is that for calculating the representation α of a new x we first have to calculate β before (3.55) can be solved. Much more interesting is the computation of the representation α by means of the *reciprocal basis* $\{\theta_i;\ i = 1, 2, 3 \ldots n\}$, which satisfies the condition

$$
\langle \varphi_i, \theta_j \rangle = \delta_{ij} \quad , \quad i, j = 1, \ldots, n,
\tag{3.57}
$$

which is known as the *biorthogonality condition*; Figure 3.3 illustrates (3.57) in the two-dimensional plane.

Multiplying both sides of (3.52) with θ_j, $j = 1, \ldots, n$ leads to

$$
\langle x, \theta_j \rangle = \sum_{i=1}^{n} \alpha_i \underbrace{\langle \varphi_i, \theta_j \rangle}_{\delta_{ij}} = \alpha_i, \quad j = 1, \ldots, n,
\tag{3.58}
$$

which means that, when using the reciprocal basis, we directly obtain the representation by forming inner products

$$
\alpha_j = \langle x, \theta_j \rangle, \quad j = 1, \ldots, n.
\tag{3.59}
$$

A vector x can be represented as

$$x = \sum_{i=1}^{n} \langle x, \theta_i \rangle \; \varphi_i, \tag{3.60}$$

and also as

$$x = \sum_{i=1}^{n} \langle x, \varphi_i \rangle \; \theta_i. \tag{3.61}$$

Parseval's relation holds only for orthonormal bases. However, also for general bases a relationship between the inner product of signals and their representations can be established. For this, one of the signals is represented by means of the basis $\{\varphi_1, \ldots, \varphi_n\}$ and a second signal by means of the corresponding reciprocal basis $\{\theta_1, \ldots, \theta_n\}$. For the inner product of two signals

$$x = \sum_{i=1}^{n} \langle x, \varphi_i \rangle \, \theta_i \tag{3.62}$$

and

$$y = \sum_{k=1}^{n} \langle y, \theta_k \rangle \, \varphi_k \tag{3.63}$$

we get

$$
\begin{aligned}
\langle x, y \rangle &= \left\langle \sum_{i=1}^{n} \langle x, \varphi_i \rangle \, \theta_i, \sum_{k=1}^{n} \langle y, \theta_k \rangle \, \varphi_k \right\rangle \\
&= \sum_{i=1}^{n} \sum_{k=1}^{n} \langle x, \varphi_i \rangle \langle y, \theta_k \rangle^* \langle \theta_i, \varphi_k \rangle \\
&= \sum_{i=1}^{n} \langle x, \varphi_i \rangle \langle y, \theta_i \rangle^*.
\end{aligned}
\tag{3.64}
$$

In the last step, the property $\langle \varphi_i, \theta_k \rangle = \delta_{ik}$ was used.

Calculation of the Reciprocal Basis. Since φ_k, $k = 1, \ldots, n$ as well as θ_j, $j = 1, \ldots, n$ are bases for X, the vectors θ_j, $j = 1, \ldots, n$ can be written as linear combinations of φ_k, $k = 1, \ldots, n$ with the yet unknown coefficients γ_{jk}:

$$\theta_j = \sum_{k=1}^{n} \gamma_{jk} \, \varphi_k, \quad j = 1, \ldots, n. \tag{3.65}$$

Multiplying this equation with φ_i, $i = 1, \ldots, n$ and using (3.57) leads to

$$
\begin{aligned}
\langle \boldsymbol{\theta}_j, \varphi_i \rangle &= \left\langle \sum_{k=1}^{n} \gamma_{jk}\, \varphi_k\, ,\, \varphi_i \right\rangle \\
&= \sum_{k=1}^{n} \langle \gamma_{jk}\, \varphi_k\, , \varphi_i \rangle \\
&= \sum_{k=1}^{n} \gamma_{jk}\, \langle \varphi_k, \varphi_i \rangle \\
&= \delta_{ij}
\end{aligned} \qquad \right\} \qquad i, j = 1, \ldots, n. \qquad (3.66)
$$

With

$$
\boldsymbol{\Gamma} = \begin{bmatrix} \gamma_{11} & \cdots & \gamma_{1n} \\ \vdots & \ddots & \vdots \\ \gamma_{n1} & \cdots & \gamma_{nn} \end{bmatrix} \qquad (3.67)
$$

and

$$
\boldsymbol{\Phi}^T = \begin{bmatrix} \langle \varphi_1, \varphi_1 \rangle & \cdots & \langle \varphi_1, \varphi_n \rangle \\ \vdots & & \vdots \\ \langle \varphi_n, \varphi_1 \rangle & \cdots & \langle \varphi_n, \varphi_n \rangle \end{bmatrix} \qquad (3.68)
$$

equation (3.66) can be written as

$$
\boldsymbol{\Gamma}\boldsymbol{\Phi}^T = \boldsymbol{I}, \qquad (3.69)
$$

so that

$$
\boldsymbol{\Gamma} = \left(\boldsymbol{\Phi}^T \right)^{-1}. \qquad (3.70)
$$

The reciprocal basis is obtained from (3.65), (3.67) and (3.70).

3.3.2   Orthogonal Projection

We consider the approximation of $x \in X$ by $\hat{x} \in M_m$, where $M_m \subset X$. For the signal spaces let $X = \mathrm{span}\,\{\varphi_1, \ldots, \varphi_n\}$ and $M_m = \mathrm{span}\,\{\varphi_1, \ldots, \varphi_m\}$ with $m < n$.

As we will see, the best approximation in the sense of

$$
\| x - \hat{x} \| \stackrel{!}{=} \min \qquad (3.71)
$$

is obtained for

$$
\hat{x} = \sum_{i=1}^{m} \langle x, \boldsymbol{\theta}_i \rangle\, \varphi_i, \qquad (3.72)
$$

where $\{\boldsymbol{\theta}_i; \; i = 1, \ldots, m\}$ is the reciprocal basis to $\{\boldsymbol{\varphi}_i; \; i = 1, \ldots, m\}$. Note that the reciprocal basis satisfies

$$M_m = \text{span}\{\boldsymbol{\varphi}_1, \ldots, \boldsymbol{\varphi}_m\} = \text{span}\{\boldsymbol{\theta}_1, \ldots, \boldsymbol{\theta}_m\}. \tag{3.73}$$

Requiring only $\langle \boldsymbol{\varphi}_i, \boldsymbol{\theta}_j \rangle = \delta_{ij}$, $i, j = 0, 1, \ldots, m$ is not sufficient for $\boldsymbol{\theta}_j$ to form the reciprocal basis.

First we consider the expression $\langle \hat{\boldsymbol{x}}, \boldsymbol{\theta}_j \rangle$ with $\hat{\boldsymbol{x}}$ according to (3.72). Because of $\langle \boldsymbol{\varphi}_i, \boldsymbol{\theta}_j \rangle = \delta_{ij}$ we obtain

$$\langle \hat{\boldsymbol{x}}, \boldsymbol{\theta}_j \rangle = \left\langle \sum_{i=1}^{m} \langle \boldsymbol{x}, \boldsymbol{\theta}_i \rangle \, \boldsymbol{\varphi}_i \, , \; \boldsymbol{\theta}_j \right\rangle = \langle \boldsymbol{x}, \boldsymbol{\theta}_j \rangle, \; j = 1, \ldots, m. \tag{3.74}$$

Hence,

$$\langle \boldsymbol{x} - \hat{\boldsymbol{x}}, \boldsymbol{\theta}_j \rangle = 0, \quad j = 1, \ldots, m. \tag{3.75}$$

Equation (3.75) shows that

$$\boldsymbol{\eta} = \boldsymbol{x} - \hat{\boldsymbol{x}} \tag{3.76}$$

is orthogonal to all $\boldsymbol{\theta}_j$, $j = 1, \ldots, m$. From (3.73) and (3.75) we conclude that $\boldsymbol{\eta}$ is orthogonal to all vectors in M_m:

$$\boldsymbol{\eta} \perp \tilde{\boldsymbol{x}} \quad \text{for all} \quad \tilde{\boldsymbol{x}} \in M_m. \tag{3.77}$$

This also means that X is decomposed into an orthogonal sum

$$X = M_m \overset{\perp}{\oplus} M_m^{\perp}. \tag{3.78}$$

For the vectors we have

$$\boldsymbol{x} = \hat{\boldsymbol{x}} + \boldsymbol{\eta}, \qquad \hat{\boldsymbol{x}} \in M_m, \quad \boldsymbol{\eta} \in M_m^{\perp}, \quad \boldsymbol{x} \in X. \tag{3.79}$$

The approximation $\hat{\boldsymbol{x}}$ according to (3.72) is the *orthogonal projection* of $\boldsymbol{x} \in X$ onto M_m.

In order to show that $\hat{\boldsymbol{x}}$ according to (3.72) is the best approximation to $\boldsymbol{x}$, we consider the distance between $\boldsymbol{x}$ and an arbitrary vector $\tilde{\boldsymbol{x}} \in M_m$ and perform some algebraic manipulations:

$$
\begin{aligned}
d^2(\boldsymbol{x}, \tilde{\boldsymbol{x}}) &= \|\boldsymbol{x} - \tilde{\boldsymbol{x}}\|^2 \\
&= \|(\boldsymbol{x} - \hat{\boldsymbol{x}}) - (\tilde{\boldsymbol{x}} - \hat{\boldsymbol{x}})\|^2 \\
&= \langle (\boldsymbol{x} - \hat{\boldsymbol{x}}) - (\tilde{\boldsymbol{x}} - \hat{\boldsymbol{x}}), (\boldsymbol{x} - \hat{\boldsymbol{x}}) - (\tilde{\boldsymbol{x}} - \hat{\boldsymbol{x}}) \rangle \\
&= \langle \boldsymbol{x} - \hat{\boldsymbol{x}}, \boldsymbol{x} - \hat{\boldsymbol{x}} \rangle - \langle \boldsymbol{x} - \hat{\boldsymbol{x}}, \tilde{\boldsymbol{x}} - \hat{\boldsymbol{x}} \rangle - \langle \tilde{\boldsymbol{x}} - \hat{\boldsymbol{x}}, \boldsymbol{x} - \hat{\boldsymbol{x}} \rangle + \langle \tilde{\boldsymbol{x}} - \hat{\boldsymbol{x}}, \tilde{\boldsymbol{x}} - \hat{\boldsymbol{x}} \rangle.
\end{aligned}
\tag{3.80}
$$

Because of $(\tilde{x} - \hat{x}) \in M_m$ and (3.75), the second and third terms in (3.80) are zero, such that

$$\|x - \tilde{x}\|^2 = \|x - \hat{x}\|^2 + \|\tilde{x} - \hat{x}\|^2 . \tag{3.81}$$

The minimum is achieved for $\tilde{x} = \hat{x}$, so that (3.72) clearly yields the best approximation.

A relationship between the norms of $x, \hat{x}$ and η is obtained from

$$
\begin{aligned}
\|x\|^2 &= \|\hat{x} + \eta\|^2 \\
&= \langle \hat{x} + \eta, \hat{x} + \eta \rangle \\
&= \langle \hat{x}, \hat{x} \rangle + \langle \hat{x}, \eta \rangle + \langle \eta, \hat{x} \rangle + \langle \eta, \eta \rangle .
\end{aligned}
\tag{3.82}
$$

Because of (3.79) the second and the third term in the last row are zero, and

$$\|x\|^2 = \|\hat{x}\|^2 + \|\eta\|^2 \tag{3.83}$$

remains.

3.3.3   Orthogonal Projection of n-Tuples

The solutions to the projection problem considered so far hold for all vectors, including n-tuples, of course. However, for n-tuples the projection can concisely be described with matrices, and we have a large number of methods at hand for solving the problem.

In the following, we consider the projection of $x = [x_1, \ldots, x_n]^T \in \mathbb{C}^n$ onto subspaces $M_m = \text{span}\{b_1, \ldots, b_m\}$, where $m < n$ and $b_i \in \mathbb{C}^n$. With

$$B = [b_1, \ldots, b_m] \qquad n \times m \;\; \text{matrix} \tag{3.84}$$

and

$$a = [a_1, \ldots, a_m]^T \qquad m \times 1 \;\; \text{vector} \tag{3.85}$$

the approximation is given by

$$\hat{x} = B \, a. \tag{3.86}$$

Furthermore, the orthogonal projection can be described by a Hermitian matrix P as

$$\hat{x} = P \, x. \tag{3.87}$$

Inner Product without Weighting. To compute the reciprocal basis $\Theta = [\boldsymbol{\theta}_1, \ldots, \boldsymbol{\theta}_n]$ the relationships (3.70), (3.56) and (3.65) are used, which can be written as

$$\begin{aligned} \boldsymbol{\Gamma}^T &= \boldsymbol{\Phi}^{-1}, \\ \boldsymbol{\Phi} &= \boldsymbol{B}^H \boldsymbol{B}, \\ \boldsymbol{\Theta} &= \boldsymbol{B}\,\boldsymbol{\Gamma}^T. \end{aligned} \tag{3.88}$$

For the reciprocal basis we then get

$$\boldsymbol{\Theta} = \boldsymbol{B}\,[\boldsymbol{B}^H \boldsymbol{B}]^{-1}. \tag{3.89}$$

Observing that the inverse of a Hermitian matrix is Hermitian itself, the representation is calculated according to (3.59) as

$$\boldsymbol{a} = \boldsymbol{\Theta}^H \boldsymbol{x} = [\boldsymbol{B}^H \boldsymbol{B}]^{-1} \boldsymbol{B}^H \boldsymbol{x}. \tag{3.90}$$

With (3.86) the orthogonal projection is

$$\hat{\boldsymbol{x}} = \boldsymbol{B}[\boldsymbol{B}^H \boldsymbol{B}]^{-1} \boldsymbol{B}^H \boldsymbol{x}. \tag{3.91}$$

If $\boldsymbol{B}$ contains an orthonormal basis, we have $\boldsymbol{B}^H \boldsymbol{B} = \boldsymbol{I}$, and the projection problem is simplified.

Note that the representation according to (3.90) is the solution of the equation

$$[\boldsymbol{B}^H \boldsymbol{B}]\,\boldsymbol{a} = \boldsymbol{B}^H \boldsymbol{x}, \tag{3.92}$$

which is known as the *normal equation.*

Inner Product with Weighting. For an inner product with a weighting matrix $\boldsymbol{G}$, equations (3.70), (3.56) and (3.65) give

$$\begin{aligned} \boldsymbol{\Gamma}^T &= \boldsymbol{\Phi}^{-1}, \\ \boldsymbol{\Phi} &= \boldsymbol{B}^H \boldsymbol{G} \boldsymbol{B}, \\ \boldsymbol{\Theta} &= \boldsymbol{B}\,\boldsymbol{\Gamma}^T. \end{aligned} \tag{3.93}$$

Thus, we obtain

$$\boldsymbol{\Theta} = \boldsymbol{B}\,[\boldsymbol{B}^H \boldsymbol{G} \boldsymbol{B}]^{-1}, \tag{3.94}$$

$$\boldsymbol{a} = \boldsymbol{\Theta}^H \boldsymbol{G} \boldsymbol{x} = [\boldsymbol{B}^H \boldsymbol{G} \boldsymbol{B}]^{-1} \boldsymbol{B}^H \boldsymbol{G} \boldsymbol{x}, \tag{3.95}$$

$$\hat{\boldsymbol{x}} = \boldsymbol{B}[\boldsymbol{B}^H \boldsymbol{G} \boldsymbol{B}]^{-1} \boldsymbol{B}^H \boldsymbol{G} \boldsymbol{x}. \tag{3.96}$$

Alternatively, $\boldsymbol{G}$ can be split into a product $\boldsymbol{G} = \boldsymbol{H}^H \boldsymbol{H}$, and the problem

$$\left. \|\boldsymbol{B\alpha} - \boldsymbol{x}\|_G \right|_{\boldsymbol{\alpha} = \boldsymbol{a}} \overset{!}{=} \min \tag{3.97}$$

can be transformed via

$$\begin{aligned} \boldsymbol{z} &= \boldsymbol{Hx} \\ \boldsymbol{V} &= \boldsymbol{HB} \end{aligned} \tag{3.98}$$

into the equivalent problem

$$\left. \|\boldsymbol{V\alpha} - \boldsymbol{z}\|_I \right|_{\boldsymbol{\alpha} = \boldsymbol{a}} \overset{!}{=} \min. \tag{3.99}$$

The indices of the norms in (3.97) and (3.99) stand for the weighting matrices involved. Thus, the projection problem with weighting can be transformed into one without weighting. Splitting $\boldsymbol{G}$ into $\boldsymbol{G} = \boldsymbol{H}^H \boldsymbol{H}$ can for instance be achieved by applying the *Cholesky decomposition* $\boldsymbol{G} = \boldsymbol{L}\boldsymbol{L}^H$ or by a *singular value decomposition*. Both methods can be applied in all cases since $\boldsymbol{G}$ must be Hermitian and positive definite in order to be a valid weighting matrix.

Note. The computation of the reciprocal basis involves the inversion of the Grammian matrix. If the Grammian matrix is poorly conditioned, numerical problems may occur. Robust methods of handling such cases are the QR decomposition and the Moore–Penrose pseudoinverse, which will be discussed in the next section.

3.4 Mathematical Tools

3.4.1 The QR Decomposition

The methods for solving the projection problem considered so far require an inversion of the Grammian matrix. The inversion does not pose a major problem so long as the vectors that span the subspace in question are linearly independent. However, because of finite-precision arithmetic, a poorly conditioned Grammian matrix may lead to considerable errors, even if the vectors are linearly independent.

A numerically robust solution of

$$\left. \|\boldsymbol{B\alpha} - \boldsymbol{x}\| \right|_{\boldsymbol{\alpha} = \boldsymbol{a}} \overset{!}{=} \min \tag{3.100}$$

is obtained by carrying out a QR decomposition of B:

$$B = Q\,R. \tag{3.101}$$

Here, Q is a unitary matrix, and R has the following form:

$$R = \begin{bmatrix} r_{11} & \cdots & r_{1m} \\ & \ddots & \vdots \\ & & r_{mm} \\ \\ \\ \end{bmatrix}. \tag{3.102}$$

The QR decomposition can, for instance, be computed by using *Householder reflections* or *Givens rotations*; see Sections 3.4.4 and 3.4.5.

In the following we will show how (3.100) can be solved via QR decomposition. Substituting (3.101) in (3.100) yields

$$\|Q R \alpha - x\|\Big|_{\alpha = a} \overset{!}{=} \min. \tag{3.103}$$

For (3.103) we can also write

$$\|Q^H Q R \alpha - Q^H x\| = \|R\alpha - Q^H x\|\Big|_{\alpha = a} \overset{!}{=} \min, \tag{3.104}$$

because a multiplication with a unitary matrix does not change the norm of a vector. Using the abbreviation $y = Q^H x$, we get

$$\|R\alpha - y\| = \left\| \begin{bmatrix} r_{11} & \cdots & r_{1m} \\ & \ddots & \vdots \\ & & r_{mm} \\ \\ \\ \end{bmatrix} \begin{bmatrix} \alpha_1 \\ \vdots \\ \alpha_m \end{bmatrix} - \begin{bmatrix} y_1 \\ \vdots \\ y_m \\ y_{m+1} \\ \vdots \\ y_n \end{bmatrix} \right\|. \tag{3.105}$$

With

$$X = \begin{bmatrix} r_{11} & \cdots & r_{1m} \\ & \ddots & \vdots \\ & & r_{mm} \end{bmatrix}, \quad z = \begin{bmatrix} y_1 \\ \vdots \\ y_m \end{bmatrix}, \quad N = \begin{bmatrix} 0 & \cdots & 0 \\ \vdots & & \vdots \\ 0 & \cdots & 0 \end{bmatrix}, \quad f = \begin{bmatrix} y_{m+1} \\ \vdots \\ y_n \end{bmatrix} \tag{3.106}$$

(3.105) becomes

$$\|R\alpha - y\| = \left\| \begin{bmatrix} X \\ N \end{bmatrix} \alpha - \begin{bmatrix} z \\ f \end{bmatrix} \right\| = \left\| \begin{bmatrix} X\alpha - z \\ N\alpha - f \end{bmatrix} \right\|. \tag{3.107}$$

The norm reaches its minimum if $\boldsymbol{\alpha} = \boldsymbol{a}$ is the solution of

$$\boldsymbol{X}\,\boldsymbol{a} = \boldsymbol{z}. \tag{3.108}$$

Note that $\boldsymbol{X}$ is an upper triangular matrix, so that $\boldsymbol{a}$ is easily computed by using Gaussian elimination. For the norm of the error we have:

$$\|\boldsymbol{Ra} - \boldsymbol{y}\| = \left\| \begin{bmatrix} \boldsymbol{X}\,\boldsymbol{a} - \boldsymbol{z} \\ \boldsymbol{f} \end{bmatrix} \right\| = \|\boldsymbol{f}\|. \tag{3.109}$$

3.4.2 The Moore–Penrose Pseudoinverse

We consider the criterion

$$\|\boldsymbol{B\alpha} - \boldsymbol{x}\|\Big|_{\boldsymbol{\alpha} = \boldsymbol{a}} \overset{!}{=} \min. \tag{3.110}$$

The solutions (3.90) and (3.91),

$$\boldsymbol{a} = \left[\boldsymbol{B}^H \boldsymbol{B}\right]^{-1} \boldsymbol{B}^H \boldsymbol{x}, \tag{3.111}$$

$$\hat{\boldsymbol{x}} = \boldsymbol{B} \left[\boldsymbol{B}^H \boldsymbol{B}\right]^{-1} \boldsymbol{B}^H \boldsymbol{x}, \tag{3.112}$$

can only be applied if $\left[\boldsymbol{B}^H \boldsymbol{B}\right]^{-1}$ exists, that is, if the columns of $\boldsymbol{B}$ are linearly independent. However, an orthogonal projection can also be carried out if $\boldsymbol{B}$ contains linearly dependent vectors. A general solution to the projection problem is obtained by introducing a matrix $\boldsymbol{B}^+$ via the following four equations

$$\boldsymbol{B}^+ \boldsymbol{B} = (\boldsymbol{B}^+ \boldsymbol{B})^H \tag{3.113}$$

$$\boldsymbol{B} \boldsymbol{B}^+ = (\boldsymbol{B} \boldsymbol{B}^+)^H \tag{3.114}$$

$$\boldsymbol{B} \boldsymbol{B}^+ \boldsymbol{B} = \boldsymbol{B} \tag{3.115}$$

$$\boldsymbol{B}^+ \boldsymbol{B} \boldsymbol{B}^+ = \boldsymbol{B}^+. \tag{3.116}$$

There is only one $\boldsymbol{B}^+$ that satisfies (3.113) – (3.116). This matrix is called the *Moore–Penrose pseudoinverse* [3]. The expressions $\boldsymbol{B}^+ \boldsymbol{B}$ and $\boldsymbol{B} \boldsymbol{B}^+$ describe orthogonal projections, since under conditions (3.113) – (3.116) we have

$$
\begin{aligned}
[\boldsymbol{x} - \boldsymbol{B} \boldsymbol{B}^+ \boldsymbol{x}]^H \boldsymbol{B} \boldsymbol{B}^+ \boldsymbol{x} &= 0, \\
[\boldsymbol{a} - \boldsymbol{B}^+ \boldsymbol{B} \boldsymbol{a}]^H \boldsymbol{B}^+ \boldsymbol{B} \boldsymbol{a} &= 0.
\end{aligned}
\tag{3.117}
$$

Assuming that $\boldsymbol{B}$ is an $n \times m$ matrix which either has rank $k = m$ or $k = n$, we have

$$
\begin{aligned}
\boldsymbol{B}^+ &= \left[\boldsymbol{B}^H \boldsymbol{B}\right]^{-1} \boldsymbol{B}^H, & k &= m, \\
\boldsymbol{B}^+ &= \boldsymbol{B}^H \left[\boldsymbol{B}\boldsymbol{B}^H\right]^{-1}, & k &= n, \\
\boldsymbol{B}^+ &= \boldsymbol{B}^{-1}, & k &= n = m.
\end{aligned}
\tag{3.118}
$$

$\boldsymbol{B}^+$ can for instance be computed via the *singular value decomposition*

$$
\boldsymbol{B} = \boldsymbol{U}\boldsymbol{\Sigma}\boldsymbol{V}^H.
\tag{3.119}
$$

$\boldsymbol{U}$ and $\boldsymbol{V}$ are unitary. For $m < n$, $\boldsymbol{\Sigma}$ has the following form:

$$
\boldsymbol{\Sigma} = \begin{bmatrix} \sigma_1 & & \\ & \ddots & \\ & & \sigma_m \\ & & \\ & & \end{bmatrix}.
\tag{3.120}
$$

The non-zero values σ_i are called the singular values of $\boldsymbol{B}$. They satisfy $\sigma_i > 0$. With

$$
\boldsymbol{\Sigma}^+ = \begin{bmatrix} \tau_1 & & \\ & \ddots & \\ & & \tau_m \end{bmatrix}, \quad \tau_i = \begin{cases} 1/\sigma_i, & \sigma_i \neq 0, \\ 0, & \sigma_i = 0 \end{cases}
\tag{3.121}
$$

the pseudoinverse $\boldsymbol{B}^+$ is given by

$$
\boldsymbol{B}^+ = \boldsymbol{V}\boldsymbol{\Sigma}^+\boldsymbol{U}^H.
\tag{3.122}
$$

It can easily be shown that the requirements (3.113) – (3.116) with $\boldsymbol{B}^+$ according to (3.122) are satisfied, so that (3.111) and (3.112) can be replaced by

$$
\begin{aligned}
\boldsymbol{a} &= \boldsymbol{B}^+\boldsymbol{x}, \tag{3.123} \\
\hat{\boldsymbol{x}} &= \boldsymbol{B}\boldsymbol{B}^+\boldsymbol{x}. \tag{3.124}
\end{aligned}
$$

Note that (3.123) is not necessarily the only solution to the problem (3.110). We will return to this topic in the next section.

By taking the products $\boldsymbol{B}^H \boldsymbol{B}$ and $\boldsymbol{B}\boldsymbol{B}^H$ we obtain equations for calculating the singular value decomposition. With $\boldsymbol{B}$ according to (3.119) we have

$$\boldsymbol{B}^H \boldsymbol{B} = \boldsymbol{V}\boldsymbol{\Sigma}^H \boldsymbol{U}^H \boldsymbol{U}\boldsymbol{\Sigma}\boldsymbol{V}^H \;\; = \;\; \boldsymbol{V}\left[\boldsymbol{\Sigma}^H \boldsymbol{\Sigma}\right]\boldsymbol{V}^H,$$

$$\boldsymbol{B}\boldsymbol{B}^H = \boldsymbol{U}\boldsymbol{\Sigma}\boldsymbol{V}^H \boldsymbol{V}\boldsymbol{\Sigma}^H \boldsymbol{U}^H \;\; = \;\; \boldsymbol{U}\left[\boldsymbol{\Sigma}\boldsymbol{\Sigma}^H\right]\boldsymbol{U}^H. \tag{3.125}$$

That is, the squares of the singular values of $\boldsymbol{B}$ are the eigenvalues of $\boldsymbol{B}^H \boldsymbol{B}$ and at the same time of $\boldsymbol{B}\boldsymbol{B}^H$. Matrix $\boldsymbol{V}$ contains the orthonormal eigenvectors of $\boldsymbol{B}^H \boldsymbol{B}$. Correspondingly, $\boldsymbol{U}$ contains the eigenvectors of $\boldsymbol{B}\boldsymbol{B}^H$. Further methods of calculating the pseudoinverse are discussed in [3].

Note. The pseudoinverse may be written as

$$\boldsymbol{B}^+ = \left[\boldsymbol{B}^H \boldsymbol{B}\right]^+ \boldsymbol{B}^H. \tag{3.126}$$

This property can be applied to continuous functions, and with $\boldsymbol{\Gamma}^T = \boldsymbol{\Phi}^+$ instead of $\boldsymbol{\Gamma}^T = \boldsymbol{\Phi}^{-1}$ we can compute a set of functions $\theta_k(t)$, which is dual to a given set $\varphi_i(t)$; see (3.65) – (3.70).

3.4.3   The Nullspace

Let us consider the problem

$$\boldsymbol{B}\,\boldsymbol{a} = \hat{\boldsymbol{x}}, \tag{3.127}$$

where $\hat{\boldsymbol{x}} = \boldsymbol{B}\,\boldsymbol{B}^+ \boldsymbol{x}$ is the orthogonal projection of an arbitrary $\boldsymbol{x}$ onto the column subspace of $\boldsymbol{B}$. It is easily observed that the solution to (3.127) also is the solution to (3.110). Depending on $\boldsymbol{B}$ we either have a unique solution $\boldsymbol{a}$, or we have an infinite number of solutions. Finding all solutions is intimately related to finding the nullspace of matrix $\boldsymbol{B}$.

The nullspace of a matrix $\boldsymbol{B}$ consists of all vectors $\boldsymbol{a}$ such that $\boldsymbol{B}\,\boldsymbol{a} = \boldsymbol{0}$. It is denoted by $\mathcal{N}(\boldsymbol{B})$. In order to describe $\mathcal{N}(\boldsymbol{B})$, let us assume that $\boldsymbol{B}$ is an $n \times m$ matrix that has rank r. If $r = m$ then $\mathcal{N}(\boldsymbol{B})$ is only the null vector, and $\boldsymbol{a} = \boldsymbol{B}^+ \hat{\boldsymbol{x}} = \boldsymbol{B}^+ \boldsymbol{x}$ is the unique solution to (3.127) and thus also to (3.110). If $r < m$ then $\mathcal{N}(\boldsymbol{B})$ is of dimension $m - r$, which means that $\mathcal{N}(\boldsymbol{B})$ is spanned by $m - r$ linearly independent vectors. These vectors can be chosen to form an orthonormal basis for the nullspace. If we define a matrix $\boldsymbol{N}$ of size $m \times (m - r)$ whose column subspace is the nullspace of $\boldsymbol{B}$ then

$$\boldsymbol{B}\,\boldsymbol{N} = \boldsymbol{0}. \tag{3.128}$$

The set of all solutions to (3.127) is then given by

$$\boldsymbol{a} = \tilde{\boldsymbol{a}} + \boldsymbol{N}\,\boldsymbol{p}, \quad \text{where} \quad \tilde{\boldsymbol{a}} = \boldsymbol{B}^+ \hat{\boldsymbol{x}} = \boldsymbol{B}^+ \boldsymbol{x}. \tag{3.129}$$

In (3.129) p is an arbitrary vector of length $m - r$. In some applications it is useful to exploit the free design parameters in p in order to find a solution a that optimizes an additional criterion. However, in most cases one will use the solution $\tilde{a}$ given by the pseudoinverse, because this is the solution with minimum Euclidean norm. In order to see this, let us determine the squared norm of a:

$$
\begin{aligned}
\|a\|_{\ell_2}^2 &= a^H a \\
&= [B^+ x + Np]^H [B^+ x + Np] \\
&= x^H (B^+)^H B^+ x + p^H N^H B^+ x + x^H (B^+)^H Np + p^H N^H Np.
\end{aligned}
$$
(3.130)

The second and third terms vanish, because $BN = 0$ implies that $N^H B^+ = 0$. Thus, we get the vector a of shortest length for $p = 0$, that is for $a = \tilde{a}$.

The matrix N that contains the basis for the nullspace is easily found from the singular value decomposition

$$
B = U \Sigma V^H.
$$
(3.131)

Let B have rank r and let the r nonzero singular values be the elements $[\Sigma]_{1,1}, \ldots, [\Sigma]_{r,r}$ of matrix Σ. Then an orthonormal matrix N is given by the last $m - r$ columns of V.

3.4.4 The Householder Transform

Householder transforms allow a simple and numerically robust way of performing QR decompositions, and thus of solving normal equations. The QR decomposition is carried out step by step by reflecting vectors at hyperplanes.

In order to explain the basic idea of the Householder transforms we consider two vectors $x, w \in \mathbb{C}^n$, and we look at the projection of x onto a one-dimensional subspace $W = \text{span} \{w\}$:

$$
P_w x = w \, \frac{1}{w^H w} \, w^H x.
$$
(3.132)

Here, $\mathbb{C}^n$ is decomposed into the orthogonal sum

$$
\mathbb{C}^n = W \overset{\perp}{\oplus} W^\perp.
$$
(3.133)

The Householder transform is given by

$$
H_w x = x - 2 \, P_w x.
$$
(3.134)
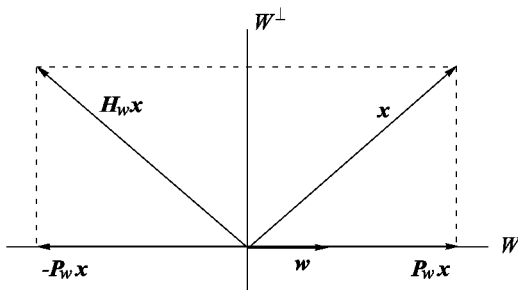
Figure 3.4. Householder reflection.

It is also known as *Householder reflection,* because it is the reflection of $\boldsymbol{x}$ at the hyperplane $W^{\perp}$, as depicted in Figure 3.4.

With $\boldsymbol{P}_w$ according to (3.132) we get

$$\boldsymbol{H}_w = \boldsymbol{I} - \frac{2}{\boldsymbol{w}^H \boldsymbol{w}}\ \boldsymbol{w}\ \boldsymbol{w}^H \tag{3.135}$$

for the *Householder matrix* $\boldsymbol{H}_w$.

From (3.135) the following property of Householder matrices can be concluded:

$$
\begin{aligned}
\boldsymbol{H}_w^H \boldsymbol{H}_w &= \boldsymbol{H}_w \boldsymbol{H}_w \\
&= \left[\boldsymbol{I} - \tfrac{2}{\boldsymbol{w}^H \boldsymbol{w}}\ \boldsymbol{w}\boldsymbol{w}^H\right]\left[\boldsymbol{I} - \tfrac{2}{\boldsymbol{w}^H \boldsymbol{w}}\ \boldsymbol{w}\boldsymbol{w}^H\right] \\
&= \boldsymbol{I} - \tfrac{4}{\boldsymbol{w}^H \boldsymbol{w}}\ \boldsymbol{w}\boldsymbol{w}^H + \tfrac{4}{\boldsymbol{w}^H \boldsymbol{w}}\ \boldsymbol{w}\boldsymbol{w}^H \boldsymbol{w}\boldsymbol{w}^H \\
&= \boldsymbol{I}.
\end{aligned} \tag{3.136}
$$

Hence $\boldsymbol{H}_w$ is unitary and Hermitian. Furthermore we have

$$\det\{\boldsymbol{H}_w\} = -1. \tag{3.137}$$

In order to make practical use of the Householder transform, we consider a vector $\boldsymbol{x}$ and try to find that vector $\boldsymbol{w}$ for which only the ith component of $\boldsymbol{H}_w\boldsymbol{x}$ is non-zero. We use the following approach:

$$\boldsymbol{w} = \boldsymbol{x} + \alpha\ \boldsymbol{e}_i, \tag{3.138}$$

where

$$e_i^T = [0, \ldots, 0, 1, 0, \ldots, 0].\qquad(3.139)$$

$$\uparrow \; i\text{th element}$$

For $\boldsymbol{H}_w\boldsymbol{x}$ we get

$$
\begin{aligned}
\boldsymbol{H}_w\boldsymbol{x} &= \boldsymbol{x} - 2\frac{\boldsymbol{w}\boldsymbol{w}^H}{\boldsymbol{w}^H\boldsymbol{w}}\,\boldsymbol{x}\\[4pt]
&= \boldsymbol{x} - 2\frac{\boldsymbol{w}^H\boldsymbol{x}}{\boldsymbol{w}^H\boldsymbol{w}}\,\boldsymbol{w}\\[4pt]
&= \boldsymbol{x} - 2\frac{\boldsymbol{w}^H\boldsymbol{x}}{\boldsymbol{w}^H\boldsymbol{w}}\,[\boldsymbol{x} + \alpha\,\boldsymbol{e}_i]\\[4pt]
&= \left(1 - 2\frac{\boldsymbol{w}^H\boldsymbol{x}}{\boldsymbol{w}^H\boldsymbol{w}}\right)\boldsymbol{x} - 2\alpha\,\frac{\boldsymbol{w}^H\boldsymbol{x}}{\boldsymbol{w}^H\boldsymbol{w}}\,\boldsymbol{e}_i.
\end{aligned}
\qquad(3.140)
$$

In order to achieve that only the ith component of $\boldsymbol{H}_w\boldsymbol{x}$ is non-zero, the expression in parentheses in (3.140) must vanish:

$$1 - 2\frac{\boldsymbol{w}^H\boldsymbol{x}}{\boldsymbol{w}^H\boldsymbol{w}} = 1 - 2\frac{\|\boldsymbol{x}\|^2 + \alpha^*x_i}{\|\boldsymbol{x}\|^2 + \alpha x_i^* + \alpha^*x_i + |\alpha|^2} = 0,\qquad(3.141)$$

where x_i is the ith component of $\boldsymbol{x}$. As can easily be verified, (3.141) is satisfied for

$$\alpha = \pm\frac{x_i}{|x_i|}\,\|\boldsymbol{x}\|.\qquad(3.142)$$

In order to avoid $\boldsymbol{w} \approx \boldsymbol{0}$ in the case of $\boldsymbol{x} \approx \beta\boldsymbol{e}_i$ for some $\beta \in \mathbb{R}$ we choose the positive sign in (3.142) and obtain

$$\boldsymbol{w} = \boldsymbol{x} + \frac{x_i}{|x_i|}\,\|\boldsymbol{x}\|\,\boldsymbol{e}_i.\qquad(3.143)$$

By substituting this solution into (3.140) we finally get

$$\boldsymbol{H}_w\boldsymbol{x} = -\frac{x_i}{|x_i|}\,\|\boldsymbol{x}\|\,\boldsymbol{e}_i.\qquad(3.144)$$

Applying the Householder transform to the QR Decomposition. We consider the problem

$$\|\boldsymbol{A}\boldsymbol{v} - \boldsymbol{b}\| \overset{!}{=} \min\qquad(3.145)$$

with

$$\boldsymbol{A} = \begin{bmatrix} a_{11}^{(1)} & \cdots & a_{1m}^{(1)}\\ \vdots & & \vdots\\ a_{n1}^{(1)} & \cdots & a_{nm}^{(1)} \end{bmatrix} \in \mathbb{C}^{n,m},\qquad n > m\qquad(3.146)$$

and try to tackle the problem by applying the QR decomposition. First, we choose x_1 to be the first column of A

$$x_1 = \left[a_{11}^{(1)}, \ldots, a_{n1}^{(1)} \right]^T. \qquad (3.147)$$

Multiplying A with the Householder matrix

$$H_1 = I - 2 \frac{w_1 w_1^H}{w_1^H w_1}, \qquad (3.148)$$

where w_1 is chosen as

$$w_1 = x_1 + \frac{a_{11}^{(1)}}{|a_{11}^{(1)}|} \|x_1\| e_1 \qquad (3.149)$$

yields a matrix where only r_{11} is non-zero in the first column:

$$H_1 A = \begin{bmatrix} r_{11} & r_{12} & \cdots & r_{1m} \\ 0 & a_{22}^{(2)} & \cdots & a_{2m}^{(2)} \\ \vdots & \vdots & & \vdots \\ 0 & a_{n2}^{(2)} & \cdots & a_{nm}^{(2)} \end{bmatrix} \qquad (3.150)$$

Then, we choose

$$x_2 = \left[0, a_{22}^{(2)}, \ldots, a_{n2}^{(2)} \right]^T,$$

$$w_2 = x_2 + \frac{a_{22}^{(2)}}{|a_{22}^{(2)}|} \|x_2\| e_2,$$

$$H_2 = I - 2 \frac{w_2 w_2^H}{w_2^H w_2}$$

and obtain

$$H_2 H_1 A = \begin{bmatrix} r_{11} & r_{12} & r_{13} & \cdots & r_{1m} \\ 0 & r_{22} & r_{23} & \cdots & r_{2m} \\ 0 & 0 & a_{33}^{(3)} & \cdots & a_{3m}^{(3)} \\ \vdots & \vdots & \vdots & & \vdots \\ 0 & 0 & a_{n3}^{(3)} & \cdots & a_{nm}^{(3)} \end{bmatrix}$$

After maximally m steps we get

$$H_m \cdots H_2 H_1 A = R, \qquad (3.151)$$

where only the upper right-hand triangular matrix of R is non-zero. This means that we have carried out the QR decomposition.

Note. If one of the values $a_{ii}^{(i)}$ becomes zero, w_i is chosen as $w_i = x_i + \|x_i\| e_i$. If $\|x_i\| = 0$, the columns must be exchanged.

3.4.5   Givens Rotations

Besides Householder reflections, rotations constitute a further possibility of performing QR decompositions. We first consider the rotation of a real-valued vector x by an angle ϕ through multiplication of x with an orthonormal rotation matrix G. For

$$x = \begin{bmatrix} x_1 \\ x_2 \end{bmatrix} = \begin{bmatrix} r \, \cos(\alpha) \\ r \, \sin(\alpha) \end{bmatrix} \tag{3.152}$$

and

$$G = \begin{bmatrix} \cos(\phi) & \sin(\phi) \\ -\sin(\phi) & \cos(\phi) \end{bmatrix} \tag{3.153}$$

we get

$$x' = Gx = \begin{bmatrix} r \, \cos(\alpha - \phi) \\ r \, \sin(\alpha - \phi) \end{bmatrix}. \tag{3.154}$$

We observe that for $\phi = \alpha$ a vector x' is obtained whose second component is zero. This special rotation matrix is

$$G = \begin{bmatrix} c & s \\ -s & c \end{bmatrix} \tag{3.155}$$

with

$$
\begin{aligned}
c &= \cos(\alpha) = \frac{x_1}{\sqrt{x_1^2 + x_2^2}} \\
s &= \sin(\alpha) = \frac{x_2}{\sqrt{x_1^2 + x_2^2}}.
\end{aligned} \tag{3.156}
$$

For the rotated vector we have

$$x' = Gx = \begin{bmatrix} r \\ 0 \end{bmatrix} = \begin{bmatrix} \sqrt{x_1^2 + x_2^2} \\ 0 \end{bmatrix}. \tag{3.157}$$

As can easily be verified, for complex-valued vectors we can apply the rotation matrix

$$G = \begin{bmatrix} c & s \\ -s^* & c \end{bmatrix} \tag{3.158}$$

with

$$c = \frac{x_1}{r}, \qquad s = \frac{x_2^*}{r}, \qquad r = \sqrt{|x_1|^2 + |x_2|^2} \tag{3.159}$$

in order to obtain $x' = [r, 0]^T$. Note that G according to (3.158) is unitary, $G^H G = I$.

We now consider a vector

$$x = [x_1, \dots, x_{i-1}, x_i, x_{i+1}, \dots, x_{j-1}, x_j, x_{j+1}, \dots, x_n]^T, \tag{3.160}$$

and want to achieve a vector

$$x' = [x_1, \ldots, x_{i-1}, r, x_{i+1}, \ldots, x_{j-1}, 0, x_{j+1}, \ldots, x_n]^T \qquad (3.161)$$

with

$$r = \sqrt{|x_i|^2 + |x_j|^2} \qquad (3.162)$$

by carrying out a rotation. The rotation is applied to the elements x_i and x_j only. We have

$$x' = G\ x \qquad (3.163)$$

with

$$G = \begin{bmatrix} 1 & & & & & & \\ & \ddots & & & & & \\ & & 1 & & & & \\ & & & c & & s & \\ & & & & 1 & & \\ & & & & & \ddots & \\ & & & & & & 1 \\ & & & -s^* & & c & \\ & & & & & & 1 \\ & & & & & & & \ddots \\ & & & & & & & & 1 \end{bmatrix} \begin{matrix} \\ \\ \\ \leftarrow i \\ \\ \\ \leftarrow j \\ \\ \end{matrix} \qquad (3.164)$$

$$\underset{\uparrow i \qquad \uparrow j}{}$$

   A QR decomposition of a matrix can be carried out by repeated application of the rotations described above.

Chapter 4

Examples of Discrete Transforms

In this chapter we discuss the most important fixed discrete transforms. We start with the z-transform, which is a fundamental tool for describing the input/output relationships in linear time-invariant (LTI) systems. Then we discuss several variants of Fourier series expansions, namely the discrete-time Fourier transform, the discrete Fourier transform (DFT), and the fast Fourier transform (FFT). The remainder of this chapter is dedicated to other discrete transforms that are of importance in digital signal processing, such as the discrete cosine transform, the discrete sine transform, the discrete Hartley transform, and the discrete Hadamard and Walsh–Hadamard transform.

4.1   The z-Transform

The z-transform of a discrete-time signal $x(n)$ is defined as

$$X(z) = \sum_{n=-\infty}^{\infty} x(n) \, z^{-n}. \qquad (4.1)$$

Note that the time index n is discrete, whereas z is a continuous parameter. Moreover, z is complex, even if $x(n)$ is real. Further note that for $z = e^{j\omega}$ the z-transform (4.1) is equal to the discrete-time Fourier transform.

In general, convergence of the sum in (4.1) depends on the sequence $x(n)$ and the value z. For most sequences we only have convergence in a certain region of the z-plane, called the *region of convergence* (ROC). The ROC can be determined by finding the values r for which

$$\sum_{n=-\infty}^{\infty} \left| x(n)\, r^{-n} \right| < \infty. \tag{4.2}$$

Proof. With $z = r\, e^{j\phi}$ we have

$$
\begin{aligned}
|X(z)| &= \left| \sum_{n=-\infty}^{\infty} x(n)\, z^{-n} \right| \\[2mm]
&= \left| \sum_{n=-\infty}^{\infty} x(n)\, r^{-n}\, e^{-j\phi n} \right| \\[2mm]
&\le \sum_{n=-\infty}^{\infty} \left| x(n)\, r^{-n}\, e^{-j\phi n} \right| \\[2mm]
&= \sum_{n=-\infty}^{\infty} \left| x(n)\, r^{-n} \right|.
\end{aligned}
\tag{4.3}
$$

Thus, $|X(z)|$ is finite if $x(n)r^{-n}$ is absolutely summable. $\square$

The inverse z-transform is given by

$$x(n) = \frac{1}{j2\pi} \oint_C X(z)\, z^{n-1} dz. \tag{4.4}$$

The integration has to be carried out counter-clockwise on a closed contour C in the complex plane, which encloses the origin and lies in the region of convergence of $X(z)$.

Proof of (4.4). We multiply both sides of (4.1) with z^{k-1} and integrate over a closed contour in a counter-clockwise manner:

$$
\begin{aligned}
\oint_C X(z)z^{k-1}dz &= \oint_C \sum_{n=-\infty}^{\infty} x(n)z^{k-1-n}dz \\[2mm]
&= \sum_{n=-\infty}^{\infty} x(n) \oint_C z^{k-1-n}dz.
\end{aligned}
\tag{4.5}
$$

Invoking the *Cauchy integral theorem*

$$\frac{1}{2\pi j} \oint_C z^{k-1-n} dz = \delta_{nk}. \tag{4.6}$$

finally yields (4.4). $\square$

Reconstruction formulae simpler than (4.4) can be found for rational $X(z)$, that is for

$$X(z) = \frac{b_0 + b_1 z^{-1} + b_2 z^{-2} \ \cdots}{a_0 + a_1 z^{-1} + a_2 z^{-2} \ \cdots}.$$

Methods based on the residue theorem, on partial fraction expansion, and on a direct expansion of $X(z)$ into a power series in z^{-1} are known. For more detail, see e.g. [80, 113].

The simplest example is the z-transform of the discrete impulse:

$$\delta(n) = \begin{cases} 1, & n = 0 \\ 0, & \text{otherwise.} \end{cases}$$

We have

$$\delta(n) \longleftrightarrow \sum_{n=-\infty}^{\infty} \delta(n) \, z^{-n} = 1. \tag{4.7}$$

For a delayed discrete impulse it follows that

$$\delta(n - n_0) \longleftrightarrow \sum_{n=-\infty}^{\infty} \delta(n - n_0) \, z^{-n} = z^{-n_0}. \tag{4.8}$$

In the following, the most important properties of the z-transform will be briefly recalled. Proofs which follow directly from the definition equation of the z-transform are omitted.

Linearity

$$v(n) = \alpha x(n) + \beta y(n) \longleftrightarrow V(z) = \alpha X(z) + \beta Y(z). \tag{4.9}$$

Convolution

$$v(n) = x(n) * y(n) \longleftrightarrow V(z) = X(z) \, Y(z). \tag{4.10}$$

Proof.

$$V(z) = \sum_{n=-\infty}^{\infty} \sum_{k=-\infty}^{\infty} x(k)\, y(n-k)\, z^{-n}$$

$$= \sum_{k=-\infty}^{\infty} x(k)\, z^{-k} \sum_{m=-\infty}^{\infty} y(m)\, z^{-m}$$

$$= X(z)\, Y(z).$$

Shifting

$$x(n-n_0) \longleftrightarrow z^{-n_0}\, X(z). \tag{4.11}$$

This result is obtained by expressing $v(n)$ as $v(n) = x(n) * \delta(n-n_0)$ and using the convolution property above.

Scaling/Modulation. For any real or complex $a \neq 0$, we have

$$a^n\, x(n) \longleftrightarrow X\left(\frac{z}{a}\right). \tag{4.12}$$

This includes $a = e^{j\omega}$ such that

$$e^{j\omega n}\, x(n) \longleftrightarrow X\left(e^{-j\omega} z\right). \tag{4.13}$$

Time Inversion

$$x(-n) \longleftrightarrow X\left(\frac{1}{z}\right). \tag{4.14}$$

Derivatives

$$n\, x(n) \longleftrightarrow -z\, \frac{d\, X(z)}{dz}. \tag{4.15}$$

Proof.

$$-z\, \frac{d\, X(z)}{dz} = -z\frac{d}{dz} \sum_{n=-\infty}^{\infty} x(n)\, z^{-n}$$

$$= \sum_{n=-\infty}^{\infty} n\, x(n)\, z^{-n}$$

$$\updownarrow$$

$$n\, x(n).$$

Conjugation. Given the correspondence $x(n) \longleftrightarrow X(z)$, we have

$$x^*(n) \longleftrightarrow X^*(z^*). \qquad (4.16)$$

Proof.

$$
\begin{aligned}
X^*(z^*) &= \left(\sum_{n=-\infty}^{\infty} x(n)\,[z^*]^{-n} \right)^* \\
&= \left(\sum_{n=-\infty}^{\infty} x(n)\,[z^{-n}]^* \right)^* \\
&= \sum_{n=-\infty}^{\infty} x^*(n)\,z^{-n}.
\end{aligned}
$$

Paraconjugation. Given the correspondence $x(n) \longleftrightarrow X(z)$, we have

$$x^*(-n) \longleftrightarrow \tilde{X}(z), \quad \text{where} \quad \tilde{X}(z) = [X(z)]^*\,|_{|z|=1}. \qquad (4.17)$$

That is, $\tilde{X}(z)$ is derived from $X(z)$ by complex conjugation on the unit circle.

Proof.

$$
\begin{aligned}
\tilde{X}(z) &= \left[\sum_{k} x(k) z^{-k} \right]^* |_{|z|=1} \\
&= \sum_{k} x^*(k) z^{k} \\
&= \sum_{n} x^*(-n) z^{-n} \\
&\quad \updownarrow \\
&\quad x^*(-n).
\end{aligned}
\qquad (4.18)
$$

For real signals $x(n)$, it follows that

$$x(-n) \longleftrightarrow \tilde{X}(z) = X(z^{-1}). \qquad (4.19)$$

Multiplication with $\cos \omega n$ and $\sin \omega n$. If $x(n) \longleftrightarrow X(z)$, then

$$\cos \omega n \; x(n) \longleftrightarrow \frac{1}{2} \left[X(e^{j\omega} z) + X(e^{-j\omega} z) \right] \qquad (4.20)$$

and

$$\sin \omega n \; x(n) \longleftrightarrow \frac{j}{2} \left[X(e^{j\omega} z) - X(e^{-j\omega} z) \right]. \qquad (4.21)$$

This follows directly from (4.13) by expressing $\cos\omega n$ and $\sin\omega n$ via Euler's formulae $\cos\alpha = \frac{1}{2}[e^{j\alpha} + e^{-j\alpha}]$ and $\sin\alpha = \frac{j}{2}[e^{j\alpha} - e^{-j\alpha}]$.

Multiplication in the Time Domain. Let $x(n)$ and $y(n)$ be real-valued sequences. Then

$$v(n) = x(n)\,y(n) \longleftrightarrow V(z) = \frac{1}{2\pi j} \oint_C X(\nu)Y\left(\frac{z}{\nu}\right)\nu^{-1}\,d\nu, \qquad (4.22)$$

where C is a closed contour that lies within the region of convergence of both $X(z)$ and $Y(\frac{1}{z})$.

    Proof. We insert (4.4) into

$$V(z) = \sum_{n=-\infty}^{\infty} x(n)\,y(n)\,z^{-n}. \qquad (4.23)$$

This yields

$$\begin{aligned}
V(z) &= \sum_{n=-\infty}^{\infty}\left[\frac{1}{j2\pi}\oint_C X(\nu)\,\nu^{n-1}d\nu\right]y(n)\,z^{-n} \\
&= \frac{1}{j2\pi}\oint_C X(\nu)\underbrace{\left[\sum_{n=-\infty}^{\infty} y(n)\left(\frac{z}{\nu}\right)^{-n}\right]}_{Y\left(\frac{z}{\nu}\right)}\nu^{-1}\,d\nu \qquad (4.24)
\end{aligned}$$

□

    Using the same arguments, we may write for complex-valued sequences

$$v(n) = x(n)\,y^*(n) \longleftrightarrow V(z) = \frac{1}{2\pi j}\oint_C X(\nu)Y^*\left(\frac{z^*}{\nu^*}\right)\nu^{-1}\,d\nu. \qquad (4.25)$$

4.2   The Discrete-Time Fourier Transform

The discrete-time Fourier transform of a sequence $x(n)$ is defined as

$$X(e^{j\omega}) = \sum_{n=-\infty}^{\infty} x(n)\,e^{-j\omega n}. \qquad (4.26)$$

Due to the 2π-periodicity of the complex exponential, $X(e^{j\omega})$ is periodic: $X(e^{j\omega}) = X(e^{j(\omega+2\pi)})$. If $x(n)$ is obtained by regular sampling of a

continuous-time signal $x_{ct}(t)$ such that $x(n) = x_{ct}(nT)$, where T is the sampling period, ω can be understood as the normalized frequency $\omega = 2\pi f T$.

The properties of the discrete-time Fourier transform are easily derived from those of the z-transform by choosing $z = e^{j\omega}$.

Shifting

$$x(n - n_0) \longleftrightarrow e^{-j\omega n_0} \, X(e^{j\omega}). \qquad (4.27)$$

Convolution

$$x(n) * y(n) \longleftrightarrow X(e^{j\omega}) \, Y(e^{j\omega}). \qquad (4.28)$$

Multiplication in the Time Domain

$$x(n)y(n) \longleftrightarrow \frac{1}{2\pi} \, X(e^{j\omega}) * Y(e^{j\omega}) \; = \; \frac{1}{2\pi} \int_{-\pi}^{\pi} X(e^{j(\omega - \nu)})Y(e^{j\nu})d\nu. \quad (4.29)$$

Reconstruction. If the sequence $x(n)$ is absolutely summable ($x \in \ell_1(-\infty, \infty)$), it can be reconstructed from $X(e^{j\omega})$ via

$$x(n) = \frac{1}{2\pi} \int_{-\pi}^{\pi} X(e^{j\omega}) \, e^{j\omega n} \, d\omega. \qquad (4.30)$$

The expression (4.30) is nothing but the inverse z-transform, evaluated on the unit circle.

Parseval's Theorem. As in the case of continuous-time signals, the signal energy can be calculated in the time and frequency domains. If a signal $x(n)$ is absolutely and square summable ($x \in \ell_1(-\infty, \infty) \cap \ell_2(-\infty, \infty)$), then

$$E_x = \sum_{n=-\infty}^{\infty} |x(n)|^2 = \frac{1}{2\pi} \int_{-\pi}^{\pi} |X(e^{j\omega})|^2 \, d\omega. \qquad (4.31)$$

Note that the expression (4.26) may be understood as a series expansion of the 2π-periodic spectrum $X(e^{j\omega})$, where the values $x(n)$ are the coefficients of the series expansion.

4.3   The Discrete Fourier Transform (DFT)

The transform pair of the *discrete Fourier transform* (DFT) is defined as

$$X(k) \;=\; \sum_{n=0}^{N-1} x(n) W_N^{nk}$$

$$\updownarrow \tag{4.32}$$

$$x(n) \;=\; \frac{1}{N} \sum_{k=0}^{N-1} X(k) W_N^{-nk},$$

where

$$W_N = e^{-j2\pi/N}. \tag{4.33}$$

Due to the periodicity of the basis functions, the DFT can be seen as the discrete-time Fourier transform of a periodic signal with period N.

With

$$\boldsymbol{x} = \begin{bmatrix} x(0) \\ x(1) \\ \vdots \\ x(N-1) \end{bmatrix}, \quad \boldsymbol{X} = \begin{bmatrix} X(0) \\ X(1) \\ \vdots \\ X(N-1) \end{bmatrix} \tag{4.34}$$

and

$$\boldsymbol{W} = \left[W_N^{kn} \right] = \begin{bmatrix} 1 & 1 & \cdots & 1 \\ 1 & W_N & \cdots & W_N^{N-1} \\ \vdots & \vdots & & \vdots \\ 1 & W_N^{N-1} & \cdots & W_N^{(N-1)(N-1)} \end{bmatrix} \tag{4.35}$$

the above relationships can also be expressed as

$$\boldsymbol{X} = \boldsymbol{W}\boldsymbol{x} \;\longleftrightarrow\; \boldsymbol{x} = \frac{1}{N} \boldsymbol{W}^H \boldsymbol{X}. \tag{4.36}$$

We see that $\boldsymbol{W}$ is orthogonal, but not orthonormal.

The DFT can be normalized as follows:

$$\boldsymbol{\alpha} = \boldsymbol{\Phi}^H \boldsymbol{x} \;\longleftrightarrow\; \boldsymbol{x} = \boldsymbol{\Phi}\boldsymbol{\alpha}, \tag{4.37}$$

where

$$\boldsymbol{\Phi} = \frac{1}{\sqrt{N}} \boldsymbol{W}^H. \tag{4.38}$$

The columns of $\boldsymbol{\Phi}$,

$$\boldsymbol{\varphi}_k = \frac{1}{\sqrt{N}} \left[1, W_N^{-k}, W_N^{-2k}, \ldots, W_N^{-(N-1)k} \right]^T, \quad k = 0, 1, \ldots, N-1$$

then form an orthonormal basis as usual.

We now briefly recall the most important properties of the DFT. For an elaborate discussion of applications of the DFT in digital signal processing the reader is referred to [113].

Shifting. A circular time shift by μ yields

$$
\begin{aligned}
x_\mu(n) &= x((n + \mu) \bmod N) \\
&\updownarrow \\
X_\mu(m) &= \sum_{n=0}^{N-1} x((n + \mu) \bmod N) W_N^{nm} \\
&= \sum_{i=0}^{N-1} x(i) W_N^{(i-\mu)m} \\
&= W_N^{-\mu m} X(m).
\end{aligned}
\tag{4.39}
$$

Accordingly,

$$
W_N^{kn} x(n) \longleftrightarrow \sum_{n=0}^{N-1} x(n) W_N^{n(m+k)} = X((m + k) \bmod N). \tag{4.40}
$$

Multiplication and Circular Convolution. For the inverse discrete Fourier transform (IDFT) of

$$
Y(m) = X_1(m) \, X_2(m)
$$

we have

$$
\begin{aligned}
y(n) &= \frac{1}{N} \sum_{m=0}^{N-1} X_1(m) \, X_2(m) \, W_N^{-mn} \\
&= \frac{1}{N} \sum_{p=0}^{N-1} \sum_{q=0}^{N-1} x_1(p) \, x_2(q) \sum_{m=0}^{N-1} W_N^{-m(n-p-q)} \\
&= \sum_{p=0}^{N-1} x_1(p) \, x_2((n - p) \bmod N).
\end{aligned}
\tag{4.41}
$$

That is, a multiplication in the frequency domain means a circular convolution

in the time domain. Accordingly,

$$x_1(n)\,x_2(n) \longleftrightarrow \sum_{n=0}^{N-1} X_1(n)\,X_2((m-n)\bmod N). \qquad (4.42)$$

Complex Conjugation. Conjugation in the time or frequency domains yields

$$x^*(n) \longleftrightarrow X^*(N-n) \qquad (4.43)$$

and

$$x^*(N-n) \longleftrightarrow X^*(n). \qquad (4.44)$$

Relationship between the DFT and the KLT. The DFT is related to the KLT due to the fact that it diagonalizes any circulant matrix

$$\boldsymbol{H} = \begin{bmatrix} h_0 & h_{N-1} & \dots & h_1 \\ h_1 & h_0 & \dots & h_2 \\ \vdots & \vdots & & \vdots \\ h_{N-1} & h_{N-2} & \dots & h_0 \end{bmatrix}. \qquad (4.45)$$

In order to show the diagonalization effect of the DFT, we consider a linear time-invariant system (FIR filter) with impulse response $h(n)$, $0 \le n \le N-1$ which is excited by the periodic signal $W_N^{-kn}/\sqrt{N}$. The output signal $y(n)$ is given by

$$y(n) = \frac{1}{\sqrt{N}} \underbrace{\left[\sum_{m=0}^{N-1} h(m) W_N^{mk}\right]}_{H(k)} W_N^{-nk} = \frac{1}{\sqrt{N}} H(k) W_N^{-nk}. \qquad (4.46)$$

Using the property $W_N^{n+N} = W_N^n$, we get

$$\begin{bmatrix} y(0) \\ y(1) \\ \vdots \\ y(N-1) \end{bmatrix} = \frac{H(k)}{\sqrt{N}} \begin{bmatrix} 1 \\ W_N^{-k} \\ \vdots \\ W_N^{-k(N-1)} \end{bmatrix}$$

$$= \frac{1}{\sqrt{N}} \begin{bmatrix} h_0 & h_{N-1} & \dots & h_1 \\ h_1 & h_0 & \dots & h_2 \\ \vdots & \vdots & & \vdots \\ h_{N-1} & h_{N-2} & \dots & h_0 \end{bmatrix} \begin{bmatrix} 1 \\ W_N^{-k} \\ \vdots \\ W_N^{-k(N-1)} \end{bmatrix}$$

$$(4.47)$$

Comparing (4.47) with (4.45) and (4.37) yields the relationship

$$H(k)\varphi_k = H\varphi_k, \quad k=0,1,\ldots,N-1. \tag{4.48}$$

Thus, the eigenvalues $\lambda_k = H(k)$ of H are derived from the DFT of the first column of H. The vectors φ_k, $k=0,1,\ldots,N-1$ are the eigenvectors of H. We have

$$\Phi^H H \Phi = \mathrm{diag}\left\{H(0), H(1), \ldots, H(N-1)\right\}. \tag{4.49}$$

4.4 The Fast Fourier Transform

For a complex-valued input signal $x(n)$ of length N the implementation of the DFT matrix W requires N^2 complex multiplications. The idea behind the fast Fourier transform (FFT) is to factorize W into a product of sparse matrices that altogether require a lower implementation cost than the direct DFT. Thus, the FFT is a fast implementation of the DFT rather than a different transform with different properties.

Several concepts for the factorization of W have been proposed in the literature. We will mainly focus on the case where the DFT length is a power of two. In particular, we will discuss the radix-2 FFTs, the radix-4 FFT, and the split-radix FFT. Section 4.4.5 gives a brief overview of FFT algorithms for cases where N is not a power of two.

We will only discuss the forward DFT. For the inverse DFT a similar algorithm can be found.

4.4.1 Radix-2 Decimation-in-Time FFT

Let us consider an N-point DFT where N is a power of two, i.e. $N = 2^K$ for some $K \in \mathbb{N}$. The first step towards a fast implementation is to decompose the time signal $x(n)$ into its even and odd numbered components

$$\left.\begin{array}{rcl} u(n) &=& x(2n) \\[2mm] v(n) &=& x(2n+1) \end{array}\right\} \quad n = 0, 1, \ldots, \frac{N}{2} - 1. \tag{4.50}$$

The DFT can be written as

$$
\begin{aligned}
X(k) &= \sum_{n=0}^{N-1} x(n) W_N^{nk} \\
&= \sum_{n=0}^{\frac{N}{2}-1} u(n) W_N^{2nk} + \sum_{n=0}^{\frac{N}{2}-1} v(n) W_N^{(2n+1)k} \\
&= \sum_{n=0}^{\frac{N}{2}-1} u(n) W_{N/2}^{nk} + W_N^k \sum_{n=0}^{\frac{N}{2}-1} v(n) W_{N/2}^{nk}, \quad k = 0, 1, \ldots, N-1.
\end{aligned}
$$
$$(4.51)$$

In the last step the properties $W_N^{2nk} = W_{N/2}^{nk}$ and $W_N^{(2n+1)k} = W_N^k W_{N/2}^{nk}$ were used. The next step is to write (4.51) for $k = 0, 1, \ldots, \frac{N}{2} - 1$ as

$$X(k) = U(k) + W_N^k V(k), \quad k = 0, 1, \ldots, \frac{N}{2} - 1 \qquad (4.52)$$

with

$$
\begin{aligned}
U(k) &= \sum_{n=0}^{\frac{N}{2}-1} u(n) W_{N/2}^{nk}, \qquad k = 0, 1, \ldots, \frac{N}{2} - 1 \\
\\
V(k) &= \sum_{n=0}^{\frac{N}{2}-1} v(n) W_{N/2}^{nk}, \qquad k = 0, 1, \ldots, \frac{N}{2} - 1.
\end{aligned}
$$
$$(4.53)$$

Due to the periodicity of the DFT the values $X(k)$ for $k = \frac{N}{2}, \ldots, N-1$ are given by

$$X(k) = U(k - \frac{N}{2}) + W_N^k V(k - \frac{N}{2}), \quad k = \frac{N}{2}, \ldots, N-1. \qquad (4.54)$$

Thus, we have decomposed an N-point DFT into two $\frac{N}{2}$-point DFTs and some extra operations for combining the two DFT outputs.

Figure 4.1 illustrates the implementation of an N-point DFT via two $\frac{N}{2}$-point DFTs. It is easily verified that the decomposition of the DFT results in a reduction of the number of multiplications: the two DFTs require $2(N/2)^2$ multiplications, and the prefactors W_N^k require another N multiplications. Thus, the overall complexity is $\frac{N^2}{2} + N$, instead of N^2 for the direct DFT. The prefactors W_N^k, which are used for the combination of the two DFTs, are called *twiddle factors*.

Since N is considered to be a power of two, the same decomposition principle can be used for the smaller DFTs and the complexity can be further
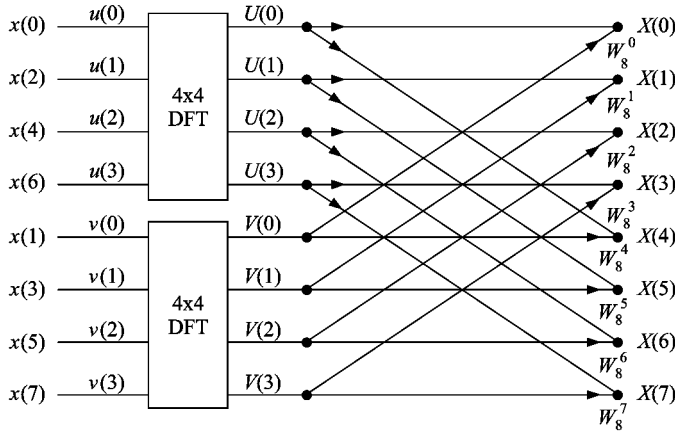
Figure 4.1. Realization of an 8-point DFT via two 4-point DFTs.

reduced. To be explicit, we decompose the sequences $u(n)$ and $v(n)$ into their even and odd numbered parts:

$$
\begin{aligned}
a(n) &= u(2n) &= x(4n)\\
b(n) &= u(2n+1) &= x(4n+2)\\
c(n) &= v(2n) &= x(4n+1)\\
d(n) &= v(2n+1) &= x(4n+3).
\end{aligned}
\tag{4.55}
$$

Observing that $W_{N/2}^k = W_N^{2k}$ we get for the $\frac{N}{2}$-point DFTs $U(k)$ and $V(k)$

$$
U(k) = \begin{cases} A(k) + W_N^{2k}\,B(k), & k = 0,1,\ldots,\dfrac{N}{4}-1\\[2mm] A(k-\tfrac{N}{4}) + W_N^{2k}\,B(k-\tfrac{N}{4}), & k = \dfrac{N}{4},\ldots,\dfrac{N}{2}-1 \end{cases}
\tag{4.56}
$$

and

$$
V(k) = \begin{cases} C(k) + W_N^{2k}\,D(k), & k = 0,1,\ldots,\dfrac{N}{4}-1\\[2mm] C(k-\tfrac{N}{4}) + W_N^{2k}\,D(k-\tfrac{N}{4}), & k = \dfrac{N}{4},\ldots,\dfrac{N}{2}-1. \end{cases}
\tag{4.57}
$$

The decomposition procedure can be continued until two-point DFTs are reached.

It turns out that all stages of the FFT are composed of so-called *butterfly graphs* as shown in Figure 4.2. The two structures in Figure 4.2 are equivalent,
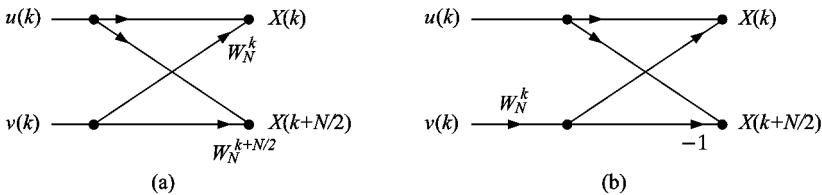
Figure 4.2. Equivalent butterfly graphs.

but the one in Figure 4.2(b) saves us one complex multiplication. The complete flow graph for an 8-point FFT based on the butterfly in Figure 4.2(b) is depicted in Figure 4.3. As we see, the output values appear in their natural order, but the input values appear in permuted order. This is the case for all N. The order of the input values is known as the *bit reversed order*. This order can be derived from the natural one as follows. First, one represents the numbers $0, 1, \ldots, N-1$ in binary form. Then the order of bits is reversed and the decimal equivalent is taken. For example, $n = 3$ is represented by [011] when an 8-point FFT is considered. This yields [110] in reversed order, and the decimal equivalent is 6. Thus, $x(6)$ has to be connected to input node 3.

Since the butterfly operations within each stage of the FFT are independent of one another, the computation of the FFT can be carried out *in place*. This means that the pair of output values of a butterfly is written over the input. After this has been done for all butterflies of a given processing stage, one can proceed to the next stage. Thus, only a memory of size $N + 1$ is required for computing an N-point FFT.

The computational complexity of the FFT is as follows. Each stage of the FFT requires $N/2$ complex multiplications and N additions. The number of stages is $\log_2 N$. This yields a total number of $\frac{1}{2} N \log_2 N$ complex multiplications and $N \log_2 N$ additions. However, since the 2-point DFTs do not require multiplications, and since the 4-point DFTs involve multiplications with $1, -1, j$, and $-j$ only, the actual number of full complex multiplications is even lower than $\frac{1}{2} N \log_2 N$.

4.4.2   Radix-2 Decimation-in-Frequency FFT

A second variant of the radix-2 FFT is the *decimation-in-frequency* algorithm. In order to derive this algorithm, we split the input sequence into the first
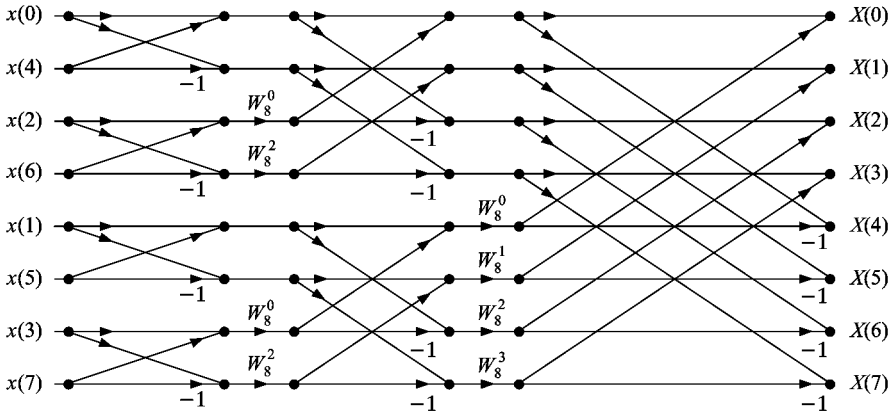
Figure 4.3. Flow graph for an 8-point decimation-in-time FFT.

and second halves and write the DFT as

$$X(k) = \sum_{n=0}^{N-1} x(n) W_N^{nk}$$

$$= \sum_{n=0}^{N/2-1} u(n) W_N^{nk} + v(n) W_N^{(n+N/2)k} \tag{4.58}$$

$$= \sum_{n=0}^{N/2-1} [u(n) + (-1)^k v(n)] W_N^{nk},$$

where

$$\left. \begin{array}{rcl} u(n) &=& x(n) \\ v(n) &=& x(n+N/2) \end{array} \right\}, \quad n = 0, 1, \ldots, \frac{N}{2} - 1. \tag{4.59}$$

In (4.58) we have used the fact that $W_N^{N/2} = -1$. For the even and odd numbered DFT points we get

$$X(2k) = \sum_{n=0}^{N-1} [u(n) + v(n)] W_N^{2nk} \tag{4.60}$$

and

$$X(2k+1) = \sum_{n=0}^{N-1} [u(n) - v(n)] W_N^n W_N^{2nk}. \tag{4.61}$$

Because of $W_N^{2nk} = W_{N/2}^{nk}$, the even numbered DFT points $X(2k)$ turn out to be the DFT of the half-length sequence $u(n) + v(n)$. The odd numbered
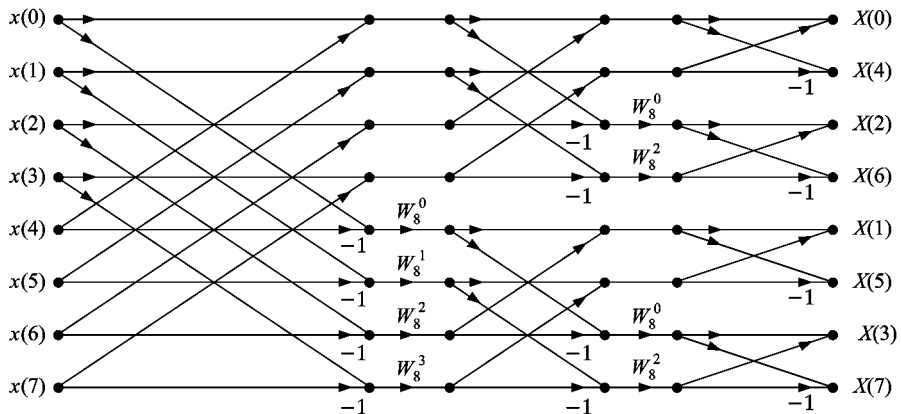
Figure 4.4. Flow graph for an 8-point decimation-in-frequency FFT.

DFT points $X(2k+1)$ are the DFT of $[u(n) - v(n)]\,W_N^n$. Thus, as with the decimation-in-time algorithm, the N-point DFT is decomposed into two $N/2$-point DFTs. Using the principle repeatedly results in an FFT algorithm where the input values appear in their natural order, but where the output values appear in bit reversed order. The complexity is the same as for the decimation-in-time FFT. Figure 4.4 shows the complete flow graph of the decimation-in-frequency FFT for the case $N = 8$. The comparison of Figures 4.3 and 4.4 shows that the two graphs can be viewed as transposed versions of one another.

4.4.3   Radix-4 FFT

The radix-4 decimation-in-frequency FFT is derived by writing the DFT as

$$
\begin{aligned}
X(k) &= \sum_{n=0}^{N-1} x(n) W_N^{nk} \\
&= \sum_{n=0}^{N/4-1} \left[\sum_{\ell=0}^{3} x\left(n + \ell\frac{N}{4}\right) W_N^{(N/4)\ell k} \right] W_N^{nk} \qquad (4.62) \\
&= \sum_{n=0}^{N/4-1} \left[\sum_{\ell=0}^{3} x\left(n + \ell\frac{N}{4}\right) (-j)^{\ell k} \right] W_N^{nk}.
\end{aligned}
$$

Splitting $X(k)$ into four subsequences $X(4k + m)$ yields

$$X(4k + m) = \sum_{n=0}^{N/4-1} \left[\sum_{\ell=0}^{3} (-j)^{\ell m} \, x(n + \ell \frac{N}{4}) W_N^{nm} \right] W_{N/4}^{nk}. \qquad (4.63)$$

Thus, we have replaced the computation of an N-point DFT by four $N/4$-point DFTs. One of these four DFTs requires no multiplication at all, and the others require one complex multiplication per point. Compared to the radix-2 FFT this means $3 \times (N/4)$ instead of $N/2$ multiplications for the twiddle factors. However, the radix-4 algorithm requires only $N/4$-point DFTs, and it requires only half as many stages as a radix-2 one. Therefore, the overall number of multiplications is lower for the radix-4 case.

4.4.4 Split-Radix FFT

The split-radix FFT [46], which is a mixture of the radix-2 and radix-4 algorithm, requires the lowest number of operations of all currently known FFT algorithms. It is also easily programmed on a computer. The radix-2 approach is used to compute the even numbered frequencies, and the radix-4 approach is used to compute two length-$(N/4)$ subsequences of the odd numbered frequencies. For this, $X(k)$ is split into the following three subsets:

$$X(2k) = \sum_{n=0}^{N/2-1} [x(n) + x(n + \frac{N}{2})] W_{N/2}^{nk}, \qquad (4.64)$$

$$X(4k+1) = \sum_{n=0}^{N/4-1} \left[[x(n) - x(n + \frac{N}{2})] \right. $$
$$\left. - j[x(n + \frac{N}{4}) - x(n + \frac{3N}{4})] \right] W_N^n W_{N/4}^{nk}, \quad (4.65)$$

$$X(4k+3) = \sum_{n=0}^{N/4-1} \left[[x(n) - x(n + \frac{N}{2})] \right. $$
$$\left. + j[x(n + \frac{N}{4}) - x(n + 3\frac{N}{4})] \right] W_N^{3n} W_{N/4}^{nk}. \quad (4.66)$$

The terms $[x(n) - x(n + \frac{N}{2})]$ and $[x(n + \frac{N}{4}) - x(n + \frac{3N}{4})]$ in (4.65) and (4.66) are the natural pairs to the terms in (4.64). Thus, a split-radix butterfly can be drawn as shown in Figure 4.5. As with the previous approaches, the decomposition principle can be used repeatedly. It turns out that the split-radix approach requires less multiplications than a pure radix-2 or radix-4 FFT, because fewer full complex multiplications occur. The split-radix
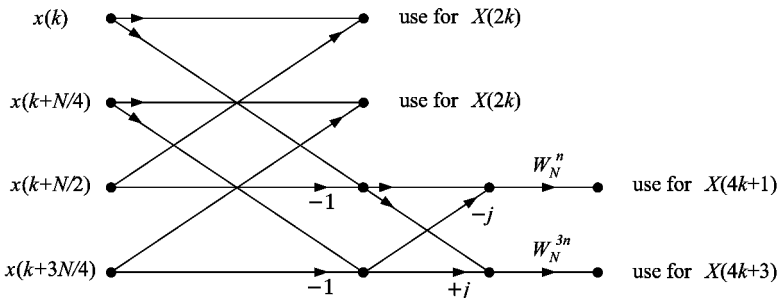
Figure 4.5. Butterfly for a split-radix FFT.

concept can be generalized to other radices [152], and special forms are available for real and real-symmetric data [45, 138].

4.4.5   Further FFT Algorithms

There are a number of algorithms available for the case where the DFT length is not necessarily a power of two. The best known one is the *Cooley–Tukey FFT* [31], which requires that the DFT-length is a composite number $N = PQ$, where P and Q are integers. The DFT can then be written as

$$
\begin{aligned}
X(kP + m) &= \sum_{i=0}^{P-1} \sum_{j=0}^{Q-1} x(iQ + j)\, W_N^{(iQ+j)(kP+m)} \\
&= \sum_{j=0}^{Q-1} W_Q^{jk}\, W_N^{jm} \sum_{i=0}^{P-1} x(iQ + j)\, W_P^{im}
\end{aligned}
\tag{4.67}
$$

for $k = 0, 1, \ldots, P - 1$ and $m = 0, 1, \ldots, Q - 1$. The inner sum in the second line of (4.67) turns out to be a P-point DFT, and the outer sum is a Q-point DFT. Thus, the N-point DFT is decomposed into P Q-point and Q P-point DFTs, plus the twiddle factors in the middle of the second line in (4.67). As can easily be verified, the complexity is lower than for the direct N-point DFT. If P and/or Q are composite themselves, the approach can be iterated, and the complexity can be further reduced. Note that the radix-2 approach occurs as a special case where $P = 2$ and $Q = N/2$.

If the DFT-length can be factored into $N = PQ$ where P and Q are relatively prime (have no common divisor other than 1) a powerful algorithm known as the *Good–Thomas FFT* can be used. The basic idea dates back to papers by Good [64] and Thomas [143]. The algorithm has been further developed in [88, 164, 20, 142]. The efficiency of the Good–Thomas FFT

results from the fact that for relatively prime P and Q the twiddle factors (they are always present in the Cooley–Tukey FFT) can be avoided. The input data can be arranged in a two-dimensional array, and the transform can be implemented as a true two-dimensional transform. The mapping is based on the Chinese remainder theorem [9].

FFTs where N is a prime number can be realized via circular convolution [120, 10]. In order to give an idea of how this is done, we follow the approach in [10] and write the DFT as

$$X(k) = \sum_{n=0}^{N-1} x(n) W_N^{nk} = W_{2N}^{k^2} \sum_{n=0}^{N-1} [x(n) W_{2N}^{n^2}] W_{2N}^{-(k-n)^2}. \qquad (4.68)$$

The sum on the right side can be identified as a circular convolution of the sequences $x(n) W_{2N}^{n^2}$ and $W_{2N}^{-n^2}$, that is

$$X(n) = W_{2N}^{k^2} [x(n) W_{2N}^{n^2} * W_{2N}^{-n^2}]. \qquad (4.69)$$

Efficiency is achieved by implementing the circular convolution via fast convolution based on the FFT, see e.g. [117].

Powerful FFT algorithms are most often associated with signal lengths that are powers of two. However, prime factor algorithms such as the Winograd FFT [164] are often competitive, if not superior, to the power-of-two approaches. Thus, when designing an algorithm where the DFT is involved, one should not be bound to certain block lengths, because for almost any length an appropriate FFT algorithm can be found.

4.5 Discrete Cosine Transforms

We distinguish the following four types of *discrete cosine transforms* (DCTs) [122]:

DCT-I:

$$c_k^I(n) = \sqrt{\frac{2}{N}} \, \gamma_k \gamma_n \, \cos\left(\frac{kn\pi}{N}\right), \qquad k, n = 0, 1, \ldots, N. \qquad (4.70)$$

DCT-II:

$$c_k^{II}(n) = \sqrt{\frac{2}{N}} \, \gamma_k \, \cos\left(\frac{k(n + \frac{1}{2})\pi}{N}\right), \qquad k, n = 0, 1, \ldots, N-1. \qquad (4.71)$$

DCT-III:

$$c_k^{III}(n) = \sqrt{\frac{2}{N}} \; \gamma_n \; \cos\left(\frac{(k+\frac{1}{2})n\pi}{N}\right), \qquad k,n = 0,1,\ldots,N-1. \quad (4.72)$$

DCT-IV:

$$c_k^{IV}(n) = \sqrt{\frac{2}{N}} \; \cos\left(\frac{(k+\frac{1}{2})(n+\frac{1}{2})\pi}{N}\right), \qquad k,n = 0,1,\ldots,N-1. \quad (4.73)$$

The constants γ_j in (4.70) – (4.72) are given by

$$\gamma_j = \begin{cases} \dfrac{1}{\sqrt{2}} & \text{for } j = 0 \text{ or } j = N, \\[2mm] 1 & \text{otherwise.} \end{cases} \quad (4.74)$$

The coefficients $c_k(n)$ are the elements of the orthonormal basis vectors

$$\boldsymbol{c}_k(n) = [c_k(0), c_k(1), \ldots]^T.$$

In order to point out clearly how (4.70) – (4.73) are to be understood, let us consider the forward and inverse DCT-II:

$$\begin{aligned} X_C^{II}(k) &= \sum_{n=0}^{N-1} x(n)\, c_k^{II}(n) \\[2mm] &= \gamma_k \sqrt{\frac{2}{N}} \sum_{n=0}^{N-1} x(n)\; \cos\left(\frac{k(n+\frac{1}{2})\pi}{N}\right), \end{aligned} \quad (4.75)$$

and

$$\begin{aligned} x(n) &= \sum_{k=0}^{N-1} X_C^{II}(k)\, c_k^{II}(n) \\[2mm] &= \sqrt{\frac{2}{N}} \sum_{k=0}^{N-1} X_C^{II}(k)\; \gamma_k\; \cos\left(\frac{k(n+\frac{1}{2})\pi}{N}\right). \end{aligned} \quad (4.76)$$

Especially the DCT-II is of major importance in signal coding because it is close to the KLT for first-order autoregressive processes with a correlation coefficient that is close to one.[1] To illustrate this, we consider the inverse of the correlation matrix of an AR(1) process, which is given by

---

[1] See Section 5.3 for the definition of an AR process.

$$
\boldsymbol{R}_{xx}^{-1} = \frac{1 + \rho^2}{\sigma^2(1 - \rho^2)}
\begin{bmatrix}
(1 - \rho\beta) & -\beta & & & \\
-\beta & 1 & -\beta & & \\
& -\beta & \ddots & \ddots & \\
& & & 1 & -\beta \\
& & & -\beta & (1 - \rho\beta)
\end{bmatrix}
\tag{4.77}
$$

with $\beta = \rho/(1 + \rho^2)$. The basis vectors of the DCT-II are the eigenvectors of tridiagonal symmetric matrices of the form

$$
\boldsymbol{Q} =
\begin{bmatrix}
(1 - \alpha) & -\alpha & & & \\
-\alpha & 1 & -\alpha & & \\
& -\alpha & \ddots & \ddots & \\
& & & 1 & -\alpha \\
& & & -\alpha & (1 - \alpha)
\end{bmatrix}.
\tag{4.78}
$$

We see that $\boldsymbol{Q}$ approaches $\boldsymbol{R}_{xx}^{-1}$ for $\rho \to 1$. Since the eigenvectors of $\boldsymbol{R}_{xx}$ are equal to those of $\boldsymbol{R}_{xx}^{-1}$ the DCT-II approaches the KLT for $\rho \to 1$. This means that the DCT-II has good decorrelation properties when the process which is to be transformed has high correlation ($\rho \to 1$). This is the case for most images, which explains why most image coding standards (e.g. JPEG, MPEG [79, 157, 108, 56]) are based on the DCT-II. Compared to the KLT, the DCT-II has the advantage that fast implementations based on the FFT algorithm exist [122].

Application in Image Coding. In most standards for transform coding of images, the two-dimensional cosine transform is used [79, 157, 108, 56]. Figure 4.6 gives an example. First, the two-dimensional signal is decomposed into non-overlapping blocks. Each of these blocks is then transformed separately. This operation can be written as $\boldsymbol{Y}_{N \times N} = \boldsymbol{U}^T \boldsymbol{X}_{N \times N} \boldsymbol{U}$, where $\boldsymbol{X}_{N \times N}$ is such a signal block and $\boldsymbol{U}$ is the DCT-II transform matrix whose columns contain the basis vectors of the DCT-II. Instead of the original $\boldsymbol{X}$, the representation $\boldsymbol{Y}$ is quantized and coded. From the quantized representation $\boldsymbol{Y}' = Q(\boldsymbol{Y})$ an approximation of the original is finally reconstructed. In Figure 4.6 we see that most of the energy of the transformed signal is concentrated in the top left sub-image. Such a concentration of signal energy in a few coefficients is the key to efficient compression. If we were to simply transmit the top left sub-image and neglect the others, we already could achieve drastic compression, while the reconstructed signal would still be relatively close to the original.
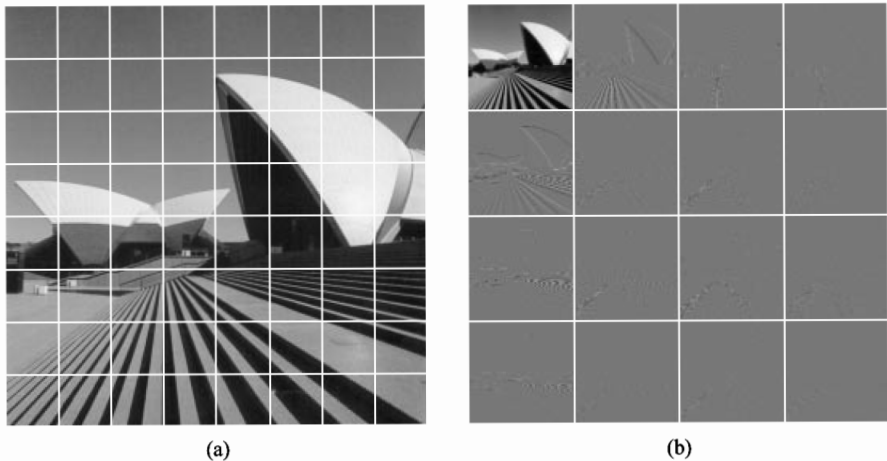
Figure 4.6. Transform coding of images; (a) original, divided into $N \times N$ blocks; (b) transformed image after rearranging the pixels.

4.6 Discrete Sine Transforms

The *discrete sine transforms (DSTs)* are classified as follows [122]:

DST-I:

$$s_k^I(n) = \sqrt{\frac{2}{N}} \, \sin\left(\frac{kn\pi}{N}\right), \qquad k, n = 1, 2, \ldots, N-1. \qquad (4.79)$$

DST-II:

$$s_k^{II}(n) = \sqrt{\frac{2}{N}} \, \gamma_{k+1} \, \sin\left(\frac{(k+1)\,(n+\frac{1}{2})\pi}{N}\right), \qquad k, n = 0, 1, \ldots, N-1. \qquad (4.80)$$

DST-III:

$$s_k^{III}(n) = \sqrt{\frac{2}{N}} \, \gamma_{n+1} \, \sin\left(\frac{(k+\frac{1}{2})\,(n+1)\pi}{N}\right), \qquad k, n = 0, 1, \ldots, N-1. \qquad (4.81)$$

DST-IV:

$$s_k^{IV}(n) = \sqrt{\frac{2}{N}} \, \sin\left(\frac{(k+\frac{1}{2})(n+\frac{1}{2})\pi}{N}\right), \qquad k, n = 0, 1, \ldots, N-1. \qquad (4.82)$$

The constants γ_j in (4.79) – (4.81) are

$$\gamma_j = \begin{cases} \dfrac{1}{\sqrt{2}} & \text{for } j = 0 \text{ or } j = N, \\ 1 & \text{otherwise.} \end{cases} \qquad (4.83)$$

To be explicit, the forward and the inverse DST-II are given by

$$
\begin{aligned}
X_S^{II}(k) &= \sum_{n=0}^{N-1} x(n)\, s_k^{II}(n) \\
&= \gamma_{k+1} \sqrt{\frac{2}{N}} \sum_{n=0}^{N-1} x(n)\ \sin\left(\frac{(k+1)\,(n+\frac{1}{2})\pi}{N}\right),
\end{aligned}
\tag{4.84}
$$

and

$$
\begin{aligned}
x(n) &= \sum_{k=0}^{N-1} X_S^{II}(k)\, s_k^{II}(n) \\
&= \sqrt{\frac{2}{N}} \sum_{k=0}^{N-1} X_S^{II}(k)\ \gamma_{k+1}\ \sin\left(\frac{(k+1)\,(n+\frac{1}{2})\pi}{N}\right).
\end{aligned}
\tag{4.85}
$$

The DST-II is related to the KLT by the fact that the KLT for an AR(1) process with correlation coefficient $\gamma \to -1$ approaches the DST-II. Thus, the DST-II has good compaction properties for processes with negative correlation of adjacent samples.

4.7 The Discrete Hartley Transform

The Hartley transform as discussed in Section 2.3 received little attention until its discrete version, the *discrete Hartley transform (DHT)*, was introduced in the early 1980s by Wang [158, 159, 160] and Bracewell [13, 14, 15]. Like other discrete transforms such as the DFT or the DCT, the DHT can be implemented efficiently through a factorization of the transform matrix. This results in fast algorithms that are closely related to the FFT, and in fact, the *fast Hartley transform (FHT)* can be computed via the FFT, and vice versa, the FFT can be implemented via the FHT [161, 14, 139]. For example, in [139] a split-radix approach for the FHT has been proposed.

The forward and inverse discrete Hartley transform pair is given by

$$
\begin{aligned}
X_H(k) &= \sum_{n=0}^{N-1} x(n)\ \mathrm{cas}\,\frac{2\pi nk}{N} \\
&\updownarrow \\
x(n) &= \frac{1}{N} \sum_{k=0}^{N-1} X_H(k)\ \mathrm{cas}\,\frac{2\pi nk}{N},
\end{aligned}
\tag{4.86}
$$

where $\operatorname{cas} \phi = \cos \phi + \sin \phi$. The signal $x(t)$ is considered to be real-valued, so that also the transform is real-valued. As with the DFT, the sequence $X_H(k)$ is periodic with period N.

Note that apart from the prefactor $1/N$ the DHT is self-inverse, which means that the same computer program or hardware can be used for the forward and inverse transform. This is not the case for the DFT, where a real-valued signal is transformed into a complex spectrum.

We may interpret the basis sequences $\operatorname{cas}(2\pi nk/N)$ as sample values of the basis functions $\operatorname{cas} \omega_k t$ with $\omega_k = 2\pi k/N$. The basis function with the highest frequency then occurs for $k = N/2$. The kth and the $(N-k)$th frequency are the same.

The relationships between the DHT and the DFT are easily derived. Using the fact that

$$e^{j\phi} = \frac{1+j}{2} \operatorname{cas} \phi + \frac{1-j}{2} \operatorname{cas}(-\phi) \tag{4.87}$$

and the periodicity in N, we get

$$\begin{aligned} \Re\{X(k)\} &= \frac{X_H(k) + X_H(N-k)}{2}, \\ \Im\{X(k)\} &= -\frac{X_H(k) - X_H(N-k)}{2}, \end{aligned} \tag{4.88}$$

where $X(k)$ denotes the DFT. The DHT can be expressed in terms of the DFT as

$$X_H(k) = \Re\{X(k)\} - \Im\{X(k)\}. \tag{4.89}$$

The properties of the DHT can easily be derived from the definition (4.86). Like in the continuous-time case, most of them are very similar to the properties of the Fourier transform. We will briefly discuss the most important ones. The proofs are essentially the same as for the continuous-time case and are omitted here.

Time Inversion. From (4.86) we see that

$$x(N-n) \longleftrightarrow X_H(N-n). \tag{4.90}$$

Shifting. A circular time shift by μ yields

$$x((n+\mu) \bmod N)$$

$$\updownarrow \tag{4.91}$$

$$\cos\left(\frac{2\pi\mu k}{N}\right) X_H(k) + \sin\left(\frac{2\pi\mu k}{N}\right) X_H(N-k).$$

Circular Convolution. The correspondence for a circular convolution of two time sequences $x(n)$ and $y(n)$ is

$$\sum_{p=0}^{N-1} x(p)\, y((n-p) \bmod N)$$

$$\updownarrow \qquad (4.92)$$

$$\frac{N}{2}\, [\, X_H(k)\, Y_H(k) - X_H(N-k)\, Y_H(N-k)$$

$$+\; X_H(k)\, Y_H(N-k) \;+\; X_H(N-k)\, Y_H(k)\,].$$

Multiplication. The correspondence for products $x(n)y(n)$ is

$$x(n)\, y(n) \longleftrightarrow \frac{N}{2}\, [\, X_H(k) * Y_H(k) + X_H(-k) * Y_H(k)$$

$$+\; X_H(k) * Y_H(-k) - X_H(-k) * Y_H(-k)\,], \qquad (4.93)$$

where the convolutions have to be carried out in a circular manner. For example an expression $Z_H(k) = X_H(k) * Y_H(-k)$ means

$$Z_H(k) = \sum_{p=0}^{N-1} X_H(p)\, Y_H((k-p) \bmod N). \qquad (4.94)$$

Remarks. The question of whether the DFT or the DHT should be used in an application very much depends on the application itself. As mentioned earlier, fast algorithms exist for both transforms, and one fast transform can be used in order to implement the other transform in an efficient way. For both the FFT and the FHT the complexity is $N \log_2 N$. An advantage of the DHT is the fact that the DHT is self-inverse, so that only one software routine or hardware device is needed for the forward and inverse FHT. For the forward and inverse FFT of a real signal, two different routines or devices are required. The DHT is somehow conceptually simpler than the DFT if the input signal is real, but all operations can be carried out with the FFT and the FHT with the same complexity.

4.8   The Hadamard and Walsh–Hadamard Transforms

The basis vectors of the *discrete Hadamard* and the *discrete Walsh–Hadamard transforms* consist of the values $\pm\alpha$; just like the Walsh functions discussed in Section 3.2.6. Both transforms are unitary. Basically they differ only in the order of the basis vectors.

We have

$$
\begin{aligned}
\boldsymbol{y} &= \boldsymbol{H}\,\boldsymbol{x}, \\
\boldsymbol{x} &= \boldsymbol{H}\,\boldsymbol{y},
\end{aligned}
\tag{4.95}
$$

where $\boldsymbol{x}$ denotes the signal, $\boldsymbol{y}$ the representation, and $\boldsymbol{H}$ the transform matrix of the Hadamard transform. $\boldsymbol{H}$ is symmetric and self-inverse:

$$
\boldsymbol{H}^T = \boldsymbol{H} = \boldsymbol{H}^{-1}.
\tag{4.96}
$$

The transform matrix of the 2×2-Hadamard transform is given by

$$
H^{(2)} = \frac{1}{\sqrt{2}} \begin{bmatrix} 1 & 1 \\ 1 & -1 \end{bmatrix}.
\tag{4.97}
$$

From this, all transform matrices $\boldsymbol{H}^{(n)}$ of size^2 $n = 2^k$, $k \in \mathbb{N}$ can be calculated recursively [133]:

$$
\boldsymbol{H}^{(2n)} = \frac{1}{\sqrt{2}} \begin{bmatrix} \boldsymbol{H}^{(n)} & \boldsymbol{H}^{(n)} \\ \boldsymbol{H}^{(n)} & -\boldsymbol{H}^{(n)} \end{bmatrix}.
\tag{4.98}
$$

The *Walsh–Hadamard transform* is obtained by taking the Hadamard transform and rearranging the basis vectors according to the number of zero crossings [66]. Somehow, this yields an order of the basis vectors with respect to their spectral properties.

---

^{2}There exist Hadamard matrices whose dimension is not a power of two.

Chapter 5

Transforms and Filters for Stochastic Processes

In this chapter, we consider the optimal processing of random signals. We start with transforms that have optimal approximation properties, in the least-squares sense, for continuous and discrete-time signals, respectively. Then we discuss the relationships between discrete transforms, optimal linear estimators, and optimal linear filters.

5.1   The Continuous-Time Karhunen–Lo`eve Transform

Among all linear transforms, the *Karhunen–Lo`eve transform* (KLT) is the one which best approximates a stochastic process in the least squares sense. Furthermore, the KLT is a signal expansion with uncorrelated coefficients. These properties make it interesting for many signal processing applications such as coding and pattern recognition. The transform can be formulated for continuous-time and discrete-time processes. In this section, we sketch the continuous-time case [81], [149]. The discrete-time case will be discussed in the next section in greater detail.

Consider a real-valued continuous-time random process $x(t)$, $a \leq t \leq b$.

We may not assume that every sample function of the random process lies in $L_2(a,b)$ and can be represented exactly via a series expansion. Therefore, a weaker condition is formulated, which states that we are looking for a series expansion that represents the stochastic process in the mean:[1]

$$x(t) = \lim_{N \to \infty} \sum_{i=1}^{N} x_i \, \varphi_i(t) \tag{5.1}$$

The "unknown" orthonormal basis $\{\varphi_i(t); \; i = 1, 2, \ldots\}$ has to be derived from the properties of the stochastic process. For this, we require that the coefficients

$$x_i = \langle \boldsymbol{x}, \boldsymbol{\varphi}_i \rangle = \int_a^b x(t) \, \varphi_i(t) \, dt \tag{5.2}$$

of the series expansion are uncorrelated. This can be expressed as

$$
\begin{aligned}
E\{x_i x_j\} &= E\{\langle \boldsymbol{x}, \boldsymbol{\varphi}_i \rangle \langle \boldsymbol{x}, \boldsymbol{\varphi}_j \rangle\} \\
&= E\left\{ \left(\int_a^b x(t) \, \varphi_i(t) \, dt \right) \cdot \left(\int_a^b x(u) \, \varphi_j(u) \, du \right) \right\} \\
&= E\left\{ \int_a^b \varphi_i(t) \int_a^b x(t) \, x(u) \, \varphi_j(u) \, du \, dt \right\} \\
&= \int_a^b \varphi_i(t) \left(\int_a^b E\{x(t) \, x(u)\} \, \varphi_j(u) \, du \right) dt \\
&\overset{!}{=} \lambda_j \, \delta_{ij}.
\end{aligned}
\tag{5.3}
$$

The kernel of the integral representation in (5.3) is the autocorrelation function

$$r_{xx}(t,u) = E\{x(t) \, x(u)\} . \tag{5.4}$$

We see that (5.3) is satisfied if

$$\lambda_j \delta_{ij} = \int_a^b \varphi_i(t) \left(\int_a^b r_{xx}(t,u) \, \varphi_j(u) \, du \right) dt. \tag{5.5}$$

Comparing (5.5) with the orthonormality relation $\delta_{ij} = \int_a^b \varphi_i(t) \, \varphi_j(t) \, dt$, we realize that

$$\int_a^b r_{xx}(t,u) \, \varphi_j(u) \, du = \lambda_j \, \varphi_j(t) \tag{5.6}$$

---

[1] l.i.m=limit in the mean[38].

must hold in order to satisfy (5.5). Thus, the solutions $\varphi_j(t)$, $j = 1, 2, \ldots$ of the integral equation (5.6) form the desired orthonormal basis. These functions are also called eigenfunctions of the integral operator in (5.6). The values λ_j, $j = 1, 2, \ldots$ are the eigenvalues. If the kernel $r_{xx}(t, u)$ is positive definite, that is, if $\int \int r_{xx}(t, u) x(t) x(u) \, dt \, du > 0$ for all $x(t) \in L_2(a, b)$, then the eigenfunctions form a complete orthonormal basis for $L_2(a, b)$. Further properties and particular solutions of the integral equation are for instance discussed in [149].

Signals can be approximated by carrying out the summation in (5.1) only for $i = 1, 2, \ldots, M$ with finite M. The mean approximation error produced thereby is the sum of those eigenvalues λ_j whose corresponding eigenfunctions are not used for the representation. Thus, we obtain an approximation with minimal mean square error if those eigenfunctions are used which correspond to the largest eigenvalues.

In practice, solving an integral equation represents a major problem. Therefore the continuous-time KLT is of minor interest with regard to practical applications. However, theoretically, that is, without solving the integral equation, this transform is an enormous help. We can describe stochastic processes by means of uncorrelated coefficients, solve estimation or recognition problems for vectors with uncorrelated components and then interpret the results for the continuous-time case.

5.2 The Discrete Karhunen–Loève Transform

We consider a real-valued zero-mean random process

$$x = \begin{bmatrix} x_1 \\ \vdots \\ x_n \end{bmatrix}, \quad x \in \mathbb{R}^n. \tag{5.7}$$

The restriction to zero-mean processes means no loss of generality, since any process z with mean m_z can be translated into a zero-mean process x by

$$x = z - m_z. \tag{5.8}$$

With an orthonormal basis $U = \{u_1, \ldots, u_n\}$, the process can be written as

$$x = U \, \alpha, \tag{5.9}$$

where the representation

$$\alpha = [\alpha_1, \ldots, \alpha_n]^T \tag{5.10}$$

is given by

$$\boldsymbol{\alpha} = \boldsymbol{U}^T \boldsymbol{x}. \tag{5.11}$$

As for the continuous-time case, we derive the KLT by demanding uncorrelated coefficients:

$$E\left\{\alpha_i \alpha_j\right\} = \lambda_j \, \delta_{ij}, \qquad i, j = 1, \ldots, n. \tag{5.12}$$

The scalars λ_j, $j = 1, \ldots, n$ are unknown real numbers with $\lambda_j \geq 0$. From (5.9) and (5.12) we obtain

$$E\left\{\boldsymbol{u}_i^T \boldsymbol{x} \, \boldsymbol{x}^T \boldsymbol{u}_j\right\} = \lambda_j \, \delta_{ij}, \qquad i, j = 1, \ldots, n. \tag{5.13}$$

With

$$\boldsymbol{R}_{xx} = E\left\{\boldsymbol{x}\boldsymbol{x}^T\right\} \tag{5.14}$$

this can be written as

$$\boldsymbol{u}_i^T \, \boldsymbol{R}_{xx} \, \boldsymbol{u}_j = \lambda_j \, \delta_{ij}, \quad i, j = 1, \ldots, n. \tag{5.15}$$

We observe that because of $\boldsymbol{u}_i^T \boldsymbol{u}_j = \delta_{ij}$, equation (5.15) is satisfied if the vectors $\boldsymbol{u}_j$, $j = 1, \ldots, n$ are solutions to the eigenvalue problem

$$\boldsymbol{R}_{xx} \, \boldsymbol{u}_j = \lambda_j \boldsymbol{u}_j, \quad j = 1, \ldots, n. \tag{5.16}$$

Since $\boldsymbol{R}_{xx}$ is a covariance matrix, the eigenvalue problem has the following properties:

1. Only real eigenvalues λ_i exist.

2. A covariance matrix is positive definite or positive semidefinite, that is, for all eigenvalues we have $\lambda_i \geq 0$.

3. Eigenvectors that belong to different eigenvalues are orthogonal to one another.

4. If multiple eigenvalues occur, their eigenvectors are linearly independent and can be chosen to be orthogonal to one another.

Thus, we see that n orthogonal eigenvectors always exist. By normalizing the eigenvectors, we obtain the orthonormal basis of the Karhunen–Loève transform.

Complex-Valued Processes. For complex-valued processes $x \in \mathbb{C}^n$, condition (5.12) becomes

$$E\left\{\alpha_i \alpha_j^*\right\} = \lambda_j \, \delta_{ij}, \ i, j = 1, \ldots, n.$$

This yields the eigenvalue problem

$$\boldsymbol{R}_{xx}\,\boldsymbol{u}_j = \lambda_j\boldsymbol{u}_j, \;\; j = 1,\ldots,n$$

with the covariance matrix

$$\boldsymbol{R}_{xx} = E\left\{\boldsymbol{xx}^H\right\}.$$

Again, the eigenvalues are real and non-negative. The eigenvectors are orthogonal to one another such that $\boldsymbol{U} = [\boldsymbol{u}_1,\ldots,\boldsymbol{u}_n]$ is unitary.

From the uncorrelatedness of the complex coefficients we cannot conclude that their real and imaginary parts are also uncorrelated; that is, $E\left\{\Re\{\alpha_i\}\,\Im\{\alpha_j\}\right\} = 0,\; i,j = 1,\ldots,n$ is not implied.

Best Approximation Property of the KLT. We henceforth assume that the eigenvalues are sorted such that $\lambda_1 \geq \ldots \geq \lambda_n$. From (5.12) we get for the variances of the coefficients:

$$E\left\{|\alpha_i|^2\right\} = \lambda_i, \qquad i = 1,\ldots,n. \tag{5.17}$$

For the mean-square error of an approximation

$$\hat{\boldsymbol{x}} = \sum_{i=1}^{m} \alpha_i\,\boldsymbol{u}_i, \quad m < n, \tag{5.18}$$

we obtain

$$
\begin{aligned}
E\left\{\|\boldsymbol{x} - \hat{\boldsymbol{x}}\|^2\right\} &= E\left\{\left\|\sum_{i=m+1}^{n}\alpha_i\boldsymbol{u}_i\right\|^2\right\} \\
&= \sum_{i=m+1}^{n} E\left\{|\alpha_i|^2\right\} \qquad\qquad (5.19) \\
&= \sum_{i=m+1}^{n} \lambda_i.
\end{aligned}
$$

It becomes obvious that an approximation with those eigenvectors $\boldsymbol{u}_1,\ldots,\boldsymbol{u}_m$, which belong to the largest eigenvectors leads to a minimal error.

In order to show that the KLT indeed yields the smallest possible error among all orthonormal linear transforms, we look at the maximization of $\sum_{i=1}^{m} E\left\{|\alpha_i|\right\}$ under the condition $\|\boldsymbol{u}_i\| = 1$. With $\alpha_i = \boldsymbol{u}_i^H\boldsymbol{x}$ this means

$$\sum_{i=1}^{m} E\left\{\boldsymbol{u}_i^H\boldsymbol{xx}^H\boldsymbol{u}_i\right\} - \gamma_i\boldsymbol{u}_i^H\boldsymbol{u}_i = \sum_{i=1}^{m}\boldsymbol{u}_i^H\boldsymbol{R}_{xx}\boldsymbol{u}_i - \gamma_i\boldsymbol{u}_i^H\boldsymbol{u}_i \overset{!}{=} \max, \tag{5.20}$$
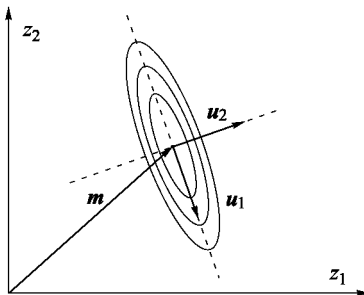
Figure 5.1. Contour lines of the pdf of a process $z = [z_1, z_2]^T$.

where γ_i are Lagrange multipliers. Setting the gradient to zero yields

$$R_{xx} u_i = \gamma_i u_i, \qquad (5.21)$$

which is nothing but the eigenvalue problem (5.16) with $\gamma_i = \lambda_i$.

Figure 5.1 gives a geometric interpretation of the properties of the KLT. We see that u_1 points towards the largest deviation from the center of gravity m.

Minimal Geometric Mean Property of the KLT.   For any positive definite matrix $X = X_{ij}$, $i, j = 1, \ldots, n$ the following inequality holds [7]:

$$\det \{ X \} \le \prod_{k=1}^{n} X_{kk}. \qquad (5.22)$$

Equality is given if X is diagonal. Since the KLT leads to a diagonal covariance matrix of the representation, this means that the KLT leads to random variables with a minimal geometric mean of the variances. From this, again, optimal properties in signal coding can be concluded [76].

The KLT of White Noise Processes.   For the special case that R_{xx} is the covariance matrix of a white noise process with

$$R_{xx} = \sigma^2 \, I$$

we have

$$\lambda_1 = \lambda_2 = \ldots = \lambda_n = \sigma^2.$$

Thus, the KLT is not unique in this case. Equation (5.19) shows that a white noise process can be optimally approximated with any orthonormal basis.

Relationships between Covariance Matrices. In the following we will briefly list some relationships between covariance matrices. With

$$\mathbf{\Lambda} = E\left\{\boldsymbol{\alpha}\ \boldsymbol{\alpha}^H\right\} = \begin{bmatrix} \lambda_1 & & \mathbf{0} \\ & \ddots & \\ \mathbf{0} & & \lambda_n \end{bmatrix}, \tag{5.23}$$

we can write (5.15) as

$$\mathbf{\Lambda} = \boldsymbol{U}^H \boldsymbol{R}_{xx} \boldsymbol{U}. \tag{5.24}$$

Observing $\boldsymbol{U}^H = \boldsymbol{U}^{-1}$, we obtain

$$\boldsymbol{R}_{xx} = \boldsymbol{U}\,\mathbf{\Lambda}\,\boldsymbol{U}^H. \tag{5.25}$$

Assuming that all eigenvalues are larger than zero, $\mathbf{\Lambda}^{-1}$ is given by

$$\mathbf{\Lambda}^{-1} = \begin{bmatrix} \frac{1}{\lambda_1} & & \mathbf{0} \\ & \ddots & \\ \mathbf{0} & & \frac{1}{\lambda_n} \end{bmatrix} = \boldsymbol{U}^H \boldsymbol{R}_{xx}^{-1} \boldsymbol{U}. \tag{5.26}$$

Finally, for $\boldsymbol{R}_{xx}^{-1}$ we obtain

$$\boldsymbol{R}_{xx}^{-1} = \boldsymbol{U}\mathbf{\Lambda}^{-1}\boldsymbol{U}^H. \tag{5.27}$$

Application Example. In pattern recognition it is important to classify signals by means of a few concise features. The signals considered in this example are taken from inductive loops embedded in the pavement of a highway in order to measure the change of inductivity while vehicles pass over them. The goal is to discriminate different types of vehicle (car, truck, bus, etc.). In the following, we will consider the two groups car and truck. After appropriate pre-processing (normalization of speed, length, and amplitude) we obtain the measured signals shown in Figure 5.2, which are typical examples of the two classes. The stochastic processes considered are z_1 (car) and z_2 (truck). The realizations are denoted as ${}^i\mathbf{z}_1$, ${}^i\mathbf{z}_2$, $i = 1 \ldots N$.

In a first step, zero-mean processes are generated:

$$\begin{aligned} \boldsymbol{x}_1 &= \boldsymbol{z}_1 - \boldsymbol{m}_1, \\ \boldsymbol{x}_2 &= \boldsymbol{z}_2 - \boldsymbol{m}_2. \end{aligned} \tag{5.28}$$

The mean values can be estimated by

$$\boldsymbol{m}_1 = E\left\{\boldsymbol{z}_1\right\} \approx \frac{1}{N}\sum_{i=1}^{N} {}^i\mathbf{z}_1 \tag{5.29}$$
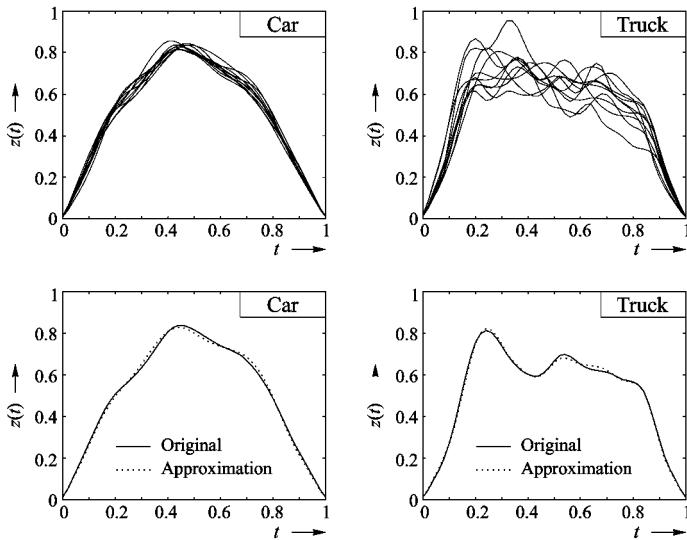
Figure 5.2. Examples of sample functions; (a) typical signal contours; (b) two sample functions and their approximations.

and

$$m_2 = E\{z_2\} \approx \frac{1}{N} \sum_{i=1}^{N} {}^i z_2. \tag{5.30}$$

Observing the *a priori* probabilities of the two classes, p_1 and p_2, a process

$$x = p_1 x_1 + p_2 x_2 \tag{5.31}$$

can be defined. The covariance matrix R_{xx} can be estimated as

$$R_{xx} = E\{xx^T\} \approx \frac{p_1}{N+1} \sum_{i=1}^{N} {}^i x_1 \, {}^i x_1^T + \frac{p_2}{N+1} \sum_{i=1}^{N} {}^i x_2 \, {}^i x_2^T, \tag{5.32}$$

where ${}^i x_1$ and ${}^i x_2$ are realizations of the zero-mean processes x_1 and x_2, respectively.

The first ten eigenvalues computed from a training set are:

λ_1	λ_2	λ_3	λ_4	λ_5	λ_6	λ_7	λ_8	λ_9	λ_{10}
212923	55460	20559	15790	10230	5262	5036	3139	2551	968

We see that by using only a few eigenvectors a good approximation can be expected. To give an example, Figure 5.2 shows two signals and their

approximations

$$
\begin{aligned}
{}^1\hat{\mathbf{z}}_1 &= \mathbf{U}\mathbf{U}^T({}^1\mathbf{z}_1 - \mathbf{m}_1) + \mathbf{m}_1, \\
{}^1\hat{\mathbf{z}}_2 &= \mathbf{U}\mathbf{U}^T({}^1\mathbf{z}_2 - \mathbf{m}_2) + \mathbf{m}_2
\end{aligned}
\tag{5.33}
$$

with the basis $\{\mathbf{u}_1, \mathbf{u}_2, \mathbf{u}_3, \mathbf{u}_4\}$.

In general, the optimality and usefulness of extracted features for discrimination is highly dependent on the algorithm that is used to carry out the discrimination. Thus, the feature extraction method described in this example is not meant to be optimal for all applications. However, it shows how a high proportion of information about a process can be stored within a few features. For more details on classification algorithms and further transforms for feature extraction, see [59, 44, 167, 58].

5.3   The KLT of Real-Valued AR(1) Processes

An *autoregressive process* of order p (AR(p) process) is generated by exciting a recursive filter of order p with a zero-mean, stationary white noise process. The filter has the system function

$$
H(z) = \frac{1}{1 - \sum\limits_{i=1}^{p} \rho(i)\, z^{-i}}, \qquad \rho(p) \neq 0.
\tag{5.34}
$$

Thus, an AR(p) process $x(n)$ is described by the difference equation

$$
x(n) = w(n) + \sum_{i=1}^{p} \rho(i)\, x(n-i),
\tag{5.35}
$$

where $w(n)$ is white noise. The AR(1) process with difference equation

$$
x(n) = w(n) + \rho\, x(n-1)
\tag{5.36}
$$

is often used as a simple model. It is also known as a *first-order Markov process*. From (5.36) we obtain by recursion:

$$
x(n) = \sum_{i=0}^{\infty} \rho^i\, w(n-i).
\tag{5.37}
$$

For determining the variance of the process $x(n)$, we use the properties

$$
m_w = E\{w(n)\} = 0 \quad \rightarrow \quad m_x = E\{x(n)\} = 0
\tag{5.38}
$$

and

$$r_{ww}(m) = E\{w(n)w(n+m)\} = \sigma^2 \delta_{m0}, \tag{5.39}$$

where δ_{m0} is the Kronecker delta. Supposing $|\rho| < 1$, we get

$$
\begin{aligned}
\sigma_x^2 &= E\{|x(n)|^2\} \\
&= \sum_{i=0}^{\infty}\sum_{j=0}^{\infty} \rho^i \, \rho^j \, E\{w(n-i)w(n-j)\} \\
&= \sigma^2 \sum_{i=0}^{\infty} \rho^{2i} \\
&= \frac{\sigma^2}{1-\rho^2}.
\end{aligned}
\tag{5.40}
$$

For the autocorrelation sequence we obtain

$$
\begin{aligned}
r_{xx}(m) &= E\{x(n)x(n+m)\} \\
&= \sum_{i=0}^{\infty}\sum_{j=0}^{\infty} \rho^i \, \rho^j \, E\{w(n-i)w(n-j+m)\} \\
&= \sigma^2 \rho^{|m|} \sum_{i=0}^{\infty} \rho^{2i} \\
&= \frac{\sigma^2}{1-\rho^2} \, \rho^{|m|}.
\end{aligned}
\tag{5.41}
$$

We see that the autocorrelation sequence is infinitely long. However, henceforth only the values $r_{xx}(-N+1), \ldots, r_{xx}(N-1)$ shall be considered. Because of the stationarity of the input process, the covariance matrix of the AR(1) process is a Toeplitz matrix. It is given by

$$
\boldsymbol{R}_{xx} = \frac{\sigma^2}{1-\rho^2}
\begin{bmatrix}
1 & \rho & \rho^2 & \cdots & \rho^{N-1} \\
\rho & 1 & \rho & & \vdots \\
\rho^2 & \rho & \ddots & \ddots & \vdots \\
\vdots & & \ddots & \ddots & \rho \\
\rho^{N-1} & \cdots & \cdots & \rho & 1
\end{bmatrix}.
\tag{5.42}
$$

The eigenvectors of $\boldsymbol{R}_{xx}$ form the basis of the KLT. For real signals and even N, the eigenvalues λ_k, $k = 0, \ldots, N-1$ and the eigenvectors were analytically derived by Ray and Driver [123]. The eigenvalues are

$$\lambda_k = \frac{1}{1 - 2\,\rho\,\cos(\alpha_k) + \rho^2}, \qquad k = 0, \ldots, N-1, \tag{5.43}$$

where $\alpha_k, \; k = 0, \ldots, N-1$ denotes the real positive roots of

$$\tan(N\alpha_k) = -\frac{(1-\rho^2)\sin(\alpha_k)}{\cos(\alpha_k) - 2\rho + \rho \, \cos(\alpha_k)}. \tag{5.44}$$

The components of the eigenvectors $u_k, \; k = 0, \ldots, N-1$ are given by

$$u_k(n) = \frac{2}{N+\lambda_k} \, \sin\left(\alpha_k \left(n - \frac{N-1}{2}\right) + (k+1)\frac{\pi}{2}\right), \qquad n, k = 0, \ldots, N-1. \tag{5.45}$$

5.4 Whitening Transforms

In this section we are concerned with the problem of transforming a colored noise process into a white noise process. That is, the coefficients of the representation should not only be uncorrelated (as for the KLT), they should also have the same variance. Such transforms, known as whitening transforms, are mainly applied in signal detection and pattern recognition, because they lead to a convenient process representation with additive white noise.

Let n be a process with covariance matrix

$$\boldsymbol{R}_{nn} = E\left\{\boldsymbol{nn}^H\right\} \quad \neq \quad \sigma^2 \boldsymbol{I}. \tag{5.46}$$

We wish to find a linear transform $\boldsymbol{T}$ which yields an equivalent process

$$\tilde{\boldsymbol{n}} = \boldsymbol{Tn} \tag{5.47}$$

with

$$E\left\{\tilde{\boldsymbol{n}}\tilde{\boldsymbol{n}}^H\right\} = E\left\{\boldsymbol{Tnn}^H\boldsymbol{T}^H\right\} = \boldsymbol{T}\boldsymbol{R}_{nn}\boldsymbol{T}^H = \boldsymbol{I}. \tag{5.48}$$

We already see that the transform cannot be unique since by multiplying an already computed matrix $\boldsymbol{T}$ with an arbitrary unitary matrix, property (5.48) is preserved.

The covariance matrix can be decomposed as follows (KLT):

$$\boldsymbol{R}_{nn} = \boldsymbol{U\Lambda U}^H = \boldsymbol{U\Sigma\Sigma}^H\boldsymbol{U}^H. \tag{5.49}$$

For $\boldsymbol{\Lambda}$ and $\boldsymbol{\Sigma}$ we have

$$\boldsymbol{\Lambda} = \begin{bmatrix} \lambda_1 & & \\ & \ddots & \\ & & \lambda_N \end{bmatrix}, \qquad \boldsymbol{\Sigma} = \begin{bmatrix} \sqrt{\lambda_1} & & \\ & \ddots & \\ & & \sqrt{\lambda_N} \end{bmatrix}.$$

Possible transforms are

$$T = \Sigma^{-1} U^H \tag{5.50}$$

or

$$T = U \Sigma^{-1} U^H. \tag{5.51}$$

This can easily be verified by substituting (5.50) into (5.48):

$$E\left\{\tilde{n}\tilde{n}^H\right\} = T R_{nn} T^H = \Sigma^{-1} \underbrace{U^H U}_{I} \Sigma \Sigma^H \underbrace{U^H U}_{I} \Sigma^{H^{-1}} = I. \tag{5.52}$$

Alternatively, we can apply the *Cholesky decomposition*

$$R_{nn} = L L^H, \tag{5.53}$$

where L is a lower triangular matrix. The whitening transform is

$$T = L^{-1}. \tag{5.54}$$

For the covariance matrix we again have

$$E\left\{\tilde{n}\tilde{n}^H\right\} = T R_{nn} T^H = L^{-1} L L^H L^{H^{-1}} = I. \tag{5.55}$$

In signal analysis, one often encounters signals of the form

$$r = s + n, \tag{5.56}$$

where s is a known signal and n is an additive colored noise processes. The whitening transforms transfer (5.56) into an equivalent model

$$\tilde{r} = \tilde{s} + \tilde{n} \tag{5.57}$$

with

$$\begin{aligned}
\tilde{r} &= T r, \\
\tilde{s} &= T s, \\
\tilde{n} &= T n,
\end{aligned} \tag{5.58}$$

where $\tilde{n}$ is a white noise process of variance $\sigma_{\tilde{n}}^2 = 1$.

5.5 Linear Estimation

In estimation the goal is to determine a set of parameters as precisely as possible from noisy observations. We will focus on the case where the estimators are linear, that is, the estimates for the parameters are computed as linear combinations of the observations. This problem is closely related to the problem of computing the coefficients of a series expansion of a signal, as described in Chapter 3.

Linear methods do not require precise knowledge of the noise statistics; only moments up to the second order are taken into account. Therefore they are optimal only under the linearity constraint, and, in general, non-linear estimators with better properties may be found. However, linear estimators constitute the globally optimal solution as far as Gaussian processes are concerned [149].

5.5.1 Least-Squares Estimation

We consider the model

$$r = S\, a + n, \tag{5.59}$$

where r is our observation, a is the parameter vector in question, and n is a noise process. Matrix S can be understood as a basis matrix that relates the parameters to the clean observation Sa.

The requirement to have an unbiased estimate can be written as

$$E\{\hat{a}(r)|\mathbf{a}\} = \mathbf{a}, \tag{5.60}$$

where $\mathbf{a}$ is understood as an arbitrary non-random parameter vector. Because of the additive noise, the estimates $\hat{a}(r)|\mathbf{a}$ again form a random process.

The linear estimation approach is given by

$$\hat{a}(r) = A\, r. \tag{5.61}$$

If we assume zero-mean noise n, matrix A must satisfy

$$A\, S = I \tag{5.62}$$

in order to ensure unbiased estimates. This is seen from

$$
\begin{aligned}
E\left\{\hat{a}(r)|\mathbf{a}\right\} &= E\left\{A\ r|\mathbf{a}\right\} \\
&= A\ E\left\{r|\mathbf{a}\right\} \\
&= A\ E\left\{Sa+n\right\} \\
&= A\ S\ \mathbf{a} \\
&\overset{!}{=} \mathbf{a}.
\end{aligned}
\tag{5.63}
$$

The *generalized least-squares estimator* is derived from the criterion

$$
\left\| \mathbf{r} - S\boldsymbol{\alpha} \right\| \Big|_{\boldsymbol{\alpha}\,=\,\hat{\mathbf{a}}(\mathbf{r})} \overset{!}{=} \min, \tag{5.64}
$$

where an arbitrary weighting matrix G may be involved in the definition of the inner product that induces the norm in (5.64). Here the observation $\mathbf{r}$ is considered as a single realization of the stochastic process r. Making use of the fact that orthogonal projections yield a minimal approximation error, we get

$$
\hat{\mathbf{a}}(\mathbf{r}) = [S^H G S]^{-1} S^H G \mathbf{r} \tag{5.65}
$$

according to (3.95). Assuming that $[S^H G S]^{-1}$ exists, the requirement (5.65) to have an unbiased estimator is satisfied for arbitrary weighting matrices, as can easily be verified.

If we choose $G = I$, we speak of a *least-squares estimator*. For weighting matrices $G \neq I$, we speak of a *generalized least-squares estimator*. However, the approach leaves open the question of how a suitable G is found.

5.5.2   The Best Linear Unbiased Estimator (BLUE)

As will be shown below, choosing $G = R_{nn}^{-1}$, where

$$
R_{nn} = E\left\{nn^H\right\} \tag{5.66}
$$

is the correlation matrix of the noise, yields an unbiased estimator with minimal variance. The estimator, which is known as the *best linear unbiased estimator* (BLUE), then is

$$
A = [S^H R_{nn}^{-1} S]^{-1} S^H R_{nn}^{-1}. \tag{5.67}
$$

The estimate is given by

$$
\hat{a}(r) = [S^H R_{nn}^{-1} S]^{-1} S^H R_{nn}^{-1}\ r. \tag{5.68}
$$

The variances of the individual estimates can be found on the main diagonal of the covariance matrix of the error $e = \hat{a}(r) - \mathbf{a}$, given by

$$\mathbf{R}_{ee} = [\mathbf{S}^H \mathbf{R}_{nn}^{-1} \mathbf{S}]^{-1}. \tag{5.69}$$

Proof of (5.69) and the optimality of (5.67). First, observe that with $\mathbf{AS} = \mathbf{I}$ we have

$$\begin{aligned}
\hat{a}(r) - \mathbf{a}|\mathbf{a} &= \mathbf{A}\,\mathbf{S}\,\mathbf{a} + \mathbf{A}\,\mathbf{n} - \mathbf{a} \\
&= \mathbf{A}\,\mathbf{n}.
\end{aligned} \tag{5.70}$$

Thus,

$$\begin{aligned}
\mathbf{R}_{ee} &= \mathbf{A}E\{\mathbf{n}\mathbf{n}^H\}\mathbf{A}^H \\
&= \mathbf{A}\mathbf{R}_{nn}\mathbf{A}^H \\
&= [\mathbf{S}^H\mathbf{R}_{nn}^{-1}\mathbf{S}]^{-1}\mathbf{S}^H\mathbf{R}_{nn}^{-1}\mathbf{R}_{nn}\mathbf{R}_{nn}^{-1}\mathbf{S}[\mathbf{S}^H\mathbf{R}_{nn}^{-1}\mathbf{S}]^{-1} \\
&= [\mathbf{S}^H\mathbf{R}_{nn}^{-1}\mathbf{S}]^{-1}.
\end{aligned} \tag{5.71}$$

In order to see whether $\mathbf{A}$ according to (5.67) is optimal, an estimation

$$\tilde{a}(r) = \tilde{\mathbf{A}}\,r \tag{5.72}$$

with

$$\tilde{\mathbf{A}} = \mathbf{A} + \mathbf{D} \tag{5.73}$$

will be considered. The unbiasedness constraint requires that

$$\tilde{\mathbf{A}}\,\mathbf{S} = \mathbf{I}. \tag{5.74}$$

Because of $\mathbf{A}\,\mathbf{S} = \mathbf{I}$ this means

$$\mathbf{D}\,\mathbf{S} = \mathbf{0} \qquad \text{(null matrix)}. \tag{5.75}$$

For the covariance matrix of the error $\tilde{e}(r) = \tilde{a}(r) - \mathbf{a}$ we obtain

$$\begin{aligned}
\mathbf{R}_{\tilde{e}\tilde{e}} &= \tilde{\mathbf{A}}\mathbf{R}_{nn}\tilde{\mathbf{A}}^H \\
&= [\mathbf{A} + \mathbf{D}]\mathbf{R}_{nn}[\mathbf{A} + \mathbf{D}]^H \\
&= \mathbf{A}\mathbf{R}_{nn}\mathbf{A}^H + \mathbf{A}\mathbf{R}_{nn}\mathbf{D}^H + \mathbf{D}\mathbf{R}_{nn}\mathbf{A}^H + \mathbf{D}\mathbf{R}_{nn}\mathbf{D}^H.
\end{aligned} \tag{5.76}$$

With

$$(AR_{nn}D^H)^H = DR_{nn}A^H \;=\; DR_{nn}R_{nn}^{-1}S[S^H R_{nn}^{-1}S]^{-1}$$
$$= \underbrace{DS}_{0}[S^H R_{nn}^{-1}S]^{-1} \tag{5.77}$$
$$= \; 0$$

(5.76) reduces to

$$R_{\tilde{e}\tilde{e}} = AR_{nn}A^H + DR_{nn}D^H. \tag{5.78}$$

We see that $R_{\tilde{e}\tilde{e}}$ is the sum of two non-negative definite expressions so that minimal main diagonal elements of $R_{\tilde{e}\tilde{e}}$ are yielded for $D = 0$ and thus for A according to (5.67). $\square$

In the case of a white noise process n, (5.68) reduces to

$$\hat{a}(r) = [S^H S]^{-1} S^H r. \tag{5.79}$$

Otherwise the weighting with $G = R_{nn}^{-1}$ can be interpreted as an implicit whitening of the noise. This can be seen by using the Cholesky decomposition $R_{nn} = LL^H$ and and by rewriting the model as

$$\tilde{r} = \tilde{S}a + \tilde{n}, \tag{5.80}$$

where

$$\tilde{r} = L^{-1}r, \;\; \tilde{S} = L^{-1}S, \;\; \tilde{n} = L^{-1}n. \tag{5.81}$$

The transformed process $\tilde{n}$ is a white noise process. The equivalent estimator then is

$$\hat{a}(\tilde{r}) = [\tilde{S}^H \tilde{S}]^{-1} \tilde{S}^H \, \tilde{r}. \tag{5.82}$$

5.5.3 Minimum Mean Square Error Estimation

The advantage of the linear estimators considered in the previous section is their unbiasedness. If we dispense with this property, estimates with smaller mean square error may be found. We will start the discussion on the assumptions

$$E\{r\} = 0, \qquad E\{a\} = 0. \tag{5.83}$$

Again, the linear estimator is described by a matrix A:

$$\hat{a}(r) = A \, r. \tag{5.84}$$

Here, r is somehow dependent on a, but the inner relationship between r and a need not be known however. The matrix A which yields minimal main diagonal elements of the correlation matrix of the estimation error $e = a - \hat{a}$ is called the *minimum mean square error (MMSE) estimator*.

In order to find the optimal A, observe that

$$\begin{aligned} R_{ee} &= E\left\{[\hat{a} - a][\hat{a} - a]^H\right\} \\ &= E\left\{aa^H\right\} - E\left\{\hat{a}a^H\right\} - E\left\{a\hat{a}^H\right\} + E\left\{\hat{a}\hat{a}^H\right\}. \end{aligned} \tag{5.85}$$

Substituting (5.84) into (5.85) yields

$$R_{ee} = R_{aa} - AR_{ar} - R_{ra}A^H + AR_{rr}A^H \tag{5.86}$$

with

$$\begin{aligned} R_{aa} &= E\left\{aa^H\right\}, \\ R_{ar} &= R_{ra}^H = E\left\{ra^H\right\}, \\ R_{rr} &= E\left\{rr^H\right\}. \end{aligned} \tag{5.87}$$

Assuming the existence of R_{rr}^{-1}, (5.86) can be extended by

$$R_{ra}R_{rr}^{-1}R_{ar} - R_{ra}R_{rr}^{-1}R_{ar}$$

and be re-written as

$$R_{ee} = \left[A - R_{ra}R_{rr}^{-1}\right]R_{rr}\left[A^H - R_{rr}^{-1}R_{ar}\right] - R_{ra}R_{rr}^{-1}R_{ar} + R_{aa}. \tag{5.88}$$

Clearly, R_{ee} has positive diagonal elements. Since only the first term on the right-hand side of (5.88) is dependent on A, we have a minimum of the diagonal elements of R_{ee} for

$$A = R_{ra}R_{rr}^{-1}. \tag{5.89}$$

The correlation matrix of the estimation error is then given by

$$R_{ee} = R_{aa} - R_{ra}R_{rr}^{-1}R_{ar}. \tag{5.90}$$

Orthogonality Principle. In Chapter 3 we saw that approximations $\hat{x}$ of signals x are obtained with minimal error if the error $\hat{x} - x$ is orthogonal to $\hat{x}$. A similar relationship holds between parameter vectors a and their MMSE estimates. With A according to (5.89) we have

$$R_{ra} = A\ R_{rr}, \quad \text{i.e.} \quad E\left\{ar^H\right\} = A\ E\left\{rr^H\right\}. \tag{5.91}$$

This means that the following orthogonality relations hold:

$$
\begin{aligned}
E\left\{[\hat{a} - a]\,\hat{a}^H\right\} &= R_{\hat{a}\hat{a}} - R_{\hat{a}a} \\
&= [AR_{rr} - R_{ra}]\,A^H \qquad (5.92)\\
&= 0.
\end{aligned}
$$

With $A\,r = \hat{a}$ the right part of (5.91) can also be written as

$$
E\left\{ar^H\right\} = E\left\{\hat{a}r^H\right\}, \qquad (5.93)
$$

which yields

$$
E\left\{[\hat{a} - a]\,r^H\right\} = 0. \qquad (5.94)
$$

The relationship expressed in (5.94) is referred to as the *orthogonality principle*. The orthogonality principle states that we get an MMSE estimate if the error $\hat{a}(r) - a$ is uncorrelated to all components of the input vector r used for computing $\hat{a}(r)$.

Singular Correlation Matrix. There are cases where the correlation matrix R_{rr} becomes singular and the linear estimator cannot be written as

$$
A = R_{ra}\,R_{rr}^{-1}. \qquad (5.95)
$$

A more general solution, which involves the replacement of the inverse by the pseudoinverse, is

$$
A = R_{ra}\,R_{rr}^{+}. \qquad (5.96)
$$

In order to show the optimality of (5.96), the estimator

$$
\tilde{A} = A + D \qquad (5.97)
$$

with A according to (5.96) and an arbitrary matrix D is considered. Using the properties of the pseudoinverse, we derive from (5.97) and (5.86):

$$
\begin{aligned}
R_{ee} &= R_{aa} - \tilde{A}R_{ar} - R_{ra}\tilde{A}^H + \tilde{A}R_{rr}\tilde{A}^H \\
&= R_{aa} - R_{ra}R_{rr}^{+}R_{ar} + DR_{rr}^{+}D^H.
\end{aligned} \qquad (5.98)
$$

Since R_{rr}^{+} is at least positive semidefinite, we get a minimum of the diagonal elements of R_{ee} for $D = 0$, and (5.96) constitutes one of the optimal solutions.

Additive Uncorrelated Noise. So far, nothing has been said about possible dependencies between a and the noise contained in r. Assuming that

$$
r = S\,a + n, \qquad (5.99)
$$

where n is an additive, uncorrelated noise process, we have

$$\begin{aligned} \boldsymbol{R}_{ra} &= \boldsymbol{R}_{ar}^H = \boldsymbol{R}_{aa}\,\boldsymbol{S}^H, \\ \boldsymbol{R}_{rr} &= \boldsymbol{S}\,\boldsymbol{R}_{aa}\,\boldsymbol{S}^H + \boldsymbol{R}_{nn}, \end{aligned} \qquad (5.100)$$

and $\boldsymbol{A}$ according to (5.89) becomes

$$\boldsymbol{A} = \boldsymbol{R}_{aa}\boldsymbol{S}^H \left[\boldsymbol{S}\boldsymbol{R}_{aa}\boldsymbol{S}^H + \boldsymbol{R}_{nn}\right]^{-1}. \qquad (5.101)$$

Alternatively, $\boldsymbol{A}$ can be written as

$$\boldsymbol{A} = \left[\boldsymbol{R}_{aa}^{-1} + \boldsymbol{S}^H \boldsymbol{R}_{nn}^{-1}\boldsymbol{S}\right]^{-1} \boldsymbol{S}^H \boldsymbol{R}_{nn}^{-1}. \qquad (5.102)$$

This is verified by equating (5.101) and (5.102), and by multiplying the obtained expression with $[\boldsymbol{R}_{aa}^{-1}+\boldsymbol{S}^H \boldsymbol{R}_{nn}^{-1}\boldsymbol{S}]$ from the left and with $[\boldsymbol{S}\boldsymbol{R}_{aa}\boldsymbol{S}^H + \boldsymbol{R}_{nn}]$ from the right, respectively:

$$\left[\boldsymbol{R}_{aa}^{-1} + \boldsymbol{S}^H \boldsymbol{R}_{nn}^{-1}\boldsymbol{S}\right] \boldsymbol{R}_{aa}\boldsymbol{S}^H = \boldsymbol{S}^H \boldsymbol{R}_{nn}^{-1}[\boldsymbol{S}\boldsymbol{R}_{aa}\boldsymbol{S}^H + \boldsymbol{R}_{nn}].$$

The equality of both sides is easily seen. The matrices to be inverted in (5.102), except $\boldsymbol{R}_{nn}$, typically have a much smaller dimension than those in (5.101). If the noise is white, $\boldsymbol{R}_{nn}^{-1}$ can be immediately stated, and (5.102) is advantageous in terms of computational cost.

For $\boldsymbol{R}_{ee}$ we get from (5.89), (5.90), (5.100) and (5.102):

$$\begin{aligned} \boldsymbol{R}_{ee} &= \boldsymbol{R}_{aa} - \boldsymbol{A}\boldsymbol{R}_{ar} \\ &= \boldsymbol{R}_{aa} - \left[\boldsymbol{R}_{aa}^{-1} + \boldsymbol{S}^H \boldsymbol{R}_{nn}^{-1}\boldsymbol{S}\right]^{-1} \boldsymbol{S}^H \boldsymbol{R}_{nn}^{-1}\boldsymbol{S}\boldsymbol{R}_{aa}. \end{aligned} \qquad (5.103)$$

Multiplying (5.103) with $[\boldsymbol{R}_{aa}^{-1} + \boldsymbol{S}^H \boldsymbol{R}_{nn}^{-1}\boldsymbol{S}]$ from the left yields

$$\begin{aligned} \left[\boldsymbol{R}_{aa}^{-1} + \boldsymbol{S}^H \boldsymbol{R}_{nn}^{-1}\boldsymbol{S}\right] \boldsymbol{R}_{ee} &= \left[\boldsymbol{R}_{aa}^{-1} + \boldsymbol{S}^H \boldsymbol{R}_{nn}^{-1}\boldsymbol{S}\right] \boldsymbol{R}_{aa} - \boldsymbol{S}^H \boldsymbol{R}_{nn}^{-1}\boldsymbol{S}\boldsymbol{R}_{aa} \\ &= \boldsymbol{I}, \end{aligned} \qquad (5.104)$$

so that the following expression is finally obtained:

$$\boldsymbol{R}_{ee} = \left[\boldsymbol{R}_{aa}^{-1} + \boldsymbol{S}^H \boldsymbol{R}_{nn}^{-1}\boldsymbol{S}\right]^{-1}. \qquad (5.105)$$

Equivalent Estimation Problems. We partition $\boldsymbol{A}$ and $\boldsymbol{a}$ into

$$\boldsymbol{a} = \begin{bmatrix} \boldsymbol{a}_1 \\ \boldsymbol{a}_2 \end{bmatrix}, \qquad \boldsymbol{A} = \begin{bmatrix} \boldsymbol{A}_1 \\ \boldsymbol{A}_2 \end{bmatrix}, \qquad (5.106)$$

such that

$$\begin{bmatrix} \hat{a}_1(r) \\ \hat{a}_2(r) \end{bmatrix} = \begin{bmatrix} A_1 \\ A_2 \end{bmatrix} r. \tag{5.107}$$

If we assume that the processes a_1, a_2 and n are independent of one another, the covariance matrix R_{aa} and its inverse R_{aa}^{-1} have the form

$$R_{aa} = \begin{bmatrix} R_{a_1 a_1} & 0 \\ 0 & R_{a_2 a_2} \end{bmatrix}, \quad R_{aa}^{-1} = \begin{bmatrix} R_{a_1 a_1}^{-1} & 0 \\ 0 & R_{a_2 a_2}^{-1} \end{bmatrix}, \tag{5.108}$$

and A according to (5.102) can be written as

$$A = \begin{bmatrix} A_1 \\ A_2 \end{bmatrix} = \begin{bmatrix} S_1^H R_{nn}^{-1} S_1 + R_{a_1 a_1}^{-1} & S_1^H R_{nn}^{-1} S_2 \\ S_2^H R_{nn}^{-1} S_1 & S_2^H R_{nn}^{-1} S_2 + R_{a_2 a_2}^{-1} \end{bmatrix}^{-1} \begin{bmatrix} S_1^H R_{nn}^{-1} \\ S_2^H R_{nn}^{-1} \end{bmatrix}, \tag{5.109}$$

where $S = [S_1, S_2]$. Applying the matrix equation

$$\begin{bmatrix} \mathcal{E} & \mathcal{F} \\ \mathcal{G} & \mathcal{H} \end{bmatrix}^{-1} = \begin{bmatrix} \mathcal{E}^{-1} + \mathcal{E}^{-1} \mathcal{F} \mathcal{D}^{-1} \mathcal{G} \mathcal{E}^{-1} & -\mathcal{E}^{-1} \mathcal{F} \mathcal{D}^{-1} \\ -\mathcal{D}^{-1} \mathcal{G} \mathcal{E}^{-1} & \mathcal{D}^{-1} \end{bmatrix}$$

$$\mathcal{D} = \mathcal{H} - \mathcal{G} \mathcal{E}^{-1} \mathcal{F} \tag{5.110}$$

yields

$$A_1 = [S_1^H R_{n_1 n_1}^{-1} S_1 + R_{a_1 a_1}^{-1}]^{-1} S_1^H R_{n_1 n_1}^{-1}, \tag{5.111}$$

$$A_2 = [S_2^H R_{n_2 n_2}^{-1} S_2 + R_{a_2 a_2}^{-1}]^{-1} S_2^H R_{n_2 n_2}^{-1} \tag{5.112}$$

with

$$R_{n_1 n_1} = R_{nn} + S_2 R_{a_2 a_2} S_2^H, \tag{5.113}$$

$$R_{n_2 n_2} = R_{nn} + S_1 R_{a_1 a_1} S_1^H. \tag{5.114}$$

The inverses $R_{n_1 n_1}^{-1}$ and $R_{n_2 n_2}^{-1}$ can be written as

$$R_{n_1 n_1}^{-1} = \left[R_{nn}^{-1} - R_{nn}^{-1} S_2 \left(S_2^H R_{nn}^{-1} S_2 + R_{a_2 a_2}^{-1} \right)^{-1} S_2^H R_{nn}^{-1} \right], \tag{5.115}$$

$$R_{n_2 n_2}^{-1} = \left[R_{nn}^{-1} - R_{nn}^{-1} S_1 \left(S_1^H R_{nn}^{-1} S_1 + R_{a_1 a_1}^{-1} \right)^{-1} S_1^H R_{nn}^{-1} \right]. \tag{5.116}$$

Equations (5.111) and (5.112) describe estimations of a_1 and a_2 in the models

$$r = S_1 a_1 + n_1, \tag{5.117}$$

$$r = S_2 a_2 + n_2 \tag{5.118}$$

with

$$\begin{aligned} n_1 &= S_2 a_2 + n, \\ n_2 &= S_1 a_1 + n. \end{aligned} \tag{5.119}$$

Thus, each parameter to be estimated can be understood as noise in the estimation of the remaining parameters. An exception is given if $S_1^H R_{nn}^{-1} S_2 = 0$, which means that S_1 and S_2 are orthogonal to each other with respect to the weighting matrix R_{nn}^{-1}. Then we get

$$A_1 = [S_1^H R_{nn}^{-1} S_1 + R_{a_1 a_1}^{-1}]^{-1} S_1^H R_{nn}^{-1}$$

and

$$R_{e_1 e_1} = [S_1^H R_{nn}^{-1} S_1 + R_{a_1 a_1}^{-1}]^{-1},$$

and we observe that the second signal component $S_2 a_2$ has no influence on the estimate.

Nonzero-Mean Processes. One could imagine that the precision of linear estimations with respect to nonzero-mean processes r and a can be increased compared to the solutions above if an additional term taking care of the mean values of the processes is considered. In order to describe this more general case, let us denote the mean of the parameters as

$$\bar{a} = E\{a\}. \tag{5.120}$$

The estimate is now written as

$$\hat{a} = Ar + \bar{a} + c, \tag{5.121}$$

where c is yet unknown. Using the shorthand

$$\begin{aligned} b &= a - \bar{a}, \\ \hat{b} &= \hat{a} - \bar{a}, \\ M &= [c, A] \\ x &= \begin{bmatrix} 1 \\ r \end{bmatrix}, \end{aligned} \tag{5.122}$$

(5.121) can be rewritten as:

$$\hat{b} = Mx. \tag{5.123}$$

The relationship between $\hat{b}$ and x is linear as usual, so that the optimal M can be given according to (5.89):

$$M = R_{xb} R_{xx}^{-1}. \tag{5.124}$$

Now let us express R_{xb} and R_{xx}^{-1} through correlation matrices of the processes a and r. From (5.122) and $E\{b\} = 0$ we derive

$$R_{xb} = [0, R_{rb}] \tag{5.125}$$

with

$$\begin{aligned} R_{rb} &= E\left\{[a - \bar{a}]\, r^H\right\} \\ &= E\left\{[a - \bar{a}]\, [r - \bar{r}]^H\right\}, \end{aligned} \tag{5.126}$$

where

$$\bar{r} = E\{r\}. \tag{5.127}$$

R_{xx} writes

$$R_{xx} = \begin{bmatrix} 1 & \bar{r}^H \\ \bar{r} & R_{rr} \end{bmatrix}. \tag{5.128}$$

Using (5.110) we obtain

$$R_{xx}^{-1} = \begin{bmatrix} 1 + \bar{r}^H\left[R_{rr} - \bar{r}\bar{r}^H\right]^{-1}\bar{r} & -\bar{r}^H\left[R_{rr} - \bar{r}\bar{r}^H\right]^{-1} \\ -\left[R_{rr} - \bar{r}\bar{r}^H\right]^{-1}\bar{r} & \left[R_{rr} - \bar{r}\bar{r}^H\right]^{-1} \end{bmatrix}. \tag{5.129}$$

From (5.122) – (5.129) and

$$\left[R_{rr} - \bar{r}\bar{r}^H\right] = E\left\{[r - \bar{r}]\, [r - \bar{r}]^H\right\} \tag{5.130}$$

we finally conclude

$$\hat{a} = E\left\{[a - \bar{a}]\, [r - \bar{r}]^H\right\}\, E\left\{[r - \bar{r}]\, [r - \bar{r}]^H\right\}^{-1} [r - \bar{r}] + \bar{a}. \tag{5.131}$$

Equation (5.131) can be interpreted as follows: the nonzero-mean processes a and r are first modified so as to become zero-mean processes $a - \bar{a}$ and $r - \bar{r}$. For the zero-mean processes the estimation problem can be solved as usual. Subsequently the mean value $\bar{a}$ is added in order to obtain the final estimate $\hat{a}$.

Unbiasedness for Random Parameter Vectors. So far the parameter vector to be estimated was assumed to be non-random. If we consider a to be a random process, various other weaker definitions of unbiasedness are possible.

The straightforward requirement

$$E\left\{\hat{a}(r)\right\} = A\, E\left\{r\right\} \stackrel{!}{=} E\left\{a\right\} \qquad (5.132)$$

is meaningless, because it is satisfied for any A as far as r and a are zero-mean.

A useful definition of unbiasedness in the case of random parameters is to consider one of the parameters contained in a (e.g. a_k) as non-random and to regard all other parameters $a_1, \ldots, a_{k-1}, a_{k+1}$ etc. as random variables:

$$E\left\{\; \hat{a}_k(r) \mid \mathrm{a}_k \;\right\} \stackrel{!}{=} \mathrm{a}_k. \qquad (5.133)$$

In order to obtain an estimator which is unbiased in the sense of (5.133), the equivalences discussed above may be applied. Starting with the model

$$\begin{aligned} r &= Sa + n \\ &= s_k a_k + \tilde{n}, \end{aligned} \qquad (5.134)$$

in which $\tilde{n}$ contains the additive noise n and the signal component produced by all random parameters a_j, $j \neq k$, we can write the unbiased estimate as

$$\hat{a}_k = h_k^H r \qquad (5.135)$$

with

$$h_k^H = \left[s_k^H R_{\tilde{n}\tilde{n}}^{-1} s_k\right]^{-1} s_k^H R_{\tilde{n}\tilde{n}}^{-1}. \qquad (5.136)$$

Then,

$$A = [h_1, h_2, \ldots]^H \qquad (5.137)$$

is an estimator which is unbiased in the sense of (5.133).

The Relationship between MMSE Estimation and the BLUE. If $R_{aa} = E\left\{aa^H\right\}$ is unknown, $R_{aa}^{-1} = 0$ is substituted into (5.102), and we obtain the BLUE (cf. (5.67)):

$$A = \left[S^H R_{nn}^{-1} S\right]^{-1} S^H R_{nn}^{-1}. \qquad (5.138)$$

In the previous discussion it became obvious that it is possible to obtain unbiased estimates of some of the parameters and to estimate the others with minimum mean square error. This result is of special interest if no unbiased estimator can be stated for all parameters because of a singular matrix $S^H R_{nn}^{-1} S$.

5.6   Linear Optimal Filters

5.6.1   Wiener Filters

We consider the problem depicted in Figure 5.3. By linear filtering of the noisy signal $r(n) = x(n) + w(n)$ we wish to make $y(n) = r(n) * h(n)$ as similar as possible to a desired signal $d(n)$. The quality criterion used for designing the optimal causal linear filter $h(n)$ is

$$E\left\{|e(n)|^2\right\} = E\left\{|d(n) - y(n)|^2\right\} \overset{!}{=} \min. \tag{5.139}$$

The solution to this optimization problem can easily be stated by applying the orthogonality principle. Assuming a causal FIR filter $h(n)$ of length p, we have

$$y(n) = \sum_{i=0}^{p-1} h(i)\, r(n - i). \tag{5.140}$$

Thus, according to (5.94), the following orthogonality condition must be satisfied by the optimal filter:

$$E\left\{\left[d(n) - \sum_{i=0}^{p-1} h(i)\, r(n - i)\right] r^*(n - j)\right\} = 0, \qquad j = 0, 1, \ldots, p - 1. \tag{5.141}$$

For stationary processes $r(n)$ and $d(n)$ this yields the discrete form of the so-called *Wiener–Hopf equation*:

$$\sum_{i=0}^{p-1} h(i)\, r_{rr}(j - i) = r_{rd}(j), \qquad j = 0, 1, \ldots, p - 1, \tag{5.142}$$

with

$$\begin{aligned} r_{rr}(m) &= E\left\{r^*(n)\, r(n + m)\right\}, \\ r_{rd}(m) &= E\left\{r^*(n)\, d(n + m)\right\}. \end{aligned} \tag{5.143}$$

The optimal filter is found by solving (5.142).

An application example is the estimation of data $d(n)$ from a noisy observation $r(n) = \sum_{\ell} c(\ell)\, d(n - \ell) + w(n)$, where $c(n)$ is a channel and $w(n)$ is noise. By using the optimal filter $h(n)$ designed according to (5.142) the data is recovered with minimal mean square error.
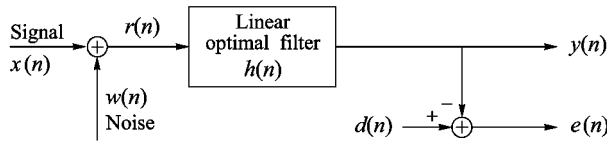
Figure 5.3. Designing linear optimal filters.

Variance. For the variance of the error we have

$$\sigma_e^2 = E\left\{|e(n|^2\right\}$$

$$= \sigma_d^2 - \sum_{i=0}^{p-1} h(i)\, r_{rd}^*(i) - \sum_{i=0}^{p-1} h^*(i)\, r_{rd}(i) \qquad (5.144)$$

$$+ \sum_{i=0}^{p-1}\sum_{j=0}^{p-1} h(i)\, h^*(j)\, r_{rr}(j-i)$$

with $\sigma_d^2 = E\left\{|d(n|^2\right\}$. Substituting the optimal solution (5.142) into (5.144) yields

$$\sigma_{e_{\min}}^2 = \sigma_d^2 - \sum_{i=0}^{p-1} h(i)\, r_{rd}^*(i). \qquad (5.145)$$

Matrix Notation. In matrix notation (5.142) is

$$\boldsymbol{R}_{rr}\, \boldsymbol{h} = \boldsymbol{r}_{rd} \qquad (5.146)$$

with

$$\boldsymbol{h}^T = [h(0), h(1), \dots, h(p-1)], \qquad (5.147)$$

$$\boldsymbol{r}_{rd}^T = [r_{rd}(0), r_{rd}(1), \dots, r_{rd}(p-1)] \qquad (5.148)$$

and

$$\boldsymbol{R}_{rr} = \begin{bmatrix} r_{rr}(0) & r_{rr}(-1) & \cdots & r_{rr}(-p+1) \\ r_{rr}(1) & r_{rr}(0) & \cdots & r_{rr}(-p+2) \\ \vdots & \vdots & & \vdots \\ r_{rr}(p-1) & r_{rr}(p-1) & \cdots & r_{rr}(0) \end{bmatrix}. \qquad (5.149)$$

From (5.146) and (5.145) we obtain the following alternative expressions for the minimal variance:

$$
\begin{aligned}
\sigma_{e_{\min}}^2 &= \sigma_d^2 - r_{rd}^H \, h \\
&= \sigma_d^2 - r_{rd}^H \, R_{rr}^{-1} \, r_{rd}.
\end{aligned}
\tag{5.150}
$$

Special Cases. The following three cases, where the desired signal is a delayed version of the clean input signal $x(n)$, are of special interest:

(i) Filtering: $d(n) = x(n)$.

(ii) Interpolation: $d(n) = x(n + D), D < 0$.

(iii) Prediction: $d(n) = x(n + D), D > 0$. Here the goal is to predict a future value.

For the three cases mentioned above the Wiener–Hopf equation is

$$
\sum_{i=0}^{p-1} h(i) \, r_{rr}(j - i) = r_{rx}(j + D), \qquad j = 0, 1, \ldots, p - 1.
\tag{5.151}
$$

Uncorrelated Noise. If the noise $w(n)$ is uncorrelated to $x(n)$, we have

$$
r_{rr}(m) = r_{xx}(m) + r_{ww}(m)
\tag{5.152}
$$

and

$$
r_{rd}(m) = r_{xx}(m + D),
\tag{5.153}
$$

and from (5.151) we derive

$$
\sum_{i=0}^{p-1} h(i) \left[r_{xx}(j - i) + r_{ww}(j - i) \right] = r_{xx}(j + D), \qquad j = 0, 1, \ldots, p - 1.
\tag{5.154}
$$

In matrix notation we get

$$
\left[R_{xx} + R_{ww} \right] h = r_{xx}(D)
\tag{5.155}
$$

with

$$
h^T = [h(0), h(1), \ldots, h(p - 1)],
\tag{5.156}
$$

$$
r_{xx}^T(D) = [r_{xx}(D), r_{xx}(D + 1), \ldots, r_{xx}(D + p - 1)]
\tag{5.157}
$$

and

$$\boldsymbol{R}_{xx} = \begin{bmatrix} r_{xx}(0) & r_{xx}(-1) & \cdots & r_{xx}(-p+1) \\ r_{xx}(1) & r_{xx}(0) & \cdots & r_{xx}(-p+2) \\ \vdots & \vdots & & \vdots \\ r_{xx}(p-1) & r_{xx}(p-1) & \cdots & r_{xx}(0) \end{bmatrix}. \qquad (5.158)$$

For the correlation matrix $\boldsymbol{R}_{ww}$ the corresponding definition holds.

The minimal variance is

$$\begin{aligned} \sigma_{e_{\min}}^2 &= \sigma_d^2 - \boldsymbol{r}_{xx}^H(D)\,\boldsymbol{h} \\[2mm] &= \sigma_d^2 - \boldsymbol{r}_{xx}^H(D)\,[\boldsymbol{R}_{xx} + \boldsymbol{R}_{ww}]^{-1}\,\boldsymbol{r}_{xx}(D). \end{aligned} \qquad (5.159)$$

5.6.2 One-Step Linear Prediction

One-step linear predictors are used in many applications such as speech and image coding (DPCM, ADPCM, LPC,...), in spectral estimation, and in feature extraction for speech recognition. Basically, they may be regarded as a special case of Wiener–Hopf filtering.
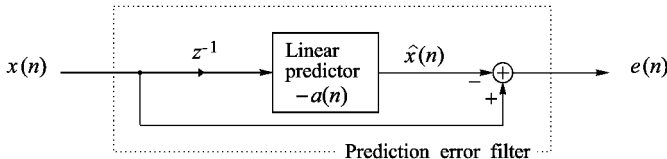
Figure 5.4. One-step linear prediction.

We consider the system in Figure 5.4. A comparison with Figure 5.3 shows that the optimal predictor can be obtained from the Wiener–Hopf equations for the special case $D = 1$ with $d(n) = x(n+1)$, while no additive noise is assumed, $w(n) = 0$. Note that the filter $a(n)$ is related to the Wiener–Hopf filter $h(n)$ as $a(n) = -h(n-1)$. With

$$\hat{x}(n) = -\sum_{i=1}^{p} a(i)\,x(n-i), \qquad (5.160)$$

where p is the length of the FIR filter $a(n)$, the error becomes

$$\begin{aligned} e(n) &= x(n) - \hat{x}(n) \\[2mm] &= x(n) + \sum_{i=1}^{p} a(i)\,x(n-i). \end{aligned} \qquad (5.161)$$

Minimizing the error with respect to the filter coefficients yields the equations

$$-\sum_{i=1}^{p} a(i)\, r_{xx}(j-i) = r_{xx}(j), \qquad j = 1, 2, \ldots, p, \tag{5.162}$$

which are known as the *normal equations of linear prediction*. In matrix notation they are

$$\begin{bmatrix} r_{xx}(0) & r_{xx}(-1) & \cdots & r_{xx}(-p+1) \\ r_{xx}(1) & r_{xx}(0) & \cdots & r_{xx}(-p+2) \\ \vdots & \vdots & & \vdots \\ r_{xx}(p-1) & r_{xx}(p-2) & \cdots & r_{xx}(0) \end{bmatrix} \begin{bmatrix} a(1) \\ a(2) \\ \vdots \\ a(p) \end{bmatrix} = - \begin{bmatrix} r_{xx}(1) \\ r_{xx}(2) \\ \vdots \\ r_{xx}(p) \end{bmatrix}, \tag{5.163}$$

that is

$$\boldsymbol{R}_{xx}\boldsymbol{a} = -\boldsymbol{r}_{xx}(1) \tag{5.164}$$

with

$$\boldsymbol{a}^T = [a(1), \ldots, a(p)]. \tag{5.165}$$

According to (5.159) we get for the minimal variance:

$$\begin{aligned} \sigma_{e_{\min}}^2 = E\left\{|e(n)|^2\right\} &= r_{xx}(0) - \boldsymbol{r}_{xx}^H(1)\, \boldsymbol{R}_{xx}^{-1}\, \boldsymbol{r}_{xx}(1) \\ &= r_{xx}(0) + \boldsymbol{r}_{xx}^H(1)\, \boldsymbol{a}. \end{aligned} \tag{5.166}$$

Autoregressive Processes and the Yule–Walker Equations. We consider an autoregressive process of order p (AR(p) process). As outlined in Section 5.3, such a process is generated by exciting a stable recursive filter with a stationary white noise process $w(n)$. The system function of the recursive system is supposed to be[2]

$$U(z) = \frac{1}{1 + \sum\limits_{i=1}^{p} a(i)\, z^{-i}}, \qquad a(p) \neq 0. \tag{5.167}$$

The input-output relation of the recursive system may be expressed via the difference equation

$$x(n) = w(n) - \sum_{i=1}^{p} a(i)\, x(n-i). \tag{5.168}$$

---

[2]In order to keep in line with the notation used in the literature, the coefficients $\rho(i)$, $i = 1, \ldots, p$ introduced in (5.34) are replaced by the coefficients $-a(i)$, $i = 1, \ldots, p$.

For the autocorrelation sequence of the process $x(n)$ we thus derive

$$
\begin{aligned}
r_{xx}(m) &= E\left\{x^*(n)x(n+m)\right\} \\
&= r_{xw}(m) - \sum_{i=1}^{p} a(i)\, r_{xx}(m-i).
\end{aligned}
\tag{5.169}
$$

The cross correlation sequence $r_{xw}(m)$ is

$$
\begin{aligned}
r_{xw}(m) &= E\left\{x^*(n)w(n+m)\right\} \\
&= \sum_{i=1}^{\infty} u^*(i)\, \underbrace{r_{ww}(i+m)}_{\sigma_w^2\,\delta(i+m)} \\
&= \sigma_w^2\, u^*(-m),
\end{aligned}
\tag{5.170}
$$

where $u(n)$ is the impulse response of the recursive filter. Since $u(n)$ is causal $(u(n) = 0$ for $n < 0)$, we derive

$$
r_{xw}(m) = \begin{cases} 0, & m < 0, \\ \sigma_w^2\, u^*(-m), & m \geq 0. \end{cases}
\tag{5.171}
$$

By combining (5.169) and (5.171) we finally get

$$
r_{xx}(m) = \begin{cases} -\sum_{i=1}^{p} a(i)\, r_{xx}(m-i), & m > 0, \\ \sigma_w^2 - \sum_{i=1}^{p} a(i)\, r_{xx}(m-i), & m = 0, \\ r_{xx}^*(-m), & m < 0. \end{cases}
\tag{5.172}
$$

The equations (5.172) are known as the *Yule–Walker equations*. In matrix form they are

$$
\begin{bmatrix}
r_{xx}(0) & r_{xx}(-1) & r_{xx}(-2) & \cdots & r_{xx}(-p) \\
r_{xx}(1) & r_{xx}(0) & r_{xx}(-1) & \cdots & r_{xx}(1-p) \\
\vdots & \vdots & \vdots & & \vdots \\
r_{xx}(p) & r_{xx}(p-1) & r_{xx}(p-1) & \cdots & r_{xx}(0)
\end{bmatrix}
\begin{bmatrix}
1 \\ a(1) \\ \vdots \\ a(p)
\end{bmatrix}
=
\begin{bmatrix}
\sigma_w^2 \\ 0 \\ \vdots \\ 0
\end{bmatrix}
\tag{5.173}
$$

As can be inferred from (5.173), we obtain the coefficients $a(i)$, $i = 1,\ldots,p$ by solving (5.163). By observing the power of the prediction error we can also determine the power of the input process. From (5.166) and (5.172) we have

$$
\begin{aligned}
\sigma_w^2 &= \sigma_{e_{\min}}^2 \\
&= r_{xx}(0) + r_{xx}^H(1)\, a.
\end{aligned}
\tag{5.174}
$$

Thus, all parameters of an autoregressive process can be exactly determined from the parameters of a one-step linear predictor.

Prediction Error Filter. The output signal of the so-called *prediction error filter* is the signal $e(n)$ in Figure 5.4 with the coefficients $a(n)$ according to (5.163). Introducing the coefficient $a(0) = 1$, $e(n)$ is given by

$$e(n) = \sum_{i=0}^{p} a(i)\, x(n-i), \quad a(0) = 1. \tag{5.175}$$

The system function of the prediction error filter is

$$A(z) = 1 + \sum_{i=1}^{p} a(i) z^{-i} = \sum_{i=0}^{p} a(i) z^{-i}, \quad a(0) = 1. \tag{5.176}$$

In the special case that $x(n)$ is an autoregressive process, the prediction error filter $A(z)$ is the inverse system to the recursive filter $U(z) \longleftrightarrow u(n)$. This also means that the output signal of the prediction error filter is a white noise process. Hence, the prediction error filter performs a whitening transform and thus constitutes an alternative to the methods considered in Section 5.4. If $x(n)$ is not truly autoregressive, the whitening transform is carried out at least approximately.

Minimum Phase Property of the Prediction Error Filter. Our investigation of autoregressive processes showed that the prediction error filter $A(z)$ is inverse to the recursive filter $U(z)$. Since a stable filter does not have poles outside the unit circle of the z-plane, the corresponding prediction error filter cannot have zeros outside the unit circle. Even if $x(n)$ is not an autoregressive process, we obtain a minimum phase prediction error filter, because the calculation of $A(z)$ only takes into account the second-order statistics, which do not contain any phase information, cf. (1.105).

5.6.3 Filter Design on the Basis of Finite Data Ensembles

In the previous sections we assumed stationary processes and considered the correlation sequences to be known. In practice, however, linear predictors must be designed on the basis of a finite number of observations.

In order to determine the predictor filter $a(n)$ from measured data $x(1), x(2), \ldots, x(N)$, we now describe the prediction error

$$e(n) = x(n) + \sum_{i=1}^{p} a(i)x(n-i)$$

via the following matrix equation:

$$e = X\,a + x, \tag{5.177}$$

where a contains the predictor coefficients, and X and x contain the input data. The term $X\,a$ describes the convolution of the data with the impulse response $a(n)$.

The criterion

$$\|e\| = \|X\,a + x\| \stackrel{!}{=} \min \tag{5.178}$$

leads to the following normal equation:

$$X^H X\,a = -X^H x. \tag{5.179}$$

Here, the properties of the predictor are dependent on the definition of X and x. In the following, two relevant methods will be discussed.

Autocorrelation Method. The *autocorrelation method* is based on the following estimation of the autocorrelation sequence:

$$\hat{r}_{xx}^{(AC)}(m) = \frac{1}{N}\sum_{n=1}^{N-|m|} x^*(n)\,x(n+m). \tag{5.180}$$

As can be seen, $\hat{r}_{xx}^{(AC)}(m)$ is a biased estimate of the true autocorrelation sequence $r_{xx}(m)$, which means that $E\{\hat{r}_{xx}^{(AC)}(m)\} \neq r_{xx}(m)$. Thus, the autocorrelation method yields a biased estimate of the parameters of an autoregressive process. However, the correlation matrix $\hat{R}_{xx}^{(AC)}$ built from $\hat{r}_{xx}^{(AC)}(m)$ has a Toeplitz structure, which enables us to efficiently solve the equation

$$\hat{R}_{xx}^{(AC)}\,\hat{a} = -\hat{r}_{xx}^{(AC)}(1) \tag{5.181}$$

by means of the *Levinson–Durbin recursion* [89, 47] or the *Schur algorithm* [130]. Textbooks that cover this topic are, for instance, [84, 99, 117].

The autocorrelation method can also be viewed as the solution to the problem (5.178) with

$$x = \begin{bmatrix} 0 \\ \vdots \\ 0 \\ x(N) \\ \vdots \\ x(p+1) \\ \vdots \\ x(2) \end{bmatrix}, \qquad X = \begin{bmatrix} & & x(N) \\ & \cdot^{\cdot^{\cdot}} & \vdots \\ x(N) & \ldots & x(N-p+1) \\ x(N-1) & \ldots & x(N-p) \\ \vdots & & \vdots \\ x(p) & \ldots & x(1) \\ \vdots & \cdot^{\cdot^{\cdot}} & \\ x(1) & & \end{bmatrix} \tag{5.182}$$

and

$$a = [a(1), a(2), \ldots, a(p)]^T. \tag{5.183}$$

We have

$$\hat{R}_{xx}^{(AC)} = X^H X \tag{5.184}$$

and

$$\hat{r}_{xx}^{(AC)}(1) = X^H x. \tag{5.185}$$

Covariance Method. The *covariance method* takes into account the prediction errors in steady state only and yields an unbiased estimate of the autocorrelation matrix. In this case X and x are defined as

$$X = \begin{bmatrix} x(N-1) & \ldots & x(N-p) \\ \vdots & & \vdots \\ x(p+1) & \ldots & x(2) \\ x(p) & \ldots & x(1) \end{bmatrix} \tag{5.186}$$

and

$$x = \begin{bmatrix} x(N) \\ \vdots \\ x(p+2) \\ x(p+1) \end{bmatrix}. \tag{5.187}$$

The equation to be solved is

$$\hat{R}_{xx}^{(CV)} \, \hat{a} = -\hat{r}_{xx}^{(CV)}(1), \tag{5.188}$$

where

$$\hat{R}_{xx}^{(CV)} = X^H X, \tag{5.189}$$

$$\hat{r}_{xx}^{(CV)}(1) = X^H x. \tag{5.190}$$

Note that $\hat{R}_{xx}^{(CV)}$ is not a Toeplitz matrix, so that solving (5.188) is much more complex than solving (5.181) via the Levinson–Durbin recursion. However, the covariance method has the advantage of being unbiased; we have

$$E\left\{\hat{R}_{xx}^{(CV)}\right\} = R_{xx}. \tag{5.191}$$

5.7 Estimation of Autocorrelation Sequences and Power Spectral Densities

5.7.1 Estimation of Autocorrelation Sequences

In the following, we will discuss methods for estimating the autocorrelation sequence of random processes from given sample values $x(n)$, $n = 0, \ldots, N-1$. We start the discussion with the estimate

$$\hat{r}_{xx}^b(m) = \frac{1}{N} \sum_{n=0}^{N-|m|-1} x^*(n) \, x(n+m), \tag{5.192}$$

which is the same as the estimate $\hat{r}_{xx}^{(AC)}(m)$, used in the autocorrelation method explained in the last section. As can easily be verified, the estimate $\hat{r}_{xx}^b(m)$ is biased with mean

$$E\left\{\hat{r}_{xx}^b(m)\right\} = \frac{N - |m|}{N} \, r_{xx}(m). \tag{5.193}$$

However, since

$$\lim_{N \to \infty} E\left\{\hat{r}_{xx}^b(m)\right\} = r_{xx}(m), \tag{5.194}$$

the estimate is asymptotically unbiased. The triangular window $\frac{N-|m|}{N}$ that occurs in (5.193) is known as the *Bartlett window*.

The variance of the estimate can be approximated as [77]

$$\text{var}[\hat{r}_{xx}^b(m)] \approx \frac{1}{N} \sum_{n=-\infty}^{\infty} |r_{xx}(n)|^2 + r_{xx}^*(n - m) \, r_{xx}(n + m). \tag{5.195}$$

Thus, as $N \to \infty$, the variance tends to zero:

$$\lim_{N \to \infty} \text{var}[\hat{r}_{xx}^b(m)] \to 0. \tag{5.196}$$

Such an estimate is said to be *consistent*. However, although consistency is given, we cannot expect good estimates for large m as long as N is finite, because the bias increases as $|m| \to N$.

Unbiased Estimate. An unbiased estimate of the autocorrelation sequence is given by

$$\hat{r}_{xx}^u(m) = \frac{1}{N - |m|} \sum_{n=0}^{N-|m|-1} x^*(n) \, x(n+m). \tag{5.197}$$

We have

$$E\left\{\hat{r}_{xx}^u(m)\right\} = r_{xx}(m), \quad |m| \le N - 1. \tag{5.198}$$

The variance of the estimate can be approximated as [77]

$$\text{var}[\hat{r}^b_{xx}(m)] \approx \frac{N}{(N-|m|)^2} \sum_{n=-\infty}^{\infty} |r_{xx}(n)|^2 + r^*_{xx}(n-m)\, r_{xx}(n+m). \quad (5.199)$$

As $N \to \infty$, this gives

$$\lim_{N \to \infty} \text{var}[\hat{r}^u_{xx}(m)] \to 0, \qquad (5.200)$$

which means that $\hat{r}^u_{xx}(m)$ is a consistent estimate. However, problems arise for large m as long as N is finite, because the variance increases for $|m| \to N$.

5.7.2 Non-Parametric Estimation of Power Spectral Densities

In many real-world problems one is interested in knowledge about the power spectral density of the data to be processed. Typically, only a finite set of observations $x(n)$ with $n = 0, 1, \dots, N-1$ is available. Since the power spectral density is the Fourier transform of the autocorrelation sequence, and since we have methods for the estimation of the autocorrelation sequence, it is a logical consequence to look at the Fourier transforms of these estimates. We start with $\hat{r}^b_{xx}(m)$. The Fourier transform of $\hat{r}^b_{xx}(m)$ will be denoted as

$$P_{xx}(e^{j\omega}) = \sum_{m=-(N-1)}^{N-1} \hat{r}^b_{xx}(m)\, e^{-j\omega m}. \qquad (5.201)$$

We know that $\hat{r}^b_{xx}(m)$ is a biased estimate of the true autocorrelation sequence $r_{xx}(m)$, so that we can conclude that the spectrum $P_{xx}(e^{j\omega})$ is a biased estimate of the true power spectral density $S_{xx}(e^{j\omega})$. In order to be explicit, let us recall that

$$E\left\{\hat{r}^b_{xx}(m)\right\} = w_B(m)\, r_{xx}(m), \qquad (5.202)$$

with $w_B(m)$ being the Bartlett window; i.e.

$$w_B(m) = \frac{N - |m|}{N}. \qquad (5.203)$$

In the spectral domain, we have

$$
\begin{aligned}
E\left\{P_{xx}(e^{j\omega})\right\} &= \sum_{m=-(N-1)}^{N-1} E\left\{\hat{r}_{xx}^{b}(m)\right\} e^{-j\omega m} \\
&= \sum_{m=-(N-1)}^{N-1} w_B(m)\, r_{xx}(m)\, e^{-j\omega m} \qquad (5.204) \\
&= \frac{1}{2\pi} \int_{-\pi}^{\pi} S_{xx}(e^{j\nu})\, W_B(e^{j(\omega-\nu)})\, d\nu,
\end{aligned}
$$

where $W_B(e^{j\omega})$ is the Fourier transform of $w_B(m)$ given by

$$
W_B(e^{j(\omega)}) = \frac{1}{N} \left(\frac{\sin(\omega N/2)}{\sin(\omega/2)} \right)^2. \qquad (5.205)
$$

Thus, $E\left\{P_{xx}(e^{j\omega})\right\}$ is a smoothed version of the true power spectral density $S_{xx}(e^{j\omega})$, where smoothing is carried out with the Fourier transform of the Bartlett window.

A second way of computing $P_{xx}(e^{j\omega})$ is to compute the Fourier transform of $x(n)$ first and to derive $P_{xx}(e^{j\omega})$ from $X(e^{j\omega})$. By inserting (5.192) into (5.201) and rearranging the expression obtained, we get

$$
P_{xx}(e^{j\omega}) = \frac{1}{N}\, |X(e^{j\omega})|^2. \qquad (5.206)
$$

In the form (5.206) $P_{xx}(e^{j\omega})$ is known as the *periodogram*.

Another way of deriving an estimate of the power spectral density is to consider the Fourier transform of the estimate $\hat{r}_{xx}^{u}(m)$. We use the notation $Q_{xx}(e^{j\omega})$ for this type of estimate:

$$
Q_{xx}(e^{j\omega}) = \sum_{m=-(N-1)}^{N-1} \hat{r}_{xx}^{u}(m)\, e^{-j\omega m}. \qquad (5.207)
$$

The expected value is

$$
\begin{aligned}
E\left\{Q_{xx}(e^{j\omega})\right\} &= \sum_{m=-(N-1)}^{N-1} E\left\{\hat{r}_{xx}^{u}(m)\right\} e^{-j\omega m} \\
&= \sum_{m=-(N-1)}^{N-1} r_{xx}(m)\, e^{-j\omega m} \\
&= \sum_{m=-\infty}^{\infty} w_{R}(m)\, r_{xx}(m)\, e^{-j\omega m} \\
&= \frac{1}{2\pi} \int_{-\pi}^{\pi} S_{xx}(e^{j\nu})\, W_{R}(e^{j(\omega-\nu)})\, d\nu,
\end{aligned}
\tag{5.208}
$$

where $w_{R}(m)$ is the rectangular window

$$
w_{R}(m) = \begin{cases} 1, & \text{for } |m| \leq N-1 \\ 0, & \text{otherwise,} \end{cases}
\tag{5.209}
$$

and $W_{R}(e^{j\omega})$ is its Fourier transform:

$$
W_{R}(e^{j(\omega)}) = \frac{\sin(\omega[2N-1]/2)}{\sin(\omega/2)}.
\tag{5.210}
$$

This means that although $\hat{r}_{xx}^{u}(m)$ is an unbiased estimate of $r_{xx}(m)$, the quantity $Q_{xx}(e^{j\omega})$ is a biased estimate of $S_{xx}(e^{j\omega})$. The reason for this is the fact that only a finite number of taps of the autocorrelation sequence is used in the computation of $Q_{xx}(e^{j\omega})$. The mean $E\left\{Q_{xx}(e^{j\omega})\right\}$ is a smoothed version of $S_{xx}(e^{j\omega})$, where smoothing is carried out with the Fourier transform of the rectangular window.

As $N \to \infty$ both estimates $\hat{r}_{xx}^{b}(m)$ and $\hat{r}_{xx}^{u}(m)$ become unbiased. The same holds for $P_{xx}(e^{j\omega})$ and $Q_{xx}(e^{j\omega})$, so that both estimates of the power spectral density are asymptotically unbiased. The behavior of the variance of the estimates is different. While the estimates of the autocorrelation sequences are consistent, those of the power spectral density are not. For example, for a Gaussian process $x(n)$ with power spectral density $S_{xx}(e^{j\omega})$, the variance of the periodogram becomes

$$
\text{var}\,[\,P_{xx}(e^{j\omega})\,] = \left[1 + \left(\frac{\sin(\omega N)}{N\sin\omega}\right)^{2}\right] S_{xx}^{2}(e^{j\omega}),
\tag{5.211}
$$

which yields

$$
\lim_{N\to\infty} \text{var}\,[\,P_{xx}(e^{j\omega})\,] = S_{xx}^{2}(e^{j\omega}).
\tag{5.212}
$$

Thus, the periodogram does not give a consistent estimate of $S_{xx}(e^{j\omega})$. The proof of (5.211) is straightforward and is omitted here.

Use of the DFT or FFT for Computing the Periodogram. Since the periodogram is computed from the Fourier transform of the finite data sequence, it can be efficiently evaluated at a discrete set of frequencies by using the FFT. Given a length-N sequence $x(n)$, we may consider a length-N DFT, resulting in

$$P_{xx}(e^{j\omega_k}) = \frac{1}{N} \left| \sum_{n=0}^{N-1} x(n) e^{-j2\pi k/N} \right|^2 \tag{5.213}$$

with $\omega_k = 2\pi k/N$. In many applications, the obtained number of samples of $P_{xx}(e^{j\omega})$ may be insufficient in order to draw a clear picture of the periodogram. Moreover, the DFT length may be inconvenient for computation, because no powerful FFT algorithm is at hand for the given length. These problems can be solved by extending the sequence $x(n)$ with zeros to an arbitrary length $N' \geq N$. This procedure is known as *zero padding*. We obtain

$$P_{xx}(e^{j\omega_k}) = \frac{1}{N'} \left| \sum_{n=0}^{N-1} x(n) e^{-j2\pi k/N'} \right|^2 \tag{5.214}$$

with $\omega_k = 2\pi k/N'$. The evaluation of (5.214) is typically carried out via the FFT.

Bartlett Method. Various methods have been proposed for achieving consistent estimates of the power spectral density. The *Bartlett method* does this by decomposing the sequence $x(n)$ into disjoint segments of smaller length and taking the ensemble average of the spectrum estimates derived from the smaller segments. With

$$x^{(i)}(n) = x(n + iM), \quad i = 0, 1, \ldots, K - 1, \quad n = 0, 1, \ldots, M - 1, \tag{5.215}$$

we get the K periodograms

$$P_{xx}^{(i)}(e^{j\omega}) = \frac{1}{M} \left| \sum_{n=0}^{M-1} x^{(i)}(n) e^{-j\omega n} \right|^2, \quad i = 0, 1, \ldots, K - 1. \tag{5.216}$$

The Bartlett estimate then is

$$P_{xx}^{B}(e^{j\omega}) = \frac{1}{K} \sum_{i=0}^{K-1} P_{xx}^{(i)}(e^{j\omega}). \tag{5.217}$$

The expected value becomes

$$E\left\{ P_{xx}^{B}(e^{j\omega}) \right\} = E\left\{ P_{xx}^{(i)}(e^{j\omega}) \right\} = \frac{1}{2\pi} \int_{-\pi}^{\pi} S_{xx}(e^{j\nu}) W_{B_M}(e^{j(\omega - \nu)}) \, d\nu, \tag{5.218}$$

with $W_{B_M}(e^{j\omega})$ being the Fourier transform of the length-M Bartlett window. Assuming a Gaussian process $x(n)$, the variance becomes

$$\text{var}\,[\,P_{xx}^B(e^{j\omega})\,] = \frac{1}{K}\,\text{var}\,[\,P_{xx}(e^{j\omega})\,] = \frac{1}{K}\left[\,1 + \left(\frac{\sin(\omega M)}{M\,\sin\omega}\right)^2\,\right]\,S_{xx}^2(e^{j\omega}).$$

(5.219)

Thus, as $N, M, K \to \infty$, the variance tends to zero and the estimate is consistent. For finite N, the decomposition of $x(n)$ into K sets results in a reduced variance, but the bias increases accordingly and the spectrum resolution decreases.

Blackman-Tukey Method. Blackman and Tukey proposed windowing the estimated autocorrelation sequence prior the Fourier transform [8]. The argument is that windowing allows us to reduce the influence of the unreliable estimates of the autocorrelation sequence for large m. Denoting the window and its Fourier transform as $w(m)$ and $W(e^{j\omega})$, respectively, the estimate can be written as

$$P_{xx}^{BT}(e^{j\omega}) = \sum_{m=-(N-1)}^{N-1} w(m)\,\hat{r}_{xx}^b(m)\,e^{-j\omega m}.$$

(5.220)

In the frequency domain, this means that

$$P_{xx}^{BT}(e^{j\omega}) = \frac{1}{2\pi}\int_{-\pi}^{\pi} P_{xx}(e^{j\nu})\,W(e^{j(\omega-\nu)})\,d\nu.$$

(5.221)

The window $w(n)$ should be chosen such that

$$W(e^{j\omega}) > 0 \quad \forall\,\omega$$

(5.222)

in order to ensure that $P_{xx}^{BT}(e^{j\omega})$ is positive for all frequencies.

The expected value of $P_{xx}^{BT}(e^{j\omega})$ is most easily expressed in the form

$$E\left\{P_{xx}^{BT}(e^{j\omega})\right\} = \sum_{m=-(N-1)}^{N-1} w(m)\,w_B(m)\,r_{xx}(m)\,e^{-j\omega m}.$$

(5.223)

Provided that $w(m)$ is wide with respect to $r_{xx}(m)$ and narrow with respect to $w_B(m)$, the expected value can be approximated as

$$E\left\{P_{xx}^{BT}(e^{j\omega})\right\} = w(0)\,S_{xx}(e^{j\omega}).$$

(5.224)

Thus, in order to achieve an asymptotically unbiased estimate, the window should satisfy

$$w(0) = 1.$$

(5.225)

For a symmetric window $w(m) = w(-m)$ the variance can be estimated as [8]

$$\text{var}\left[\,P_{xx}^{BT}(e^{j\omega})\,\right] \approx \frac{1}{N}\left[\sum_{m=-(N-1)}^{N-1} w^2(n)\right] S_{xx}^2(e^{j\omega}). \qquad (5.226)$$

This approximation is based on the assumption that $W(e^{j\omega})$ is wide with respect to $W_B(e^{j\omega})$ and narrow with respect to the variations of $S_{xx}(e^{j\omega})$.

Welch Method. In the *Welch method* [162] the data is divided into overlapping blocks

$$x^{(i)}(n) = x(n + iD), \quad i = 0, 1, \ldots, K-1, \quad n = 0, 1, \ldots, M-1 \qquad (5.227)$$

with $D \leq M$. For $D = M$ we approach the decomposition in the Bartlett method. For $D < M$ we have more segments than in the Bartlett method.

Each block is windowed prior to computation of the periodogram, resulting in K spectral estimates

$$V_{xx}^{(i)}(e^{j\omega}) = \frac{1}{\alpha M}\left|\sum_{n=0}^{M-1} x^{(i)}(n)\,w(n)\,e^{-j\omega n}\right|^2, \quad i = 0, 1, \ldots, K-1. \qquad (5.228)$$

The factor α is chosen as

$$\alpha = \frac{1}{M}\sum_{m=0}^{M-1} w^2(m) = \frac{1}{M}\frac{1}{2\pi}\int_{-\pi}^{\pi} S_{ww}^E(e^{j\omega})\,d\omega, \qquad (5.229)$$

which means that the analysis is carried out with a window of normalized energy. Taking the average yields the final estimate

$$P_{xx}^W(e^{j\omega}) = \frac{1}{K}\sum_{i=0}^{K-1} V_{xx}^{(i)}(e^{j\omega}). \qquad (5.230)$$

The expected value becomes

$$E\left\{P_{xx}^W(e^{j\omega})\right\} = E\left\{V_{xx}^{(i)}(e^{j\omega})\right\} \qquad (5.231)$$

with

$$E\left\{V_{xx}^{(i)}(e^{j\omega})\right\} = \frac{1}{\alpha M}\sum_{n=0}^{M-1}\sum_{m=0}^{M-1} w(n)\,w(m)\,r_{xx}(n-m)\,e^{-j\omega(n-m)}. \qquad (5.232)$$

In the spectral domain, this can be rewritten as

$$E\left\{V_{xx}^{(i)}(e^{j\omega})\right\} = \frac{1}{\alpha M}\frac{1}{2\pi}\int_{-\pi}^{\pi} S_{xx}(e^{j\nu})\,S_{ww}^E(e^{j(\omega-\nu)})\,d\nu, \qquad (5.233)$$

where

$$S_{ww}^E(e^{j\omega}) = \left| W(e^{j\omega}) \right|^2. \qquad (5.234)$$

With increasing N and M, $S_{ww}^E(e^{j(\omega - \nu)})$ becomes narrow with respect to $S_{xx}(e^{j\nu})$ and the expected value tends to

$$E\left\{ V_{xx}^{(i)}(e^{j\omega}) \right\} = \frac{1}{\alpha M}\, S_{xx}(e^{j\omega})\, \frac{1}{2\pi} \int_{-\pi}^{\pi} S_{ww}^E(e^{j\omega})\, d\omega = S_{xx}(e^{j\omega}). \quad (5.235)$$

This shows that the Welch method is asymptotically unbiased.

For a Gaussian process, the variance of the estimate is

$$\mathrm{var}\,[\,P_{xx}^W(e^{j\omega})\,] = \frac{1}{K^2} \sum_{i=0}^{K-1} \sum_{j=0}^{K-1} E\left\{ V_{xx}^{(i)}(e^{j\omega})\, V_{xx}^{(j)}(e^{j\omega}) \right\} - \left[E\left\{ V_{xx}^{(i)}(e^{j\omega}) \right\} \right]^2.$$

$$(5.236)$$

If no overlap is considered $(D = M)$, the expression reduces to

$$\mathrm{var}\,[\,P_{xx}^W(e^{j\omega})\,] = \frac{1}{K}\, \mathrm{var}\,[\,V_{xx}^{(i)}(e^{j\omega})\,] \approx \frac{1}{K}\, S_{xx}^2(e^{j\omega}). \qquad (5.237)$$

For $k \to \infty$ the variance approaches zero, which shows that the Welch method is consistent.

Various windows with different properties are known for the purpose of spectral estimation. In the following, a brief overview is given.

Hanning Window.

$$w(n) = \begin{cases} 0.5 - 0.5 \cos\left(\frac{2\pi n}{N-1}\right), & n = 0, 1, \ldots, N-1 \\ 0, & \text{otherwise.} \end{cases} \qquad (5.238)$$

Hamming Window.

$$w(n) = \begin{cases} 0.54 - 0.46 \cos\left(\frac{2\pi n}{N-1}\right), & n = 0, 1, \ldots, N-1 \\ 0, & \text{otherwise.} \end{cases} \qquad (5.239)$$

Blackman Window.

$$w(n) = \begin{cases} 0.42 - 0.5 \cos\left(\frac{2\pi n}{N-1}\right) + 0.08 \cos\left(\frac{4\pi n}{N-1}\right), & n = 0, 1, \ldots, N-1 \\ 0, & \text{otherwise.} \end{cases}$$

$$(5.240)$$
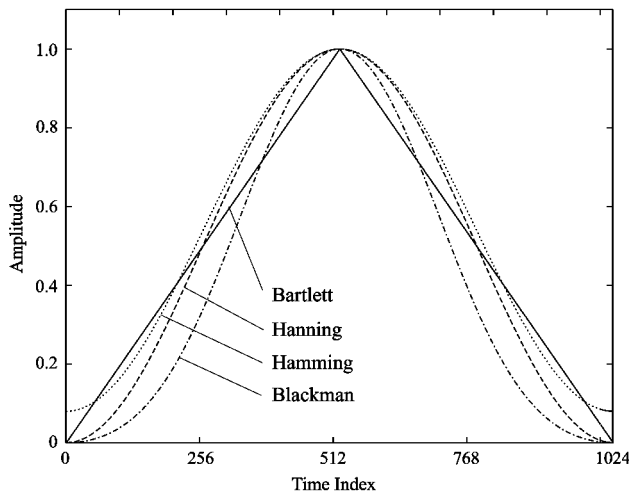
Figure 5.5. Window functions.

Figure 5.5 shows the windows, and Figure 5.6 shows their magnitude frequency responses. The spectrum of the Bartlett window is positive for all frequencies, which also means that the bias due to the Bartlett window is strictly positive. The spectra of the Hanning and Hamming window have relatively large negative side lobes, so that the estimated power spectral density may have a negative bias in the vicinity of large peaks in $S_{xx}(e^{j\omega})$. The Blackman window is a compromise between the Bartlett and the Hanning/Hamming approaches.

5.7.3   Parametric Methods in Spectral Estimation

Parametric methods in spectral estimation have been the subject of intensive research, and many different methods have been proposed. We will consider the simplest case only, which is related to the Yule–Walker equations. A comprehensive treatment of this subject would go far beyond the scope of this section.

Recall that in Section 5.6.2 we showed that the coefficients of a linear one-step predictor are identical to the parameters describing an autoregressive process. Hence the power spectral density may be estimated as

$$\hat{S}_{xx}(e^{j\omega}) = \frac{\hat{\sigma}_w^2}{\left| 1 + \displaystyle\sum_{n=1}^{p} \hat{a}(n)e^{-j\omega n} \right|^2}. \tag{5.241}$$

The coefficients $\hat{a}(n)$ in (5.241) are the predictor coefficients determined from
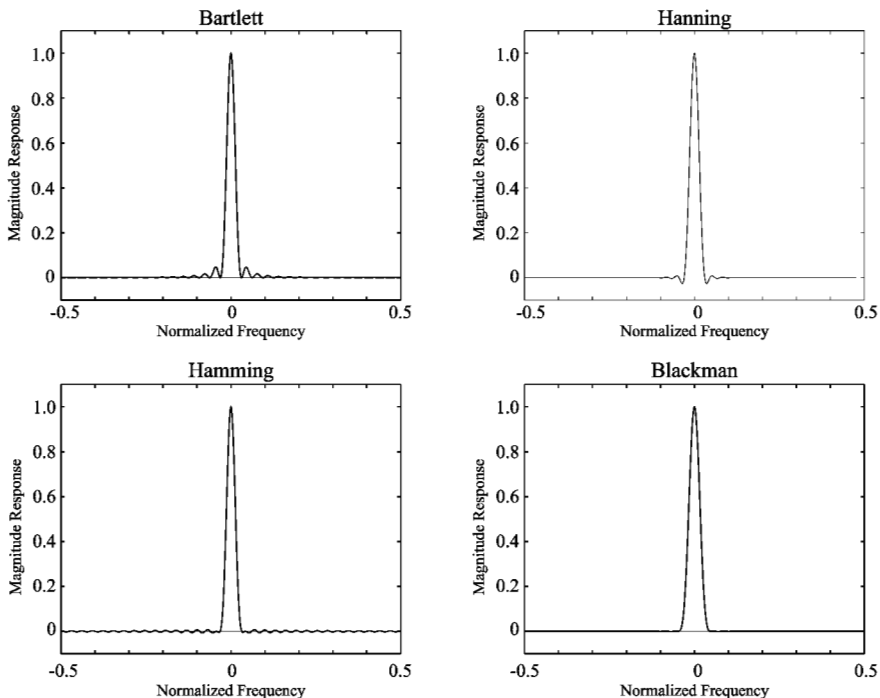
Figure 5.6. Magnitude frequency responses of common window functions.

the observed data, and $\hat{\sigma}_w^2$ is the power of the white input process estimated according to (5.174):

$$\hat{\sigma}_w^2 = \hat{r}_{xx}(0) + \hat{r}_{xx}^H(1)\ \hat{a}. \tag{5.242}$$

If we apply the autocorrelation method to the estimation of the predictor coefficients $\hat{a}(n)$, the estimated autocorrelation matrix has a Toeplitz structure, and the prediction filter is always minimum phase, just as when using the true correlation matrix $\boldsymbol{R}_{xx}$. For the covariance method this is not the case.

Finally, it shall be remarked that besides a forward prediction a backward prediction may also be carried out. By combining both predictors one can obtain an improved estimation of the power spectral density compared to (5.241). An example is the *Burg method* [19].

Chapter 6

Filter Banks

Filter banks are arrangements of low pass, bandpass, and highpass filters used for the spectral decomposition and composition of signals. They play an important role in many modern signal processing applications such as audio and image coding. The reason for their popularity is the fact that they easily allow the extraction of spectral components of a signal while providing very efficient implementations. Since most filter banks involve various sampling rates, they are also referred to as *multirate systems*. To give an example, Figure 6.1 shows an M-channel filter bank. The input signal is decomposed into M so-called *subb and signals* by applying M analysis filters with different passbands. Thus, each of the subband signals carries information on the input signal in a particular frequency band. The blocks with arrows pointing downwards in Figure 6.1 indicate downsampling (subsampling) by factor N, and the blocks with arrows pointing upwards indicate upsampling by N. Subsampling by N means that only every Nth sample is taken. This operation serves to reduce or eliminate redundancies in the M subband signals. Upsampling by N means the insertion of $N - 1$ consecutive zeros between the samples. This allows us to recover the original sampling rate. The upsamplers are followed by filters which replace the inserted zeros with meaningful values. In the case $M = N$ we speak of *critical subsampling*, because this is the maximum downsampling factor for which *perfect reconstruction* can be achieved. Perfect reconstruction means that the output signal is a copy of the input signal with no further distortion than a time shift and amplitude scaling.
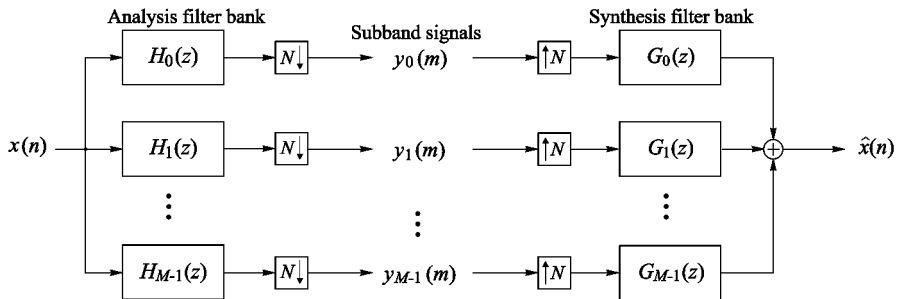
Figure 6.1. M-channel filter bank.

From the mathematical point of view, a filter bank carries out a series expansion, where the subband signals are the coefficients, and the time-shifted variants $g_k(n-iN)$, $i \in \mathbb{Z}$, of the synthesis filter impulse responses $g_k(n)$ form the basis. The main difference to the block transforms is that the lengths of the filter impulse responses are usually larger than N so that the basis sequences overlap.

6.1   Basic Multirate Operations

6.1.1   Decimation and Interpolation

In this section, we derive spectral interpretations for the decimation and interpolation operations that occur in every multirate system. For this, we consider the configuration in Figure 6.2. The sequence $v(n)$ results from inserting zeros into $y(m)$. Because of the different sampling rates we obtain the following relationship between $Y(z)$ and $V(z)$:

$$Y(z^N) = V(z). \tag{6.1}$$

After downsampling and upsampling by N the values $v(nN)$ and $u(nN)$ are still equal, while all other samples of $v(n)$ are zero. Using the correspondence

$$\frac{1}{N} \sum_{i=0}^{N-1} e^{j2\pi in/N} = \begin{cases} 1 & \text{for } n/N \in \mathbb{Z}, \\ 0 & \text{otherwise}, \end{cases} \tag{6.2}$$

the relationship between $v(n)$ and $u(n)$ can be written as

$$v(n) = u(n)\frac{1}{N} \sum_{i=0}^{N-1} W_N^{-in}, \tag{6.3}$$
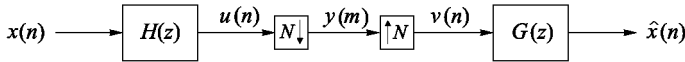
Figure 6.2. Typical components of a filter bank.

where

$$W_N = e^{-j2\pi/N}.$$ (6.4)

The z-transform is given by

$$
\begin{aligned}
V(z) &= \sum_{n=-\infty}^{\infty} v(n)z^{-n} \\
&= \frac{1}{N} \sum_{i=0}^{N-1} \sum_{n=-\infty}^{\infty} u(n) \left[W_N^i z\right]^{-n} \qquad (6.5) \\
&= \frac{1}{N} \sum_{i=0}^{N-1} U(W_N^i z).
\end{aligned}
$$

The relationship between $Y(z)$ and $U(z)$ is concluded from (6.1) and (6.5):

$$Y(z) = \frac{1}{N} \sum_{i=0}^{N-1} U(W_N^i z^{\frac{1}{N}}).$$ (6.6)

With (6.6) and $U(z) = H(z)X(z)$ we have the following relationship between $Y(z)$ and $X(z)$:

$$Y(z) = \frac{1}{N} \sum_{i=0}^{N-1} H(W_N^i z^{\frac{1}{N}}) \, X(W_N^i z^{\frac{1}{N}}).$$ (6.7)

From (6.1) and (6.7) we finally conclude

$$
\begin{aligned}
\hat{X}(z) &= G(z) \, Y(z^N) \\
&= \frac{1}{N} \sum_{i=0}^{N-1} G(z) H(W_N^i z) X(W_N^i z).
\end{aligned}
$$ (6.8)
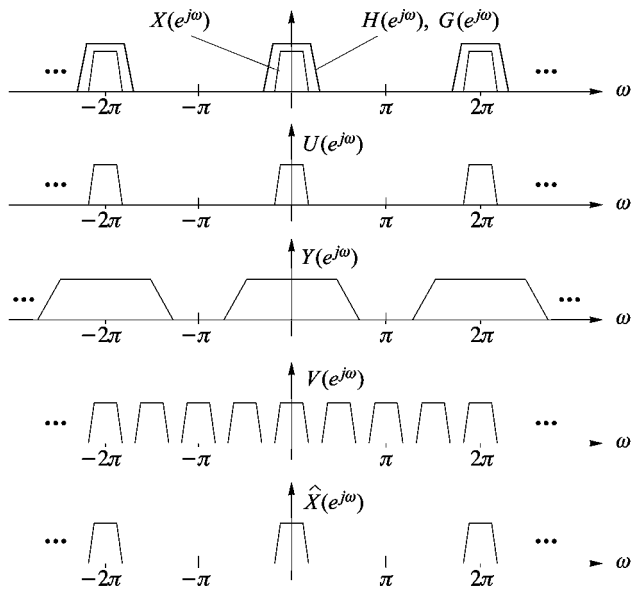
Figure 6.3. Signal spectra for decimation and interpolation according to the structure in Figure 6.2 (non-aliased case).
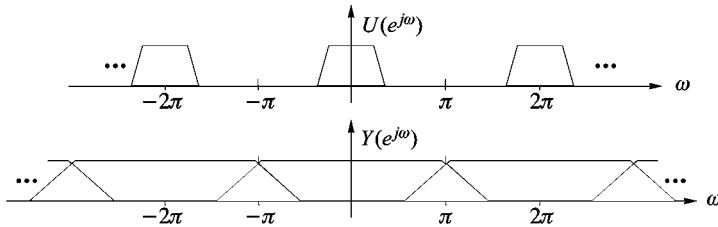
Figure 6.4. Signal spectra in the aliased case.

The spectra of the signals occurring in Figure 6.2 are illustrated in Figure 6.3 for the case of a narrowband lowpass input signal $x(n)$, which does not lead to aliasing effects. This means that the products $G(z)(H(W_N^i z)X(W_N^i z))$ in (6.8) are zero for $i \neq 0$. The general case with aliasing occurs when the spectra become overlapping. This is shown in Figure 6.4, where the shaded areas indicate the aliasing components that occur due to subsampling. It is clear that $x(n)$ can only be recovered from $y(m)$ if no aliasing occurs. However, the aliased case is the normal operation mode in multirate filter banks. The reason why such filter banks allow perfect reconstruction lies in the fact that they can be designed in such a way that the aliasing components from all parallel branches compensate at the output.
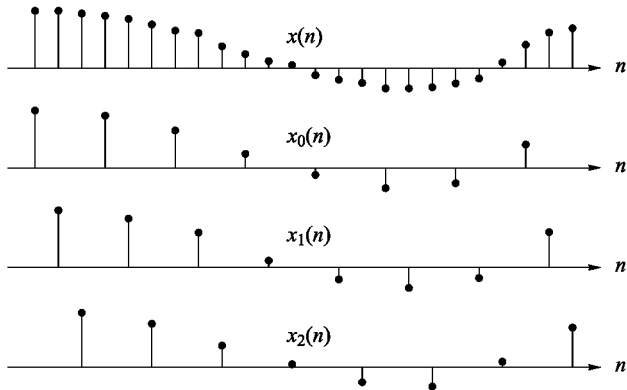
Figure 6.5. Type-1 polyphase decomposition for $M = 3$.

6.1.2 Polyphase Decomposition

Consider the decomposition of a sequence $x(n)$ into sub-sequences $x_i(m)$, as shown in Figure 6.5. Interleaving all $x_i(m)$ again yields the original $x(n)$. This decomposition is called a *polyphase decomposition*, and the $x_i(m)$ are the *polyphase components* of $x(n)$. Several types of polyphase decompositions are known, which are briefly discussed below.

Type-1. A type-1 polyphase decomposition of a sequence $x(n)$ into M components is given by

$$X(z) = \sum_{\ell=0}^{M-1} z^{-\ell} X_\ell(z^M), \qquad (6.9)$$

where

$$X_\ell(z) \longleftrightarrow x_\ell(n) = x(nM + \ell). \qquad (6.10)$$

Figure 6.5 shows an example of a type-1 decomposition.

Type-2. The decomposition into type-2 polyphase components is given by

$$X(z) = \sum_{\ell=0}^{M-1} z^{-(M-1-\ell)} X_\ell'(z^M), \qquad (6.11)$$

where

$$X_\ell'(z) \longleftrightarrow x_\ell'(n) = x(nM + M - 1 - \ell). \qquad (6.12)$$

Thus, the only difference between a type-1 and a type-2 decomposition lies in the indexing:

$$X_\ell(z) = X'_{M-1-\ell}(z). \tag{6.13}$$

Type-3. A type-3 decomposition reads

$$X(z) = \sum_{\ell=0}^{M-1} z^\ell \, \bar{X}_\ell(z^M), \tag{6.14}$$

where

$$\bar{X}_\ell(z) \longleftrightarrow \bar{x}_\ell(n) = x(nM - \ell). \tag{6.15}$$

The relation to the type-1 polyphase components is

$$\begin{aligned}
X_0(z) &= \bar{X}_0(z), \\
X_\ell(z) &= z^{-1}\bar{X}_{M-\ell}(z), \quad \ell = 1,\ldots,M-1.
\end{aligned} \tag{6.16}$$

Polyphase decompositions are frequently used for both signals and filters. In the latter case we use the notation $H_{ik}(z)$ for the kth type-1 polyphase component of filter $H_i(z)$. The definitions for type-2 and type-3 components are analogous.

6.2   Two-Channel Filter Banks

6.2.1   PR Condition

Let us consider the two-channel filter bank in Figure 6.6. The signals are related as

$$Y_0(z^2) = \tfrac{1}{2} \left[H_0(z) \, X(z) + H_0(-z) \, X(-z) \right],$$

$$Y_1(z^2) = \tfrac{1}{2} \left[H_1(z) \, X(z) + H_1(-z) \, X(-z) \right], \tag{6.17}$$

$$\hat{X}(z) = \left[Y_0(z^2) \, G_0(z) + Y_1(z^2) \, G_1(z) \right].$$

Combining these equations yields the input-output relation

$$\begin{aligned}
\hat{X}(z) = \quad & \tfrac{1}{2} \left[H_0(z) \, G_0(z) + H_1(z) \, G_1(z) \right] X(z) \\
+ & \tfrac{1}{2} \left[H_0(-z) \, G_0(z) + H_1(-z) \, G_1(z) \right] X(-z).
\end{aligned} \tag{6.18}$$

The first term describes the transmission of the signal $X(z)$ through the system, while the second term describes the aliasing component at the output
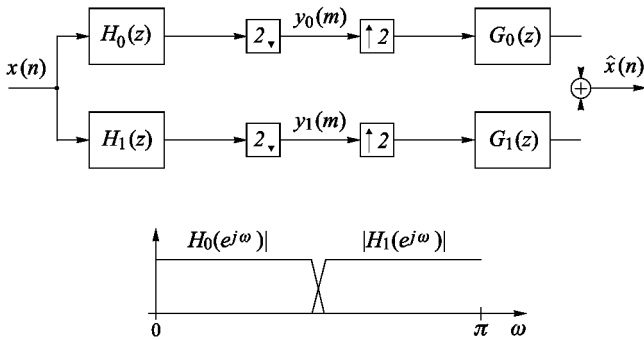
Figure 6.6. Two-channel filter bank.

of the filter bank. Perfect reconstruction is given if the output signal is nothing but a delayed version of the input signal. That is, the transfer function for the signal component, denoted as $S(z)$, must satisfy

$$S(z) = H_0(z)\,G_0(z) + H_1(z)\,G_1(z) = 2\,z^{-q}, \tag{6.19}$$

and the transfer function $F(z)$ for the aliasing component must be zero:

$$F(z) = H_0(-z)\,G_0(z) + H_1(-z)\,G_1(z) = 0. \tag{6.20}$$

If (6.20) is satisfied, the output signal contains no aliasing, but amplitude distortions may be present. If both (6.19) and (6.20) are satisfied, the amplitude distortions also vanish. Critically subsampled filter banks that allow perfect reconstruction are also known as biorthogonal filter banks. Several methods for satisfying these conditions either exactly or approximately can be found in the literature. The following sections give a brief overview.

6.2.2 Quadrature Mirror Filters

Quadrature mirror filter banks (QMF banks) provide complete aliasing cancellation at the output, but condition (6.19) is only approximately satisfied. The principle was introduced by Esteban and Galand in [52]. In QMF banks, $H_0(z)$ is chosen as a linear phase lowpass filter, and the remaining filters are constructed as

$$
\begin{aligned}
G_0(z) &= H_0(z) \\
H_1(z) &= H_0(-z) \\
G_1(z) &= -H_1(z).
\end{aligned}
\tag{6.21}
$$
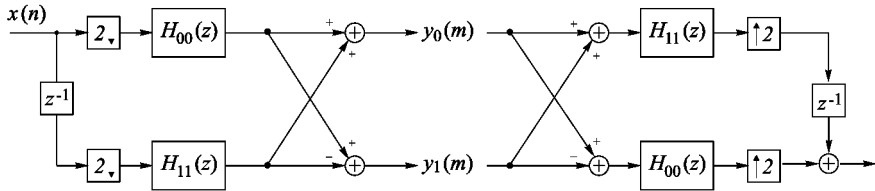
Figure 6.7. QMF bank in polyphase structure.

As can easily be verified, independent of the filter $H_0(z)$, the condition $F(z) = 0$ is structurally satisfied, so that one only has to ensure that $S(z) = H_0^2(z) + H_0^2(-z) \approx 2z^{-q}$. The name QMF is due to the mirror image property

$$|H_1(e^{j\frac{\pi}{2} - \omega})| = |H_0(e^{j\frac{\pi}{2} + \omega})|$$

with symmetry around $\pi/2$.

QMF bank prototypes with good coding properties have for instance been designed by Johnston [78].

One important property of the QMF banks is their efficient implementation due to the modulated structure, where the highpass and lowpass filters are related as $H_1(z) = H_0(-z)$. For the polyphase components this means that $H_{10}(z) = H_{00}(z)$ and $H_{11}(z) = -H_{01}(z)$. The resulting efficient polyphase realization is depicted in Figure 6.7.

6.2.3   General Perfect Reconstruction Two-Channel Filter Banks

A method for the construction of PR filter banks is to choose

$$
\begin{aligned}
G_0(z) &= z^{-\ell} H_1(-z) \\
G_1(z) &= -z^{-\ell} H_0(-z).
\end{aligned}
\tag{6.22}
$$

Is is easily verified that (6.20) is satisfied. Inserting the above relationships into (6.19) yields

$$H_0(z)G_0(z) + (-1)^{\ell+1} H_0(-z)G_0(-z) = 2z^{-q}. \tag{6.23}$$

Using the abbreviation

$$T(z) = G_0(z) \, H_0(z), \tag{6.24}$$
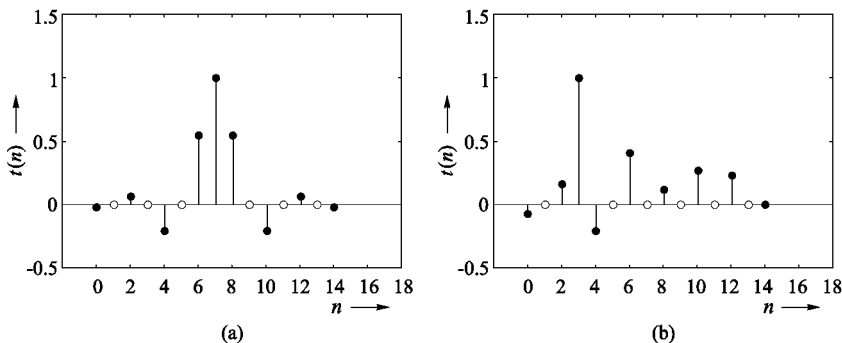
Figure 6.8. Examples of Nyquist filters $T(z)$; (a) linear-phase; (b) short overall delay.

this becomes

$$2z^{-q} = T(z) + (-1)^{\ell+1}\ T(-z). \tag{6.25}$$

Note that $\frac{1}{2}[T(z) + T(-z)]$ is the z-transform of a sequence that only has non-zero even taps, while $\frac{1}{2}[T(z) - T(-z)]$ is the z-transform of a sequence that only has non-zero odd taps. Altogether we can say that in order to satisfy (6.25), the system $T(z)$ has to satisfy

$$t(n) = \begin{cases} 1 & n = q \\ 0 & n = q + 2\ell,\ \ell \neq 0 \qquad \ell \in \mathbb{Z} \\ \text{arbitrary} & n = q + 2\ell + 1. \end{cases} \tag{6.26}$$

In communications, condition (6.26) is known as the *first Nyquist condition*. Examples of impulse responses $t(n)$ satisfying the first Nyquist condition are depicted in Figure 6.8. The arbitrary taps are the free design parameters, which may be chosen in order to achieve good filter properties. Thus, filters can easily be designed by choosing a filter $T(z)$ and factoring it into $H_0(z)$ and $G_0(z)$. This can be done by computing the roots of $T(z)$ and dividing them into two groups, which form the zeros of $H_0(z)$ and $G_0(z)$. The remaining filters are then chosen according to (6.24) in order to yield a PR filter bank. This design method is known as *spectral factorization*.

6.2.4   Matrix Representations

Matrix representations are a convenient and compact way of describing and characterizing filter banks. In the following we will give a brief overview of the most important matrices and their relation to the analysis and synthesis filters.

Modulation Matrix. The input-output relations of the two-channel filter bank may also be written in matrix form. For this, we introduce the vectors

$$\boldsymbol{x}_m(z) = \begin{bmatrix} X(z) \\ X(-z) \end{bmatrix}, \tag{6.27}$$

$$\boldsymbol{y}_p(z) = \begin{bmatrix} Y_0(z) \\ Y_1(z) \end{bmatrix} \tag{6.28}$$

and the so-called *modulation matrix* or *alias component (AC) matrix*

$$\boldsymbol{H}_m(z) = \begin{bmatrix} H_0(z) & H_1(z) \\ H_0(-z) & H_1(-z) \end{bmatrix}, \tag{6.29}$$

which contains the filters $H_0(z)$ and $H_1(z)$ and their modulated versions $H_0(-z)$ and $H_1(-z)$. We get

$$\boldsymbol{y}_p(z^2) = \frac{1}{2} \boldsymbol{H}_m^T(z) \, \boldsymbol{x}_m(z), \tag{6.30}$$

$$\hat{X}(z) = [G_0(z), \, G_1(z)] \, \boldsymbol{y}_p(z^2)$$

$$= \frac{1}{2} [G_0(z), \, G_1(z)] \, \boldsymbol{H}_m^T(z) \, \boldsymbol{x}_m(z). \tag{6.31}$$

Polyphase Representation of the Analysis Filter Bank. Let us consider the analysis filter bank in Figure 6.9(a). The signals $y_0(m)$ and $y_1(m)$ may be written as

$$y_0(m) = \sum_n h_0(n) \, x(2m - n)$$

$$= \sum_k h_0(2k) \, x(2m - 2k) + \sum_k h_0(2k + 1) \, x(2m - 2k - 1)$$

$$= \sum_k h_{00}(k) \, \bar{x}_0(m - k) + \sum_k h_{01}(k) \, \bar{x}_1(m - k) \tag{6.32}$$

and

$$y_1(m) = \sum_n h_1(n) \, x(2m - n)$$

$$= \sum_k h_{10}(k) \, \bar{x}_0(m - k) + \sum_k h_{11}(k) \, \bar{x}_1(m - k), \tag{6.33}$$
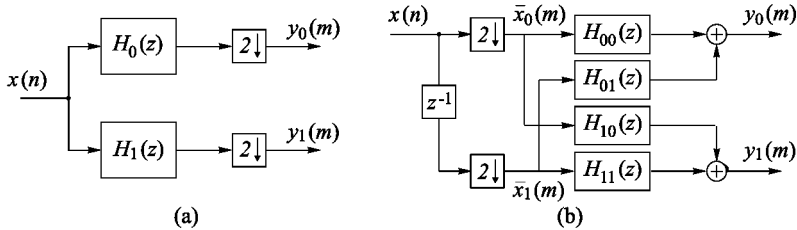
Figure 6.9. Analysis filter bank. (a) direct implementation; (b) polyphase realization.

where we used the following polyphase components:

$$
\begin{aligned}
h_{00}(k) &= h_0(2k), \\
h_{01}(k) &= h_0(2k+1), \\
h_{10}(k) &= h_1(2k), \\
h_{11}(k) &= h_1(2k+1), \\
\bar{x}_0(k) &= x(2k), \\
\bar{x}_1(k) &= x(2k-1).
\end{aligned}
$$

The last rows of (6.32), and (6.33) respectively, show that the complete analysis filter bank can be realized by operating solely with the polyphase components, as depicted in Figure 6.9(b). The advantage of the polyphase realization compared to the direct implementation in Figure 6.9(a) is that only the required output values are computed. When looking at the first rows of (6.32) and (6.33) this sounds trivial, because these equations are easily implemented and do not produce unneeded values. Thus, unlike in the QMF bank case, the polyphase realization does not necessarily lead to computational savings compared to a proper direct implementation of the analysis equations. However, it allows simple filter design, gives more insight into the properties of a filter bank, and leads to efficient implementations based on lattice structures; see Sections 6.2.6 and 6.2.7.

It is convenient to describe (6.32) and (6.33) in the z-domain using matrix notation:

$$
\boldsymbol{y}_p(z) = \boldsymbol{E}(z)\, \bar{\boldsymbol{x}}_p(z), \tag{6.34}
$$

where

$$
\boldsymbol{E}(z) = \begin{bmatrix} H_{00}(z) & H_{01}(z) \\ H_{10}(z) & H_{11}(z) \end{bmatrix}, \tag{6.35}
$$

$$
\bar{\boldsymbol{x}}_p(z) = \begin{bmatrix} \bar{X}_0(z) \\ \bar{X}_1(z) \end{bmatrix}. \tag{6.36}
$$

Matrix $\boldsymbol{E}(z)$ is called the *polyphase matrix* of the analysis filter bank. As can easily be seen by inspection, it is related to the modulation matrix as follows:

$$\boldsymbol{H}_m(z) = \boldsymbol{W}^H \, \boldsymbol{D}(z) \, \boldsymbol{E}^T(z^2),$$

$$\boldsymbol{E}(z^2) = \tfrac{1}{2} \, \boldsymbol{H}_m^T(z) \, \boldsymbol{W} \, \boldsymbol{D}(z^{-1}),$$

(6.37)

with

$$\boldsymbol{W} = \begin{bmatrix} 1 & 1 \\ 1 & -1 \end{bmatrix},$$

(6.38)

and

$$\boldsymbol{D}(z) = \begin{bmatrix} 1 & \\ & z^{-1} \end{bmatrix}$$

(6.39)

Here, $\boldsymbol{W}$ is understood as the $2{\times}2$-DFT matrix. In view of the general M-channel case, we use the notation $\boldsymbol{W}^{-1} = \tfrac{1}{2}\boldsymbol{W}^H$ for the inverse.

Polyphase Representation of the Synthesis Filter Bank. We consider the synthesis filter bank in Figure 6.10(a). The filters $G_0(z)$ and $G_1(z)$ can be written in terms of their type-2 polyphase components as

$$G_0(z) = z^{-1}G'_{00}(z^2) + G'_{01}(z^2)$$

(6.40)

and

$$G_1(z) = z^{-1}G'_{10}(z^2) + G'_{11}(z^2).$$

(6.41)

This gives rise to the following z-domain matrix representation:

$$\hat{X}(z) = \begin{bmatrix} z^{-1} & 1 \end{bmatrix} \underbrace{\begin{bmatrix} G'_{00}(z) & G'_{10}(z) \\ G'_{01}(z) & G'_{11}(z) \end{bmatrix}}_{\boldsymbol{R}(z)} \begin{bmatrix} Y_0(z) \\ Y_1(z) \end{bmatrix}.$$

(6.42)

The corresponding polyphase realization is depicted in Figure 6.10. Perfect reconstruction up to an overall delay of $q = 2m_0 + 1$ samples is achieved if

$$\boldsymbol{R}(z)\boldsymbol{E}(z) = z^{-m_0} \, \boldsymbol{I}.$$

(6.43)

The PR condition for an even overall delay of $q = 2m_0$ samples is

$$\boldsymbol{R}(z)\boldsymbol{E}(z) = z^{-m_0} \begin{bmatrix} 0 & 1 \\ z^{-1} & 0 \end{bmatrix}.$$

(6.44)
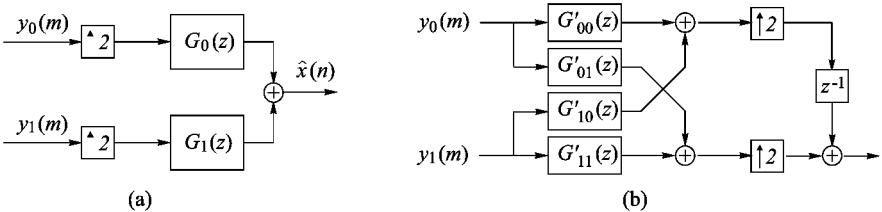
Figure 6.10. Synthesis filter bank. (a) direct implementation; (b) polyphase realization.

6.2.5 Paraunitary Two-Channel Filter Banks

The inverse of a unitary matrix is given by the Hermitian transpose. A similar property can be stated for polyphase matrices as follows:

$$\boldsymbol{E}^{-1}(z) = \tilde{\boldsymbol{E}}(z), \tag{6.45}$$

where

$$\tilde{\boldsymbol{E}}(z) = (\boldsymbol{E}(z))^H, \quad |z| = 1, \tag{6.46}$$

such that

$$\boldsymbol{E}(z)\,\tilde{\boldsymbol{E}}(z) = \tilde{\boldsymbol{E}}(z)\,\boldsymbol{E}(z) = \boldsymbol{I}. \tag{6.47}$$

Analogous to ordinary matrices, $(\boldsymbol{E}(z))^H$ stands for transposing the matrix and simultaneously conjugating the elements:

$$\boldsymbol{E}(z) = \begin{bmatrix} H_{00}(z) & H_{01}(z) \\ H_{10}(z) & H_{11}(z) \end{bmatrix} \Rightarrow \tilde{\boldsymbol{E}}(z) = \begin{bmatrix} \tilde{H}_{00}(z) & \tilde{H}_{10}(z) \\ \tilde{H}_{01}(z) & \tilde{H}_{11}(z) \end{bmatrix}.$$

In the case of real-valued filter coefficients we have $\tilde{H}_{ik}(z) = H_{ik}(z^{-1})$, such that $\tilde{\boldsymbol{E}}(z) = \boldsymbol{E}^T(z^{-1})$ and

$$\boldsymbol{E}(z)\,\boldsymbol{E}^T(z^{-1}) = \boldsymbol{E}^T(z^{-1})\,\boldsymbol{E}(z) = \boldsymbol{I}. \tag{6.48}$$

Since $\boldsymbol{E}(z)$ is dependent on z, and since the operation (6.46) has to be carried out on the unit circle, and not at some arbitrary point in the z plane, a matrix $\boldsymbol{E}(z)$ satisfying (6.47) is said to be paraunitary.

Modulation Matrices. As can be seen from (6.37) and (6.47), we have

$$\boldsymbol{H}_m(z)\tilde{\boldsymbol{H}}_m(z) = \tilde{\boldsymbol{H}}_m(z)\boldsymbol{H}_m(z) = 2\,\boldsymbol{I} \tag{6.49}$$

for the modulation matrices of paraunitary two-channel filter banks.

Matched Filter Condition. From (6.49) we may conclude that the analysis and synthesis filters in a paraunitary two-channel filter bank are related as

$$G_k(z) = \tilde{H}_k(z) \quad \longleftrightarrow \quad g_k(n) = h_k^*(-n), \qquad k = 0, 1. \tag{6.50}$$

This means that an analysis filter and its corresponding synthesis filter together yield a Nyquist filter (cf. (6.24)) whose impulse response is equivalent to the autocorrelation sequence of the filters in question:

$$t_k(n) = r^E_{h_k h_k}(n) = r^E_{g_k g_k}(n) = h_k(n) * h_k^*(-n). \qquad (6.51)$$

Here we find parallels to data transmission, where the receiver input filter is matched to the output filter of the transmitter such that the overall result is the autocorrelation sequence of the filter. This is known as the *matched-filter condition*. The reason for choosing this special input filter is that it yields a maximum signal-to-noise ratio if additive white noise interferes on the transmission channel.

Power-Complementary Filters. From (6.49) we conclude

$$2 = H_0(z)\tilde{H}_0(z) + H_0(-z)\tilde{H}_0(-z), \qquad (6.52)$$

which for $z = e^{j\omega}$ implies the requirement

$$2 = \left|H_0(e^{j\omega})\right|^2 + \left|H_0(e^{j(\omega + \pi)})\right|^2. \qquad (6.53)$$

We observe that the filters $H_0(e^{j\omega})$ and $H_0(e^{j(\omega + \pi)})$ must be power-complementary to one another. For constructing paraunitary filter banks we therefore have to find a Nyquist filter $T(z)$ which can be factored into

$$T(z) = H_0(z) \, \tilde{H}_0(z). \qquad (6.54)$$

Note that a factorization is possible only if $T(e^{j\omega})$ is real and positive. A filter that satisfies this condition is said to be *valid*. Since $T(e^{j\omega})$ has symmetry around $\omega = \pi/2$ such a filter is also called a *valid halfband filter*. This approach was introduced by Smith and Barnwell in [135].

Given Prototype. Given an FIR prototype $H(z)$ that satisfies condition (6.53), the required analysis and synthesis filters can be derived as

$$\begin{aligned}
H_0(z) &= H(z) \\
H_1(z) &= z^{-(L-1)}\tilde{H}(-z) \\
G_0(z) &= z^{-(L-1)}\tilde{H}_0(z) \\
G_1(z) &= z^{-(L-1)}\tilde{H}_1(z).
\end{aligned} \qquad (6.55)$$

Here, L is the number of coefficients of the prototype.

Number of Coefficients. Prototypes for paraunitary two-channel filter banks have even length. This is seen by formulating (6.52) in the time domain and assuming an FIR filter with coefficients $h_0(0), \ldots, h_0(2k)$:

$$\delta_{\ell 0} = \sum_{n=0}^{2k} h_0(n) h_0^*(n - 2\ell).$$
(6.56)

For $\ell = k$, $n = 2k$, $k \neq 0$, this yields the requirement $0 = h_0(2k) h_0^*(0)$, which for $h_0(0) \neq 0$ can only be satisfied by $h_0(2k) = 0$. This means that the filter has to have even length.

Filter Energies. It is easily verified that all filters in a paraunitary filter bank have energy one:

$$\|h_0\|_{\ell_2}^2 = \|h_1\|_{\ell_2}^2 = \|g_0\|_{\ell_2}^2 = \|g_1\|_{\ell_2}^2 = 1.$$
(6.57)

Non-Linear Phase Property. We will show that paraunitary two-channel filter banks are non-linear phase with one exception. The following proof is based on Vaidyanathan [145]. We assume that two filters $H(z)$ and $G(z)$ are power-complementary and linear-phase:

$$c^2 \quad = H(z)\tilde{H}(z) + G(z)\tilde{G}(z)$$

$$\left.\begin{array}{ll} \tilde{H}(z) & = e^{j\alpha} \, z^L \, H(z), \quad \alpha \in \mathbb{R} \\ \tilde{G}(z) & = e^{j\beta} \, z^L \, G(z), \quad \beta \in \mathbb{R} \end{array}\right\} \quad \text{(linear-phase property).}$$
(6.58)

We conclude

$$(H(z)e^{j\alpha/2} + jG(z)e^{j\beta/2}) \, (H(z)e^{j\alpha/2} - jG(z)e^{j\beta/2}) = c^2 \, z^{-L}.$$
(6.59)

Both factors on the left are FIR filters, so that

$$\left.\begin{array}{ll} H(z)e^{j\alpha/2} + jG(z)e^{j\beta/2} & = pz^{-L_1} \\ H(z)e^{j\alpha/2} - jG(z)e^{j\beta/2} & = qz^{-L_2} \end{array}\right\} \quad L_1 + L_2 = L, \quad pq = c^2$$
(6.60)

Adding and subtracting both equations shows that $H(z)$ and $G(z)$ must have the form

$$\begin{array}{ll} H(z) & = \quad az^{-L_1} + bz^{-L_2}, \\ G(z) & = \quad \gamma(az^{-L_1} - bz^{-L_2}), \quad |\gamma| = 1 \end{array}$$
(6.61)

in order to be both power-complementary and linear-phase. In other words, power-complementary linear-phase filters cannot have more than two coefficients.

6.2.6 Paraunitary Filter Banks in Lattice Structure

Paraunitary filter banks can be efficiently implemented in a lattice structure [53], [147]. For this, we decompose the polyphase matrix $E(z)$ as follows:

$$E(z) = B_{N-1}D(z)B_{N-2} \cdots D(z)B_0. \tag{6.62}$$

Here, the matrices B_k, $k = 0, \ldots, N-1$ are rotation matrices:

$$B_k = \begin{bmatrix} \cos\beta_k & \sin\beta_k \\ -\sin\beta_k & \cos\beta_k \end{bmatrix}, \quad k = 0, \ldots, N-1, \tag{6.63}$$

and $D(z)$ is the delay matrix

$$D = \begin{bmatrix} 1 & 0 \\ 0 & z^{-1} \end{bmatrix}. \tag{6.64}$$

It can be shown that such a decomposition is always possible [146].

Provided $\cos\beta_k \neq 0$, $k = 0, 1, \ldots, N-1$, we can also write

$$E(z) = c\, A_{N-1}D(z)A_{N-2} \cdots D(z)A_0 \tag{6.65}$$

with

$$A_k = \begin{bmatrix} 1 & \alpha_k \\ -\alpha_k & 1 \end{bmatrix}, \quad c = \prod_{k=0}^{N-1} \frac{1}{\sqrt{1+\alpha_k^2}}. \tag{6.66}$$

This basically allows us to reduce the total number of multiplications. The realization of the filter bank by means of the decomposed polyphase matrix is pictured in Figure 6.11(a). Given α_k, $k = 0, \ldots, N-1$, we obtain filters of length $L = 2N$.

Since this lattice structure leads to a paraunitary filter bank for arbitrary α_k, we can thus achieve perfect reconstruction even if the coefficients must be quantized due to finite precision. In addition, this structure may be used for optimizing the filters. For this, we excite the filter bank with $x_{even}(n) = \delta_{n0}$ and $x_{odd}(n) = \delta_{n1}$ and observe the polyphase components of $H_0(z)$ and $H_1(z)$ at the output.

The polyphase matrix of the synthesis filter bank has the following factorization:

$$R(z) = B_0^T D'(z)B_1^T \cdots D'(z)B_{N-1}^T \tag{6.67}$$

with $D'(z) = J D(z)J$, such that $D'(z)D(z) = z^{-1}I$. This means that all rotations are inverted and additional delay is introduced. The implementation is shown in Figure 6.11(b).
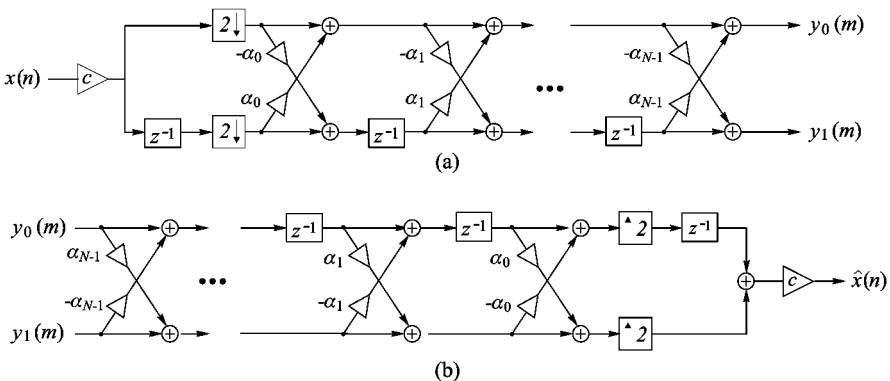
Figure 6.11. Paraunitary filter bank in lattice structure; (a) analysis; (b) synthesis.

6.2.7   Linear-Phase Filter Banks in Lattice Structure

Linear-phase PR two-channel filter banks can be designed and implemented in various ways. Since the filters do not have to be power-complementary, we have much more design freedom than in the paraunitary case. For example, any factorization of a Nyquist filter into two linear-phase filters is possible. A Nyquist filter with $P = 6$ zeros can for instance be factored into two linear-phase filters each of which has three zeros, or into one filter with four and one filter with two zeros. However, realizing the filters in lattice structure, as will be discussed in the following, involves the restriction that the number of coefficients must be even and equal for all filters.

The following factorization of $E(z)$ is used [146]:

$$E(z) = L_{N-1}D(z)L_{N-2} \cdots D(z)L_0 \qquad (6.68)$$

with

$$L_k = \begin{bmatrix} 1 & \alpha_k \\ \alpha_k & 1 \end{bmatrix}, \quad L_{N-1} = \begin{bmatrix} 1 & 1 \\ 1 & -1 \end{bmatrix}, \quad D = \begin{bmatrix} 1 & 0 \\ 0 & z^{-1} \end{bmatrix}, \quad k = 0, \dots, N-2.$$

It results in a linear-phase PR filter bank. The realization of the filter bank with the decomposed polyphase matrix is depicted in Figure 6.12. As in the case of paraunitary filter banks in Section 6.2.6, we can achieve PR if the coefficients must be quantized because of finite-precision arithmetic. In addition, the structure is suitable for optimizing filter banks with respect to given criteria while conditions such as linear-phase and PR are structurally guaranteed. The number of filter coefficients is $L = 2(N + 1)$ and thus even in any case.
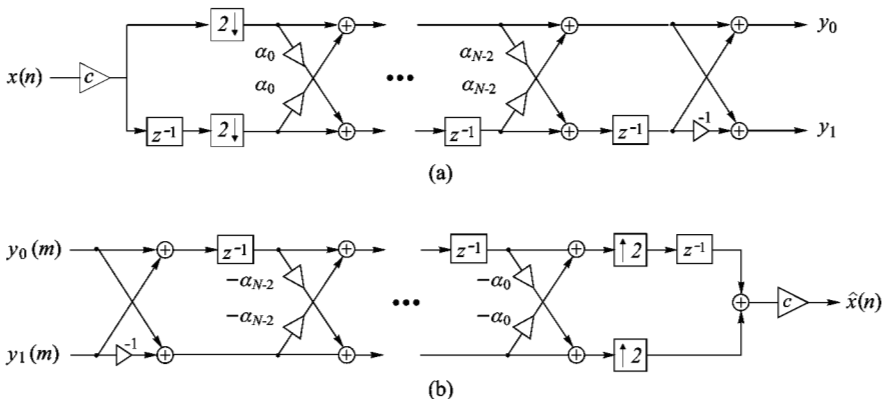
Figure 6.12. Linear-phase filter bank in lattice structure; (a) analysis; (b) synthesis.

6.2.8   Lifting Structures

Lifting structures have been suggested in [71, 141] for the design of biorthogonal wavelets. In order to explain the discrete-time filter bank concept behind lifting, we consider the two-channel filter bank in Figure 6.13(a). The structure obviously yields perfect reconstruction with a delay of one sample. Now we incorporate a system $A(z)$ and a delay z^{-a}, $a \geq 0$ in the polyphase domain as shown in Figure 6.13(b). Clearly, the overall structure still gives PR, while the new subband signal $y_0(m)$ is different from the one in Figure 6.13(a). In fact, the new $y_0(m)$ results from filtering $x(n)$ with the filter

$$H_0(z) = z^{-2a} + z^{-1}A(z^2)$$

and subsampling. The overall delay has increased by $2a$. In the next step in Figure 6.13(c), we use a dual lifting step that allows us to construct a new (longer) filter $H_1(z)$ as

$$H_1(z) = z^{-2b-1} + z^{-2a}B(z^2) + z^{-1}A(z^2)B(z^2).$$

Now the overall delay is $2a + 2b + 1$ with $a, b \geq 0$. Note that, although we may already have relatively long filters $H_0(z)$ and $H_1(z)$, the delay may be unchanged if we have chosen $a = b = 0$. This technique allows us to design PR filter banks with high stopband attenuation and low overall delay. Such filters are for example very attractive for real-time communications systems, where the overall delay has to be kept below a given threshold.

(a)

(b)

(c)
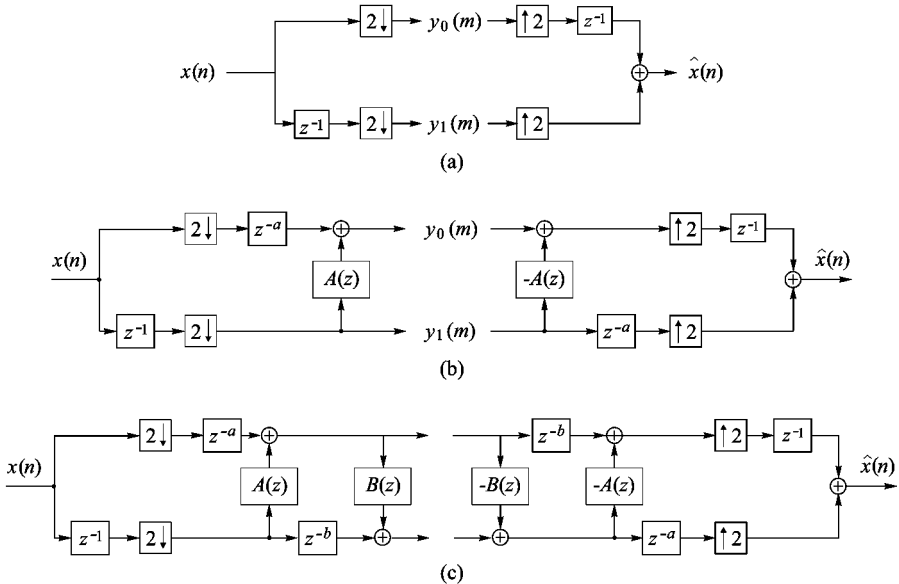
Figure 6.13. Two-channel filter banks in lifting structure.
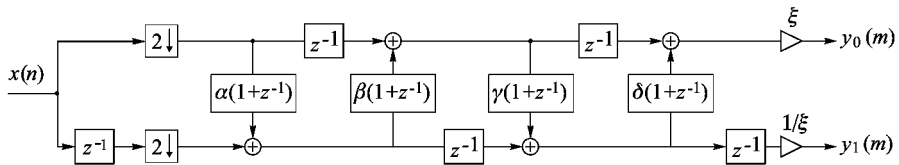
Figure 6.14. Lifting implementation of the 9-7 filters from [5] according to [37]. The parameters are $\alpha = -1.586134342$, $\beta = -0.05298011854$, $\gamma = 0.8829110762$, $\delta = 0.4435068522$, $\xi = 1.149604398$.

In general, the filters constructed via lifting are non-linear phase. However, the lifting steps can easily be chosen to yield linear-phase filters.

Both lattice and lifting structures are very attractive for the implementation of filter banks on digital signal processors, because coefficient quantization does not affect the PR property. Moreover, due to the joint realization of $H_0(z)$ and $H_1(z)$, the total number of operations is lower than for the direct polyphase implementation of the same filters. To give an example, Figure 6.14 shows the lifting implementation of the 9-7 filters from [5], which are very popular in image compression.

An important result is that any two-channel filter bank can be factored into a finite number of lifting steps [37]. The proof is based on the Euclidean algorithm [9]. The decomposition of a given filter bank into lifting steps is not unique, so that many implementations for the same filter bank can be found. Unfortunately, one cannot say *a priori* which implementation will perform best if the coefficients have to be quantized to a given number of bits.

6.3   Tree-Structured Filter Banks

In most applications one needs a signal decomposition into more than two, say M, frequency bands. A simple way of designing the required filters is to build cascades of two-channel filter banks. Figure 6.15 shows two examples, (a) a regular tree structure and (b) an octave-band tree structure. Further structures are easily found, and also signal-adaptive concepts have been developed, where the tree is chosen such that it is best matched to the problem. In all cases, PR is easily obtained if the two-channel filter banks, which are used as the basic building blocks, provide PR.

In order to describe the system functions of cascaded filters with sampling rate changes, we consider the two systems in Figure 6.16. It is easily seen that both systems are equivalent. Their system function is

$$\frac{1}{2}\, H_1(z^2)\, \left[H_0(z) + H_0(-z)\right].$$

For the system $B_2(z^2)$ we have

$$B_2(z^2) = H_0(z)H_1(z^2).$$

With this result, the system functions of arbitrary cascades of two-channel filter banks are easily obtained.

An example of the frequency responses of non-ideal octave-band filter banks in tree structure is shown in Figure 6.17. An effect, which results from the overlap of the lowpass and highpass frequency responses, is the occurrence of relatively large side lobes.
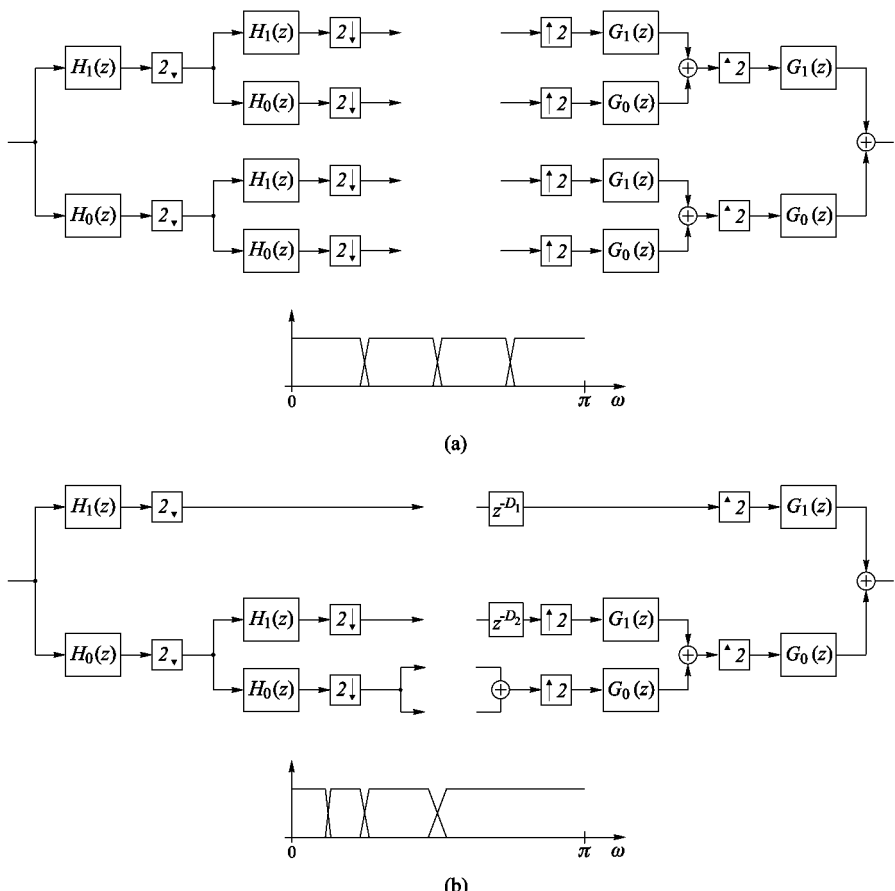
Figure 6.15. Tree-structured filter banks; (a) regular tree structure; (b) octave-band tree structure.
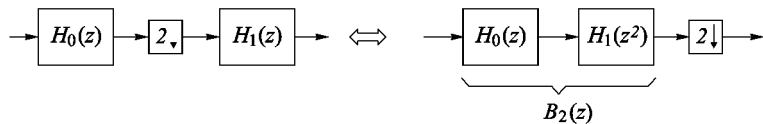
Figure 6.16. Equivalent systems.
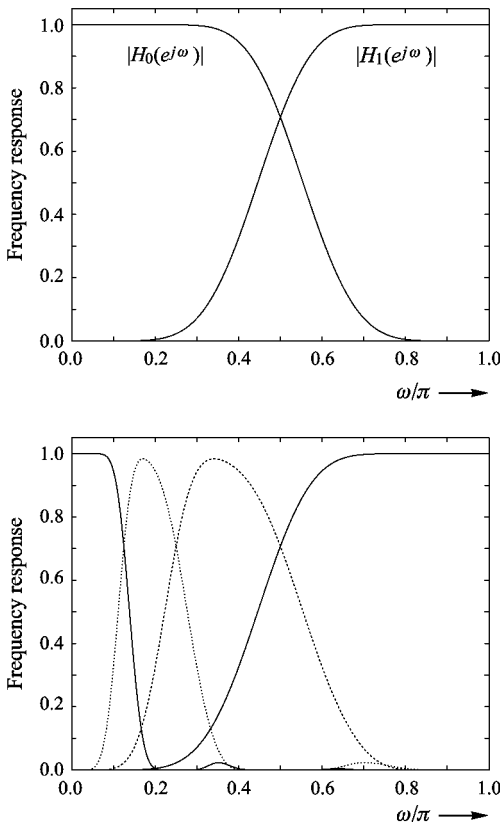
Figure 6.17. Frequency responses in tree-structured filter banks; (a) two-channel filter bank; (b) octave-band filter bank.

6.4   Uniform *M*-Channel Filter Banks

This section addresses uniform *M*-channel filter banks for which the sampling rate is reduced by N in all subbands. Figure 6.1 shows such a filter bank, and Figure 6.18 shows some frequency responses. In order to obtain general results for uniform *M*-channel filter banks, we start by assuming $N \leq M$, where M is the number of subbands.

6.4.1   Input-Output Relations

We consider the multirate filter bank depicted in Figure 6.1. From equations (6.7) and (6.8) we obtain
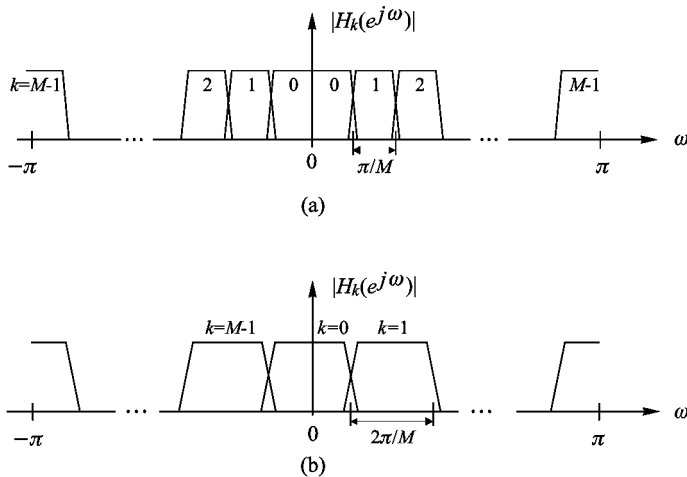
Figure 6.18. Frequency responses of the analysis filters in a uniform M-channel filter bank; (a) cosine-modulated filter bank; (b) DFT filter bank.

$$Y_k(z) = \frac{1}{N} \sum_{i=0}^{N-1} H_k(W_N^i z^{\frac{1}{N}}) \, X(W_N^i z^{\frac{1}{N}}), \quad k = 0, \ldots, M-1, \tag{6.69}$$

and

$$\hat{X}(z) = \frac{1}{N} \sum_{k=0}^{M-1} \sum_{i=0}^{N-1} G_k(z) H_k(W_N^i z) X(W_N^i z). \tag{6.70}$$

In order to achieve perfect reconstruction, suitable filters $H_k(z)$ and $G_k(z)$, $k = 0, \ldots, M-1$, and parameters N and M must be chosen. We obtain the PR requirement by first changing the order of the summation in (6.70):

$$\hat{X}(z) = \frac{1}{N} \sum_{i=0}^{N-1} X(W_N^i z) \sum_{k=0}^{M-1} G_k(z) H_k(W_N^i z). \tag{6.71}$$

Equation (6.71) shows that $\hat{X}(z) = z^{-q} \, X(z)$ holds if the filters satisfy

$$\sum_{k=0}^{M-1} G_k(z) H_k(W_N^i z) = N \, z^{-q} \, \delta_{i0}, \quad 0 \le i \le N-1. \tag{6.72}$$

Using the notation

$$
\boldsymbol{H}_m(z) = \begin{bmatrix} H_0(z) & H_1(z) & \cdots & H_{M-1}(z) \\ H_0(zW_N) & H_1(zW_N) & \cdots & H_{M-1}(zW_N) \\ \vdots & \vdots & \ddots & \vdots \\ H_0(zW_N^{N-1}) & H_1(zW_N^{N-1}) & \cdots & H_{M-1}(zW_N^{N-1}) \end{bmatrix}, \quad (6.73)
$$

and

$$
\boldsymbol{g}(z) = [G_0(z), G_1(z), \ldots, G_{M-1}(z)]^T, \tag{6.74}
$$

$$
\boldsymbol{x}_m(z) = [X(z), X(zW_N), \ldots, X(zW_N^{M-1})]^T, \tag{6.75}
$$

the input-output relations may also be written as

$$
\hat{X}(z) = \frac{1}{N}\, \boldsymbol{g}^T(z)\, \boldsymbol{H}_m^T(z)\, \boldsymbol{x}_m(z). \tag{6.76}
$$

Thus, PR requires that

$$
\frac{1}{N}\, \boldsymbol{g}^T(z)\, \boldsymbol{H}_m^T(z) = z^{-q}\, [1, 0, \ldots, 0]. \tag{6.77}
$$

6.4.2   The Polyphase Representation

In Section 6.2 we explained the polyphase representation of two-channel filter banks. The generalization to M channels with subsampling by N is outlined below. The implementation of such a filter bank is depicted in Figure 6.19.

Analysis. The analysis filter bank is described by

$$
\boldsymbol{y}_p(z) = \boldsymbol{E}(z)\, \boldsymbol{x}_p(z), \tag{6.78}
$$

where

$$
\boldsymbol{x}_p(z) = \left[\bar{X}_0(z), \bar{X}_1(z), \ldots, \bar{X}_{N-1}(z)\right]^T \tag{6.79}
$$

$$
\boldsymbol{y}_p(z) = \left[Y_0(z), Y_1(z), \ldots, Y_{M-1}(z)\right]^T \tag{6.80}
$$

$$
\boldsymbol{E}(z) = \begin{bmatrix} H_{00}(z) & H_{01}(z) & \cdots & H_{0,N-1}(z) \\ H_{10}(z) & H_{11}(z) & \cdots & H_{1,N-1}(z) \\ \vdots & \vdots & \ddots & \vdots \\ H_{M-1,0}(z) & H_{M-1,1}(z) & \cdots & H_{M-1,N-1}(z) \end{bmatrix} \tag{6.81}
$$
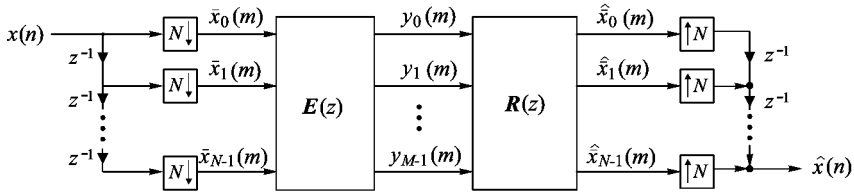
Figure 6.19. Filter bank in polyphase structure.

Synthesis. Synthesis may be described in a similar way:

$$\hat{x}_p(z) = R(z)\, y_p(z) \tag{6.82}$$

with

$$
R(z) = \begin{bmatrix}
G'_{00}(z) & G'_{10}(z) & \cdots & G'_{M-1,0}(z) \\
G'_{01}(z) & G'_{11}(z) & \cdots & G'_{M-1,1}(z) \\
\vdots & \vdots & \ddots & \vdots \\
G'_{0,N-1}(z) & G'_{1,N-1}(z) & \cdots & G'_{M-1,N-1}(z)
\end{bmatrix} \tag{6.83}
$$

Perfect Reconstruction. From (6.78) and (6.82) we conclude the PR requirement

$$R(z)\, E(z) = z^{-q_0}\, I, \tag{6.84}$$

which results in an overall delay of $Mq_0 + M - 1$ samples. The generalization to any arbitrary delay of $Mq_0 + r + M - 1$ samples is

$$R(z)\, E(z) = z^{-q_0} \begin{bmatrix} 0 & I_{M-r} \\ z^{-1}I_r & 0 \end{bmatrix}, \tag{6.85}$$

where $0 \le r \le M - 1$ [146].

FIR Filter Banks. Let us write (6.84) as

$$R(z) = z^{-q_0}\, E^{-1}(z) = z^{-q_0}\, \frac{\mathrm{Adj}\{E(z)\}}{\det\{E(z)\}} \tag{6.86}$$

and let us assume that all elements of $E(z)$ are FIR. We see that the elements of $R(z)$ are also FIR if $\det\{E(z)\}$ is a monomial in z. The same arguments hold for the more general PR condition (6.85). Thus, FIR solutions for both the analysis and synthesis filters of a PR filter bank require that the determinants of the polyphase matrices are just delays.

6.4.3   Paraunitary Filter Banks

The paraunitary case is characterized by the fact that the sum of the energies of all subband signals is equal to the energy of the input signal. This may be expressed as $\|\boldsymbol{y}_p\| = \|\boldsymbol{x}_p\| \; \forall \; \boldsymbol{x}_p$ with $\|\boldsymbol{x}_p\| < \infty$, where $\boldsymbol{x}_p(z)$ is the polyphase vector of a finite-energy input signal and $\boldsymbol{y}_p(z) = \boldsymbol{E}(z)\,\boldsymbol{x}_p(z)$ is the vector of subband signals. It can easily be verified that filter banks (oversampled and critically sampled) are paraunitary if the following condition holds:

$$\tilde{\boldsymbol{E}}(z)\,\boldsymbol{E}(z) = \boldsymbol{I}. \tag{6.87}$$

This also implies that

$$h_k(n) = g_k^*(-n) \;\longleftrightarrow\; H_k(z) = \tilde{G}_k(z), \quad k = 0, \ldots, M-1. \tag{6.88}$$

Especially in the critically subsampled case where $N = M$, the impulse responses $h_k(n-mM)$ and $g_k(n-mM)$, $k = 0, \ldots, M-1$, $m \in \mathbb{Z}$, respectively, form orthonormal bases:

$$\sum_n h_j^*(mM + n)\,h_k(n) = \delta_{m0}\,\delta_{jk}, \tag{6.89}$$

$$\sum_n g_j^*(mM + n)\,g_k(n) = \delta_{m0}\,\delta_{jk}. \tag{6.90}$$

6.4.4   Design of Critically Subsampled M-Channel FIR Filter Banks

Analogous to the lattice structures introduced in Sections 6.2.6 and 6.2.7, we consider the following factorization of $\boldsymbol{E}(z)$:

$$\boldsymbol{E}(z) = \boldsymbol{A}_K \boldsymbol{D}(z)\boldsymbol{A}_{K-1}\boldsymbol{D}(z)\cdots\boldsymbol{D}(z)\boldsymbol{A}_0, \tag{6.91}$$

where

$$\boldsymbol{D}(z) = \begin{bmatrix} \boldsymbol{I}_{M-1} & \boldsymbol{0} \\ \boldsymbol{0} & z^{-1} \end{bmatrix}. \tag{6.92}$$

The matrices $\boldsymbol{A}_k$, $k = 0, 1, \ldots, K$ are arbitrary non-singular matrices. The elements of these matrices are the free design parameters, which can be chosen in order to obtain some desired filter properties. To achieve this, a useful objective function has to be defined and the free parameters have to be found via non-linear optimization. Typically, one tries to minimize the stopband energy of the filters.

The corresponding synthesis polyphase matrix can be designed as

$$\boldsymbol{R}(z) = \boldsymbol{A}_0^{-1}\boldsymbol{\Gamma}(z)\boldsymbol{A}_1^{-1}\boldsymbol{\Gamma}(z)\cdots\boldsymbol{\Gamma}(z)\boldsymbol{A}_K^{-1}, \qquad (6.93)$$

where

$$\boldsymbol{\Gamma}(z) = \begin{bmatrix} z^{-1}\boldsymbol{I}_{M-1} & \boldsymbol{0} \\ \boldsymbol{0} & 1 \end{bmatrix}. \qquad (6.94)$$

Clearly, both $\boldsymbol{E}(z)$ and $\boldsymbol{R}(z)$ contain FIR filters. The overall transfer matrix is

$$\boldsymbol{R}(z)\boldsymbol{E}(z) = z^{-K}\boldsymbol{I}. \qquad (6.95)$$

Figure 6.20 illustrates the implementation of the filter bank according to the above factorizations. A simple parameterization for the matrices $\boldsymbol{A}_k$ that guarantees the existence of $\boldsymbol{A}_k^{-1}$ is to use triangular matrices with ones on the main diagonal. The inverses then are also triangular, so that the implementation cost is somehow reduced. Examples are given in [146].

Paraunitary FIR Filter Banks based on Rotations. Paraunitary filter banks are easily derived from the above scheme by restricting the matrices $\boldsymbol{A}_k$ to be unitary. Interestingly, not all matrices have to be fully parameterized rotation matrices in order to cover all possible unitary filter banks [41]. The matrices $\boldsymbol{A}_0,\ldots,\boldsymbol{A}_{K-1}$ only have to belong to the subset of all possible $M \times M$ unitary matrices which can be written as a sequence of $M-1$ Givens rotations performed successively on the elements $k, k+1$ for $k = 0,1,\ldots,M-2$.

$$\boldsymbol{A}_k = \begin{bmatrix} \cos\phi_0^{(k)} & \sin\phi_0^{(k)} & & & \\ -\sin\phi_0^{(k)} & \cos\phi_0^{(k)} & & & \\ & & 1 & & \\ & & & \ddots & \\ & & & & 1 \end{bmatrix} \cdots \begin{bmatrix} 1 & & & & \\ & \ddots & & & \\ & & 1 & & \\ & & & \cos\phi_{K-1}^{(k)} & \sin\phi_{K-1}^{(k)} \\ & & & -\sin\phi_{K-1}^{(k)} & \cos\phi_{K-1}^{(k)} \end{bmatrix}$$

$$(6.96)$$

The last matrix $\boldsymbol{A}_K$ has to be a general rotation matrix. Filter design can be carried out by defining an objective function and optimizing the rotation angles.

Paraunitary FIR Filter Banks based on Reflections. A second way of parameterizing paraunitary filter banks was proposed in [148]. Here, the polyphase matrix is written as follows:

$$\boldsymbol{E}(z) = \boldsymbol{V}_K(z)\boldsymbol{V}_{K-1}(z)\cdots\boldsymbol{V}_1(z)\boldsymbol{U}. \qquad (6.97)$$

The matrices $\boldsymbol{V}_k(z)$ are reflection-like matrices of the type

$$\boldsymbol{V}_k = \boldsymbol{I} - \boldsymbol{v}_k\boldsymbol{v}_k^T + z^{-1}\boldsymbol{v}_k\boldsymbol{v}_k^T, \qquad (6.98)$$
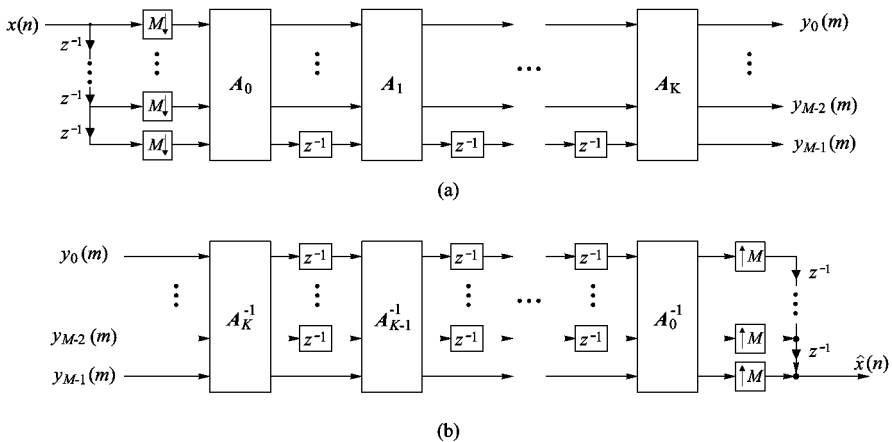
Figure 6.20. *M*-channel filter bank with FIR filters; (a) analysis; (b) synthesis.

where $\boldsymbol{v}_k$ is an $M \times 1$ vector with $\|\boldsymbol{v}_k\| = \boldsymbol{v}^T\boldsymbol{v} = 1$. It is easily proven that $\boldsymbol{V}_k^T(z^{-1})\boldsymbol{V}_k(z) = \boldsymbol{I}$, so that the matrices can indeed be used for parameterization. The matrix $\boldsymbol{U}$ has to be a general unitary matrix. The parameterization (6.97) directly leads to an efficient implementation, which is similar to the one discussed in Section 3.4.4 for the implementation of Householder reflections: instead of multiplying an input vector $\boldsymbol{x}(z)$ with an entire matrix $\boldsymbol{V}_k(z)$, one computes $\boldsymbol{x}(z) - \boldsymbol{v}_k[1 - z^{-1}][\boldsymbol{v}_k^T\boldsymbol{x}(z)]$ in order to obtain $\boldsymbol{V}_k(z)\boldsymbol{x}(z)$.

In addition to the above parameterizations, which generally yield non-linear phase filters, methods for designing linear-phase paraunitary filter banks have also been developed. For this special class the reader is referred to [137].

6.5   DFT Filter Banks

DFT filter banks belong to the class of modulated filter banks, where all filters are derived from prototypes via modulation. Modulated filter banks have the great advantage that only suitable prototypes must be found, not the complete set of analysis and synthesis filters. One prototype is required for the analysis and one for the synthesis side, and in most cases the same prototypes can be used for both sides. Due to the modulated structure very efficient implementations are possible.

In DFT banks, the analysis and synthesis filters, $H_k(z)$ and $G_k(z)$, are

related to the analysis and synthesis prototypes, $P(z)$ and $Q(z)$, as

$$H_k(z) = P(W_M^k z) \quad \longleftrightarrow \quad h_k(n) = p(n)\ W_M^{-kn}$$

$$G_k(z) = Q(W_M^k z) \quad \longleftrightarrow \quad g_k(n) = q(n)\ W_M^{-kn}.$$

$$(6.99)$$

In order to explain the efficient implementation of DFT banks, let us consider the critically subsampled case. The analysis equation is

$$
\begin{aligned}
y_k(m) &= \sum_{n=0}^{L-1} h_k(n)\ x(mM - n) \\
&= \sum_{n=0}^{L-1} p(n)\ W_M^{-kn}\ x(mM - n).
\end{aligned}
$$

$$(6.100)$$

We now substitute $n = iM + j$, $L = ML_p$ and rewrite (6.100) as

$$
\begin{aligned}
y_k(m) &= \sum_{j=0}^{M-1} \sum_{i=0}^{L_p-1} p(iM + j)\ W_M^{-k(iM+j)}\ x(mM - iM - j) \\
&= \sum_{j=0}^{M-1} W_M^{-kj} \sum_{i=0}^{L_p-1} p(iM + j)\ x(mM - iM - j) \\
&= \sum_{j=0}^{M-1} W_M^{-kj} \sum_{i=0}^{L_p-1} p_j(i)\ \bar{x}_j(m - i).
\end{aligned}
$$

$$(6.101)$$

Thus, the subband signals can be computed by filtering the polyphase components of the input signal with the polyphase components of the prototype, followed by an IDFT (without pre-factor $1/M$). On the synthesis side, the same principle can be used. The complete analysis/synthesis system, which requires extremely low computation effort, is depicted in Figure 6.21.

For critical subsampling, as shown in Figure 6.21, the PR condition is easily found to be

$$P_k(z)\ Q_{M-1-k}(z) = \frac{z^{-q_0}}{M}.$$

$$(6.102)$$

This means that the polyphase components of PR FIR prototypes are restricted to length one, and the filtering degenerates to pointwise scalar multiplication. Thus, critically subsampled DFT filter banks with PR mainly reduce to the DFT.

If oversampling by a factor $\mu = \frac{M}{N} \in \mathbb{Z}$ is considered, the PR condition becomes [33, 86]

$$\sum_{\ell=0}^{\mu-1} P_{k+\ell N}(z)\ Q_{M-1-k-\ell N}(z) = \frac{z^{-q_0}}{M}.$$

$$(6.103)$$
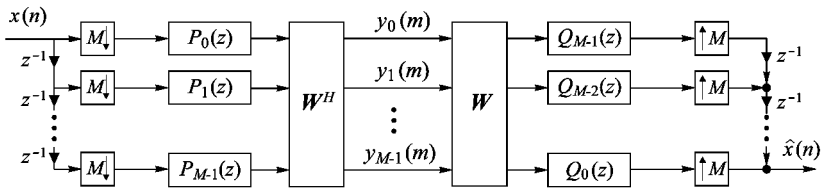
Figure 6.21. DFT polyphase filter bank with critical subsampling.

Clearly, if a filter bank provides PR in the critically subsampled case, it also provides PR in the oversampled case, provided the output signal is downscaled by the oversampling factor. Thus, (6.102) is included in (6.103). This is most easily seen from (6.103) for $\mu = 2$:

$$\underbrace{P_k(z)\, Q_{M-1-k}(z)}_{\frac{z^{-q_0}}{M}} + \underbrace{P_{k+N}(z)\, Q_{M-1-k-N}(z)}_{\frac{z^{-q_0}}{M}} = 2\frac{z^{-q_0}}{M}.$$

In general, (6.103) means an increased design freedom compared to (6.102). This freedom can be exploited in order to design FIR prototypes $P(z)$ and $Q(z)$ with good filter properties.

The prototypes are typically designed to be lowpass filters. A common design criterion is to minimize the stopband energy and the passband ripple:

$$\int_{\text{passband}} \alpha\, (|P(e^{j\omega})| - 1)^2\, d\omega + \int_{\text{stopband}} \beta\, |P(e^{j\omega})|^2\, d\omega \overset{!}{=} \min. \qquad (6.104)$$

At this point it should be mentioned that all PR prototypes for M-channel cosine-modulated filter banks, which will be discussed in the next section, also serve as PR prototypes for oversampled $2M$-channel DFT filter banks. On the other hand, satisfying only (6.103) is not sufficient in the cosine-modulated case. Thus, oversampled DFT filter banks offer more design freedom than cosine-modulated ones.

MDFT Filter Bank. Figure 6.22 shows the MDFT filter bank introduced by Fliege. Compared to the simple DFT filter banks described above, this filter bank is modified in such a way that PR is achieved with FIR filters [55], [82]. The key to PR is subsampling the filter output signals by $M/2$, extracting the real and imaginary parts, and using them to compose the complex subband signals $y_k(m)$, $k = 0, \ldots, M - 1$. As can be seen in Figure 6.22, the extraction of the real and imaginary parts takes place in adjoining channels in reverse order.
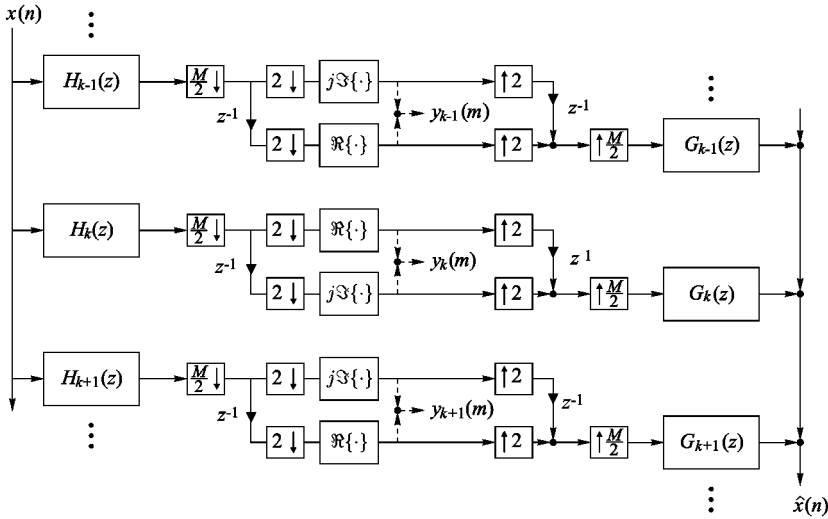
Figure 6.22. Modified complex modulated filter bank with critical subsampling.

DFT Polyphase Filter Bank with IIR Filters and Perfect Reconstruction.

We consider the DFT filter bank in Figure 6.21. Husøy and Ramstad proposed to construct the polyphase components of the prototype as first-order IIR allpass filters [74]:

$$P_i(z) = \frac{1}{\sqrt{M}} \frac{a_i + z^{-1}}{1 + a_i z^{-1}}, \qquad i = 0, \ldots, M-1. \tag{6.105}$$

Using the synthesis filters

$$Q_{M-1-i}(z) = P_i(z^{-1}) = \frac{1}{\sqrt{M}} \frac{1 + a_i z^{-1}}{a_i + z^{-1}}, \qquad i = 0, \ldots, M-1, \tag{6.106}$$

then ensures perfect reconstruction. Unfortunately, this leads to a problem concerning stability: if the analysis filters are stable, the synthesis filters determined according to (6.106) are not. This problem can be avoided by filtering the subband signals "backwards" using the stable analysis filters. Then, the desired output signal is formed by another temporal reversal. This is not a feasible strategy if we work with one-dimensional signals, but in image processing we *a priori* have finite-length signals so that this method can be applied nevertheless.

The quality of a filter bank is not only dependent on whether it reconstructs perfectly or not. The actual purpose of the filter bank is to separate different frequency bands, for example in order to provide a maximal coding

gain. The stopband attenuation of the prototype $P(z)$ composed of IIR allpasses is determined by the parameters a_i, $i = 0, \ldots, M - 1$, so that these are the design parameters. Husøy and Ramstad state a stopband attenuation of 36.4 dB for the prototype $P(z)$ of an eight-channel filter bank [74]. In view of the extremely low computational cost this is an astonishing value.

6.6   Cosine-Modulated Filter Banks

Cosine-modulated filter banks are very popular due to their real-valued nature and their efficient implementation via polyphase structure and fast DCT [116, 127, 94, 121, 87, 100, 110, 129, 68]. Cosine-modulated filter banks can be designed as pseudo QMF banks [127], paraunitary filter banks [94, 121, 87, 100, 103], and also as biorthogonal filter banks allowing low reconstruction delay [110, 129, 68, 83, 86]. Perfect reconstruction is easily achieved by choosing an appropriate prototype. For example, the MPEG audio standard [17] is based on cosine-modulated filter banks.

In the following, we will consider biorthogonal cosine-modulated filter banks where the analysis filters $h_k(n)$, $k = 0, \ldots, M - 1$, are derived from an FIR prototype $p(n)$ and the synthesis filters $g_k(n)$, $k = 0, \ldots, M - 1$, from an FIR prototype $q(n)$ according to

$$h_k(n) = 2p(n) \cos\left[\frac{\pi}{M}\left(k + \frac{1}{2}\right)\left(n - \frac{D}{2}\right) + \phi_k\right], \quad n = 0, \ldots, L_p - 1$$

$$g_k(n) = 2q(n) \cos\left[\frac{\pi}{M}\left(k + \frac{1}{2}\right)\left(n - \frac{D}{2}\right) - \phi_k\right], \quad n = 0, \ldots, L_q - 1.$$

The length of the analysis prototype is L_p, and the length of the synthesis prototype is L_q. The variable D denotes the overall delay of the analysis-synthesis system. A suitable choice for ϕ_k is given by $\phi_k = (-1)^k \pi/4$ [87, 95].

For the sake of brevity, we confine ourselves to even M, analysis and synthesis prototypes with lengths $L_p = 2mM$ and $L_q = 2m'M$, $m, m' \in \mathbb{N}$, and an overall delay of $D = 2sM + 2M - 1$ samples. Note that the delay can be chosen independently of the filter length, so that the design of low-delay banks is included here. The most common case within this framework is the one where the same prototype is used for analysis and synthesis. However, in order to demonstrate some of the design freedom, we start with a more general approach where different prototypes are used for analysis and synthesis. Generalizations to all filter lengths and delays are given in [68].

In order to derive the conditions that must be met by the prototypes $P(z)$ and $Q(z)$ to yield perfect reconstruction, we first decompose them into $2M$ polyphase components. Note that in the case of DFT filter banks, only M polyphase components were used to describe an M-channel filter bank. We use the type-1 decomposition given by

$$P_j(z) = \sum_{\ell=0}^{m-1} p(2\ell M + j) \, z^{-\ell}, \qquad j = 0, \ldots, 2M - 1. \tag{6.107}$$

6.6.1 Critically Subsampled Case

In the critically subsampled case the analysis polyphase matrix can be written as [112, 68]

$$\boldsymbol{E}(z) = \boldsymbol{T}_1 \begin{bmatrix} \boldsymbol{P}_0(z^2) \\ z^{-1}\boldsymbol{P}_1(z^2) \end{bmatrix}, \tag{6.108}$$

where

$$\begin{aligned}[\boldsymbol{T}_1]_{k,j} &= 2\cos\left[\tfrac{\pi}{M}\left(k+\tfrac{1}{2}\right)\left(j-\tfrac{D}{2}\right)+\phi_k\right], \\ &\qquad k = 0, \ldots, M-1, \quad j = 0, \ldots, 2M-1,\end{aligned} \tag{6.109}$$

and

$$\begin{aligned}\boldsymbol{P}_0(z^2) &= \operatorname{diag}\left[P_0(-z^2), P_1(-z^2), \ldots, P_{M-1}(-z^2)\right], \\ \boldsymbol{P}_1(z^2) &= \operatorname{diag}\left[P_M(-z^2), P_{M+1}(-z^2), \ldots, P_{2M-1}(-z^2)\right].\end{aligned} \tag{6.110}$$

Note that the matrices $\boldsymbol{P}_0(z^2)$ and $\boldsymbol{P}_1(z^2)$ contain upsampled and modulated versions of the polyphase filters.

For the synthesis polyphase matrix we get

$$\boldsymbol{R}(z) = \left[z^{-1}\boldsymbol{Q}_1(z^2),\ \boldsymbol{Q}_0(z^2)\right]\boldsymbol{T}_2^{\mathrm{T}}, \tag{6.111}$$

where

$$\begin{aligned}[\boldsymbol{T}_2]_{k,j} &= 2\cos\left[\tfrac{\pi}{M}\left(k+\tfrac{1}{2}\right)\left(2M-1-j-\tfrac{D}{2}\right)-\phi_k\right], \\ &\qquad k = 0, \ldots, M-1, \quad j = 0, \ldots, 2M-1,\end{aligned} \tag{6.112}$$

and

$$\begin{aligned}\boldsymbol{Q}_0(z^2) &= \operatorname{diag}\left[Q_{M-1}(-z^2), \ldots, Q_1(-z^2), Q_0(-z^2)\right], \\ \boldsymbol{Q}_1(z^2) &= \operatorname{diag}\left[Q_{2M-1}(-z^2), \ldots, Q_{M+1}(-z^2), Q_M(-z^2)\right].\end{aligned} \tag{6.113}$$

The perfect reconstruction conditions are obtained by setting

$$\boldsymbol{R}(z)\boldsymbol{E}(z) = z^{-q_0}\,\boldsymbol{I}_M. \tag{6.114}$$

Using the property [87]

$$\boldsymbol{T}_2^{\mathrm{T}}\boldsymbol{T}_1 = (-1)^s\,2M\,\boldsymbol{I}_{2M} + 2M\begin{bmatrix} \boldsymbol{J}_M & 0 \\ 0 & -\boldsymbol{J}_M \end{bmatrix}, \tag{6.115}$$

this yields the conditions

$$P_k(z)\,Q_{2M-1-k}(z) + P_{M+k}(z)\,Q_{M-1-k}(z) \;\overset{!}{=}\; \frac{z^{-s}}{2M}, \tag{6.116}$$

$$P_k(z)\,Q_{M+k}(z) - P_{M+k}(z)\,Q_k(z) \;\overset{!}{=}\; 0, \tag{6.117}$$

which have to be met for $k = 0, \ldots, \frac{M}{2} - 1$. The relationship between q_0 and s is

$$q_0 = 2s + 1. \tag{6.118}$$

The condition (6.117) is satisfied for $Q_k(z) = \alpha z^{-\beta} P_k(z)$ and $Q_{M+k}(z) = \alpha z^{-\beta} P_{M+k}(z)$ with arbitrary α, β, which suggests the use of the same prototype for both analysis and synthesis. Thus, with $Q(z) = P(z)$, the remaining condition is

$$P_{2M-1-k}(z)\,P_k(z) + P_{M+k}(z)\,P_{M-1-k}(z) \overset{!}{=} \frac{z^{-s}}{2M}, \qquad k = 0, \ldots, \frac{M}{2} - 1. \tag{6.119}$$

The $M/2$ equations in (6.119) may be understood as PR conditions on $M/2$ non-subsampled two-channel filter banks. The prototype can for instance be designed by using the quadratic-constrained least-squares (QCLS) approach, which was proposed by Nguyen [111]. Here, we write all constraints given by (6.119) in quadratic form and optimize the prototype using constrained numerical optimization. The approach does not inherently guarantee PR, but the PR constraints can be satisfied with arbitrary accuracy.

Another approach, which guarantees PR and also leads to a very efficient implementation of the filter bank, is to design the filters via lifting [129, 83]. For this, we write the PR conditions as

$$\boldsymbol{V}(z)\boldsymbol{U}(z) = \frac{z^{-1}(-z^{-2})^s}{2M}\,\boldsymbol{I}, \tag{6.120}$$

where

$$U(z) = \begin{bmatrix} P_k(-z^2) & (-1)^s P_{M-1-k}(-z^2) \\ (-1)^{s-1} z^{-1} P_{k+M}(-z^2) & z^{-1} P_{2M-1-k}(-z^2) \end{bmatrix}$$

$$V(z) = \begin{bmatrix} z^{-1} Q_{2M-1-k}(-z^2) & (-1)^{s-1} Q_{2M-1-k-M}(-z^2) \\ (-1)^s z^{-1} Q_{k+M}(-z^2) & Q_k(-z^2) \end{bmatrix}.$$

$$(6.121)$$

It is easily verified that (6.120) includes (6.117) and (6.116), but (6.120) can also be derived straightforwardly from (6.114) by using the properties of the cosine functions [83]. The filter design is as follows. We start with

$$U_0(z) = \begin{bmatrix} p_0 & p_1 \\ -p_2 z^{-1} & p_3 z^{-1} \end{bmatrix}$$

$$V_0(z) = \frac{1}{2M} \frac{1}{p_0 p_3 - p_1 p_2} \begin{bmatrix} p_3 z^{-1} & -p_1 \\ -p_2 z^{-1} & p_0 \end{bmatrix},$$

$$(6.122)$$

where the subscript 0 indicates that this is the 0th iteration. We have

$$V_0(z) U_0(z) = \frac{z^{-1}}{2M} I. \qquad (6.123)$$

Longer filters with the same delay are constructed by introducing matrices of the type

$$A_i^{-1}(z) A_i(z) = I \qquad (6.124)$$

with

$$A_i(z) = \begin{bmatrix} a_i z^{-1} & 1 \\ 1 & 0 \end{bmatrix}, \qquad A_i^{-1}(z) = \begin{bmatrix} 0 & 1 \\ 1 & -a_i z^{-1} \end{bmatrix} \qquad (6.125)$$

in between the product $V_i(z) U_i(z)$:

$$U_{i+1}(z) = A_i(z) U_i(z),$$

$$V_{i+1}(z) = V_i(z) A_i^{-1}(z).$$

$$(6.126)$$

Note that $U_{i+1}(z)$ and $V_{i+1}(z)$ retain the structure given in (6.121). From the new matrices the polyphase components of the prototype are easily extracted. The operation (6.126) can be repeated until the filters contained in $U_i(z)$ and $V_i(z)$ have the desired length. Since the overall delay remains constant, this operation is called zero-delay lifting.

A second possibility is to introduce matrices

$$B_i(z) = \begin{bmatrix} 0 & -z^{-1} \\ -z^{-1} & c_i \end{bmatrix}, \qquad C_i(z) = \begin{bmatrix} c_i & z^{-1} \\ z^{-1} & 0 \end{bmatrix} \qquad (6.127)$$

and to construct the new filters as

$$
\begin{aligned}
\boldsymbol{U}_{i+1}(z) &= \boldsymbol{C}_i(z)\boldsymbol{U}_i(z), \\
\boldsymbol{V}_{i+1}(z) &= \boldsymbol{V}_i(z)\boldsymbol{B}_i(z).
\end{aligned}
\tag{6.128}
$$

This type of lifting is known as maximum-delay lifting. Again, $\boldsymbol{U}_{i+1}(z)$ and $\boldsymbol{V}_{i+1}(z)$ have the structure given in (6.121), and since (6.120) is satisfied, PR is structurally guaranteed. Thus, filter optimization can be carried out by optimizing the lifting coefficients in an unrestricted way.

Also other lifting schemes can easily be found. The advantage of the above approach is that only one lifting step with one lifting coefficient a_i or c_i is needed in order to increase the length of two polyphase components of each prototype.

Implementation Issues. The straightforward polyphase implementation of (6.108) is depicted in Figure 6.23. On the analysis side, we see that always those two systems are fed with the same input signal which are connected in (6.116). In the synthesis bank, the output signals of the corresponding synthesis polyphase filters are added. This already suggests the joint implementation of pairs of two filters. However, a more efficient structure can be obtained by exploiting the periodicies in the rectangular matrices $\boldsymbol{T}_1$ and $\boldsymbol{T}_2$ and by replacing them with $M \times M$ cosine modulation matrices $\tilde{\boldsymbol{T}}_1$ and $\tilde{\boldsymbol{T}}_2 = \tilde{\boldsymbol{T}}_1^T = \tilde{\boldsymbol{T}}_1^{-1}$ [83]:

$$
[\tilde{\boldsymbol{T}}_1]_{k,j} =
\begin{cases}
2\cos\left[\frac{\pi}{M}\left(k+\frac{1}{2}\right)\left(j-\frac{D}{2}\right)+\phi_k\right], & j = 0,\ldots,\frac{M}{2}-1 \\[2mm]
2\cos\left[\frac{\pi}{M}\left(k+\frac{1}{2}\right)\left(M+j-\frac{D}{2}\right)+\phi_k\right], & j = \frac{M}{2},\ldots,M-1
\end{cases}
\tag{6.129}
$$

for $k = 0,\ldots,M-1$. This structure is depicted in Figure 6.24. Note that the following signals are needed as input signals for the cosine transform:

$$
\begin{bmatrix} \bar{Z}_k(z) \\ \bar{Z}_{M-1-k}(z) \end{bmatrix} =
\begin{bmatrix} P_k(-z^2) & (-1)^s P_{M-1-k}(-z^2) \\ (-1)^{s-1}z^{-1}P_{k+M}(-z^2) & z^{-1}P_{2M-1-k}(-z^2) \end{bmatrix}
\begin{bmatrix} \bar{X}_k(z) \\ \bar{X}_{M-1-k}(z) \end{bmatrix}
\tag{6.130}
$$

Thus, all polyphase filtering operations can be carried out via the lifting scheme described above where four filters are realized jointly.

(a)

(b)
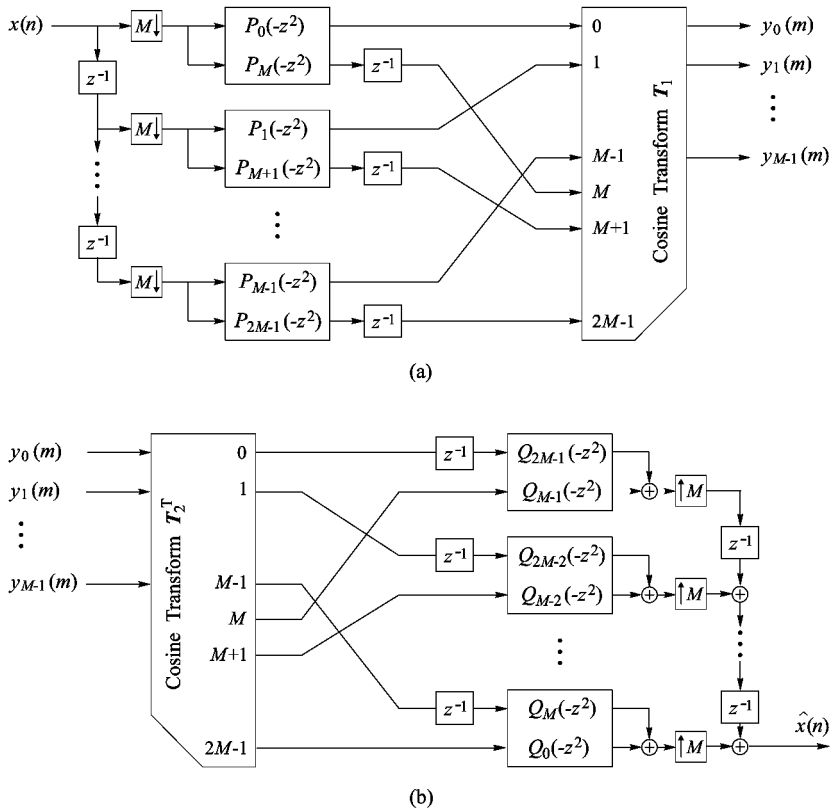
Figure 6.23. Cosine-modulated filter bank with critical subsampling. (a) analysis; (b) synthesis.

6.6.2 Paraunitary Case

In the paraunitary case with critical subsampling we have

$$\tilde{\boldsymbol{E}}(z)\,\boldsymbol{E}(z) = \boldsymbol{I}_M, \tag{6.131}$$

which leads to the following constraints on the prototype:

1. The prototype has to be linear-phase, that is, $p(L-1-n) = p(n)$.
2. The same prototype is required for both analysis and synthesis.
3. The prototype has to satisfy

$$\tilde{P}_k(z)P_k(z) + \tilde{P}_{M+k}(z)P_{M+k}(z) = \frac{1}{2M}. \tag{6.132}$$
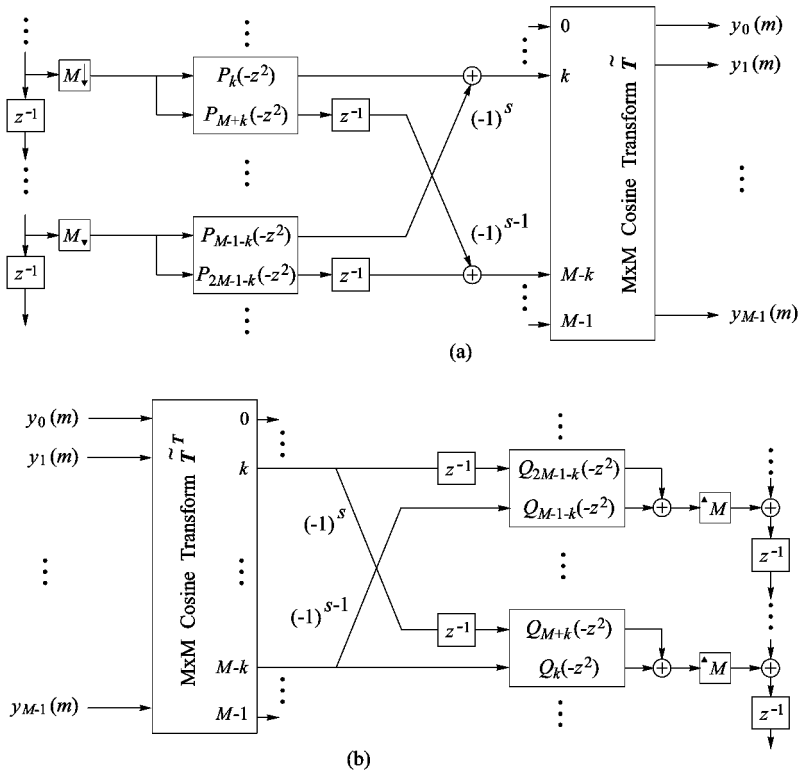
Figure 6.24. Cosine-modulated filter bank with critical subsampling and efficient implementation structure. (a) analysis; (b) synthesis.

The filter design may for instance be carried out by parameterizing the polyphase components using the lattice structure shown in Figure 6.25 and choosing the rotation angles so as to minimize an arbitrary objective function. For this method a good starting point is required, because we have to optimize angles in a cascade of lattices and the relationships between the angles and the impulse response are highly nonlinear. Alternatively, the QCLS approach [111] can be used, which typically is less sensitive to the starting point.

As in the biorthogonal case, the polyphase filters can be realized jointly. One can use the structure in Figure 6.23 and implement two filters at a time via the lattice in Figure 6.25. However, the more efficient structure in Figure 6.24 can also be used, where four filters are realized via a common lattice. This was shown in [95] for special filter lengths. A generalization is given in [62].
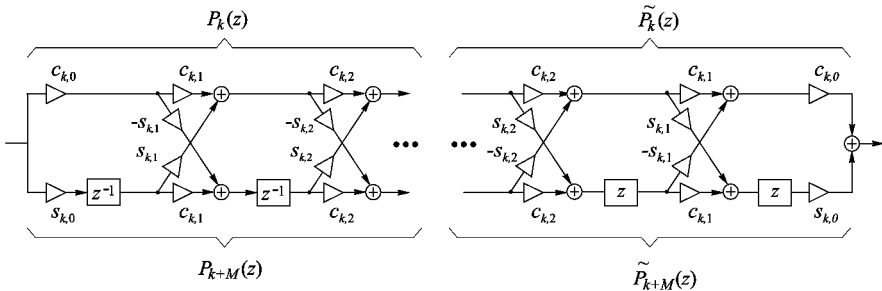
Figure 6.25. Lattice structure for the design and implementation of cosine-modulated filters.

In [103] a method has been proposed that allows the design of discrete-coefficient linear-phase prototypes for the paraunitary case. The design procedure is based on a subspace approach that allows us to perform linear combinations of PR prototype filters in such a way that the resulting filter is also a linear-phase PR prototype. The filter design is carried out iteratively, while the PR property is guaranteed throughout the design process. In order to give some design examples, Table 6.1 shows impulse responses of 8-band prototypes with integer coefficients and filter length $L = 32$. Because of symmetry, only the first 16 coefficients are listed. The frequency responses of the filters #3 and #6 are depicted in Figure 6.26.

Closed Form Solutions. For filter length $L = 2M$ and $L = 4M$ closed form solutions for PR prototypes are known. The special case $L = 2M$ is known as the *modulated lapped transform* (MLT), which was introduced by Princen and Bradley [116]. In this case the PR condition (6.132) reduces to

$$p_k(0)^2 + p_{M+k}(0)^2 = \frac{1}{2M},$$

which means

$$p^2(n) + p^2(M + n) = \frac{1}{2M}. \tag{6.133}$$

An example of an impulse response that satisfies (6.133) is

$$p(n) = \frac{1}{\sqrt{2M}} \, \sin\left[(n + \frac{1}{2})\frac{\pi}{2M}\right]. \tag{6.134}$$

The case $L = 4M$ is known as the *extended lapped transform* (ELT). The ELT was introduced by Malvar, who suggested the following prototype [95]:

$$p(n) = -\frac{1}{4\sqrt{M}} + \frac{1}{2\sqrt{2M}} \cos\left[(n + \frac{1}{2})\frac{\pi}{2M}\right]. \tag{6.135}$$

(a)

(b)
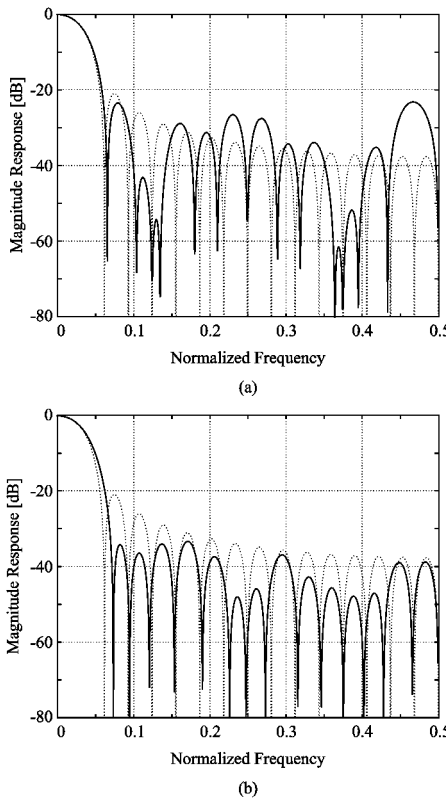
Figure 6.26. Frequency responses of 8-channel prototypes from Table 3.1. (a) filter #3; (b) filter #6. For comparison the frequency response of the ELT prototype is depicted with dotted lines.

Table 6.1.

Perfect reconstruction prototypes for 8-band filter banks with integer coefficients $(p(L - 1 - n) = p(n))$.

n	$p(n)$					
	#1	#2	#3	#4	#5	#6
0			-1	-6	-72	-2190
1			-1	-4	-97	-1901
2			0	0	-41	-1681
3			0	-6	-48	-426
4			0	7	56	497
5			0	0	62	2542
6			2	8	194	3802
7			2	17	204	6205
8		1	4	24	390	9678
9		1	4	33	524	13197
10		1	6	41	656	16359
11		1	6	48	774	19398
12	1	2	7	56	903	22631
13	1	2	7	62	992	24738
14	1	2	8	66	1048	26394
15	1	2	8	68	1105	27421

6.6.3 Oversampled Cosine-Modulated Filter Banks

In the oversampled case with oversampling by $\mu = \frac{M}{N} \in \mathbb{Z}$, the polyphase matrices may be written as

$$E^{(\mu)}(z) = \frac{1}{\sqrt{\mu}} \cdot T \begin{bmatrix} P_0(z^{2\mu}) \\ z^{-1} P_1(z^{2\mu}) \\ \vdots \\ z^{-(2\mu-1)} P_{2\mu-1}(z^{2\mu}) \end{bmatrix} \tag{6.136}$$

and

$$R^{(\mu)}(z) = \frac{1}{\sqrt{\mu}} \cdot \left[z^{-(2\mu-1)} Q_{2\mu-1}(z^{2\mu}), \ldots z^{-1} Q_1(z^{2\mu}), Q_0(z^{2\mu}) \right] T^{\mathrm{T}} \tag{6.137}$$

with

$$P_\ell(z^{2\mu}) = \operatorname{diag} \left\{ P_{\ell N}(-z^{2\mu}), P_{\ell N+1}(-z^{2\mu}), \ldots, P_{\ell N+(N-1)}(-z^{2\mu}) \right\}, \tag{6.138}$$

$$Q_\ell(z^{2\mu}) = \operatorname{diag} \left\{ Q_{\ell N+(N-1)}(-z^{2\mu}), \ldots, Q_{\ell N+1}(-z^{2\mu}), Q_{\ell N}(-z^{2\mu}) \right\}. \tag{6.139}$$

The superscript (μ) indicates the oversampling factor. Requiring

$$R^{(\mu)}(z)\ E^{(\mu)}(z) = z^{-q_0^{(\mu)}} \tag{6.140}$$

for perfect reconstruction yields [86]

$$\sum_{\ell=0}^{2\mu-1} P_{k+\ell N}(z)\ Q_{2M-1-k-\ell N}(z) \overset{!}{=} \frac{z^{-s}}{2M} \tag{6.141}$$

and

$$P_{k+\ell N}(z)\ Q_{M+k+\ell N}(z) - P_{M+k+\ell N}(z)\ Q_{k+\ell N}(z) \overset{!}{=} 0 \tag{6.142}$$

for $k = 0, \ldots, N-1$; $\ell = 0, \ldots, \mu-1$. The delay $q_0^{(\mu)}$ is related to s as

$$q_0^{(\mu)} = 2\mu s + 2\mu - 1, \tag{6.143}$$

and the overall delay amounts to

$$q = N - 1 + q_0^{(\mu)} N. \tag{6.144}$$

As we see, these conditions offer increased design freedom for an increasing oversampling rate. This is further discussed in [86], where solutions based on a nullspace approach are presented.

If we restrict an oversampled cosine-modulated filter bank to be parauni-
tary, that is, $\tilde{\boldsymbol{E}}^{(\mu)}(z)\,\boldsymbol{E}^{(\mu)}(z) = \boldsymbol{I}_N$, we get the following constraints on the
prototype $P(z)$ [85, 86]:

$$\sum_{\ell=0}^{2\mu-1} \tilde{P}_{k+\ell N}(z)\, P_{k+\ell N}(z) \overset{!}{=} \frac{1}{2M} \quad \text{for} \quad k = 0, \ldots, \left\lceil \frac{N}{2} \right\rceil - 1. \qquad (6.145)$$

Interestingly, for $\mu > 1$, we still may choose different prototypes $P(z)$ and
$Q(z)$ such that

$$\boldsymbol{R}^{(\mu)}(z) = z^{-(2mL-1)}\,\tilde{\boldsymbol{E}}^{(\mu)}(z) + \boldsymbol{N}^{(\mu)}(z)$$

with

$$\boldsymbol{N}^{(\mu)}(z)\boldsymbol{E}^{(\mu)}(z) = \boldsymbol{0}.$$

Example. We consider a 16-band filter bank with linear-phase prototype and
an overall delay of 255 samples. Figure 6.27 shows a comparison of frequency
responses for the critically sampled and the oversampled case. It turns out
that the PR prototype for the oversampled filter bank has a much higher
stopband attenuation. This demonstrates the increased design freedom in the
oversampled case.

6.6.4 Pseudo-QMF Banks

In *pseudo-QMF banks*, one no longer seeks perfect reconstruction, but *nearly
perfect reconstruction*. Designing a pseudo-QMF bank is done as follows [127].
One ensures that the aliasing components of adjacent channels compensate
exactly. This requires power complementarity of frequency shifted versions of
the prototype, as illustrated in Figure 6.28. Furthermore, one tries to suppress
the remaining aliasing components by using filters with very high stopband
attenuation. Through filter optimization the linear distortions are kept as
small as possible. An efficient design method was proposed in [166]. Since
the constraints on the prototype are less restrictive than in the PR case, the
prototypes typically have a higher stopband attenuation than the PR ones.
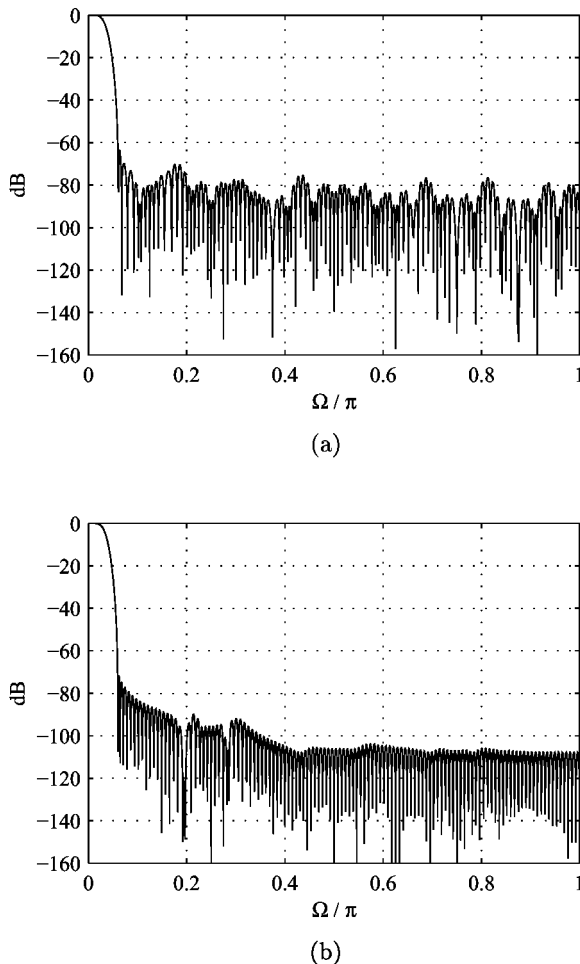
Figure 6.27. Frequency responses of 16-channel prototypes. (a) critical subsampling; (b) oversampling by $\mu = 2$.
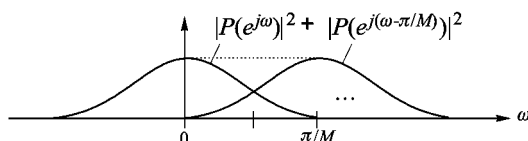
Figure 6.28. Design of pseudo-QMF banks.

6.7   Lapped Orthogonal Transforms

Lapped orthogonal transforms (LOTs) were introduced in [21] and have been further studied in [93, 97, 2]. Unlike block transforms, they have overlapping basis functions, which better allow us to smooth out blocking artifacts in coding applications. LOTs may also be seen as a special kind of critically subsampled paraunitary filter banks. Typically, an overlap of one block is considered, which means that the basis functions are of length $L = 2M$ when the number of channels is M. Longer transforms have been designed in [118] and are called generalized lapped orthogonal transforms (GenLOTs). More recently, biorthogonal lapped transforms have also been proposed [96, 144].

Figure 6.29. Transform matrix of a lapped orthogonal transform.

Figure 6.29 illustrates the structure of the transform matrix of a lapped orthogonal transform. Like in an M-channel filter bank with length-$2M$ filters, $2M$ input samples are combined in order to form M transform coefficients. We will first consider the constraints on the $M \times M$ submatrices $\boldsymbol{P}_0$ and $\boldsymbol{P}_1$. From the condition of orthogonality,

$$\boldsymbol{T}^T \boldsymbol{T} = \boldsymbol{T} \boldsymbol{T}^T = \boldsymbol{I} \tag{6.146}$$

it follows that

$$\boldsymbol{P}_0^T \boldsymbol{P}_0 + \boldsymbol{P}_1^T \boldsymbol{P}_1 = \boldsymbol{P}_0 \boldsymbol{P}_0^T + \boldsymbol{P}_1 \boldsymbol{P}_1^T = \boldsymbol{I}_{M \times M} \tag{6.147}$$

and

$$\boldsymbol{P}_0^T \boldsymbol{P}_1 = \boldsymbol{P}_0 \boldsymbol{P}_1^T = \boldsymbol{0}_{M \times M}. \tag{6.148}$$

Now let $\boldsymbol{B} = \boldsymbol{P}_0 + \boldsymbol{P}_1$. Note that $\boldsymbol{B}$ is orthogonal if $\boldsymbol{P}_0$ and $\boldsymbol{P}_1$ satisfy the above conditions. Moreover, $\boldsymbol{P}_0\boldsymbol{P}_0^T$ and $\boldsymbol{P}_1\boldsymbol{P}_1^T$ are orthogonal projections onto two subspaces that are orthogonal to one another. Define $\boldsymbol{A} = \boldsymbol{P}_0\boldsymbol{P}_0^T$ and verify that $\boldsymbol{P}_1\boldsymbol{P}_1^T = \boldsymbol{I} - \boldsymbol{A}$. Thus,

$$\boldsymbol{P}_0 = \boldsymbol{A}\,\boldsymbol{B}, \qquad \boldsymbol{P}_1 = [\boldsymbol{I} - \boldsymbol{A}]\,\boldsymbol{B}. \tag{6.149}$$

The most general way of constructing LOTs is to start with two matrices A and B, where A is a projection and B is orthogonal. The desired matrices P_0 and P_1 are then found from (6.149). This method, however, does not automatically yield linear-phase filters, which are desired in many applications.

In [98], a fast linear-phase LOT based on the DCT was presented, which will be briefly explained in the following. For this, let D_e and D_o be matrices that contain the rows of the transposed DCT-II matrix with even and odd symmetry, respectively. Then,

$$Q^{(0)} = \left[P_0^{(0)}, P_1^{(0)} \right] = \frac{1}{2} \begin{bmatrix} D_e - D_o & (D_e - D_o)J \\ D_e - D_o & -(D_e - D_o)J \end{bmatrix} \qquad (6.150)$$

is a LOT matrix that already satisfies the above conditions. J is the counter identity matrix with entries $J_{i,k} = \delta_{i,N-i-1}$, $i = 0, 1, \ldots, N - 1$. In an expression of the form $X J$, it flips the columns of X from left to right. Due to the application of J in (6.150), the first $M/2$ rows of $Q^{(0)}$ have even and the last $M/2$ rows have odd symmetry. A transform matrix with better properties (e.g. for coding) can be obtained by rotating the columns of $Q^{(0)}$ such that

$$Q = Z \, Q^{(0)}, \qquad (6.151)$$

where Z is unitary. For the fast LOT, Z is chosen to contain only three plane rotations, which help to improve the performance, but do not significantly increase the complexity. The matrix $Q^{(0)}$ already has a fast implementation based on the fast DCT. See Figure 6.30 for an illustration of the fast LOT. The angles proposed by Malvar are $\theta_1 = 0.13\pi$, $\theta_2 = 0.16\pi$, and $\theta_3 = 0.13\pi$.
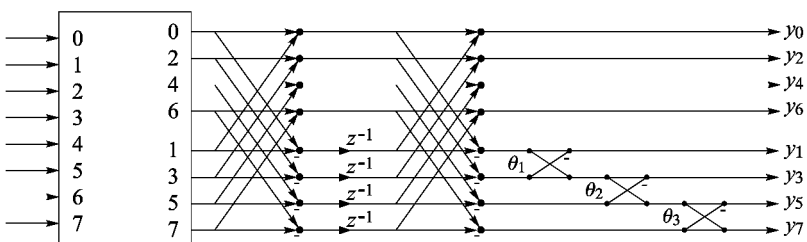
Figure 6.30. The fast lapped orthogonal transform for $M = 8$ based on the DCT and three plane rotations.

6.8   Subband Coding of Images

Two-dimensional filter banks for the decomposition of images can be realized as separable and non-separable filter banks. For the sake of simplicity, we will restrict ourselves to the separable case. Information on non-separable filter banks and the corresponding filter design methods is given in [1, 154].

In separable filter banks, the rows and columns of the input signal (image) are filtered successively. The procedure is illustrated in Figure 6.31 for an octave-band decomposition based on cascades of one-dimensional two-channel filter banks. In Figure 6.32 an example of such an octave-band decomposition is given. Note that this decomposition scheme is also known as the discrete wavelet transform; see Chapter 8. In Figure 6.32(b) we observe that most information is contained in the lower subbands. Moreover, local high-frequency information is kept locally within the subbands. These properties make such filter banks very attractive for image coding applications. In order to achieve high compression ratios, one quantizes the decomposed image, either by scalar quantization, or using a technique known as *embedded zerotree coding* [131, 128]; see also Section 8.9. The codewords describing the quantized values are usually further compressed in a lossless way by *arithmetic* or *Huffman coding* [76, 63]. To demonstrate the characteristics of subband coding with octave-band filter banks, Figures 6.32(c) and (d) show coding results at different bit rates.
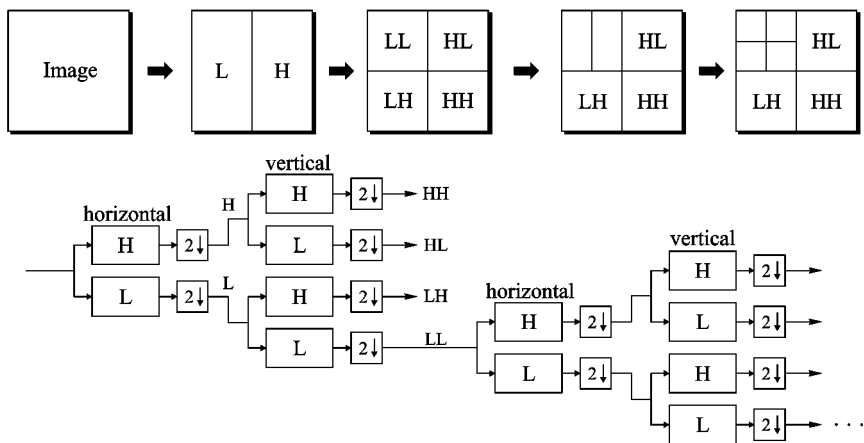
Figure 6.31. Separable two-dimensional octave-band filter bank.
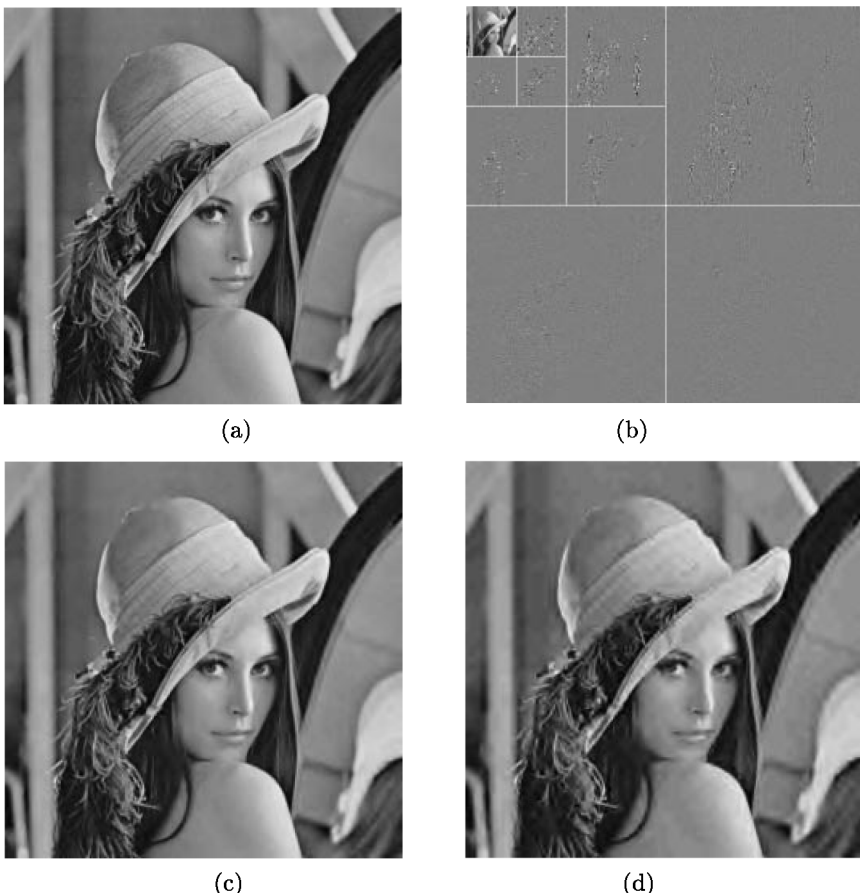
Figure 6.32. Examples of subband coding; (a) original image of size 512×512; (b) ten-band octave decomposition; (c) coding at 0.2 bits per pixel; (d) coding at 0.1 bits per pixel.

6.9 Processing of Finite-Length Signals

The term "critical sampling", used in the previous sections, was used under the assumption of infinitely long signals. This assumption is justified with sufficient accuracy for audio and speech coding. However, if we want to decompose an image by means of a critically subsampled filter bank, we see that the number of subband samples is larger than the number of input values. Figure 6.33 gives an example. If we simply truncate the number of subband samples to the number of input values – which would be desirable for coding – then PR is not possible any longer. Solutions to this problem that yield PR
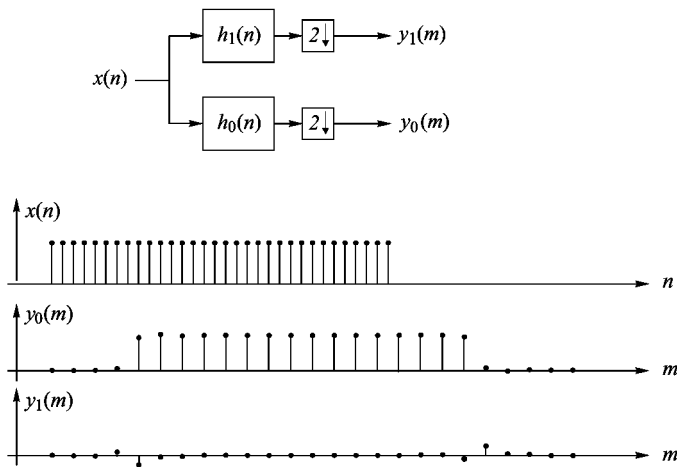
Figure 6.33. Two-channel decomposition of a finite-length signal.

with a minimum number of subband samples are discussed in the following.

Circular Convolution. Assuming that the length of the signal to be processed is a multiple of the number of channels, the problem mentioned above can be solved by circular convolution. In this method, the input signal is extended periodically prior to decomposition [165], which yields periodic subband signals of which only one period has to be stored or transmitted. Figures 6.34(a) and 6.34(c) give an illustration. Synthesis is performed by extending the subband signals according to their symmetry, filtering the extended signals, and extracting the required part of the output signal. A drawback of circular convolution is the occurrence of discontinuities at the signal boundaries, which may lead to annoying artifacts after reconstruction from quantized subband signals.

Symmetric Reflection. In this method, the input signal is extended periodically by reflection at the boundaries as indicated in Figures 6.34(b) and 6.34(d), [136, 16, 23, 6]. Again, we get periodic subband signals, but the period is twice as long as with circular convolution. However, only half a period of the subband signals is required if linear-phase filters are used, because they lead to symmetry in the subbands. By comparing Figures 6.34(a) and (b) (or 6.34(c) and (d)) we see that symmetric reflection leads to smoother transitions at the boundaries than circular convolution does. Thus, when quantizing the subband signals, this has the effect of less severe boundary distortions.

The exact procedure depends on the filter bank in use and on the signal
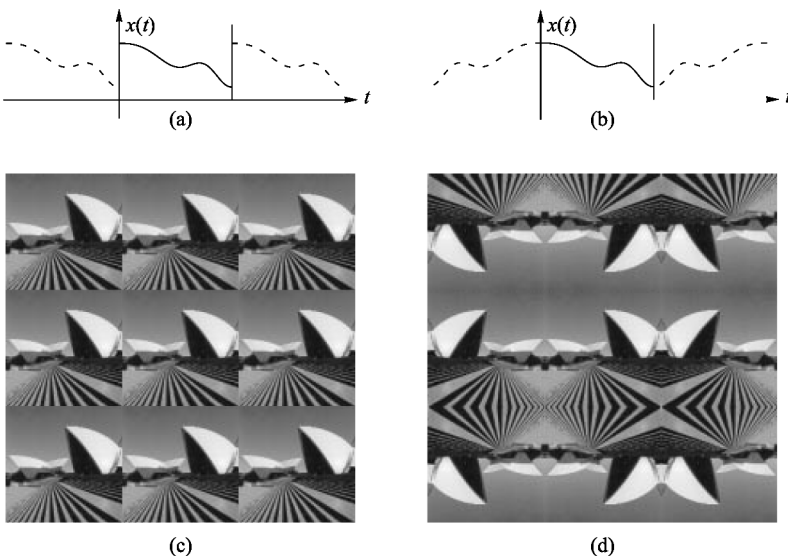
Figure 6.34. Periodic extension of the input signal; (a) one-dimensional circular convolution; (b) one-dimensional symmetric reflection; (c) two-dimensional circular convolution; (d) two-dimensional symmetric reflection.

length. Figure 6.35(a) shows a scheme suitable for the two-band decomposition of an even-length signal with linear-phase odd-length biorthogonal filters. The input signal is denoted as $x_0, x_1, \ldots, x_7$, and the filter impulse responses are $\{A, B, C, B, A\}$ for the lowpass and $\{-a, b, -a\}$ for the highpass. The upper row shows the extended input signal, where the given input samples are shown in solid boxes. The lowpass and highpass subband samples, c_n and d_n, respectively, are computed by taking the inner products of the impulse responses in the displayed positions with the corresponding part of the extended input signal. We see that only four different lowpass and highpass coefficients occur and have to be transmitted. A second scheme for the same filters which also allows the decomposition of even-length signals into lowpass and highpass components of half the length is depicted in Figure 6.35(b). In order to distinguish between both methods we say that the starting position in Figure 6.35(a) is even and the one in Figure 6.35(b) is odd, as indicated by the indices of the samples. Combinations of both schemes can be used to decompose odd-length signals. Moreover, these schemes can be used for the decomposition of 2-D objects with arbitrary shape. We will return to this topic at the end of this section.

Schemes for the decomposition of even-length signals with even-length

(a)

x_2 x_1 | x_0 x_1 x_2 x_3 x_4 x_5 x_6 x_7 x_6 x_5 x_4

A B C B A
　A B C B A
　　A B C B A
　　　A B C B A
$-a$ b $-a$
　$-a$ b $-a$
　　$-a$ b $-a$
　　　$-a$ b $-a$

c_1 d_0 | c_0 d_0 c_1 d_1 c_2 d_2 c_3 d_3 c_3 d_2 c_2

(b)

x_4 x_3 x_2 | x_1 x_2 x_3 x_4 x_5 x_6 x_7 x_8 x_7 x_6

A B C B A
　A B C B A
　　A B C B A
　　　A B C B A
$-a$ b $-a$
　$-a$ b $-a$
　　$-a$ b $-a$
　　　$-a$ b $-a$

c_2 d_1 c_1 | d_0 c_1 d_1 c_2 d_2 c_3 d_3 c_4 d_3 c_3

(c)

x_1 x_0 | x_0 x_1 x_2 x_3 x_4 x_5 x_6 x_7 x_7 x_6 x_5

A B B A
　A B B A
　　A B B A
　　　A B B A
a b $-b$ $-a$
　a b $-b$ $-a$
　　a b $-b$ $-a$
　　　a b $-b$ $-a$

c_0 $-d_0$ | c_0 d_0 c_1 d_1 c_2 d_2 c_3 d_3 c_3 $-d_3$ c_2

(d)

x_3 x_2 x_1 | x_1 x_2 x_3 x_4 x_5 x_6 x_7 x_8 x_8 x_7

A B B A
　A B B A
　　A B B A
　　　A B B A
　　　　A B B A
a b $-b$ $-a$
　a b $-b$ $-a$
　　a b $-b$ $-a$

c_1 $-d_1$ c_0 0 c_1 d_1 c_2 d_2 c_3 d_3 c_4 0 c_3

d_0 c_1 d_1 c_2 d_2 c_3 d_3 c_4

Figure 6.35. Symmetric reflection for even-length signals. (a) odd-length filters, segment starting at an even position; (b) odd-length filters, segment starting at an odd position; (c) even-length filters, segment starting at an even position; (d) even-length filters, segment starting at an odd position.

linear-phase filters are depicted in Figures 6.35(c) and (d). The filter impulse responses are $\{A, B, B, A\}$ for the lowpass and $\{-a, -b, b, a\}$ for the highpass. Note that a different type of reflection is used and that we have other symmetries in the subbands. While the scheme in Figure 6.35(c) results in the same number of lowpass and highpass samples, the one in Figure 6.35(d) yields an extra lowpass value, while the corresponding highpass value is zero. However, the additional lowpass samples can be turned into highpass values by subtracting them from the following lowpass value and storing the differences in the highpass band.

In object based image coding, for instance MPEG-4 [109], it is required to carry out subband decompositions of arbitrarily shaped objects. Figure 6.36

2	1	0	1	2	3	4	5	6	7	8	9	8	7	6
2	1	0	1	2	3	4	5	6	7	8	7	6	5	4
4	3	2	1	2	3	4	5	6	7	8	7	6	5	4
4	3	2	1	2	3	4	5	6	7	6	5	4	3	2
6	5	4	3	2	3	4	5	6	7	6	5	4	3	2
6	5	4	3	2	3	4	5	6	5	4	3	2	3	4
4	5	6	5	4	3	4	5	6	5	4	3	4	5	6
4	3	4	5	4	3	4	5	4	3	4	5	4	3	4
4	5	4	5	4	5	4	5	4	5	4	5	4	5	4
4	4	4	4	4	4	4	4	4	4	4	4	4	4	4

(a)

A B C B A
  A B C B A
    A B C B A
      A B C B A
        A B C B A
          A B C B A

(b)

-a b -a
  -a b -a
    -a b -a
      -a b -a
        -a b -a

(c)

(d) (e) (f) (h) (g) (i)
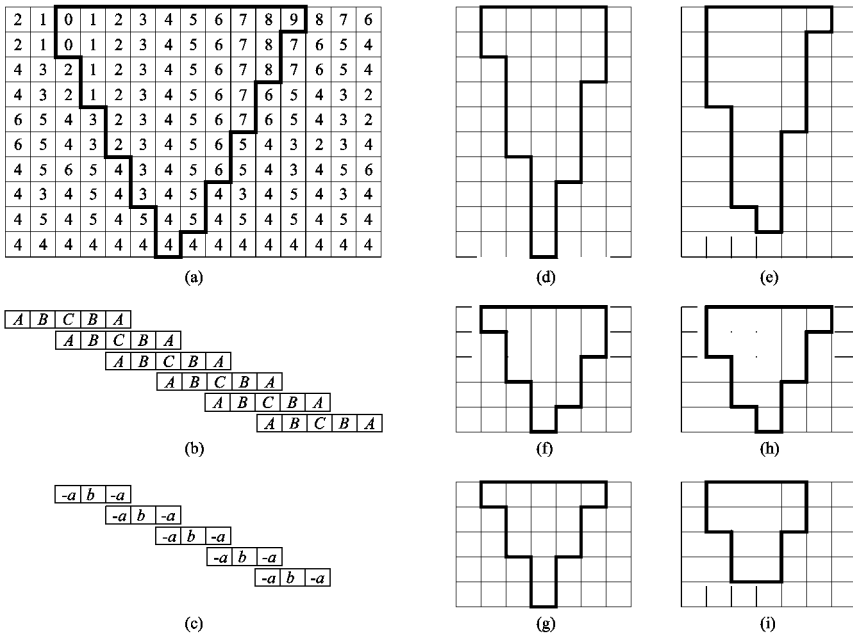
Figure 6.36. Shape adaptive image decomposition using symmetric reflection for odd-length two-channel filter banks; (a) arbitrarily shaped object and horizontal extension with pixel values as indicated; (b) lowpass filter; (c) highpass filter; (d) and (e) lowpass and highpass subbands after horizontal filtering; (f) and (g) lowpass and highpass decompositions of the signal in (d); (h) and (i) lowpass and highpass decompositions of the signal in (e).

shows a scheme which is suitable for this task using odd-length filters. The arbitrarily shaped input signal is shown in the marked region, and the extension for the first horizontal decomposition is found outside this region. Figures 6.36(d) and (e) show the shape of the lowpass and highpass band, respectively. Figures 6.36(f)–(i) finally show the object shapes after the vertical decomposition of the signals in Figures 6.36(d) and (e) based on the same reflection scheme. Such schemes are often called shape adaptive wavelet transforms. Note that the overall number of subband samples is equal to the number of input pixels. Moreover, the scheme yields a decomposition where the interior region of an object is processed as if the object was of infinite size. Thus, the actual object shape only influences the subband samples close to the boundaries. The 2-D decomposition is carried out in such a way that the horizontal decomposition introduces minimal distortion for the next vertical one and vice versa.

1	0	0	1	2	3	4	5	6	7	8	9	9
1	0	0	1	2	3	4	5	6	7	8	8	7
3	2	1	1	2	3	4	5	6	7	8	8	7
3	2	1	1	2	3	4	5	6	7	7	6	5
5	4	3	2	2	3	4	5	6	7	7	6	5
5	4	3	2	2	3	4	5	6	6	5	4	3
6	6	5	4	3	3	4	5	6	6	5	4	3
4	5	5	4	3	3	4	5	5	4	3	3	4
5	4	4	5	5	4	4	5	5	4	4	5	5
4	4	4	4	4	4	4	4	4	4	4	4	4

(a)

(b): rows of `A B B A` staggered

(c): rows of `a b -b -a` staggered

(d) (e) (f) (h) (g) (i)
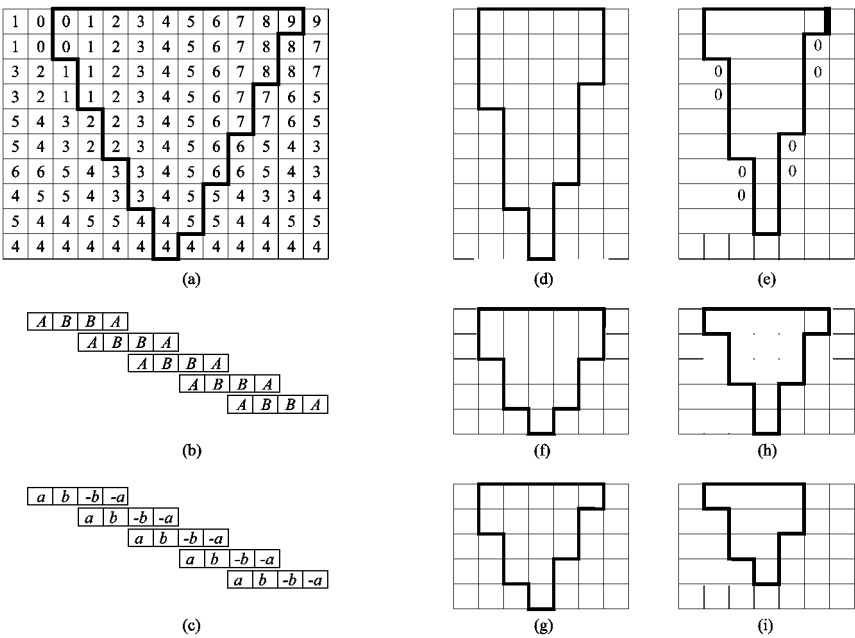
Figure 6.37. Shape adaptive image decomposition using symmetric reflection for even-length two-channel filter banks; see the comments to Figure 6.36 for further explanation.

A scheme for the decomposition of arbitrarily shaped 2-D objects with even-length filters is depicted in Figure 6.37. Note that in this case, the lowpass band grows faster than the highpass band. The shaded regions in Figures 6.37(d) and (e) show the shape of the lowpass and highpass band after horizontal filtering. The brighter regions within the object in Figure 6.37(d) indicate the extra lowpass samples. The zero-marked fields in Figure 6.37(e) are positions where the highpass samples are exactly zero.

If the faster growing of the lowpass band is unwanted the manipulation indicated in Figure 6.35(d) can be applied. Then the subbands obtained with even-length filters will have the same shape as the ones in Figure 6.36.

In addition to the direct use of symmetric reflection, one can optimize the boundary processing schemes in order to achieve better coding properties. Methods for this task have been proposed in [70, 69, 101, 27, 102, 39, 40]. These include the two-band, the more general M-band, and the paraunitary case with non-linear phase filters.

6.10   Transmultiplexers

Transmultiplexers are systems that convert time-division multiplexed (TDM) signals into frequency-division multiplexed (FDM) signals and vice versa [151]. Essentially, these systems are filter banks as shown in Figure 6.38. Contrary to the subband coding filter banks considered so far, the synthesis filter bank is applied first and the analysis filter bank is then used to recover the subband samples $y_k(m)$, which may be understood as components of a TDM signal. At the output of the synthesis filter bank we have an FDM signal where each data stream $y_k(m)$ covers a different frequency band.

The transmission from input i to output k is described by the impulse responses

$$t_{i,k}(m) = q_{i,k}(mM), \tag{6.152}$$

where

$$q_{i,k}(n) = g_i(n) * h_k(n). \tag{6.153}$$

In the noise-free case, perfect reconstruction of the input data with a delay of m_0 samples can be obtained when the following condition holds:

$$t_{i,k}(m) = \delta_{ik}\,\delta_{mm_0}, \qquad i,k = 0,1,\ldots,M-1. \tag{6.154}$$

Using the notation of modulation matrices these PR conditions may be written as

$$\boldsymbol{T}(z^M) = \boldsymbol{H}_m^T(z)\,\boldsymbol{G}_m(z) = M\,z^{-m_0 M}\,\boldsymbol{I}, \tag{6.155}$$

where the overall transfer matrix depends on z^M. This essentially means that any PR subband coding filter bank yields a PR transmultiplexer if the overall delay is a multiple of M.

Practical problems with transmultiplexers mainly occur due to non-ideal transmission channels. This means that intersymbol interference, crosstalk between different channels, and additive noise need to be considered in the transmultiplexer design. An elaborate discussion of this topic is beyond the scope of this section.
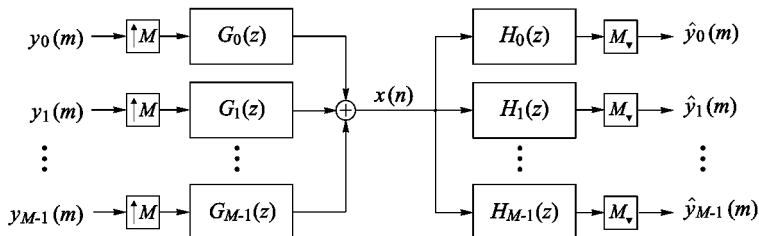
Figure 6.38. Transmultiplexer filter bank.

Chapter 7

Short-Time

Fourier Analysis

A fundamental problem in signal analysis is to find the spectral components contained in a measured signal $x(t)$ and/or to provide information about the time intervals when certain frequencies occur. An example of what we are looking for is a sheet of music, which clearly assigns time to frequency, see Figure 7.1. The classical Fourier analysis only partly solves the problem, because it does not allow an assignment of spectral components to time. Therefore one seeks other transforms which give insight into signal properties in a different way. The short-time Fourier transform is such a transform. It involves both time and frequency and allows a time-frequency analysis, or in other words, a signal representation in the time-frequency plane.

7.1 Continuous-Time Signals

7.1.1 Definition

The *short-time Fourier transform* (STFT) is the classical method of time-frequency analysis. The concept is very simple. We multiply $x(t)$, which is to be analyzed, with an analysis window $\gamma^*(t - \tau)$ and then compute the Fourier

Figure 7.1. Time-frequency representation.
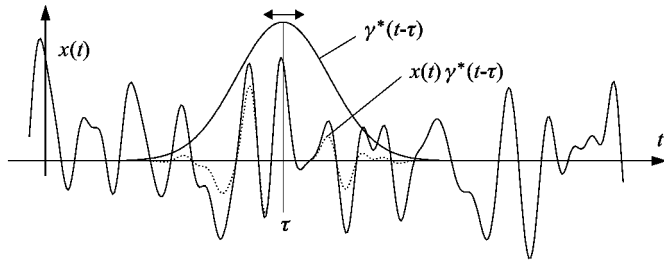
Figure 7.2. Short-time Fourier transform.

transform of the windowed signal:

$$\mathcal{F}_x^\gamma(\tau,\omega) = \int_{-\infty}^{\infty} x(t)\ \gamma^*(t-\tau)\ e^{-j\omega t}\ dt. \tag{7.1}$$

The analysis window $\gamma^*(t-\tau)$ suppresses $x(t)$ outside a certain region, and the Fourier transform yields a local spectrum. Figure 7.2 illustrates the application of the window. Typically, one will choose a real-valued window, which may be regarded as the impulse response of a lowpass. Nevertheless, the following derivations will be given for the general complex-valued case.

If we choose the Gaussian function to be the window, we speak of the *Gabor transform*, because Gabor introduced the short-time Fourier transform with this particular window [61].

Shift Properties. As we see from the analysis equation (7.1), a time shift $x(t) \rightarrow x(t-t_0)$ leads to a shift of the short-time Fourier transform by t_0. Moreover, a modulation $x(t) \rightarrow x(t)\ e^{j\omega_0 t}$ leads to a shift of the short-time Fourier transform by ω_0. As we will see later, other transforms, such as the discrete wavelet transform, do not necessarily have this property.

7.1.2   Time-Frequency Resolution

Applying the shift and modulation principle of the Fourier transform we find
the correspondence

$$
\begin{aligned}
\gamma_{\tau;\omega}(t) &:= \gamma(t-\tau)\, e^{j\omega t} \\
&\updownarrow \\
\Gamma_{\tau;\omega}(\nu) &:= \int_{-\infty}^{\infty} \gamma(t-\tau)\, e^{-j(\nu-\omega)t}\, dt = \Gamma(\nu-\omega)\, e^{-j(\nu-\omega)\tau}
\end{aligned}
\tag{7.2}
$$

From Parseval's relation in the form

$$
\begin{aligned}
\langle x, \gamma_{\tau;\omega} \rangle &= \int_{-\infty}^{\infty} x(t)\, \gamma^*(t-\tau)\, e^{-j\omega t}\, dt \\[2mm]
&= \tfrac{1}{2\pi} \langle X, \Gamma_{\tau;\omega} \rangle \\[2mm]
&= \tfrac{1}{2\pi} \int_{-\infty}^{\infty} X(\nu)\, \Gamma^*(\nu-\omega)\, e^{j(\nu-\omega)\tau}\, d\nu
\end{aligned}
\tag{7.3}
$$

we conclude

$$
\mathcal{F}_x^\gamma(\tau,\omega) = e^{-j\omega\tau}\, \frac{1}{2\pi} \int_{-\infty}^{\infty} X(\nu)\, \Gamma^*(\nu-\omega)\, e^{j\nu\tau}\, d\nu.
\tag{7.4}
$$

That is, windowing in the time domain with $\gamma^*(t-\tau)$ simultaneously leads
to windowing in the spectral domain with the window $\Gamma^*(\nu-\omega)$.

Let us assume that $\gamma^*(t-\tau)$ and $\Gamma^*(\nu-\omega)$ are concentrated in the time
and frequency intervals

$$
[\tau + t_0 - \Delta_t \ , \ \tau + t_0 + \Delta_t]
\tag{7.5}
$$

and

$$
[\omega + \omega_0 - \Delta_\omega \ , \ \omega + \omega_0 + \Delta_\omega],
\tag{7.6}
$$

respectively. Then $\mathcal{F}_x^\gamma(\tau,\omega)$ gives information on a signal $x(t)$ and its spectrum
$X(\omega)$ in the time-frequency window

$$
[\tau + t_0 - \Delta_t \ , \ \tau + t_0 + \Delta_t] \ \times \ [\omega + \omega_0 - \Delta_\omega \ , \ \omega + \omega_0 + \Delta_\omega].
\tag{7.7}
$$

The position of the time-frequency window is determined by the parameters τ
and ω. The form of the time-frequency window is independent of τ and ω, so
that we obtain a uniform resolution in the time-frequency plane, as indicated
in Figure 7.3.
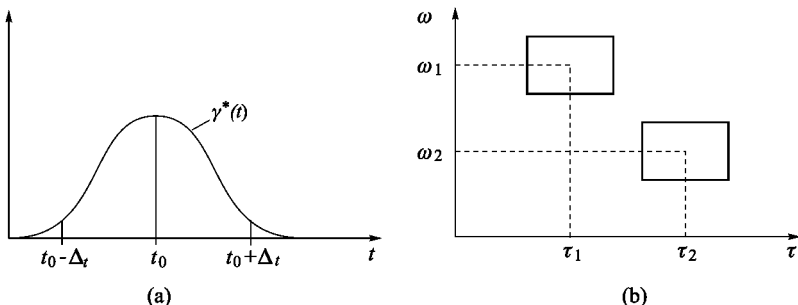
Figure 7.3. Time-frequency window of the short-time Fourier transform.

Let us now have a closer look at the size and position of the time-frequency window. Basic requirements for $\gamma^*(t)$ to be called a time window are $\gamma^*(t) \in L_2(\mathbb{R})$ and $t\,\gamma^*(t) \in L_2(\mathbb{R})$. Correspondingly, we demand that $\Gamma^*(\omega) \in L_2(\mathbb{R})$ and $\omega\,\Gamma^*(\omega) \in L_2(\mathbb{R})$ for $\Gamma^*(\omega)$ being a frequency window. The center t_0 and the radius Δ_t of the time window $\gamma^*(t)$ are defined analogous to the mean value and the standard deviation of a random variable:

$$t_0 = \int_{-\infty}^{\infty} t \cdot \frac{|\gamma(t)|^2}{\|\gamma\|^2}\,dt, \tag{7.8}$$

$$\Delta_t = \left(\int_{-\infty}^{\infty} (t - t_0)^2 \cdot \frac{|\gamma(t)|^2}{\|\gamma\|^2}\,dt \right)^{\frac{1}{2}}. \tag{7.9}$$

Accordingly, the center ω_0 and the radius Δ_ω of the frequency window $\Gamma^*(\omega)$ are defined as

$$\omega_0 = \int_{-\infty}^{\infty} \omega \cdot \frac{|\Gamma(\omega)|^2}{\|\Gamma\|^2}\,d\omega, \tag{7.10}$$

$$\Delta_\omega = \left(\int_{-\infty}^{\infty} (\omega - \omega_0)^2 \cdot \frac{|\Gamma(\omega)|^2}{\|\Gamma\|^2}\,d\omega \right)^{\frac{1}{2}}. \tag{7.11}$$

The radius Δ_ω may be viewed as half of the bandwidth of the filter $\gamma^*(-t)$.

In time-frequency analysis one intends to achieve both high time and frequency resolution if possible. In other words, one aims at a time-frequency window that is as small as possible. However, the uncertainty principle applies, giving a lower bound for the area of the window. Choosing a short time window leads to good time resolution and, inevitably, to poor frequency resolution. On the other hand, a long time window yields poor time resolution, but good frequency resolution.

7.1.3   The Uncertainty Principle

Let us consider the term $(\Delta_t \Delta_\omega)^2$, which is the square of the area in the time-frequency plane being covered by the window. Without loss of generality we may assume $\int t\,|\gamma(t)|^2\,dt = 0$ and $\int \omega\,|\Gamma(\omega)|^2\,d\omega = 0$, because these properties are easily achieved for any arbitrary window by applying a time shift and a modulation. With (7.9) and (7.11) we have

$$(\Delta_t \Delta_\omega)^2 = \frac{\left(\int_{-\infty}^{\infty} t^2\,|\gamma(t)|^2\,dt\right)\left(\int_{-\infty}^{\infty} \omega^2\,|\Gamma(\omega)|^2\,d\omega\right)}{\|\gamma\|^2\,\|\Gamma\|^2}. \tag{7.12}$$

For the left term in the numerator of (7.12), we may write

$$\int_{-\infty}^{\infty} t^2\,|\gamma(t)|^2\,dt = \|\boldsymbol{\xi}\|^2 \tag{7.13}$$

with $\xi(t) = t\,\gamma(t)$. Using the differentiation principle of the Fourier transform, the right term in the numerator of (7.12) may be written as

$$\begin{aligned}
\int_{-\infty}^{\infty} \omega^2\,|\Gamma(\omega)|^2\,d\omega &= \int_{-\infty}^{\infty} |\mathcal{F}\{\gamma'(t)\}|^2\,d\omega \\
&= 2\pi\,\|\gamma'\|^2
\end{aligned} \tag{7.14}$$

where $\gamma'(t) = \frac{d}{dt}\gamma(t)$. With (7.13), (7.14) and $\|\Gamma\|^2 = 2\pi\,\|\gamma\|^2$ we get for (7.12)

$$(\Delta_t \Delta_\omega)^2 = \frac{1}{\|\gamma\|^4}\,\|\boldsymbol{\xi}\|^2\,\|\gamma'\|^2. \tag{7.15}$$

Applying the Schwarz inequality yields

$$\begin{aligned}
(\Delta_t \Delta_\omega)^2 &\geq \tfrac{1}{\|\gamma\|^4}\,|\langle \boldsymbol{\xi}, \gamma'\rangle|^2 \\
&\geq \tfrac{1}{\|\gamma\|^4}\,|\Re\{\langle \boldsymbol{\xi}, \gamma'\rangle\}|^2 \\
&= \tfrac{1}{\|\gamma\|^4}\,\left|\Re\left\{\int_{-\infty}^{\infty} t\,\gamma(t)\,\gamma'^*(t)\,dt\right\}\right|^2.
\end{aligned} \tag{7.16}$$

By making use of the relationship

$$\Re\{t\,\gamma(t)\,\gamma'^*(t)\} = \frac{1}{2}\,t\,\frac{d}{dt}\,|\gamma(t)|^2, \tag{7.17}$$

which can easily be verified, we may write the integral in (7.16) as

$$\Re\left\{\int_{-\infty}^{\infty} t\,\gamma(t)\,\gamma'^*(t)\,dt\right\} = \frac{1}{2}\int_{-\infty}^{\infty} t\,\frac{d}{dt}\,|\gamma(t)|^2\,dt. \tag{7.18}$$

Partial integration yields

$$\frac{1}{2}\int_{-\infty}^{\infty} t \,\frac{d}{dt}\,|\gamma(t)|^2 \,\,dt = \frac{1}{2}\,t\,|\gamma(t)|^2 \,\Big|_{-\infty}^{\infty} \,-\,\frac{1}{2}\int_{-\infty}^{\infty}|\gamma(t)|^2 \,\,dt. \tag{7.19}$$

The property

$$\lim_{|t|\to\infty} t\,|\gamma(t)|^2 = 0, \tag{7.20}$$

which immediately follows from $t\,\gamma(t) \in L_2$, implies that

$$\Re\left\{\int_{-\infty}^{\infty} t\,\gamma(t)\,\gamma'^*(t)\,dt\right\} = -\frac{1}{2}\,\|\gamma\|^2, \tag{7.21}$$

so that we may conclude that

$$(\Delta_t\Delta_\omega)^2 \,\geq\, \frac{1}{4}, \tag{7.22}$$

that is

$$\Delta_t\Delta_\omega \,\geq\, \frac{1}{2}. \tag{7.23}$$

The relation (7.23) is known as the *uncertainty principle*. It shows that the size of a time-frequency windows cannot be made arbitrarily small and that a perfect time-frequency resolution cannot be achieved.

In (7.16) we see that equality in (7.23) is only given if $t\,\gamma(t)$ is a multiple of $\gamma'(t)$. In other words, $\gamma(t)$ must satisfy the differential equation

$$t\,\gamma(t) = c\,\gamma'(t), \tag{7.24}$$

whose general solution is given by

$$\gamma(t) = \alpha\,e^{-\frac{t^2}{2\beta^2}}. \tag{7.25}$$

Hence, equality in (7.23) is achieved only if $\gamma(t)$ is the Gaussian function. If we relax the conditions on the center of the time-frequency window of $\gamma(t)$, the general solution with a time-frequency window of minimum size is a modulated and time-shifted Gaussian.

7.1.4 The Spectrogram

Since the short-time Fourier transform is complex-valued in general, we often use the so-called *spectrogram* for display purposes or for further processing stages. This is the squared magnitude of the short-time Fourier transform:

$$S_x(\tau,\omega) = |\,\mathcal{F}_x^\gamma(\tau,\omega)|^2 = \left|\,\int_{-\infty}^{\infty} x(t)\,\gamma^*(t-\tau)\,e^{-j\omega t}\,dt\,\right|^2. \tag{7.26}$$
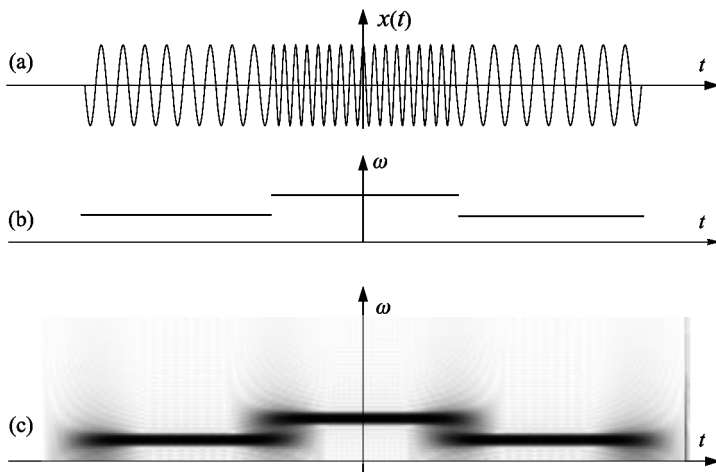
Figure 7.4. Example of a short-time Fourier analysis; (a) test signal; (b) ideal time-frequency representation; (c) spectrogram.

Figure 7.4 gives an example of a spectrogram; the values $S_x(\tau, \omega)$ are represented by different shades of gray. The uncertainty of the STFT in both time and frequency can be seen by comparing the result in Figure 7.4(c) with the ideal time-frequency representation in Figure 7.4(b).

A second example that shows the application in speech analysis is pictured in Figure 7.5. The regular vertical striations of varying density are due to the pitch in speech production. Each striation corresponds to a single pitch period. A high pitch is indicated by narrow spacing of the striations. Resonances in the vocal tract in voiced speech show up as darker regions in the striations. The resonance frequencies are known as the formant frequencies. We see three of them in the voiced section in Figure 7.5. Fricative or unvoiced sounds are shown as broadband noise.

7.1.5   Reconstruction

A reconstruction of $x(t)$ from $\mathcal{F}_x^\gamma(\tau, \omega)$ is possible in the form

$$x(t) = \frac{1}{2\pi} \int_{-\infty}^{\infty} \int_{-\infty}^{\infty} \mathcal{F}_x^\gamma(\tau, \omega)\ g(t - \tau)\ e^{j\omega t}\ d\tau\ d\omega. \qquad (7.27)$$

Here, the synthesis window $g(t)$ must satisfy the condition

$$\int_{-\infty}^{\infty} \gamma^*(t)\ g(t)\ dt\ =\ 1. \qquad (7.28)$$
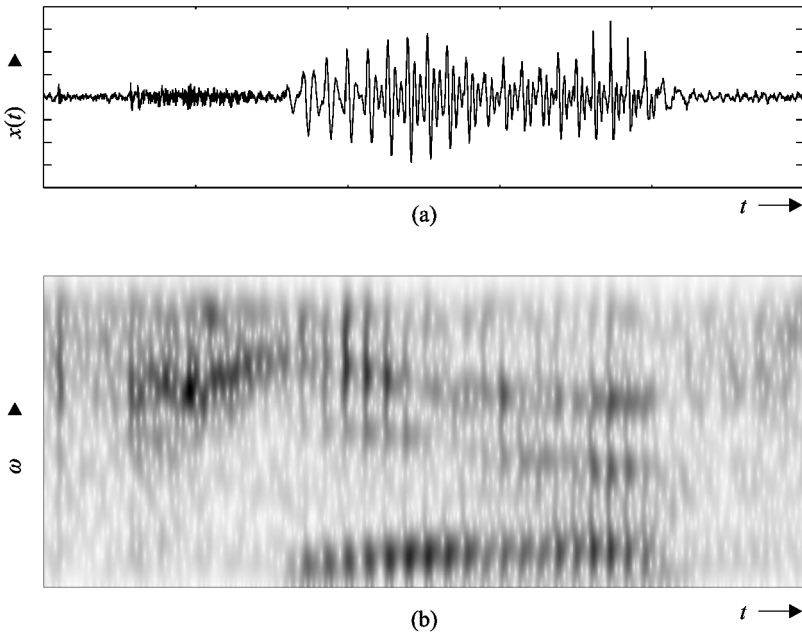
Figure 7.5. Spectrogram of a speech signal; (a) signal; (b) spectrogram.

We can verify this by substituting (7.1) into (7.27) and by rewriting the expression obtained:

$$
\begin{aligned}
x(t) &= \frac{1}{2\pi} \int \int \int x(t') \, \gamma^*(t' - \tau) \, e^{-j\omega t'} \, dt' \, g(t - \tau) \, e^{j\omega t} \, d\tau \, d\omega \\
&= \int x(t') \int \gamma^*(t' - \tau) \, g(t - \tau) \, \frac{1}{2\pi} \int e^{j\omega(t - t')} \, d\omega \, d\tau \, dt' \qquad (7.29) \\
&= \int x(t') \int \gamma^*(t' - \tau) \, g(t - \tau) \, \delta(t - t') \, d\tau \, dt'.
\end{aligned}
$$

For (7.29) to be satisfied,

$$
\delta(t - t') = \int_{-\infty}^{\infty} \gamma^*(t' - \tau) \, g(t - \tau) \, \delta(t - t') \, d\tau \qquad (7.30)
$$

must hold, which is true if (7.28) is satisfied.

The restriction (7.28) is not very tight, so that an infinite number of windows $g(t)$ can be found which satisfy (7.28). The disadvantage of (7.27) is of course that the complete short-time spectrum must be known and must be involved in the reconstruction.

7.1.6   Reconstruction via Series Expansion

Since the transform (7.1) represents a one-dimensional signal in the two-dimensional plane, the signal representation is redundant. For reconstruction purposes this redundancy can be exploited by using only certain regions or points of the time-frequency plane. Reconstruction from discrete samples in the time-frequency plane is of special practical interest. For this we usually choose a grid consisting of equidistant samples as shown in Figure 7.6.
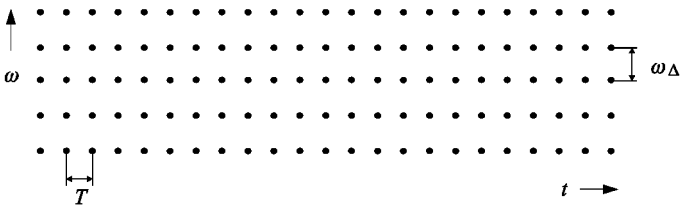
Figure 7.6. Sampling the short-time Fourier transform.

Reconstruction is given by

$$x(t) = \sum_{m=-\infty}^{\infty} \sum_{k=-\infty}^{\infty} \mathcal{F}_x^\gamma(mT, k\omega_\Delta)\, g(t - mT)\, e^{jk\omega_\Delta t}. \qquad (7.31)$$

The sample values $\mathcal{F}_x^\gamma(mT, k\omega_\Delta)$, $m, k \in \mathbb{Z}$ of the short-time Fourier transform are nothing but the coefficients of a series expansion of $x(t)$. In (7.31) we observe that the set of functions used for signal reconstruction is built from time-shifted and modulated versions of the same prototype $g(t)$. Thus, each of the synthesis functions covers a distinct area of the time-frequency plane of fixed size and shape. This type of series expansion was introduced by Gabor [61] and is also called a *Gabor expansion*.

Perfect reconstruction according to (7.31) is possible if the condition

$$\frac{2\pi}{\omega_\Delta} \sum_{m=-\infty}^{\infty} g(t - mT)\, \gamma^*(t - mT - \ell\frac{2\pi}{\omega_\Delta}) = \delta_{\ell 0} \quad \forall\, t \qquad (7.32)$$

is satisfied [72], where $\delta_{\ell 0}$ is the Kronecker delta. For a given window $\gamma(t)$, (7.32) represents a linear set of equations for determining $g(t)$. However, here, as with Shannon's sampling theorem, a minimal sampling rate must be guaranteed, since (7.32) can be satisfied only for [35, 72]

$$T\, \omega_\Delta \le 2\pi. \qquad (7.33)$$

Unfortunately, for critical sampling, that is for $T\,\omega_\Delta = 2\pi$, and equal analysis and synthesis windows, it is impossible to have both a good time and a good frequency resolution. If $\gamma(t) = g(t)$ is a window that allows perfect reconstruction with critical sampling, then either Δ_t or Δ_ω is infinite. This relationship is known as the *Balian–Low theorem* [36]. It shows that it is impossible to construct an orthonormal short-time Fourier basis where the window is differentiable and has compact support.

7.2 Discrete-Time Signals

The short-time Fourier transform of a discrete-time signal $x(n)$ is obtained by replacing the integration in (7.1) by a summation. It is then given by [4, 119, 32]

$$\mathcal{F}_x^\gamma(m, e^{j\omega}) = \sum_n x(n)\,\gamma^*(n - mN)\,e^{-j\omega n}. \tag{7.34}$$

Here we assume that the sampling rate of the signal is higher (by the factor $N \in \mathbb{N}$) than the rate used for calculating the spectrum. The analysis and synthesis windows are denoted as γ^* and g, as in Section 7.1; in the following they are meant to be discrete-time. Frequency ω is normalized to the sampling frequency.

In (7.34) we must observe that the short-time spectrum is a function of the discrete parameter m and the continuous parameter ω. However, in practice one would consider only the discrete frequencies

$$\omega_k = 2\pi k/M, \qquad k = 0, \ldots, M - 1. \tag{7.35}$$

Then the discrete values of the short-time spectrum can be given by

$$X(m, k) = \sum_n x(n)\,\gamma^*(n - mN)\,W_M^{kn}, \tag{7.36}$$

where

$$X(m, k) = \mathcal{F}_x^\gamma(m, e^{j\omega_k}) \tag{7.37}$$

and

$$W_M = e^{-j2\pi/M}. \tag{7.38}$$

Synthesis. As in (7.31), signal reconstruction from discrete values of the spectrum can be carried out in the form

$$\hat{x}(n) = \sum_{m=-\infty}^{\infty} \sum_{k=0}^{M-1} X(m, k)\,g(n - mN)\,W_M^{-kn}. \tag{7.39}$$

The reconstruction is especially easy for the case $N = 1$ (no subsampling), because then all PR conditions are satisfied for $g(n) = \delta_{n0} \longleftrightarrow G(e^{j\omega}) = 1$ and any arbitrary length-M analysis window $\gamma(n)$ with $\gamma(0) = 1/M$ [4, 119]. The analysis and synthesis equations (7.36) and (7.39) then become

$$X(m, k) = \sum_n x(n) \ \gamma^*(n - m) \ W_M^{kn} \tag{7.40}$$

and

$$\hat{x}(n) = \sum_{k=0}^{M-1} X(n, k) \ W_M^{-kn}. \tag{7.41}$$

This reconstruction method is known as *spectral summation*. The validity of $\hat{x}(n) = x(n)$ provided $\gamma(0) = 1/M$ can easily be verified by combining these expressions.

Regarding the design of windows allowing perfect reconstruction in the subsampled case, the reader is referred to Chapter 6. As we will see below, the STFT may be understood as a DFT filter bank.

Realizations using Filter Banks. The short-time Fourier transform, which has been defined as the Fourier transform of a windowed signal, can be realized with filter banks as well. The analysis equation (7.36) can be interpreted as filtering the modulated signals $x(n)W_M^{kn}$ with a filter

$$h(n) = \gamma^*(-n). \tag{7.42}$$

The synthesis equation (7.39) can be seen as filtering the short-time spectrum with subsequent modulation. Figure 7.7 shows the realization of the short-time Fourier transform by means of a filter bank. The windows $g(n)$ and $\gamma(n)$ typically have a lowpass characteristic.

Alternatively, signal analysis and synthesis can be carried out by means of equivalent bandpass filters. By rewriting (7.36) as

$$X(m, k) = W_M^{kmN} \sum_n x(n) \ \gamma^*(n - mN) \ W_M^{k(n-mN)} \tag{7.43}$$

we see that the analysis can also be realized by filtering the sequence $x(n)$ with the bandpass filters

$$h_k(n) = \gamma^*(-n) \ W_M^{-kn}, \qquad k = 0, \ldots, M - 1 \tag{7.44}$$

and by subsequent modulation.
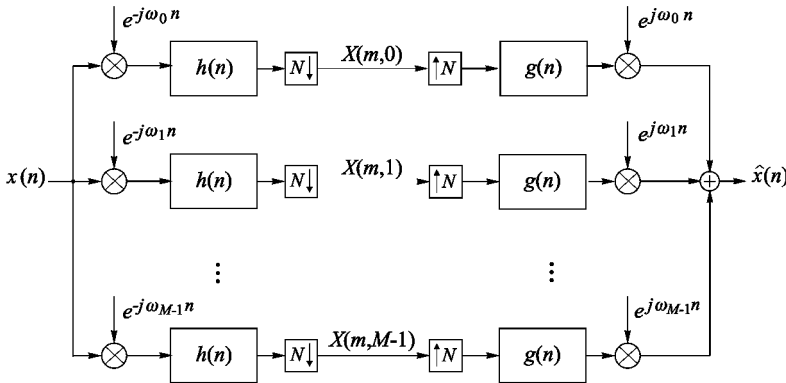
Figure 7.7. Lowpass realization of the short-time Fourier transform.

Rewriting (7.39) as

$$\hat{x}(n) = \sum_{m=-\infty}^{\infty} \sum_{k=0}^{M-1} X(m,k) \, W_M^{-kmN} \, g(n-mN) \, W_M^{-k(n-mN)} \qquad (7.45)$$

shows that synthesis can be achieved with modulated filters as well. To accomplish this, first the short-time spectrum is modulated, then filtering with the bandpass filters

$$g_k(n) = g(n) \, W_M^{-kn}, \qquad k = 0, \ldots, M-1, \qquad (7.46)$$

takes place; see Figure 7.8.

We realize that the short-time Fourier transform belongs to the class of modulated filter banks. On the other hand, it has been introduced as a transform, which illustrates the close relationship between filter banks and short-time transforms.

The most efficient realization of the STFT is achieved when implementing it as a DFT polyphase filter bank as outlined in Chapter 6.

7.3 Spectral Subtraction based on the STFT

In many real-word situations one encounters signals distorted by additive noise. Several methods are available for reducing the effect of noise in a more or less optimal way. For example, in Chapter 5.5 optimal linear filters that yield a maximum signal-to-noise ratio were presented. However, linear methods are
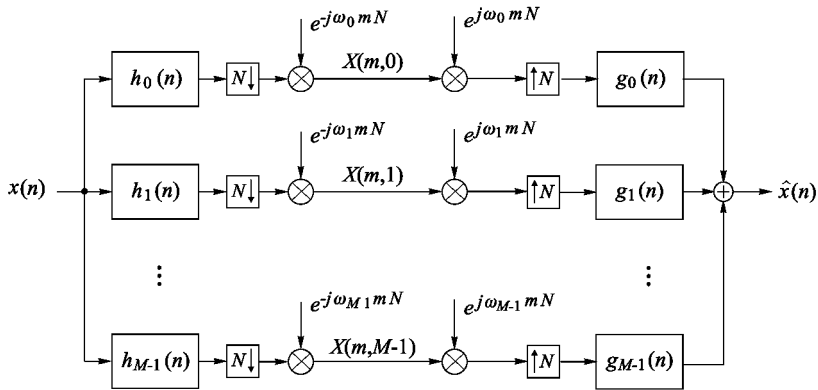
Figure 7.8. Bandpass realization of the short-time Fourier transform.

not necessarily the optimal ones, especially if a subjective signal quality with respect to human perception is of importance. Spectral subtraction is a non-linear method for noise reduction, which is very well suited for the restoration of speech signals.

We start with the model

$$y(t) = x(t) + n(t), \tag{7.47}$$

where we assume that the additive noise process $n(t)$ is statistically independent of the signal $x(t)$. Assuming that the Fourier transform of $y(t)$ exists, we have

$$Y(\omega) = X(\omega) + N(\omega) \tag{7.48}$$

in the frequency domain. Due to statistical independence between signal and noise, the energy density may be written as

$$|Y(\omega)|^2 = |X(\omega)|^2 + |N(\omega)|^2. \tag{7.49}$$

If we now assume that $E\left\{|N(\omega)|^2\right\}$ is known, the least squares estimate for $|X(\omega)|^2$ can be obtained as

$$|\hat{X}(\omega)|^2 = |Y(\omega)|^2 - E\left\{|N(\omega)|^2\right\}. \tag{7.50}$$

In spectral subtraction, one only tries to restore the magnitude of the spectrum, while the phase is not attached. Thus, the denoised signal is given in the frequency domain as

$$\hat{X}(\omega) = |\hat{X}(\omega)| \angle Y(\omega). \tag{7.51}$$

Keeping the noisy phase is motivated by the fact that the phase is of minor importance for speech quality.

So far, the time dependence of the statistical properties of the signal and the noise process has not been considered. Speech signals are highly nonstationary, but within intervals of about 20 msec, the signal properties do not change significantly, and the assumption of stationarity is valid on a short-time basis. Therefore, one replaces the above spectra by the short-time spectra computed by the STFT. Assuming a discrete implementation, this yields

$$Y(m,k) = X(m,k) + N(m,k), \tag{7.52}$$

where m is the time and k is the frequency index. $Y(m,k)$ is the STFT of $y(m)$.

Instead of subtracting an average noise spectrum $E\left\{|N(\omega)|^2\right\}$, one tries to keep track of the actual (time-varying) noise process. This can for instance be done by estimating the noise spectrum in the pauses of a speech signal. Equations (7.50) and (7.51) are then replaced by

$$|\hat{X}(m,k)|^2 = |Y(m,k)|^2 - |\widehat{N(m,k)}|^2 \tag{7.53}$$

and

$$\hat{X}(m,k) = |\hat{X}(m,k)| \angle Y(m,k), \tag{7.54}$$

where $|\widehat{N(m,k)}|^2$ is the estimated noise spectrum.

Since it cannot be assured that the short-time spectra satisfy $|Y(m,k)|^2 - |\widehat{N(m,k)}|^2 > 0$, $\forall m, k$, one has to introduce further modifications such as clipping. Several methods for solving this problem and for keeping track of the time-varying noise have been proposed. For more detail, the reader is referred to [12, 50, 51, 60, 49]. Finally, note that a closely related technique, known as wavelet-based denoising, will be studied in Section 8.10.

Chapter 8

Wavelet Transform

The *wavelet transform* was introduced at the beginning of the 1980s by Morlet *et al.*, who used it to evaluate seismic data [105],[106]. Since then, various types of wavelet transforms have been developed, and many other applications ha v ebeen found. The continuous-time wavelet transform, also called the *integral wavelet transform* (IWT), finds most of its applications in data analysis, where it yields an affine invariant time-frequency representation. The most famous version, however, is the discrete wavelet transform(DWT). This transform has excellent signal compaction properties for many classes of real-world signals while being computationally very efficient. Therefore, it has been applied to almost all technical fields including image compression, denoising, numerical integration, and pattern recognition.

8.1   The Continuous-Time Wavelt   Transform

The wavelet transform $\mathcal{W}_x(b, a)$ of a continuous-time signal $x(t)$ is defined as

$$\mathcal{W}_x(b, a) = |a|^{-\frac{1}{2}} \int_{-\infty}^{\infty} x(t) \; \psi^* \left(\frac{t-b}{a} \right) \; dt. \qquad (8.1)$$

Thus, the wavelet transform is computed as the inner product of $x(t)$ and translated and scaled versions of a single function $\psi(t)$, the so-called *wavelet*.

If we consider $\psi(t)$ to be a bandpass impulse response, then the wavelet analysis can be understood as a bandpass analysis. By varying the scaling

210

parameter a the center frequency and the bandwidth of the bandpass are influenced. The variation of b simply means a translation in time, so that for a fixed a the transform (8.1) can be seen as a convolution of $x(t)$ with the time-reversed and scaled wavelet:

$$\mathcal{W}_x(t, a) = |a|^{-\frac{1}{2}} x(t) * \psi_a(t), \quad \psi_a(t) = \psi^* \left(\frac{-t}{a} \right).$$

The prefactor $|a|^{-1/2}$ is introduced in order to ensure that all scaled functions $|a|^{-1/2} \psi^*(t/a)$ with $a \in \mathbb{R}$ have the same energy.

Since the analysis function $\psi(t)$ is scaled and not modulated like the kernel of the STFT, a wavelet analysis is often called a *time-scale analysis* rather than a time-frequency analysis. However, both are naturally related to each other by the bandpass interpretation. Figure 8.1 shows examples of the kernels of the STFT and the wavelet transform. As we can see, a variation of the time delay b and/or of the scaling parameter a has no effect on the form of the transform kernel of the wavelet transform. However, the time and frequency resolution of the wavelet transform depends on a. For high analysis frequencies (small a) we have good time localization but poor frequency resolution. On the other hand, for low analysis frequencies, we have good frequency but poor time resolution. While the STFT is a constant bandwidth analysis, the wavelet analysis can be understood as a constant-Q or octave analysis.

When using a transform in order to get better insight into the properties of a signal, it should be ensured that the signal can be perfectly reconstructed from its representation. Otherwise the representation may be completely or partly meaningless. For the wavelet transform the condition that must be met in order to ensure perfect reconstruction is

$$C_\psi = \int_{-\infty}^{\infty} \frac{|\Psi(\omega)|^2}{|\omega|} \, d\omega \quad < \infty, \tag{8.2}$$

where $\Psi(\omega)$ denotes the Fourier transform of the wavelet. This condition is known as the *admissibility condition* for the wavelet $\psi(t)$. The proof of (8.2) will be given in Section 8.3.

Obviously, in order to satisfy (8.2) the wavelet must satisfy

$$\Psi(0) = \int_{-\infty}^{\infty} \psi(t) \, dt = 0. \tag{8.3}$$

Moreover, $|\Psi(\omega)|$ must decrease rapidly for $|\omega| \to 0$ and for $|\omega| \to \infty$. That is, $\psi(t)$ must be a bandpass impulse response. Since a bandpass impulse response looks like a small wave, the transform is named wavelet transform.
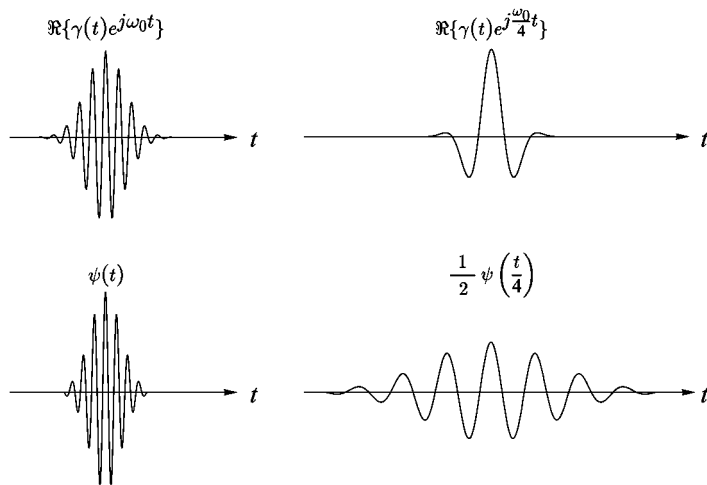
Figure 8.1. Comparison of the analysis kernels of the short-time Fourier transform (top, the real part is shown) and the wavelet transform (bottom, real wavelet) for high and low analysis frequencies.

Calculation of the Wavelet Transform from the Spectrum $X(\omega)$. Using the abbreviation

$$\psi_{b,a}(t) = |a|^{-\frac{1}{2}} \psi\left(\frac{t-b}{a}\right) \tag{8.4}$$

the integral wavelet transform introduced by equation (8.1) can also be written as

$$\mathcal{W}_x(b,a) = \langle x, \psi_{b,a}\rangle. \tag{8.5}$$

With the correspondences $X(\omega) \longleftrightarrow x(t)$ and $\Psi(\omega) \longleftrightarrow \psi(t)$, and the time and frequency shift properties of the Fourier transform, we obtain

$$\begin{aligned} \Psi_{b,a}(\omega) &= |a|^{\frac{1}{2}} e^{-j\omega b} \Psi(a\omega) \\ &\updownarrow \\ \psi_{b,a}(t) &= |a|^{-\frac{1}{2}} \psi\left(\tfrac{t-b}{a}\right). \end{aligned} \tag{8.6}$$

By making use of Parseval's relation we finally get

$$\begin{aligned} \mathcal{W}_x(b,a) &= \frac{1}{2\pi}\langle X, \Psi_{b,a}\rangle \\[2mm] &= |a|^{\frac{1}{2}} \frac{1}{2\pi}\int_{-\infty}^{\infty} X(\omega)\, \Psi^*(a\omega)\, e^{j\omega b}\, d\omega. \end{aligned} \tag{8.7}$$

Equation (8.7) states that the wavelet transform can also be calculated by means of an inverse Fourier transform from the windowed spectrum $X(\omega)\,\Psi^*(a\omega)$.

Time-Frequency Resolution. In order to describe the time-frequency resolution of the wavelet transform we consider the time-frequency window associated with the wavelet. The center (t_0, ω_0) and the radii Δ_t and Δ_ω of the window are calculated according to (7.8) and (7.11). This gives

$$t_0 = \int_{-\infty}^{\infty} t \cdot \frac{|\psi(t)|^2}{\|\psi\|^2}\, dt, \tag{8.8}$$

$$\omega_0 = \int_{-\infty}^{\infty} \omega \cdot \frac{|\Psi(\omega)|^2}{\|\Psi\|^2}\, d\omega \tag{8.9}$$

and

$$\Delta_t = \left(\int_{-\infty}^{\infty} (t - t_0)^2 \cdot \frac{|\psi(t)|^2}{\|\psi\|^2}\, dt \right)^{\frac{1}{2}}, \tag{8.10}$$

$$\Delta_\omega = \left(\int_{-\infty}^{\infty} (\omega - \omega_0)^2 \cdot \frac{|\Psi(\omega)|^2}{\|\Psi\|^2}\, d\omega \right)^{\frac{1}{2}}. \tag{8.11}$$

For the center and the radii of the scaled function $\psi(\frac{t}{a}) \longleftrightarrow |a|\Psi(a\omega)$ we have $\{a \cdot t_0,\ \frac{1}{a}\omega_0\}$ and $\{a \cdot \Delta_t,\ \frac{1}{a}\Delta_\omega\}$, respectively. This means that the wavelet transform $\mathcal{W}_x(b, a)$ provides information on a signal $x(t)$ and its spectrum $X(\omega)$ in the time-frequency window

$$[b + a \cdot t_0 - a \cdot \Delta_t,\ b + a \cdot t_0 + a \cdot \Delta_t] \times [\frac{\omega_0}{a} - \frac{\Delta_\omega}{a},\ \frac{\omega_0}{a} + \frac{\Delta_\omega}{a}]. \tag{8.12}$$

The area $4\Delta_t\Delta_\omega$ is independent of the parameters a and b; it is determined only by the used wavelet $\psi(t)$. The time window narrows when a becomes small, and it widens when a becomes large. On the other hand, the frequency window becomes wide when a becomes small, and it becomes narrow when a becomes large. As mentioned earlier, a short analysis window leads to good time resolution on the one hand, but on the other to poor frequency resolution. Accordingly, a long analysis window yields good frequency resolution but poor time resolution. Figure 8.2 illustrates the different resolutions of the short-time Fourier transform and the wavelet transform.

Affine Invariance. Equation (8.1) shows that if the signal is scaled $(x(t) \to x(t/c))$, the wavelet representation $\mathcal{W}_x(b, a)$ is scaled as well; except this, $\mathcal{W}_x(b, a)$ undergoes no other modification. For this reason we also speak of an
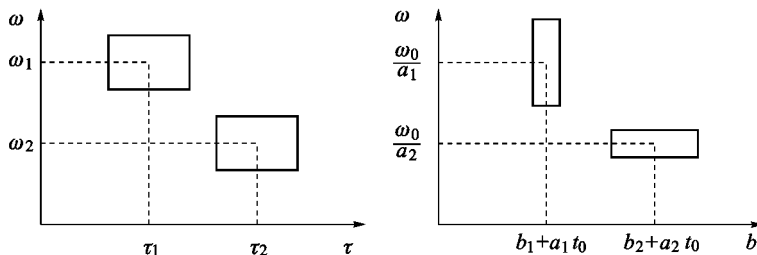
Figure 8.2. Resolution of the short-time Fourier transform (left) and the wavelet transform (right).

affine invariant transform. Furthermore, the wavelet transform is *translation invariant*, i.e. a shift of the signal $(x(t) \to x(t - t_0))$ leads to a shift of the wavelet representation $\mathcal{W}_x(b, a)$ by t_0, but $\mathcal{W}_x(b, a)$ undergoes no other modification.

8.2 Wavelets for Time-Scale Analysis

In time-scale signal analysis one aims at inferring certain signal properties from the wavelet transform in a convenient way. *Analytic wavelets* are especially suitable for this purpose. Like an *analytic signal*, they contain only positive frequencies. In other words, for the Fourier transform of an analytic wavelet $\psi_{b,a}(t)$ the following holds:

$$\Psi_{b,a}(\omega) = 0 \qquad \text{for} \qquad \omega \le 0. \tag{8.13}$$

Analytic wavelets have a certain property, which will be discussed briefly below. For this consider the real signal $x(t) = \cos(\omega_0 t)$. The spectrum is

$$X(\omega) = \pi \left[\delta(\omega - \omega_0) + \delta(\omega + \omega_0) \right] \quad \longleftrightarrow \quad x(t) = \cos(\omega_0 t). \tag{8.14}$$

Substituting $X(\omega)$ according to (8.14) into (8.7) yields

$$
\begin{aligned}
\mathcal{W}_x(b, a) &= \tfrac{1}{2} |a|^{\frac{1}{2}} \int_{-\infty}^{\infty} \left(\delta(\omega - \omega_0) + \delta(\omega + \omega_0) \right) \Psi^*(a\omega) \, e^{j\omega b} \, d\omega \\
&\qquad\qquad\qquad\qquad\qquad\qquad\qquad\qquad\qquad\qquad (8.15) \\
&= \tfrac{1}{2} |a|^{\frac{1}{2}} \left[\Psi^*(a\,\omega_0) \, e^{j\omega_0 b} + \Psi^*(-a\,\omega_0) \, e^{-j\omega_0 b} \right].
\end{aligned}
$$

Hence, for an analytic wavelet:

$$\mathcal{W}_x(b, a) = \frac{1}{2} |a|^{\frac{1}{2}} \, \Psi^*(a\omega_0) \, e^{j\omega_0 b}. \tag{8.16}$$

Since only the argument of the complex exponential in (8.16) depends on b, the frequency of $x(t)$ can be inferred from the phase of $\mathcal{W}_x(b, a)$. For this, any horizontal line in the time-frequency plane can be considered. The magnitude of $\mathcal{W}_x(b, a)$ is independent of b, so that the amplitude of $x(t)$ can be seen independent of time. This means that the magnitude of $\mathcal{W}_x(b, a)$ directly shows the time-frequency distribution of signal energy.

The Scalogram. A *scalogram* is the squared magnitude of the wavelet transform:

$$|\mathcal{W}_x(b, a)|^2 = \left| \; |a|^{-\frac{1}{2}} \int_{-\infty}^{\infty} x(t) \; \psi^* \left(\frac{t - b}{a} \right) \, dt \; \right|^2. \qquad (8.17)$$

Scalograms, like spectrograms, can be represented as images in which intensity is expressed by different shades of gray. Figure 8.3 depicts scalograms for $x(t) = \delta(t)$. We see that here analytic wavelets should be chosen in order to visualize the distribution of the signal energy in relation to time and frequency (and scaling, respectively).

The Morlet Wavelet. The complex wavelet most frequently used in signal analysis is the Morlet wavelet, a modulated Gaussian function:

$$\psi(t) = e^{j\omega_0 t} \; e^{-\beta^2 t^2 / 2}. \qquad (8.18)$$

Note that the Morlet wavelet satisfies the admissibility condition (8.2) only approximately. However, by choosing proper parameters ω_0 and β in (8.18) one can make the wavelet at least "practically" admissible. In order to show this, let us consider the Fourier transform of the wavelet, which, for $\omega = 0$, does not vanish exactly:

$$\Psi(\omega) = \frac{1}{\beta} \; e^{-(\omega - \omega_0)^2 / (2\beta^2)} \; > 0 \quad \forall \; \omega. \qquad (8.19)$$

By choosing

$$\omega_0 \geq 2\pi\beta \qquad (8.20)$$

we get $\Psi(\omega) \leq 2.7 \times 10^{-9}$ for $\omega \leq 0$, which is sufficient for most applications [132]. Often $\omega_0 \geq 5\beta$ is taken to be sufficient [65], which leads to $\Psi(\omega) \leq 10^{-5}$, $\omega \leq 0$.

Example. The example considered below is supposed to give a visual impression of a wavelet analysis and illustrates the difference from a short-time Fourier analysis. The chosen test signal is a discrete-time signal; it contains
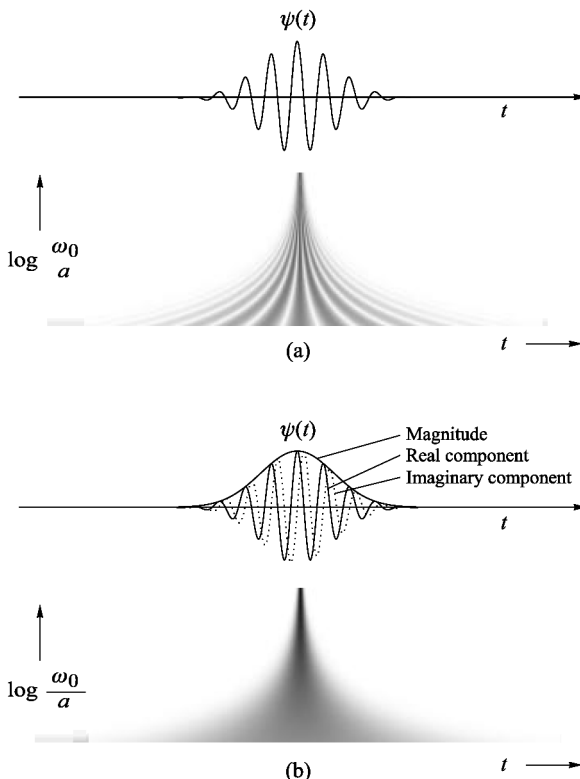
Figure 8.3. Scalogram of a delta impulse $(\mathcal{W}_\delta(b,a) = |\psi(b/a)|^2)$; (a) real wavelet; (b) analytic wavelet.

two periodic parts and two impulses.[1] An almost analytic, sampled Morlet wavelet is used. The signal is depicted in Figure 8.4(a). Figures 8.4(b) and 8.4(c) show two corresponding spectrograms (short-time Fourier transforms) with Gaussian analysis windows. We see that for a very short analysis window the discrimination of the two periodic components is impossible whereas the impulses are quite visible. A long window facilitates good discrimination of the periodic component, but the localization of the impulses is poor. This is not the case in the wavelet analysis represented in Figure 8.4(d). Both the periodic components and the impulses are clearly visible. Another property of the wavelet analysis, which is well illustrated in Figure 8.4(d), is that it clearly indicates non-stationarities of the signal.

---

[1]In Section 8.8 the question of how the wavelet transform of a discrete-time signal can be calculated will be examined in more detail.
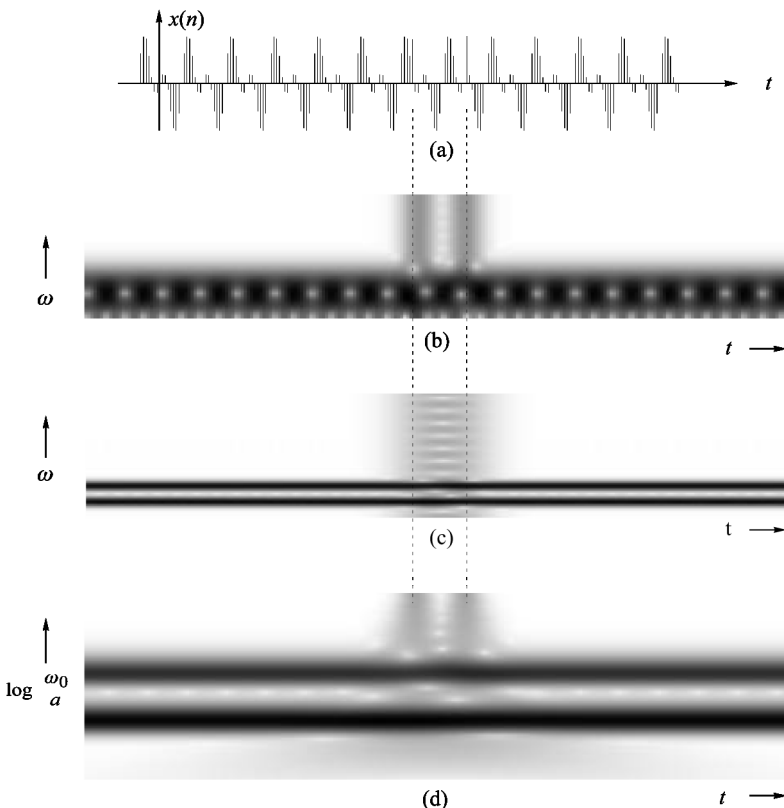
Figure 8.4. Examples of short-time Fourier and wavelet analyses; (a) test signal; (b) spectrogram (short window); (c) spectrogram (long window); (d) scalogram.

8.3 Integral and Semi-Discrete Reconstruction

In this section, two variants of continuous wavelet transforms will be considered; they only differ in the way reconstruction is handled. Specifically, we will look at integral reconstruction from the entire time-frequency plane and at a semi-discrete reconstruction.

8.3.1 Integral Reconstruction

As will be shown, the inner product of two signals $x(t)$ and $y(t)$ is related to the inner product of their wavelet transforms as

$$\langle x, y \rangle = \frac{1}{C_\psi} \int_{-\infty}^{\infty} \int_{-\infty}^{\infty} \mathcal{W}_x(b, a) \, \mathcal{W}_y^*(b, a) \, \frac{da \, db}{a^2} \qquad (8.21)$$

with C_ψ as in (8.2).

Given the inner product (8.21), we obtain a synthesis equation by choosing

$$y_t(t') = \delta(t' - t), \tag{8.22}$$

because then the following relationship holds:

$$\langle x, y_t \rangle = \int_{-\infty}^{\infty} f(t')\, \delta(t' - t)\, dt' = x(t). \tag{8.23}$$

Substituting (8.22) into (8.21) gives

$$\langle x, y_t \rangle = \frac{1}{C_\psi} \int_{-\infty}^{\infty}\int_{-\infty}^{\infty} \mathcal{W}_x(b, a)\, |a|^{-\frac{1}{2}} \int_{-\infty}^{\infty} \delta(t' - t)\, \psi\left(\frac{t' - b}{a}\right) dt'\, \frac{da\ db}{a^2}.$$

From this we obtain the reconstruction formula

$$x(t) = \frac{1}{C_\psi} \int_{-\infty}^{\infty}\int_{-\infty}^{\infty} \mathcal{W}_x(b, a)\, |a|^{-\frac{1}{2}}\, \psi\left(\frac{t - b}{a}\right)\ \frac{da\ db}{a^2}. \tag{8.24}$$

Proof of (8.2) and (8.21). With

$$P_a(\omega) = X(\omega)\, \Psi^*(\omega a) \tag{8.25}$$

equation (8.7) can be written as

$$\mathcal{W}_x(b, a) = |a|^{\frac{1}{2}}\, \frac{1}{2\pi} \int_{-\infty}^{\infty} P_a(\omega)\, e^{j\omega b} d\omega. \tag{8.26}$$

Using the correspondence $P_a(\omega) \longleftrightarrow p_a(b)$ we obtain

$$\mathcal{W}_x(b, a) = |a|^{\frac{1}{2}}\, p_a(b). \tag{8.27}$$

Similarly, for the wavelet transform of $y(t)$ we get

$$Q_a(\omega) = Y(\omega)\, \Psi^*(\omega a) \longleftrightarrow q_a(b), \tag{8.28}$$

which means that

$$\mathcal{W}_y(b, a) = |a|^{\frac{1}{2}}\, q_a(b). \tag{8.29}$$

Substituting (8.27) and (8.28) into the right term of (8.21) and rewriting the obtained expression by applying Parseval's relation yields

$$\int_{-\infty}^{\infty}\int_{-\infty}^{\infty} \mathcal{W}_x(b,a)\,\mathcal{W}_y^*(b,a)\,\frac{da\,db}{a^2} = \int_{-\infty}^{\infty}\frac{1}{|a|}\int_{-\infty}^{\infty} p_a(b)\,q_a^*(b)\,db\,da$$

$$= \int_{-\infty}^{\infty}\frac{1}{|a|}\langle p_a, q_a\rangle\,da$$

$$= \int_{-\infty}^{\infty}\frac{1}{|a|}\frac{1}{2\pi}\langle P_a, Q_a\rangle\,da$$

$$= \frac{1}{2\pi}\int_{-\infty}^{\infty} X(\nu)\,Y^*(\nu)\int_{-\infty}^{\infty}\frac{|\Psi(\nu a)|^2}{|a|}\,da\,\,d\nu.$$

$$(8.30)$$

By substituting $\omega = \nu a$ we can show that the inner integral in the last line of (8.30) is a constant, which only depends on $\psi(t)$:

$$C_\psi = \int_{-\infty}^{\infty}\frac{|\Psi(\nu a)|^2}{|a|}\,da = \int_{-\infty}^{\infty}\frac{|\Psi(\omega)|^2}{|\omega|}\,d\omega. \qquad (8.31)$$

Hence (8.30) is

$$\int_{-\infty}^{\infty}\int_{-\infty}^{\infty} \mathcal{W}_x(b,a)\,\mathcal{W}_y^*(b,a)\,\frac{da\,db}{a^2} = C_\psi\,\frac{1}{2\pi}\int_{-\infty}^{\infty} X(\nu)\,Y^*(\nu)\,d\nu$$

$$= C_\psi\int_{-\infty}^{\infty} x(\tau)\,y^*(\tau)\,d\tau.$$

$$(8.32)$$

This completes the proof of (8.2) and (8.21). $\square$

8.3.2 Semi-Discrete Dyadic Wavelets

We speak of semi-discrete dyadic wavelets if every signal $x(t) \in L_2(\mathbb{R})$ can be reconstructed from semi-discrete values $\mathcal{W}_x(b, a_m)$, where a_m, $m \in \mathbb{Z}$ are dyadically arranged:

$$a_m = 2^m. \qquad (8.33)$$

That is, the wavelet transform is calculated solely along the lines $\mathcal{W}_x(b, 2^m)$:

$$\mathcal{W}_x(b, 2^m) = 2^{-\frac{m}{2}}\int_{-\infty}^{\infty} x(t)\,\psi^*(2^{-m}(t - b))\,dt. \qquad (8.34)$$

The center frequencies of the scaled wavelets are

$$\omega_m = \frac{\omega_0}{a_m} = 2^{-m}\,\omega_0, \qquad m \in \mathbb{Z}, \tag{8.35}$$

with ω_0 according to (8.9). The radii of the frequency windows are

$$\frac{\Delta_\omega}{a_m} = 2^{-m}\,\Delta_\omega, \qquad m \in \mathbb{Z}. \tag{8.36}$$

In order to ensure that neighboring frequency windows

$$\left[\frac{\omega_0 - \Delta_\omega}{a_m}, \frac{\omega_0 + \Delta_\omega}{a_m}\right]$$

and

$$\left[\frac{\omega_0 - \Delta_\omega}{a_{m+1}}, \frac{\omega_0 + \Delta_\omega}{a_{m+1}}\right]$$

do adjoin, we assume

$$\omega_0 = 3\,\Delta_\omega. \tag{8.37}$$

This condition can easily be satisfied, because by modulating a given wavelet $\psi_o(t)$ the center frequency can be varied freely. From (8.33), (8.35) and (8.37) we get for the center frequencies of the scaled wavelets:

$$\omega_m = 3 \cdot 2^{-m}\,\Delta_\omega, \qquad m \in \mathbb{Z}. \tag{8.38}$$

Synthesis. Consider the signal analysis and synthesis shown in Figure 8.5. Mathematically, we have the following synthesis approach using a dual (also dyadic) wavelet $\tilde{\psi}(t)$:

$$x(t) = \sum_{m=-\infty}^{\infty} 2^{-\frac{3}{2}m} \int_{-\infty}^{\infty} \mathcal{W}_x(b, 2^m)\, \tilde{\psi}(2^{-m}(t-b))\, db. \tag{8.39}$$

In order to express the required dual wavelet $\tilde{\psi}(t)$ by $\psi(t)$, (8.39) is rearranged

as

$$x(t) = \sum_{m=-\infty}^{\infty} 2^{-\frac{3}{2}m} \int_{-\infty}^{\infty} \mathcal{W}_x(b, 2^m) \tilde{\psi}(2^{-m}(t-b))\, db$$

$$= \sum_{m=-\infty}^{\infty} 2^{-\frac{3}{2}m} \left\langle \mathcal{W}_x(\,\cdot\,, 2^m), \tilde{\psi}^*(2^{-m}(t-\,\cdot\,)) \right\rangle$$

$$= \sum_{m=-\infty}^{\infty} 2^{-\frac{3}{2}m} \frac{1}{2\pi} \left\langle \mathcal{F}\{\mathcal{W}_x(\,\cdot\,, 2^m)\}, \mathcal{F}\{\tilde{\psi}^*(2^{-m}(t-\,\cdot\,))\} \right\rangle$$

$$= \sum_{m=-\infty}^{\infty} 2^{-\frac{3}{2}m} \frac{1}{2\pi} \int_{-\infty}^{\infty} \left[X(\omega)\, 2^{\frac{m}{2}} \Psi^*(2^m \omega) \right] \left[2^m \tilde{\Psi}(2^m \omega) e^{j\omega t} \right]\, d\omega$$

$$= \frac{1}{2\pi} \int_{-\infty}^{\infty} X(\omega) \left[\sum_{m=-\infty}^{\infty} \Psi^*(2^m \omega) \tilde{\Psi}(2^m \omega) \right] e^{j\omega t}\, d\omega.$$

$$(8.40)$$

For the sum in the last row of (8.40)

$$\sum_{m=-\infty}^{\infty} \Psi^*(2^m \omega)\, \tilde{\Psi}(2^m \omega) = 1 \tag{8.41}$$

must hold in order to allow reconstruction. Hence, $\tilde{\psi}(t)$ can be computed from $\psi(t)$ as

$$\tilde{\Psi}(\omega) = \frac{\Psi(\omega)}{\displaystyle\sum_{m=-\infty}^{\infty} |\Psi(2^m \omega)|^2}. \tag{8.42}$$

If two positive constants A and B with $0 < A \le B < \infty$ exist such that

$$A \le \sum_{m=-\infty}^{\infty} |\Psi(2^m \omega)|^2 \le B \tag{8.43}$$

we achieve stability. Therefore, (8.43) is referred to as a *stability condition*. A wavelet $\psi(t)$ which satisfies (8.43) is called a dyadic wavelet. Note that because of (8.42), for the dual dyadic wavelet, we have:

$$\frac{1}{B} \le \sum_{m=-\infty}^{\infty} \left| \tilde{\Psi}(2^m \omega) \right|^2 \le \frac{1}{A}. \tag{8.44}$$

Thus, for $\tilde{\Psi}(\omega)$ according to (8.42) we have stability, provided that (8.43) is satisfied. Note that the dual wavelet is not necessarily unique [25]. One may find other duals that also satisfy the stability condition.
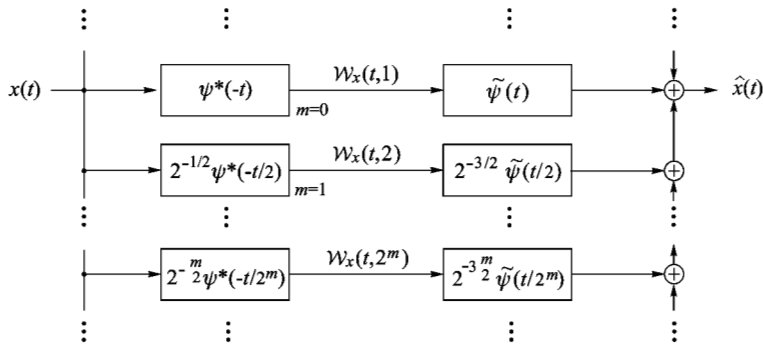
Figure 8.5. Octave-band analysis and synthesis filter bank.

Finally it will be shown that if condition (8.43) holds the admissibility condition (8.2) is also satisfied. Dividing (8.43) by ω and integrating the obtained expression over the interval $(1,2)$ yields:

$$A \int_1^2 \frac{d\omega}{\omega} \leq \sum_{m=-\infty}^{\infty} \int_1^2 \frac{|\Psi(2^m\omega)|^2}{\omega} d\omega \leq B \int_1^2 \frac{d\omega}{\omega}. \qquad (8.45)$$

With

$$\int_1^2 \frac{|\Psi(2^m\omega)|^2}{\omega} d\omega = \int_{2^m}^{2^{m+1}} \frac{|\Psi(\nu)|^2}{\nu} d\nu \qquad (8.46)$$

we obtain the following result for the center term in (8.45):

$$\sum_{m=-\infty}^{\infty} \int_1^2 \frac{|\Psi(2^m\omega)|^2}{\omega} d\omega = \int_0^\infty \frac{|\Psi(\omega)|^2}{\omega} d\omega. \qquad (8.47)$$

Thus

$$A \ln 2 \leq \int_0^\infty \frac{|\Psi(\omega)|^2}{\omega} d\omega \leq B \ln 2. \qquad (8.48)$$

Dividing (8.43) by $-\omega$ and integrating over $(-1,-2)$ gives

$$A \ln 2 \leq \int_0^\infty \frac{|\Psi(-\omega)|^2}{\omega} d\omega \leq B \ln 2. \qquad (8.49)$$

Thus the admissibility condition (8.2) is satisfied in any case, and reconstruction according to (8.24) is also possible.

8.4 Wavelet Series

8.4.1 Dyadic Sampling

In this section, we consider the reconstruction from discrete values of the wavelet transform. The following dyadically arranged sampling points are used:

$$a_m = 2^m, \qquad b_{mn} = a_m \, n \, T = 2^m n T, \tag{8.50}$$

This yields the values $\mathcal{W}_x \left(b_{mn}, a_m \right) = \mathcal{W}_x \left(2^m n T, 2^m \right)$. Figure 8.6 shows the sampling grid.

Using the abbreviation

$$
\begin{aligned}
\psi_{mn}(t) &= |a_m|^{-\frac{1}{2}} \cdot \psi \left(\frac{t - b_{mn}}{a_m} \right) \\
&= 2^{-\frac{m}{2}} \cdot \psi(2^{-m} t - nT),
\end{aligned}
\tag{8.51}
$$

we may write the wavelet analysis as

$$\mathcal{W}_x \left(b_{mn}, a_m \right) = \mathcal{W}_x \left(2^m n T, 2^m \right) = \langle x, \psi_{mn} \rangle. \tag{8.52}$$

The values $\{ \mathcal{W}_x \left(2^m n T, 2^m \right), \ m, n \in \mathbb{Z} \}$ form the representation of $x(t)$ with respect to the wavelet $\psi(t)$ and the chosen grid.

Of course, we cannot assume that any set $\psi_{mn}(t)$, $m, n \in \mathbb{Z}$ allows reconstruction of all signals $x(t) \in L_2(\mathbb{R})$. For this a dual set $\tilde{\psi}_{mn}(t)$, $m, n \in \mathbb{Z}$ must exist, and both sets must span $L_2(\mathbb{R})$. The dual set need not necessarily be built from wavelets. However, we are only interested in the case where $\tilde{\psi}_{mn}(t)$ is derived as

$$\tilde{\psi}_{mn}(t) = 2^{-\frac{m}{2}} \cdot \tilde{\psi}(2^{-m} t - nT), \qquad m, n \in \mathbb{Z} \tag{8.53}$$

from a dual wavelet $\tilde{\psi}(t)$. If both sets $\psi_{mn}(t)$ and $\tilde{\psi}_{mn}(t)$ with $m, n \in \mathbb{Z}$ span the space $L_2(\mathbb{R})$, any $x(t) \in L_2(\mathbb{R})$ may be written as

$$x(t) = \sum_{m=-\infty}^{\infty} \sum_{n=-\infty}^{\infty} \langle x, \psi_{mn} \rangle \, \tilde{\psi}_{mn}(t). \tag{8.54}$$

Alternatively, we may write $x(t)$ as

$$x(t) = \sum_{m=-\infty}^{\infty} \sum_{n=-\infty}^{\infty} \left\langle x, \tilde{\psi}_{mn} \right\rangle \psi_{mn}(t). \tag{8.55}$$
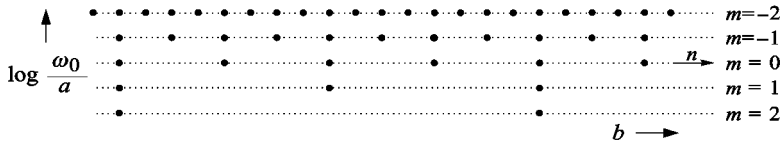
Figure 8.6. Dyadic sampling of the wavelet transform.

For a given wavelet $\psi(t)$, the possibility of perfect reconstruction is depen-
dent on the sampling interval T. If T is chosen very small (oversampling), the
values $\mathcal{W}_x\left(2^m nT, 2^m\right)$, $m, n \in \mathbb{Z}$ are highly redundant, and reconstruction is
very easy. Then the functions $\psi_{mn}(t)$, $m, n \in \mathbb{Z}$ are linearly dependent, and
an infinite number of dual sets $\tilde{\psi}_{mn}(t)$ exists. The question of whether a dual
set $\tilde{\psi}_{mn}(t)$ exists at all can be answered by checking two frame bounds[2] A
and B. It can be shown that the existence of a dual set and the completeness
are guaranteed if the stability condition

$$A\left\|x\right\|^2 \leq \sum_{m=-\infty}^{\infty} \sum_{n=-\infty}^{\infty} \left|\langle x, \psi_{mn}\rangle\right|^2 \leq B\left\|x\right\|^2 \tag{8.56}$$

with the frame bounds $0 < A \leq B < \infty$ is satisfied [35]. In the case of a
tight frame, $A = B$, perfect reconstruction with $\tilde{\psi}_{mn}(t) = \psi_{mn}(t)$ is possible.
This is also true if the samples $\mathcal{W}_x\left(2^m nT, 2^m\right)$ contain redundancy, that is, if
the functions $\psi_{mn}(t)$, $m, n \in \mathbb{Z}$ are linearly dependent. The tighter the frame
bounds are, the smaller is the reconstruction error if the reconstruction is
carried out according to

$$\hat{x}(t) = \frac{2}{A+B} \sum_{m=-\infty}^{\infty} \sum_{n=-\infty}^{\infty} \langle x, \psi_{mn}\rangle \, \psi_{mn}(t). \tag{8.57}$$

If T is chosen just large enough that the samples $\mathcal{W}_x\left(2^m nT, 2^m\right)$, $m, n \in \mathbb{Z}$
contain no redundancy at all (critical sampling), the functions $\psi_{mn}(t)$, $m, n \in$
$\mathbb{Z}$ are linearly independent. If (8.56) is also satisfied with $0 < A \leq B < \infty$,
the functions $\psi_{mn}(t)$, $m, n \in \mathbb{Z}$ form a basis for $L_2(\mathbb{R})$. Then the following
relation, which is known as the *biorthogonality condition*, holds:

$$\left\langle \psi_{mn}, \tilde{\psi}_{lk} \right\rangle = \delta_{ml}\,\delta_{nk}, \quad m, n, l, k \in \mathbb{Z}. \tag{8.58}$$

Wavelets that satisfy (8.58) are called *biorthogonal wavelets*.   As a special
case, we have the *orthonormal wavelets*. They are self-reciprocal and satisfy

---

[2]The problem of calculating the frame bounds will be discussed at the end of this section
in detail.

the orthonormality condition

$$\langle \psi_{mn}, \psi_{lk} \rangle = \delta_{ml}\,\delta_{nk}, \qquad m,n,l,k \in \mathbb{Z}. \tag{8.59}$$

Thus, in the orthonormal case, the functions $\psi_{mn}(t)$, $m,n \in \mathbb{Z}$ can be used for both analysis and synthesis. Orthonormal bases always have the same frame bounds (tight frame), because, in that case, (8.56) is a special form of Parseval's relation.

8.4.2 Better Frequency Resolution — Decomposition of Octaves

An octave-band analysis is often insufficient. Rather, we would prefer to decompose every octave into M subbands in order to improve the frequency resolution by the factor M.

We here consider the case where the same sampling rate is used for all M subbands of an octave. This corresponds to a nesting of M dyadic wavelet analyses with the scaled wavelets

$$\psi^{(k)}(t) = 2^{\frac{k}{2M}}\,\psi(2^{\frac{k}{M}}t), \qquad k = 0,1,\ldots,M-1. \tag{8.60}$$

Figure 8.7 shows the sampling grid of an analysis with three voices per octave. Sampling the wavelet transform can be further generalized by choosing the sampling grid

$$a_m = a_0^m, \qquad b_{mn} = a_m\,n\,T, \qquad m,n \in \mathbb{Z} \tag{8.61}$$

with an arbitrary $a_0 > 1$. This corresponds to M nested wavelet analyses with the wavelets

$$\psi^{(k)}(t) = a_0^{\frac{k}{2M}}\,\psi(a_0^{\frac{k}{M}}t), \qquad k = 0,1,\ldots,M-1. \tag{8.62}$$

For this general case we will list the formulae for the frame bounds A and B in (8.56) as derived by Daubechies [35]. The conditions for the validity of the formulae are:[3]

$$\operatorname*{ess\,inf}_{|\omega|\in[1,a_0]}\ \sum_{m=-\infty}^{\infty} |\Psi(a_0^m\omega)|^2 \ >\ 0, \tag{8.63}$$

$$\operatorname*{ess\,sup}_{|\omega|\in[1,a_0]}\ \sum_{m=-\infty}^{\infty} |\Psi(a_0^m\omega)|^2 \ <\ \infty, \tag{8.64}$$

and

$$\sup_{s\in\mathbb{R}}\left[(1+s^2)^{(1+\varepsilon)/2}\,\beta(s)\right] = C_\varepsilon < \infty \qquad \text{(for an } \varepsilon > 0) \tag{8.65}$$

---

[3] By "ess inf" and "ess sup" we mean the essential infimum and supremum.
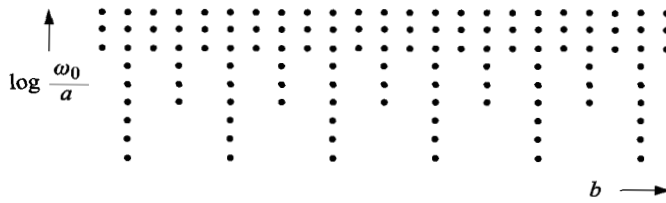
Figure 8.7. Sampling of the wavelet transform with three voices per octave.

with

$$\beta(s) = \sup_{|\omega| \in [1, a_0]} \sum_{m=-\infty}^{\infty} |\Psi(a_0^m \omega)| \; |\Psi(a_0^m \omega + s)|. \tag{8.66}$$

If (8.63) – (8.65) are satisfied for all wavelets defined in (8.62), the frame bounds A and B can be estimated on the basis of the quantities

$$c = \operatorname*{ess\,inf}_{|\omega| \in [1, a_0]} \sum_{k=0}^{M-1} \sum_{m=-\infty}^{\infty} \left| \Psi^{(k)}(a_0^m \omega) \right|^2, \tag{8.67}$$

$$C = \operatorname*{ess\,sup}_{|\omega| \in [1, a_0]} \sum_{k=0}^{M-1} \sum_{m=-\infty}^{\infty} \left| \Psi^{(k)}(a_0^m \omega) \right|^2, \tag{8.68}$$

$$\beta^{(k)}(s) = \sup_{|\omega| \in [1, a_0]} \sum_{m=-\infty}^{\infty} \left| \Psi^{(k)}(a_0^m \omega) \right| \; \left| \Psi^{(k)}(a_0^m \omega + s) \right|. \tag{8.69}$$

Provided the sampling interval T is chosen such that

$$2 \sum_{k=0}^{M-1} \sum_{\ell=1}^{\infty} \left[\beta^{(k)} \left(\ell \, \frac{2\pi}{T} \right) \; \beta^{(k)} \left(-\ell \, \frac{2\pi}{T} \right) \right]^{\frac{1}{2}} < c, \tag{8.70}$$

we finally have the following estimates for A and B:

$$A \geq \frac{2\pi}{T} \left(c - 2 \sum_{k=0}^{M-1} \sum_{\ell=1}^{\infty} \left[\beta^{(k)} \left(\ell \, \frac{2\pi}{T} \right) \; \beta^{(k)} \left(-\ell \, \frac{2\pi}{T} \right) \right]^{\frac{1}{2}} \right) \tag{8.71}$$

$$B \leq \frac{2\pi}{T} \left(C + 2 \sum_{k=0}^{M-1} \sum_{\ell=1}^{\infty} \left[\beta^{(k)} \left(\ell \, \frac{2\pi}{T} \right) \; \beta^{(k)} \left(-\ell \, \frac{2\pi}{T} \right) \right]^{\frac{1}{2}} \right). \tag{8.72}$$

8.5 The Discrete Wavelet Transform (DWT)

In this section the idea of *multiresolution analysis* and the efficient realization of the discrete wavelet transform based on multirate filter banks will be addressed. This framework has mainly been developed by Meyer, Mallat and Daubechies for the orthonormal case [104, 91, 90, 34]. Since biorthogonal wavelets formally fit into the same framework [153, 36], the derivations will be given for the more general biorthogonal case.

8.5.1 Multiresolution Analysis

In the following we assume that the sets

$$
\begin{aligned}
\psi_{mn}(t) &= 2^{-\frac{m}{2}}\,\psi(2^{-m}t - n), \\
&\qquad\qquad\qquad\qquad m, n \in \mathbb{Z} \qquad (8.73) \\
\tilde{\psi}_{mn}(t) &= 2^{-\frac{m}{2}}\,\tilde{\psi}(2^{-m}t - n),
\end{aligned}
$$

are bases for $L_2(\mathbb{R})$ satisfying the biorthogonality condition (8.58). Note that $T = 1$ is chosen in order to simplify notation. We will mainly consider the representation (8.55) and write it as

$$
x(t) = \sum_{m=-\infty}^{\infty} \sum_{n=-\infty}^{\infty} d_m(n)\,\psi_{mn}(t) \qquad (8.74)
$$

with

$$
d_m(n) = \mathcal{W}_x^{\tilde{\psi}}(2^m n, 2^m) = \left\langle x, \tilde{\psi}_{mn} \right\rangle, \qquad m, n \in \mathbb{Z}. \qquad (8.75)
$$

Since a basis consists of linearly independent functions, $L_2(\mathbb{R})$ may be understood as the direct sum of subspaces

$$
L_2(\mathbb{R}) = \ldots \oplus W_{-1} \oplus W_0 \oplus W_1 \oplus \ldots \qquad (8.76)
$$

with

$$
W_m = \operatorname{span}\left\{\psi(2^{-m}t - n),\ n \in \mathbb{Z}\right\}, \qquad m \in \mathbb{Z}. \qquad (8.77)
$$

Each subspace W_m covers a certain frequency band. For the subband signals we obtain from (8.74):

$$
y_m(t) = \sum_{n=-\infty}^{\infty} d_m(n)\,\psi_{mn}(t), \qquad y_m(t) \in W_m. \qquad (8.78)
$$

Every signal $x(t) \in L_2(\mathbb{R})$ can be represented as

$$
x(t) = \sum_{m=-\infty}^{\infty} y_m(t), \qquad y_m(t) \in W_m. \qquad (8.79)
$$

Now we define the subspaces V_m, $m \in \mathbb{Z}$ as the direct sum of V_{m+1} and W_{m+1}:

$$V_m = V_{m+1} \oplus W_{m+1}. \tag{8.80}$$

Here we may assume that the subspaces V_m contain lowpass signals and that the bandwidth of the signals contained in V_m reduces with increasing m.

From (8.77), (8.76), and (8.80) we derive the following properties:

(i) We have a nested sequence of subspaces

$$\ldots \subset V_{m+1} \subset V_m \subset V_{m-1} \subset \ldots \tag{8.81}$$

(ii) Scaling of $x(t)$ by the factor two $(x(t) \to x(2t))$ makes the scaled signal $x(2t)$ an element of the next larger subspace and vice versa:

$$x(t) \in V_m \quad \Leftrightarrow \quad x(2t) \in V_{m-1}. \tag{8.82}$$

(iii) If we form a sequence of functions $x_m(t)$ by projection of $x(t) \in L_2(\mathbb{R})$ onto the subspaces V_m, this sequence converges towards $x(t)$:

$$\lim_{m \to -\infty} x_m(t) = x(t), \quad x(t) \in L_2(\mathbb{R}), \quad x_m(t) \in V_m. \tag{8.83}$$

Thus, any signal may be approximated with arbitrary precision.

Because of the scaling property (8.82) we may assume that the subspaces V_m are spanned by scaled and time-shifted versions of a single function $\phi(t)$:

$$V_m = \mathrm{span}\left\{\phi(2^{-m}t - n), \ n \in \mathbb{Z}\right\}. \tag{8.84}$$

Thus, the subband signals $x_m(t) \in V_m$ are expressed as

$$x_m(t) = \sum_{n=-\infty}^{\infty} c_m(n) \ \phi_{mn}(t) \tag{8.85}$$

with

$$\phi_{mn}(t) = 2^{-\frac{m}{2}} \phi(2^{-m}t - n). \tag{8.86}$$

The function $\phi(t)$ is called a *scaling function*.

Orthonormal Wavelets. If the functions $\psi_{mn}(t) = 2^{-\frac{m}{2}} \psi(2^{-m}t - n)$, $m, n \in \mathbb{Z}$ form an orthonormal basis for $L_2(\mathbb{R})$, then $L_2(\mathbb{R})$ is decomposed into an orthogonal sum of subspaces:

$$L_2(\mathbb{R}) = \ldots \overset{\perp}{\oplus} W_{-1} \overset{\perp}{\oplus} W_0 \overset{\perp}{\oplus} W_1 \overset{\perp}{\oplus} \ldots \tag{8.87}$$

In this case (8.80) becomes an orthogonal decomposition:

$$V_m = V_{m+1} \overset{\perp}{\oplus} W_{m+1}. \tag{8.88}$$

If we assume $\|\phi\| = 1$, then the functions

$$\phi_{mn}(t) = 2^{-\frac{m}{2}} \phi(2^{-m}t - n), \qquad m, n \in \mathbb{Z}, \tag{8.89}$$

form orthonormal bases for the spaces V_m, $m \in \mathbb{Z}$.

Signal Decomposition. From (8.80) we derive

$$x_m(t) = x_{m+1}(t) + y_{m+1}(t). \tag{8.90}$$

If we assume that one of the signals $x_m(t)$, for example $x_0(t)$, is known, this signal can be successively decomposed according to (8.90):

$$
\begin{array}{ccccccc}
y_1(t) & & y_2(t) & & y_3(t) & & y_4(t) \\
\nearrow & & \nearrow & & \nearrow & & \nearrow \\
x_0(t) \;\to\; & x_1(t) & \to & x_2(t) & \to & x_3(t) & \to & x_4(t) & \to\,.
\end{array}
$$

The signals $y_1(t)$, $y_2(t), \ldots$ contain the high-frequency components of $x_0(t)$, $x_1(t)$, etc., so that the decomposition is a successive lowpass filtering accompanied by separating bandpass signals. Since the successive lowpass filtering results in an increasing loss of detail information, and since these details are contained in $y_1(t)$, $y_2(t), \ldots$ we also speak of a multiresolution analysis (MRA).

Assuming a known sequence $\{c_0(n)\}$, the sequences $\{c_m(n)\}$ and $\{d_m(n)\}$ for $m > 0$ may also be derived directly according to the scheme

$$
\begin{array}{ccccccc}
\{d_1(\ell)\} & & \{d_2(m)\} & & \{d_3(k)\} & & \{d_4(j)\} \\
\nearrow & & \nearrow & & \nearrow & & \nearrow \\
\{c_0(n)\} \;\to\; & \{c_1(\ell)\} & \to & \{c_2(m)\} & \to & \{c_3(k)\} & \to & \{c_4(j)\} & \to\,.
\end{array}
$$

In the next section we will discuss this very efficient method in greater detail.

Example: Haar Wavelets. The *Haar function* is the simplest example of an orthonormal wavelet:

$$\psi(t) = \begin{cases} 1 & \text{for } 0 \leq t < 0.5 \\ -1 & \text{for } 0.5 \leq t < 1 \\ 0 & \text{otherwise.} \end{cases}$$
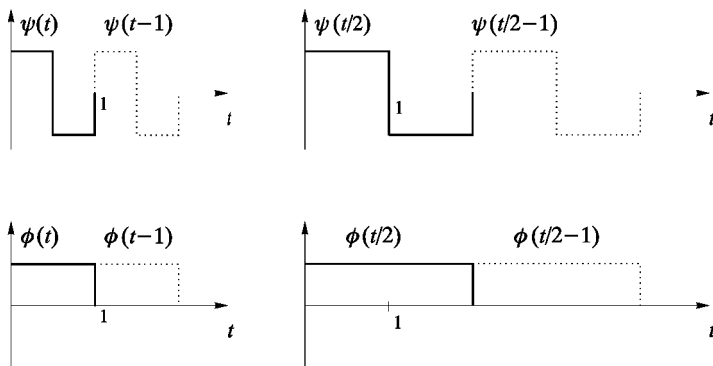
Figure 8.8. Haar wavelet and scaling function.

The corresponding scaling function is

$$\phi(t) = \begin{cases} 1, & \text{for } 0 \le t < 1 \\ 0, & \text{otherwise.} \end{cases}$$

The functions $\psi(t - n)$, $n \in \mathbb{Z}$ span the subspace W_0, and the functions $\psi(\frac{1}{2}t - n)$, $n \in \mathbb{Z}$ span W_1. Furthermore, the functions $\phi(t - n)$, $n \in \mathbb{Z}$ span V_0 and the functions $\phi(\frac{1}{2}t - n)$, $n \in \mathbb{Z}$ span V_1. The orthogonality among the basis functions $\psi(2^{-m}t - n)$, $m, n \in \mathbb{Z}$ and the orthogonality of the functions $\psi(2^{-m}t - n)$, $m, n \in \mathbb{Z}$ and $\phi(2^{-j}t - n)$, $j \ge m$ is obvious, see Figure 8.8.

Example: Shannon Wavelets. The *Shannon wavelets* are impulse responses of ideal bandpass filters:

$$\psi(t) = \frac{\sin \frac{\pi}{2}t}{\frac{\pi}{2}t} \cos \frac{3\pi}{2}t. \tag{8.91}$$

In the frequency domain this is

$$\Psi(\omega) = \begin{cases} 1 & \text{for } \pi \le |\omega| \le 2\pi, \\ 0 & \text{otherwise.} \end{cases} \tag{8.92}$$

The scaling function that belongs to the Shannon wavelet is the impulse response of the ideal lowpass:

$$\phi(t) \quad = \quad \frac{\sin \pi t}{\pi t} \tag{8.93}$$

$$\updownarrow \tag{8.94}$$

$$\Phi(\omega) \quad = \quad \begin{cases} 1 & \text{for } 0 \le |\omega| \le \pi, \\ 0 & \text{otherwise.} \end{cases} \tag{8.95}$$
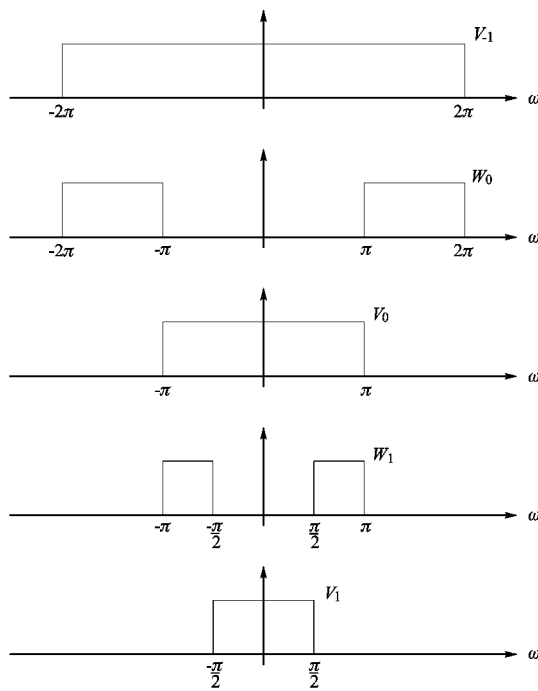
Figure 8.9. Subspaces of Shannon wavelets.

The coefficients $c_m(n)$, $m, n \in \mathbb{Z}$ in (8.85) can be understood as the sample values of the ideally lowpass-filtered signal. Figure 8.9 illustrates the decomposition of the signal space.

The Shannon wavelets form an orthonormal basis for $L_2(\mathbb{R})$. The orthogonality between different scales is easily seen, because the spectra do not overlap. For the inner product of translated versions of $\phi(t)$ at the same scale, we get

$$
\begin{aligned}
\int_{-\infty}^{\infty} \phi(t - m)\phi^*(t - n) &= \frac{1}{2\pi} \int_{-\pi}^{\pi} \Phi(\omega)\Phi^*(\omega)e^{-j(m - n)\omega}d\omega \\
&= \frac{1}{2\pi} \int_{-\pi}^{\pi} e^{-j(m - n)\omega}d\omega \qquad (8.96) \\
&= \delta_{mn}
\end{aligned}
$$

by using Parseval's relation. The orthogonality of translated wavelets at the same scale is shown using a similar derivation.

A drawback of the Shannon wavelets is their infinite support and the

poor time resolution due to the slow decay. On the other hand, the frequency resolution is perfect. For the Haar wavelets, we observed the opposite behavior. They had perfect time, but unsatisfactory frequency resolution.

8.5.2   Wavelet Analysis by Multirate Filtering

Because of $V_0 = V_1 \oplus W_1$ the functions $\phi_{0n}(t) = \phi(t - n) \in V_0$, $n \in \mathbb{Z}$ can be written as linear combinations of the basis functions for the spaces V_1 and W_1. With the coefficients $h_0(2\ell - n)$ and $h_1(2\ell - n)$, $\ell, n \in \mathbb{Z}$ the approach is

$$\phi_{0n}(t) = \sum_{\ell} h_0(2\ell - n) \ \phi_{1\ell}(t) + h_1(2\ell - n) \ \psi_{1\ell}(t). \tag{8.97}$$

Equation (8.97) is known as the *decomposition relation,* for which the following notation is used as well:

$$\sqrt{2} \ \phi(2t - n) = \sum_{\ell} h_0(2\ell - n) \ \phi(t - \ell) + h_1(2\ell - n) \ \psi(t - \ell). \tag{8.98}$$

We now consider a known sequence $\{c_0(n)\}$, and we substitute (8.97) into (8.85) for $m = 0$. We get

$$\begin{aligned}
x_0(t) \ &= \sum_{n} c_0(n) \ \phi_{0n}(t) \\
&= \sum_{n} c_0(n) \sum_{\ell} h_0(2\ell - n) \ \phi_{1\ell}(t) + h_1(2\ell - n) \ \psi_{1\ell}(t) \\
&= \sum_{\ell} \underbrace{\sum_{n} c_0(n) \ h_0(2\ell - n)}_{c_1(\ell)} \ \phi_{1\ell}(t) + \sum_{\ell} \underbrace{\sum_{n} c_0(n) \ h_1(2\ell - n)}_{d_1(\ell)} \ \psi_{1\ell}(t) \\
&= x_1(t) + y_1(t),
\end{aligned}$$

$$\tag{8.99}$$

where $x_0 \in V_0$, $x_1 \in V_1$, and $y_1 \in W_1$. This method allows us to compute $\{c_{m+1}(\ell)\}$ and $\{d_{m+1}(\ell)\}$ from $\{c_m(n), \ m, n \in \mathbb{Z}\}$:

$$\left. \begin{aligned}
c_{m+1}(\ell) \ &= \sum_{n} c_m(n) \ h_0(2\ell - n) \\
d_{m+1}(\ell) \ &= \sum_{n} c_m(n) \ h_1(2\ell - n)
\end{aligned} \right\}, \qquad i, \ell \in \mathbb{Z}. \tag{8.100}$$

We see that the sequences $\{c_{m+1}(\ell)\}$ and $\{d_{m+1}(\ell)\}$ occur with half the sampling rate of $\{c_m(n)\}$. Altogether, the decomposition (8.100) is equivalent to a two-channel filter bank analysis with the analysis filters $h_0(n)$ and $h_1(n)$.
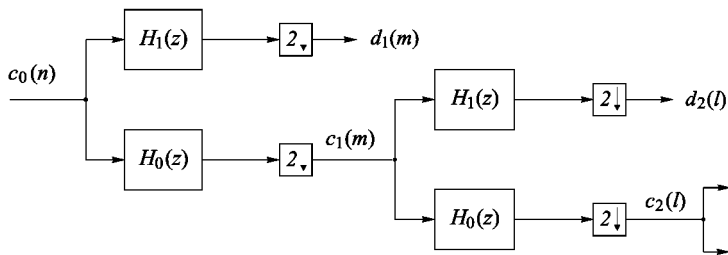
Figure 8.10. Analysis filter bank for computing the DWT.

If we assume that $x_0(t)$ is a sufficiently good approximation of $x(t)$, and if we know the coefficients $c_0(n)$, we are able to compute the coefficients $c_{m+1}(n)$, $d_{m+1}(n)$, $m > 0$, and thus the values of the wavelet transform using the discrete-time filter bank depicted in Figure 8.10. This is the most efficient way of computing the DWT of a signal.

8.5.3 Wavelet Synthesis by Multirate Filtering

Let us consider two sequences $g_0(n)$ and $g_1(n)$, which allow us to express the functions $\phi_{10}(t) = 2^{-1/2}\phi(t/2) \in V_1$ and $\psi_{10}(t) = 2^{-1/2}\psi(t/2) \in W_1$ as linear combinations of $\phi_{0n}(t) = \phi(t - n) \in V_0$, $n \in \mathbb{Z}$ in the form

$$
\begin{aligned}
\phi_{10}(t) &= \sum_n g_0(n)\,\phi_{0n}(t), \\
\psi_{10}(t) &= \sum_n g_1(n)\,\phi_{0n}(t),
\end{aligned}
\tag{8.101}
$$

or equivalently as

$$
\begin{aligned}
\phi(t) &= \sum_n g_0(n)\,\sqrt{2}\,\phi(2t - n), \\
\psi(t) &= \sum_n g_1(n)\,\sqrt{2}\,\phi(2t - n).
\end{aligned}
\tag{8.102}
$$

Equations (8.101) and (8.102), respectively, are referred to as the *two-scale relation*. For time-shifted functions the two-scale relation is

$$
\begin{aligned}
\phi_{1\ell}(t) &= \sum_n g_0(n - 2\ell)\,\phi_{0n}(t), \\
\psi_{1\ell}(t) &= \sum_n g_1(n - 2\ell)\,\phi_{0n}(t).
\end{aligned}
\tag{8.103}
$$
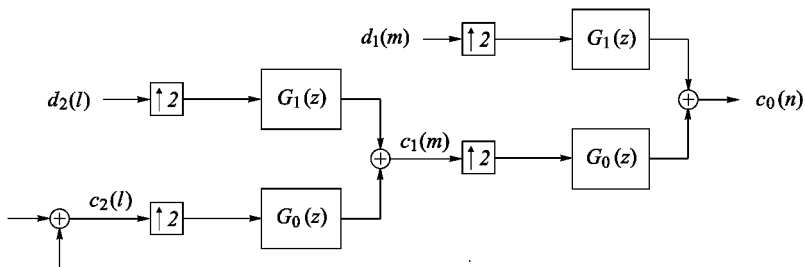
Figure 8.11. Synthesis filter bank.

From (8.103), (8.78), (8.85) and (8.90) we derive

$$
\begin{aligned}
x_0(t) &= x_1(t) + y_1(t) \\
&= \sum_\ell c_1(\ell)\ \phi_{1\ell}(t) + \sum_\ell d_1(\ell)\ \psi_{1\ell}(t) \\
&= \sum_\ell c_1(\ell)\ \sum_n g_0(n - 2\ell)\ \phi_{0n}(t) + \sum_\ell d_1(\ell)\ \sum_n g_1(n - 2\ell)\ \phi_{0n}(t) \\
&= \sum_n \left(\sum_\ell c_1(\ell)\ g_0(n - 2\ell) + d_1(\ell)\ g_1(n - 2\ell) \right)\ \phi_{0n}(t) \\
&= \sum_n c_0(n)\ \phi_{0n}(t).
\end{aligned}
$$

$$(8.104)$$

The generalization of (8.104) yields

$$
c_m(n) = \sum_\ell c_{m+1}(\ell)\ g_0(n - 2\ell) + d_{m+1}(\ell)\ g_1(n - 2\ell). \tag{8.105}
$$

The sequences $g_0(n)$ and $g_1(n)$ may be understood as the impulse responses of discrete-time filters, and (8.105) describes a discrete-time two-channel synthesis filter bank. The filter bank is shown in Figure 8.11.

8.5.4   The Relationship between Filters and Wavelets

Let us consider the decomposition relation (8.97), that is

$$
\phi_{0n}(t) = \sum_\ell h_0(2\ell - n)\ \phi_{1\ell}(t) + h_1(2\ell - n)\ \psi_{1\ell}(t). \tag{8.106}
$$

Taking the inner product of (8.106) with $\tilde{\phi}_{1\ell}(t)$ and $\tilde{\psi}_{1\ell}(t)$ yields

$$\left\langle \phi_{0n}, \tilde{\phi}_{1\ell} \right\rangle = \sum_m h_0(2m - n) \left\langle \phi_{1m}, \tilde{\phi}_{1\ell} \right\rangle + h_1(2m - n) \left\langle \psi_{1m}, \tilde{\phi}_{1\ell} \right\rangle,$$

$$\left\langle \phi_{0n}, \tilde{\psi}_{1\ell} \right\rangle = \sum_m h_0(2m - n) \left\langle \phi_{1m}, \tilde{\psi}_{1\ell} \right\rangle + h_1(2m - n) \left\langle \psi_{1m}, \tilde{\psi}_{1\ell} \right\rangle.$$

$$(8.107)$$

Observing that

$$\begin{aligned}
\left\langle \phi_{1m}, \tilde{\phi}_{1\ell} \right\rangle &= \delta_{\ell m}, \\
\left\langle \psi_{1m}, \tilde{\psi}_{1\ell} \right\rangle &= \delta_{\ell m}, \\
\left\langle \phi_{1m}, \tilde{\psi}_{1\ell} \right\rangle &= 0, \\
\left\langle \psi_{1m}, \tilde{\phi}_{1\ell} \right\rangle &= 0,
\end{aligned}$$

$$(8.108)$$

we obtain

$$\begin{aligned}
h_0(2\ell - n) &= \left\langle \phi_{0n}, \tilde{\phi}_{1\ell} \right\rangle, \\
h_1(2\ell - n) &= \left\langle \phi_{0n}, \tilde{\psi}_{1\ell} \right\rangle.
\end{aligned}$$

$$(8.109)$$

Similarly, the two-scale relation (8.101) yields

$$\begin{aligned}
g_0(n) &= \left\langle \phi_{10}, \tilde{\phi}_{0n} \right\rangle, \\
g_1(n) &= \left\langle \psi_{10}, \tilde{\phi}_{0n} \right\rangle.
\end{aligned}$$

$$(8.110)$$

Substituting (8.101) into (8.108) yields

$$\begin{aligned}
\delta_{\ell 0} &= \sum_n g_0(n) \left\langle \phi_{0n}, \tilde{\phi}_{1\ell} \right\rangle, \\
\delta_{\ell 0} &= \sum_n g_1(n) \left\langle \phi_{0n}, \tilde{\psi}_{1\ell} \right\rangle, \\
0 &= \sum_n g_0(n) \left\langle \phi_{0n}, \tilde{\psi}_{1\ell} \right\rangle, \\
0 &= \sum_n g_1(n) \left\langle \phi_{0n}, \tilde{\phi}_{1\ell} \right\rangle,
\end{aligned}$$

$$(8.111)$$

and by comparing (8.111) with (8.109) we obtain

$$\begin{aligned}
\delta_{\ell 0} &= \sum_n g_0(n) \, h_0(2\ell - n), \\
\delta_{\ell 0} &= \sum_n g_1(n) \, h_1(2\ell - n), \\
0 &= \sum_n g_0(n) \, h_1(2\ell - n), \\
0 &= \sum_n g_1(n) \, h_0(2\ell - n).
\end{aligned}$$

$$(8.112)$$

The conditions (8.112) are nothing but the PR conditions for critically subsampled two-channel filter banks, formulated in the time domain, cf. Section 6.2. By z-transform of (8.112) we obtain

$$
\begin{aligned}
2 &= G_0(z)\,H_0(z) + G_0(-z)\,H_0(-z), \\
2 &= G_1(z)\,H_1(z) + G_1(-z)\,H_1(-z), \\
0 &= G_0(z)\,H_1(z) + G_0(-z)\,H_1(-z), \\
0 &= G_1(z)\,H_0(z) + G_1(-z)\,H_0(-z).
\end{aligned}
\tag{8.113}
$$

Orthonormal Wavelets. If the sets $\phi_{mn}(t)$ and $\psi_{mn}(t)$, $m,n \in \mathbb{Z}$ according to (8.51) and (8.89) are orthonormal bases for V_m and W_m, $m \in \mathbb{Z}$, (8.109) becomes

$$
\begin{aligned}
h_0(2\ell - n) &= \langle \phi_{0n}, \phi_{1\ell} \rangle, \\
h_1(2\ell - n) &= \langle \phi_{0n}, \psi_{1\ell} \rangle.
\end{aligned}
\tag{8.114}
$$

Substituting the two-scale relation (8.103) into (8.114) yields

$$
\begin{aligned}
h_0(2\ell - n) &= \sum_k g_0^*(k - 2\ell)\,\langle \phi_{0n}, \phi_{0k} \rangle, \\
h_1(2\ell - n) &= \sum_k g_1^*(k - 2\ell)\,\langle \phi_{0n}, \phi_{0k} \rangle.
\end{aligned}
\tag{8.115}
$$

Observing $\langle \phi_{0n}, \phi_{0k} \rangle = \delta_{nk}$, we derive

$$
\begin{aligned}
h_0(n) &= g_0^*(-n) \quad \longleftrightarrow \quad H_0(z) = \tilde{G}_0(z), \\
h_1(n) &= g_1^*(-n) \quad \longleftrightarrow \quad H_1(z) = \tilde{G}_1(z).
\end{aligned}
\tag{8.116}
$$

Thus equations (8.112) and (8.113) become

$$
\begin{aligned}
\delta_{\ell 0} &= \sum_n g_0(n)\,g_0^*(n - 2\ell), \\
\delta_{\ell 0} &= \sum_n g_1(n)\,g_1^*(n - 2\ell), \\
0 &= \sum_n g_0(n)\,g_1^*(n - 2\ell), \\
0 &= \sum_n g_1(n)\,g_0^*(n - 2\ell)
\end{aligned}
\tag{8.117}
$$

and

$$
\begin{aligned}
2 &= G_0(z)\,\tilde{G}_0(z) + G_0(-z)\,\tilde{G}_0(-z), \\
2 &= G_1(z)\,\tilde{G}_1(z) + G_1(-z)\,\tilde{G}_1(-z), \\
0 &= G_0(z)\,\tilde{G}_1(z) + G_0(-z)\,\tilde{G}_1(-z), \\
0 &= G_1(z)\,\tilde{G}_0(z) + G_1(-z)\,\tilde{G}_0(-z).
\end{aligned}
\tag{8.118}
$$

These are nothing but the requirements for paraunitary two-channel filter banks, as derived in Chapter 6.

8.6 Wavelets from Filter Banks

8.6.1 General Procedure

In the previous sections we assumed that the wavelets and scaling functions are given. Due to the properties of the wavelet transform we were able to show the existence of sequences $h_0(n), h_1(n), g_0(n)$, and $g_1(n)$, which allow us to realize the transform via a multirate filter bank. When constructing wavelets and scaling functions one often adopts the reverse strategy. One chooses the coefficients of a PR two-channel filter bank in such a way that the wavelets and scaling functions associated with these filters have the desired properties.

Scaling Function. The starting point for constructing scaling functions is the first part of the two-scale relation (8.102):

$$\phi(t) = \sum_n g_0(n) \sqrt{2} \, \phi(2t - n). \tag{8.119}$$

In the following the Fourier transform of equation (8.119) is required, which, using

$$\phi(2t - n) \longleftrightarrow \frac{1}{2} \, \Phi(\frac{\omega}{2}) \, e^{-\frac{j\omega n}{2}}, \tag{8.120}$$

is

$$\Phi(\omega) = \Phi(\frac{\omega}{2}) \frac{1}{\sqrt{2}} \sum_n g_0(n) \, e^{-\frac{j\omega n}{2}}. \tag{8.121}$$

With

$$G_0(e^{j\frac{\omega}{2}}) = \sum_n g_0(n) \, e^{-\frac{j\omega n}{2}} \tag{8.122}$$

equation (8.121) is

$$\Phi(\omega) = \frac{1}{\sqrt{2}} \, G_0(e^{j\frac{\omega}{2}}) \, \Phi(\frac{\omega}{2}). \tag{8.123}$$

Since the scaling function $\phi(t)$ is supposed to be a lowpass impulse response, we may introduce the normalization

$$\Phi(0) = \int_{-\infty}^{\infty} \phi(t) \, dt = 1. \tag{8.124}$$

If we now apply (8.119) and (8.123) K times, we obtain

$$\Phi(\omega) = \left(\prod_{k=1}^{K} \frac{1}{\sqrt{2}} \, G_0(e^{j\omega/2^k}) \right) \Phi(\frac{\omega}{2^K}). \tag{8.125}$$

Now we let $K \to \infty$. If the product in (8.125) converges for $K \to \infty$ to a continuous function, it converges to

$$\Phi(\omega) = \prod_{k=1}^{\infty} \frac{1}{\sqrt{2}} G_0(e^{j\omega/2^k}), \tag{8.126}$$

because we have specified $\Phi(0) = 1$. Thus (8.119) allows us to determine the scaling function recursively. When starting with

$$x_0(t) = \begin{cases} 1 & \text{for } 0 \leq t < 1, \\ 0 & \text{otherwise}, \end{cases} \tag{8.127}$$

we obtain the piecewise constant functions $x_i(t)$ by means of the recursion

$$x_{i+1}(t) = \sqrt{2} \sum_n g_0(n) \, x_i(2t - n), \tag{8.128}$$

which approaches the scaling function for $i \to \infty$.

Figure 8.12 illustrates the recursive calculation of the scaling function $\phi(t)$. However, the convergence of the product does not guarantee that the obtained scaling function is smooth. Figures 8.13 and 8.14 show examples leading to smooth and fractal scaling functions, respectively.

Wavelet. If the scaling function $\phi(t)$ is known, $\psi(t)$ can be calculated by using the second part of the two-scale relation (8.102):

$$\psi(t) = \sum_n g_1(n) \, \sqrt{2} \, \phi(2t - n). \tag{8.129}$$

It is obvious that a smooth $\phi(t)$ results in a smooth $\psi(t)$, regardless of the coefficients $g_1(n)$, so that all concerns regarding smoothness are related to the lowpass $g_0(n)$.

Summary of Construction Formulae. According to (8.126), the synthesis scaling function is related to the synthesis lowpass as

$$\Phi(\omega) = \prod_{k=1}^{\infty} \frac{1}{\sqrt{2}} G_0(e^{j\omega/2^k}). \tag{8.130}$$

For the synthesis wavelet we get from (8.129) and (8.130)

$$\Psi(\omega) = \frac{1}{\sqrt{2}} G_1(e^{j\omega/2}) \prod_{k=2}^{\infty} \frac{1}{\sqrt{2}} G_0(e^{j\omega/2^k}). \tag{8.131}$$
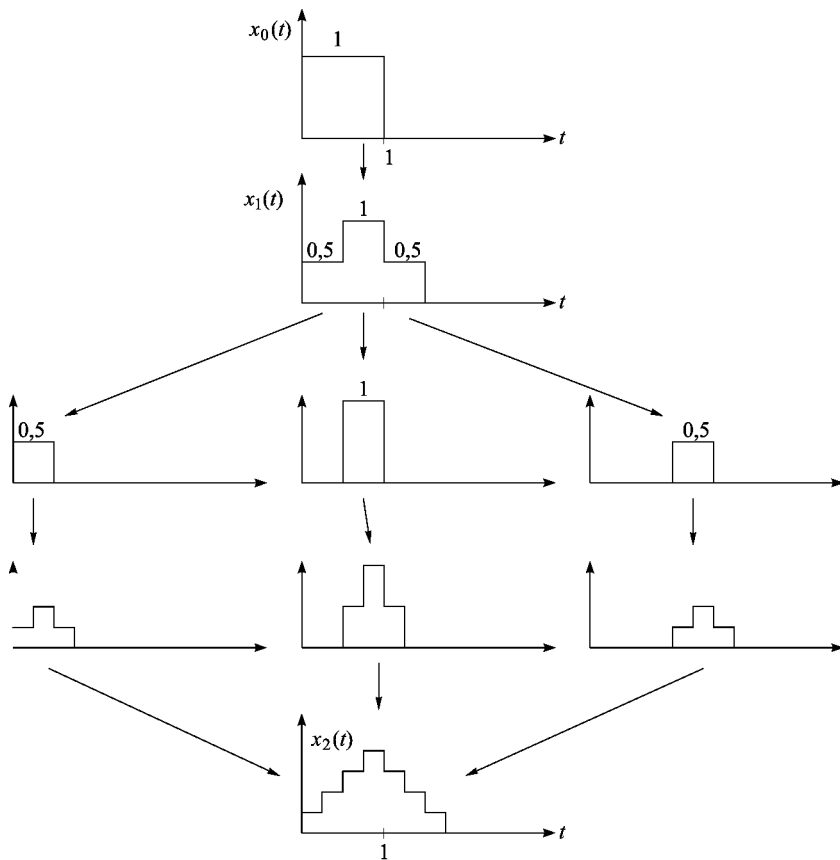
Figure 8.12. Recursive calculation of the scaling function $\phi(t)$; the first two steps of the recursion are shown (coefficients: $\{g_0(n)\} = \frac{\sqrt{2}}{2}\{\frac{1}{2}, 1, \frac{1}{2}\}$).

The analysis scaling function $\tilde{\phi}(t)$ and the wavelet $\tilde{\psi}(t)$ are related to the time-reversed and complex conjugated analysis filters $h_0^*(-n)$ and $h_1^*(-n)$ in the same way as $\phi(t)$ and $\psi(t)$ are related to $g_0(n)$ and $g_1(n)$. Thus, they may be given in the frequency domain as

$$\tilde{\Phi}(\omega) = \prod_{k=1}^{\infty} \frac{1}{\sqrt{2}} \, H_0(e^{-j\omega/2^k}) \tag{8.132}$$

and

$$\tilde{\Psi}(\omega) = \frac{1}{\sqrt{2}} \, H_1(e^{-j\omega/2}) \prod_{k=2}^{\infty} \frac{1}{\sqrt{2}} \, H_0(e^{-j\omega/2^k}). \tag{8.133}$$
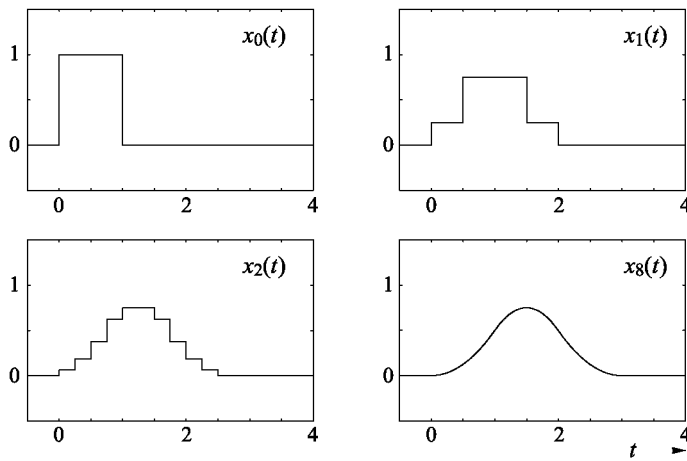
Figure 8.13. Recursive calculation of the scaling function $\phi(t)$ (coefficients $\{g_0(n)\} = \frac{\sqrt{2}}{8}\{1\ 3\ 3\ 1\}$).
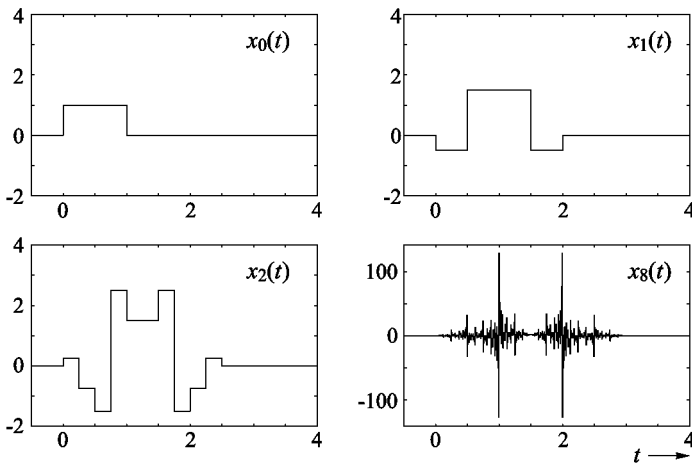
Figure 8.14. Recursive calculation of the scaling function $\phi(t)$ (coefficients $\{g_0(n)\} = \frac{\sqrt{2}}{4}\{-1\ 3\ 3\ -1\}$).

Non-Linear Phase Property of Orthonormal Wavelets. In Chapter 6 we have shown that paraunitary two-channel filter banks have non-linear phase filters in general. This property is transferred directly to the scaling functions and wavelets constructed with these filters. Thus, orthonormal wavelets have non-linear phase in general. Exceptions are the Haar and Shannon wavelets.

8.6.2 Requirements to be Met by the Coefficients

We have already shown that to construct biorthogonal and orthonormal scaling functions and wavelets the coefficients of PR two-channel filter banks are required. But, in order to satisfy (8.124), the coefficients must be scaled appropriately. The correct scaling for the lowpass can be found by integrating (8.119):

$$\int_{-\infty}^{\infty} \phi(t) \ dt \ = \ \frac{1}{\sqrt{2}} \sum_n g_0(n) \int_{-\infty}^{\infty} \phi(2t - n) \ d(2t). \tag{8.134}$$

This yields

$$\sum_n g_0(n) = \sqrt{2}. \tag{8.135}$$

By integrating equation (8.129) we obtain

$$\int_{-\infty}^{\infty} \psi(t) \ dt = \frac{1}{\sqrt{2}} \sum_n g_1(n) \int_{-\infty}^{\infty} \phi(2t - n) \ d(2t), \tag{8.136}$$

and with (8.124) and $\int \psi(t) \ dt = 0$ we conclude

$$\sum_n g_1(n) = 0. \tag{8.137}$$

This means that the highpass filters in the two-channel filter bank must have zero mean in order to allow the construction of wavelets.

8.6.3 Partition of Unity

In order to enforce a lowpass characteristic of $G_0(z)$, it is useful to require

$$G_0(-1) = 0 \quad \longleftrightarrow \quad \sum_n (-1)^n g_0(n) = 0. \tag{8.138}$$

As will be shown in the following, (8.135), (8.135), and (8.138) result in

$$\Phi(2\pi k) = \begin{cases} 1 & k = 0 \\ 0 & k \neq 0. \end{cases} \tag{8.139}$$

In the time domain, this property of the scaling function, which is known as the partition of unity, is written

$$\sum_{n=-\infty}^{\infty} \phi(t - n) = 1. \tag{8.140}$$

Proof of (8.139). We consider (8.123) for $\omega = 2\pi k$, observing (8.135) and (8.138):

$$\Phi(2\pi k) \quad = \quad \tfrac{1}{\sqrt{2}} G_0(e^{j\pi k}) \Phi(\pi k)$$

$$= \quad \tfrac{1}{\sqrt{2}} G_0((-1)^k) \Phi(\pi k) \qquad (8.141)$$

$$= \quad \begin{cases} \Phi(\pi k) & k \text{ even}, \\ 0 & k \text{ odd}. \end{cases}$$

For $k = 0, 1, 2, 3, 4, \ldots$ we obtain

$$\begin{array}{llll}
k = 0: & \Phi(0) & = \Phi(0) & = 1, \\
k = 1: & \Phi(2\pi) & = 0 \cdot \Phi(\pi) & = 0, \\
k = 2: & \Phi(4\pi) & = 1 \cdot \Phi(2\pi) & = 0, \\
k = 3: & \Phi(6\pi) & = 0 \cdot \Phi(3\pi) & = 0, \\
k = 4: & \Phi(8\pi) & = 1 \cdot \Phi(4\pi) & = 0, \\
\vdots & & & \vdots
\end{array} \qquad (8.142)$$

We may proceed in a similar way for the negative indices, and it turns out that (8.139) holds. $\square$

8.6.4   The Norm of Constructed Scaling Functions and Wavelets

When the coefficients $g_0(n)$ belong to a paraunitary filter bank, (8.124) directly leads to

$$\|\phi\| = 1. \qquad (8.143)$$

We realize this by forming the inner product of (8.140) with $\phi_{00}(t)$ and by making use of orthogonality:

$$\underbrace{\left\langle \phi_{00}, \textstyle\sum_{n=-\infty}^{\infty} \phi_{0n} \right\rangle}_{\langle \phi_{00}, \phi_{00} \rangle} = \underbrace{\langle \phi_{00}, \mathbf{1} \rangle}_{\Phi(0)=1} . \qquad (8.144)$$

Forming the inner product $\langle \psi_{00}, \psi_{00} \rangle$ by using (8.101) yields

$$\begin{aligned}
\langle \psi_{00}, \psi_{00} \rangle &= \left\langle \textstyle\sum_k g_1(k)\, \phi_{1k} \, , \, \sum_n g_1(n)\, \phi_{1n} \right\rangle \\
&= \textstyle\sum_k \sum_n g_1(k)\, g_1^*(n) \underbrace{\langle \phi_{1k}, \phi_{1n} \rangle}_{\delta_{nk}} = \|g_1\|^2 = 1, \qquad (8.145)
\end{aligned}$$

which shows that

$$\|\psi\| = 1 \tag{8.146}$$

for the norm of the wavelet $\psi(t)$. Assuming $\Phi(0) = \alpha$ leads to $\|\phi\| = \|\psi\| = \alpha$.

In the biorthogonal case the relationship between the norm of the coefficients and the norm of the scaling function is much more complicated.

8.6.5 Moments

Multiresolution signal decompositions are often carried out in order to compress signals, so that the compaction properties of such decompositions are of crucial importance. Most signals to be compressed are of a lowpass nature and can be well approximated locally by low-order polynomials. Therefore, it is useful to seek wavelets with good approximation properties for low-order polynomials. As we shall see, the approximation properties of a multiresolution decomposition are intimately related to the number of vanishing wavelet moments.

The kth moment of a wavelet $\psi(t)$ is given by

$$m_k = \int_{-\infty}^{\infty} t^k \, \psi(t) \; dt. \tag{8.147}$$

Using the property (2.40) of the Fourier transform, the moments can also be expressed as

$$m_k = (-j)^{-k} \frac{d^k \, \Psi(\omega)}{d\omega^k} \bigg|_{\omega = 0} \tag{8.148}$$

Thus, if $\Psi(\omega)$ has N_ψ zeros at $\omega = 0$, the wavelet has N_ψ vanishing moments, that is

$$\int_{-\infty}^{\infty} t^k \, \psi(t) \; dt = 0 \quad \text{for} \quad k = 0, 1, \ldots, N_\psi - 1. \tag{8.149}$$

Clearly, the inner product of an analysis wavelet $\tilde{\psi}(t)$ having $N_{\tilde{\psi}}$ vanishing moments with a signal

$$x(t) = \sum_{k=0}^{N_{\tilde{\psi}}-1} a_k \, t^k$$

is zero, and, consequently, all wavelet coefficients are zero. Thus, polynomial signals of order $N_{\tilde{\psi}} - 1$ are solely represented by the lowpass component, that is, by the coefficients of the scaling function.

The number of vanishing moments is easily controlled when constructing wavelets from filter banks. In order to see this, let us recall equation (8.133):

$$\tilde{\Psi}(\omega) = \frac{1}{\sqrt{2}} \, H_1(e^{-j\omega/2}) \prod_{k=2}^{\infty} \frac{1}{\sqrt{2}} \, H_0(e^{-j\omega/2^k}). \tag{8.150}$$

$N_{\tilde{\psi}}$ is given by the number of zeros of $H_1(e^{j\omega})$ at $\omega = 0$, or, equivalently, by the number of zeros of $H_1(z)$ at $z = 1$. Note that according to (6.22), $H_1(z)$ is a modulated version of the synthesis lowpass $G_0(z)$, so that we may alternatively say that $N_{\tilde{\psi}}$ is given by the number of zeros of $G_0(z)$ at $z = -1$. Similarly, the number of vanishing moments of the synthesis wavelet is equal to the number of zeros of the analysis lowpass at $z = -1$.

The discrete-time filters also have vanishing moments and corresponding approximation properties for discrete-time polynomial signals. For the kth derivative of

$$H_1(e^{j\omega}) = \sum_n h_1(n) \, e^{-j\omega n} \tag{8.151}$$

we get

$$\frac{d^k \, H_1(e^{j\omega})}{d\omega^k} = \sum_n (-jn)^k \, h_1(n) \, e^{-j\omega n}. \tag{8.152}$$

From this expression we see that if $H_1(z)$ has $N_{\tilde{\psi}}$ zeros at $z = 1$, then $h_1(n)$ has $N_{\tilde{\psi}}$ vanishing moments in the discrete-time sense:

$$\sum_n n^k \, h_1(n) = 0 \quad \text{for} \quad k = 0, 1, \dots, N_\psi - 1. \tag{8.153}$$

This means that sampled polynomial signals of order $N_{\tilde{\psi}} - 1$ are solely represented by the lowpass component.

8.6.6   Regularity

In Figures 8.13 and 8.14 we saw that different filters may have completely different convergence properties. Typically, one prefers smooth functions $\phi(t)$, which should possibly have several continuous derivatives. Daubechies derived a test that can check the regularity and thus the convergence of the product in (8.125) [34]. Assuming that $G_0(z)$ has N zeros at $z = -1$, $G_0(z)$ can be written as

$$G_0(z) = \sqrt{2} \, \left(\frac{1 + z^{-1}}{2} \right)^N S(z). \tag{8.154}$$

Note that $N \geq 1$ because of (8.137). Further note that $S(1) = 1$ because of (8.135). Pointwise convergence of the functions $x_i(t)$ defined in (8.128)

towards a continuous function $x_\infty(t) = \phi(t)$ is guaranteed if

$$\sup_{0 \le \omega \le 2\pi} |S(e^{j\omega})| < 2^{N-1}. \tag{8.155}$$

Clearly, if $G_0(z)$ has no zero at $z = -1$, then (8.155) cannot be satisfied because $S(1) = 1$.

If N is larger than the minimum number that is required to satisfy (8.155), then the function $\phi(t)$ will also have continuous derivatives. Precisely, $\phi(t)$ is m-times continuously differentiable if

$$\sup_{0 \le \omega \le 2\pi} |S(e^{j\omega})| < 2^{N-m-1}. \tag{8.156}$$

Regularity is only associated with the lowpass filters $g_0(n)$ and $h_0(n)$, respectively. Given a continuous function $\phi(t)$, the function $\psi(t)$ according to (8.129) will be continuous for any sequence $g_1(n)$.

Hölder Regularity. Rioul introduced the concept of Hölder regularity, which can be expressed as follows: if a scaling function is m-times continuously differentiable and its mth derivative $\psi^{(m)}(t)$ is Hölder continuous of order α, then its regularity is $r = m + \alpha$ [125]. The Hölder exponent α is the maximum α for which

$$|\psi^{(m)}(t) - \psi^{(m)}(t+\tau)| \le C\,|\tau|^\alpha \quad \forall\, t, \tau \tag{8.157}$$

8.6.7 Wavelets with Finite Support

If $g_0(n)$ and $g_1(n)$ are FIR filters, then the resulting scaling functions and wavelets have finite support [34]. The proof is straightforward. One merely has to consider the iteration (8.128) with the L coefficients $g_0(0), \dots, g_0(L-1)$ while assuming that $x_i(t)$ is restricted to the interval $[0, L-1]$:

$$x_{i+1}(t) = \sqrt{2} \sum_{n=0}^{L-1} g_0(n)\, x_i(2t-n). \tag{8.158}$$

Then, all recursively constructed functions are restricted to $0 \le 2t-n \le L-1$. Since the convergence is unique, $x_\infty(t) = \phi(t)$ is restricted to $[0, L-1]$ for any arbitrary $x_0(t)$.

The fact that the support is known can be exploited to calculate the values of $\phi(t)$ at the times $t_{nm} = n2^m$. This, again, is based on the two-scale relation (8.119):

$$\phi(t) = \sqrt{2} \sum_\ell g_0(\ell)\, \phi(2t-\ell). \tag{8.159}$$

Let us assume that the initial values $\phi(n)$ are known. By writing (8.159) as

$$\phi(\tfrac{k}{2}) = \sqrt{2} \sum_\ell g_0(\ell)\, \phi(k - \ell),$$

$$\phi(\tfrac{k}{4}) = \sqrt{2} \sum_\ell g_0(\ell)\, \phi(\tfrac{k}{2} - \ell), \qquad (8.160)$$

$$\vdots$$

we realize that we obtain the intermediate values at each iteration step. However, so far we only know the values $\phi(0) = 0$ and $\phi(L) = 0$. The initial values required can be determined by exploiting the fact that the initial values remain unchanged during the iteration (8.160). With

$$\boldsymbol{m} = [\phi(1), \ldots, \phi(L - 1)]^T \qquad (8.161)$$

we get

$$\boldsymbol{m} = \boldsymbol{M} \cdot \boldsymbol{m} \qquad (8.162)$$

according to (8.160), where the $L - 1 \times L - 1$ matrix $\boldsymbol{M}$ is given by

$$[\boldsymbol{M}]_{ij} := \sqrt{2}\, g_0(2i - j). \qquad (8.163)$$

Recalling (8.140) it becomes obvious that we obtain the initial values by determining the right eigenvector $\boldsymbol{m}$ of $\boldsymbol{M}$ which belongs to the eigenvalue 1.

Note. We conclude from (8.135) and (8.138) that the sum of the even coefficients equals the sum of the odd coefficients:

$$\sum_n g_0(2n) = \sum_n g_0(2n + 1) = \frac{\sqrt{2}}{2}. \qquad (8.164)$$

Since the columns of $\boldsymbol{M}$ contain either all even coefficients $g_0(2n)$ or all odd coefficients $g_0(2n + 1)$, the sum of all elements of the columns of $\boldsymbol{M}$ is one. Thus, conditions (8.135) and (8.138) guarantee the existence of a left eigenvector $[1, 1, \ldots, 1]$ with eigenvalue one.

Example. Let $g_0(n)$ consist of five coefficients $g_0(0), \ldots, g_0(4)$, and let $G_0(z)$ satisfy $G_0(-1) = 0$. Matrix $\boldsymbol{M}$ is given by

$$\boldsymbol{M} = \sqrt{2} \begin{bmatrix} g_0(1) & g_0(0) & \\ g_0(3) & g_0(2) & g_0(1) \\ & g_0(4) & g_0(3) \end{bmatrix}. \qquad (8.165)$$

Because of (8.164) we have

$$\sqrt{2}\, [1, 1, 1] \begin{bmatrix} g_0(1) & g_0(0) & \\ g_0(3) & g_0(2) & g_0(1) \\ & g_0(4) & g_0(3) \end{bmatrix} = 1 \cdot [1, 1, 1], \qquad (8.166)$$

and we see that the eigenvalue 1 exists. The eigenvalue problem we have to solve is given by

$$\sqrt{2} \begin{bmatrix} g_0(1) & g_0(0) & \\ g_0(3) & g_0(2) & g_0(1) \\ & g_0(4) & g_0(3) \end{bmatrix} \cdot \begin{bmatrix} \phi(1) \\ \phi(2) \\ \phi(3) \end{bmatrix} = 1 \cdot \begin{bmatrix} \phi(1) \\ \phi(2) \\ \phi(3) \end{bmatrix}. \tag{8.167}$$

8.7 Wavelet Families

Various wavelet families are defined in the literature. We will only consider a few of those constructed from filter banks. For further design methods the reader is referred to [36, 154].

8.7.1 Design of Biorthogonal Linear-Phase Wavelets

In this section, we consider the design of linear-phase biorthogonal wavelets according to Cohen, Daubechies and Feauveau [28]. We start the discussion with the first equation in (8.113), which is the PR condition for two-channel filter banks without delay. We consider an overall delay of τ, that is

$$H_0(z) \, G_0(z) + H_0(-z) \, G_0(-z) = 2 \, z^{-\tau}. \tag{8.168}$$

On the unit circle, this means

$$H_0(e^{j\omega}) \, G_0(e^{j\omega}) + H_0(e^{j(\omega+\pi)}) \, G_0(e^{j(\omega+\pi)}) = 2 \, e^{-j\omega\tau}. \tag{8.169}$$

In order to yield linear-phase wavelets, both filter $H_0(z)$ and $G_0(z)$ have to be linear-phase. Furthermore, the filters need to satisfy the regularity condition as outlined in Section 8.6.6 in order to allow the construction of continuous scaling functions and wavelets.

When expressing the linear-phase property, two types of symmetry have to be considered, depending on whether the filter length is even or odd. We will outline these properties for the filter $H_0(z)$ and start with odd-length filters. The second filter $G_0(z)$, which completes a perfect reconstruction pair, has the same type of symmetry.

Odd-Length Filters. Odd-length linear-phase filters satisfy

$$H_0(e^{j\omega}) = e^{-j\omega\tau_h} \, H_0'(\cos\omega), \tag{8.170}$$

where the delay τ_h is an integer. Assuming that $H_0'(\cos\omega)$ has ℓ zeros at $\omega = \pi$, we may write

$$H_0'(e^{j\omega}) = \sqrt{2} \, (\cos\frac{\omega}{2})^{2\ell} \, P(\cos\omega). \tag{8.171}$$

It is easily shown that $G_0(e^{j\omega})$ has the same type of factorization, so that

$$G_0(e^{j\omega}) = e^{-j\omega\tau_g} \sqrt{2} \, (\cos\frac{\omega}{2})^{2\tilde{\ell}} \, Q(\cos\omega), \qquad (8.172)$$

where $\tau = \tau_h + \tau_g$.

Even-Length Filters. Symmetric even-length filters can be expressed as

$$H_0(e^{j\omega}) = e^{-j\omega(\tau_h + \frac{1}{2})} \, \cos\frac{\omega}{2} \, H_0'(\cos\omega), \qquad (8.173)$$

and according to the above considerations, we may write

$$H_0(e^{j\omega}) = \sqrt{2} \, e^{-j\omega(\tau_h + \frac{1}{2})} \, (\cos\frac{\omega}{2})^{2\ell+1} \, P(\cos\omega), \qquad (8.174)$$

where it is again assumed that $H_0(e^{j\omega})$ has ℓ zeros at $\omega = \pi$. $G_0(e^{j\omega})$ then has a factorization of the form

$$G_0(e^{j\omega}) = \sqrt{2} \, e^{-j\omega(\tau_g + \frac{1}{2})} \, (\cos\frac{\omega}{2})^{2\tilde{\ell}+1} \, Q(\cos\omega). \qquad (8.175)$$

Filter Construction.   Substituting the factorizations for $H_0(e^{j\omega})$ and $G_0(e^{j\omega})$ into (8.169) yields

$$(\cos\frac{\omega}{2})^{2k} \, M(\cos\omega) + (\sin\frac{\omega}{2})^{2k} \, M(-\cos\omega) = 1 \qquad (8.176)$$

with

$$M(\cos\omega) = P(\cos\omega) \, Q(\cos\omega) \qquad (8.177)$$

and $k = \ell + \tilde{\ell}$ if the filter length is odd and $k = \ell + \tilde{\ell} + 1$ if it is even. This expression will now be reformulated by rewriting $M(\cos\omega)$ as a polynomial in $(1 - \cos\omega)/2 = \sin^2\omega/2$, so that $M(\cos\omega) := F(\sin^2\omega/2)$. We get

$$(\cos\frac{\omega}{2})^{2k} \, F(\sin^2\omega/2) + (\sin\frac{\omega}{2})^{2k} \, F(\cos^2\omega/2) = 1, \qquad (8.178)$$

or equivalently,

$$(1 - x)^k \, F(x) + x^k \, F(1 - x) = 1 \qquad (8.179)$$

with $x = \sin^2\omega/2$. Hence,

$$F(x) = (1 - x)^{-k} - x^k \, (1 - x)^{-k} \, F(1 - x). \qquad (8.180)$$

Using Bezout's theorem, one can show that this condition is satisfied by a unique polynomial $F(x)$ with a degree of at most $k - 1$ [28]. Based on this property, the polynomial $F(x)$ of maximum degree $k - 1$ can be found by

expanding the right-hand side of (8.180) into a Taylor series where only the first k terms are needed. This gives

$$F(x) = \sum_{n=0}^{k-1} \binom{k+n-1}{n} x^n. \tag{8.181}$$

The general solution of higher degree can be written as

$$F(x) = \sum_{n=0}^{k-1} \binom{k+n-1}{n} x^n + x^k R(1-2x), \tag{8.182}$$

where $R(x)$ is an odd polynomial. Based on this expression, filters can be found by factorizing a given $F(\sin^2\omega/2)$ into $P(\cos\omega)$ and $Q(\cos\omega)$. Given $P(\cos\omega)$ and $Q(\cos\omega)$ one easily finds $H_0(e^{j\omega})$ and $G_0(e^{j\omega})$ from (8.170) – (8.175).

Spline Wavelets. Spline wavelets based on odd-length filters are constructed by choosing $R(x) \equiv 0$ and

$$G_0(e^{j\omega}) = \sqrt{2}\, e^{-j\omega\tau_g} \left(\cos\frac{\omega}{2}\right)^{2\tilde{\ell}}. \tag{8.183}$$

The corresponding analysis filter is

$$H_0(e^{j\omega}) = \sqrt{2}\, e^{-j\omega\tau_h} \left(\cos\frac{\omega}{2}\right)^{2\ell} \sum_{n=0}^{\ell+\tilde{\ell}-1} \binom{\ell+\tilde{\ell}+n-1}{n} \left(\sin^2\frac{\omega}{2}\right)^n. \tag{8.184}$$

Even-length filters are given by

$$G_0(e^{j\omega}) = \sqrt{2}\, e^{-j\omega(\tau_g + \frac{1}{2})} \left(\cos\frac{\omega}{2}\right)^{2\tilde{\ell}+1} \tag{8.185}$$

and

$$H_0(e^{j\omega}) = \sqrt{2}\, e^{-j\omega(\tau_h + \frac{1}{2})} \left(\cos\frac{\omega}{2}\right)^{2\ell+1} \sum_{n=0}^{\ell+\tilde{\ell}} \binom{\ell+\tilde{\ell}+n}{n} \left(\sin^2\frac{\omega}{2}\right)^n. \tag{8.186}$$

The scaling function $\phi(t)$ constructed from $G_0(z)$ according to (8.183) is a B-spline centered around τ_g, and the one constructed from $G_0(z)$ according to (8.185) is a B-spline centered around $\tau_g + \frac{1}{2}$.

Filters with Almost Equal Length. In the spline case, the length of $H_0(z)$ is typically much higher than the length of $G_0(z)$. In order to design filters with almost equal length, one groups the zeros of $F(x)$ into real zeros and pairs of conjugate complex zeros and rewrites $F(x)$ as

$$F(x) = A \prod_{i=1}^{I} (x - x_i) \prod_{j=1}^{J} (x^2 - 2\Re\{z_j\} x + |z_j|). \qquad (8.187)$$

Any regrouping into two polynomials yields a PR filter pair. This allows us to choose filters with equal or almost equal length. For example, the 9-7 filters have been found this way [28]; they are known for their excellent coding performance in wavelet-based image compression [155, 134].

Examples. Table 8.1 shows some examples of odd-length filters. While the coefficients of the spline filters (5-3 and 9-3) are dyadic fractions, those of the 9-7 filters constructed from (8.187) are not even rational. This means an implementation advantage for the spline filters in real-time applications. However, the 9-7 filters have superior coding performance. For illustration, Figures 8.15 and 8.16 show the analysis and synthesis scaling functions and wavelets generated from the 9-3 and 9-7 filters in Table 8.1.

Table 8.1.
Linear-phase odd-length biorthogonal wavelet filters.

	5-3		9-3		9-7	
n	$4 \cdot g_0$	$4 \cdot h_0$	$16 \cdot g_0$	$16 \cdot h_0$	g_0	h_0
0	1	-1	1	3	-0.06453888265083	0.03782845543778
1	2	2	2	-6	-0.04068941758680	-0.02384946495431
2	1	6	1	-16	0.41809227351029	-0.11062440401143
3		2		38	0.78848561689252	0.37740285554759
4		-1		90	0.41809227351029	0.85269867833384
5				38	-0.04068941758680	0.37740285554759
6				-16	-0.06453888265083	-0.11062440401143
7				-6		-0.02384946495431
8				3		0.03782845543778
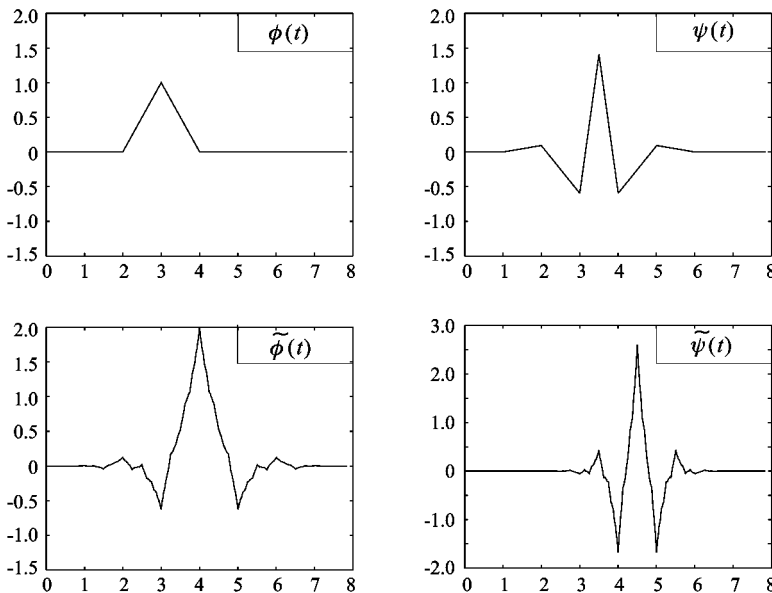
Figure 8.15. Scaling functions and wavelets constructed from the 9-3 filters.
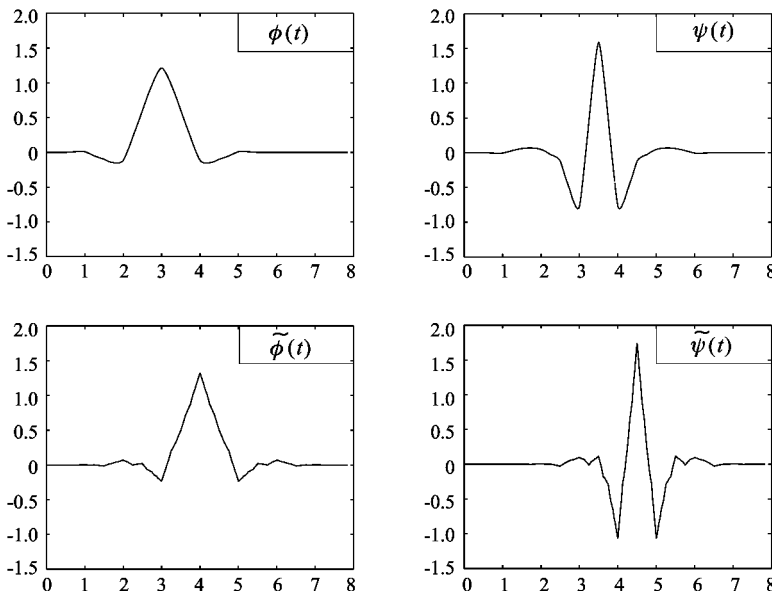
Figure 8.16. Scaling functions and wavelets constructed from the 9-7 filters.

8.7.2   The Orthonormal Daubechies Wavelets

Daubechies designed a family of orthonormal wavelets with a maximal number of vanishing moments for a given support [34]. In order to control the regularity, the following factorization of $H_0(e^{j\omega})$ is considered:

$$H_0(e^{j\omega}) = \sqrt{2} \left(\frac{1 + e^{-j\omega}}{2} \right)^k P(e^{j\omega}). \tag{8.188}$$

Because of orthonormality, the PR condition to be met by the prototype filter is

$$\left| H_0(e^{j\omega}) \right|^2 + \left| H_0(e^{j(\omega + \pi)}) \right|^2 = 2. \tag{8.189}$$

Since $h_0(n)$ is considered to be real, the term $|H_0(e^{j\omega})|^2$ may be written as

$$\left| H_0(e^{j\omega}) \right|^2 = \sqrt{2} \left(\cos^2 \frac{\omega}{2} \right)^k M(\cos \omega) \tag{8.190}$$

with

$$M(\cos \omega) = |P(e^{j\omega})|^2. \tag{8.191}$$

Inserting (8.190) into (8.189) yields

$$(\cos^2 \frac{\omega}{2})^k M(\cos \omega) + (\sin^2 \frac{\omega}{2})^k M(-\cos \omega) = 1. \tag{8.192}$$

Using the same arguments as in the last section, (8.192) can also be written as

$$(\cos^2 \frac{\omega}{2})^k F(\sin^2 \omega/2) + (\sin^2 \frac{\omega}{2})^k F(\cos^2 \omega/2) = 1, \tag{8.193}$$

or equivalently as

$$(1 - x)^k F(x) + x^k F(1 - x) = 1 \tag{8.194}$$

with $x = \sin^2 \omega/2$. This is essentially the same condition that occurred in the biorthogonal case, but we now have to satisfy $F(\sin^2 \omega/2) \geq 0 \ \forall \ \omega$, because $F(\sin^2 \omega/2) = |P(e^{j\omega})|^2$.

Daubechies proposed to choose

$$F(x) = \sum_{n=0}^{k-1} \binom{k + n - 1}{n} x^n + x^k R(1 - 2x), \tag{8.195}$$

where $R(x)$ is an odd polynomial such that $F(x) \geq 0$ for $x \in [0,1]$. The family of Daubechies wavelets is derived for $R(x) \boxminus 0$ by spectral factorization of $F(x)$ into $F(x) = P(x)P(x^{-1})$. For this, the zeros of $F(x)$ have to be computed and grouped into zeros inside and outside the unit circle. $P(x)$ then

contains all zeros inside the unit circle. This factorization results in minimum phase scaling functions. For filters $H_0(z)$ with at least eight coefficients, more symmetric factorizations are also possible. The magnitude frequency responses, however, are the same as for the minimum phase case.

Figure 8.17 shows some Daubechies wavelets, the corresponding scaling functions and the frequency responses of the filters. We observe that the scaling functions and wavelets become smoother with increasing filter length. For comparison, some Daubechies wavelets with maximal symmetry, known as *symmlets*, and the corresponding scaling functions are depicted in Figure 8.18. The frequency responses are the same as in Figure 8.17. Recall that with a few exceptions (Haar and Shannon wavelets), perfect symmetry is impossible.

8.7.3 Coiflets

The orthonormal Daubechies wavelets have a maximum number of vanishing wavelet moments for a given support. Vanishing moments of the scaling function have not been considered. The idea behind the Coiflet wavelets is to trade off some of the vanishing wavelet moments to the scaling function. This can be expressed as

$$\int_{-\infty}^{\infty} t^k \, \phi(t) \, dt = \begin{cases} 1, & \text{for } k = 0 \\ 0, & \text{for } k = 1, 2, \ldots, \ell - 1 \end{cases} \qquad (8.196)$$

and

$$\int_{-\infty}^{\infty} t^k \, \psi(t) \, dt = 0 \quad \text{for} \quad k = 0, 1, \ldots, \ell - 1. \qquad (8.197)$$

Note that the 0th moments of a scaling function is still fixed to one. Further note that the same parameter ℓ, called the order of the coiflet, is used for the wavelet and the scaling function.

The frequency domain formulations of (8.196) and (8.197) are

$$\frac{d^k \omega \, \Phi(\omega)}{d\omega^k} \bigg|_{\omega = 0} = \begin{cases} 1, & \text{for } k = 0 \\ 0, & \text{for } k = 1, 2, \ldots, \ell - 1 \end{cases} \qquad (8.198)$$

and

$$\frac{d^k \omega \, \Psi(\omega)}{d\omega^k} \bigg|_{\omega = 0} = 0 \quad \text{for} \quad k = 0, 1, \ldots, \ell - 1. \qquad (8.199)$$

Condition (8.198) means for the filter $H_0(e^{j\omega})$ that

$$H_0(e^{j\omega}) = 1 + (1 - e^{-j\omega})^{\ell} \, U(e^{j\omega}) \qquad (8.200)$$
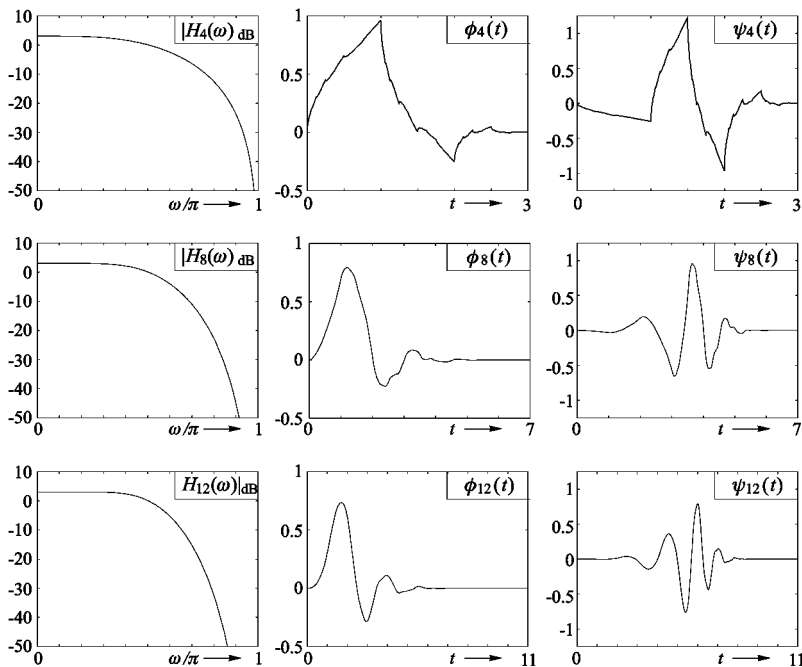
Figure 8.17. Frequency responses of the minimum-phase Daubechies filters and the corresponding scaling functions and wavelets (the indices indicate filter length).
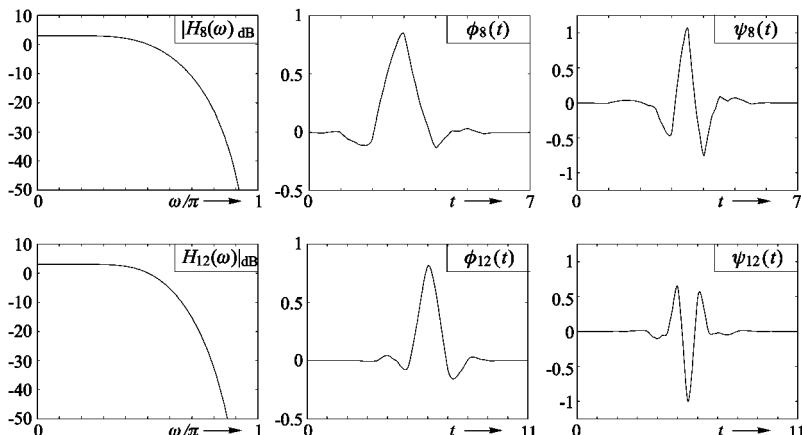
Figure 8.18. Frequency responses of the maximally symmetric Daubechies filters and the corresponding scaling functions and wavelets (the indices indicate filter length; the frequency responses are equal to those in Figure 8.17).

for some $U(e^{j\omega})$. From (8.199) it follows that $H_0(e^{j\omega})$ can also be written in the form (8.188)

$$H_0(e^{j\omega}) = \sqrt{2}\,\left(\frac{1 + e^{-j\omega}}{2}\right)^\ell\,P(e^{j\omega}). \qquad (8.201)$$

For even ℓ, solutions to this problem can be formulated as [36]

$$P(e^{j\omega}) = \sum_{n=0}^{\ell/2-1} \binom{\ell/2 + n - 1}{n}\,\left(\sin^2\frac{\omega}{2}\right)^n + \left(\sin^2\frac{\omega}{2}\right)^{\frac{\ell}{2}}\,f(e^{j\omega}), \quad (8.202)$$

where $f(e^{j\omega})$ has to be found such that (8.189) is satisfied. This results in $\ell/2$ quadratic equations for $\ell/2$ unknowns [36].

8.8 The Wavelet Transform of Discrete-Time Signals

In the previous sections we assumed continuous-time signals and wavelets throughout. It could be shown that sample values of the wavelet transform can be computed by means of a PR filter bank, provided the coefficients $c_0(n)$ for representing an approximation $x_0(t) = \sum_n c_0(n)\tilde{\phi}(t - n)$ are known. For the sequences $d_m(n)$, $m > 0$, successively computed from $c_0(n)$, we had

$$\begin{aligned} d_m(n) &= \mathcal{W}_x\left(2^m n, 2^m\right) = \langle x, \psi_{mn}\rangle \\ &= 2^{-\frac{m}{2}} \int_{-\infty}^{\infty} x(t)\,\psi^*(2^{-m}t - n)\,dt, \end{aligned} \qquad (8.203)$$

that is, the values $d_m(n)$ were sample values of the wavelet transform of a continuous-time signal. A considerable problem is the generation of the discrete-time signal $c_0(n)$ because in digital signal processing the signals to be processed are usually obtained by filtering continuous-time signals with a standard anti-aliasing filter and sampling. Only if the impulse response $h(t)$ of the prefilter is chosen such that $x_0(t) = x(t) * h(t) \in V_0$, we obtain a "genuine" wavelet analysis.

If we wish to apply the theory outlined above to "ordinary" discrete-time signals $x(n)$, it is helpful to discretize the integral in (8.203):

$$w_x(2^m n, 2^m) = 2^{-\frac{m}{2}} \sum_k x(k)\,\psi^*(2^{-m}k - n). \qquad (8.204)$$

Here, the values $\psi(2^{-m}k - n)$, $m > 0$, $k, n \in \mathbb{Z}$ are to be regarded as samples of a given wavelet $\psi(t)$ where the sampling interval is $T = 1$.

Translation Invariance. We are mainly interested in dyadically arranged values according to (8.204). In this form the wavelet analysis is not translation invariant because a delayed input signal $x(n - \ell)$ leads to

$$
\begin{aligned}
w_x\big(2^m(n - 2^{-m}\ell), 2^m\big) &= 2^{-\frac{m}{2}} \sum_k x(k - \ell) \, \psi^*(2^{-m}k - n) \\
&= 2^{-\frac{m}{2}} \sum_i x(i) \, \psi^*(2^{-m}i - [n - 2^{-m}\ell]).
\end{aligned}
$$
$$(8.205)$$

Only if ℓ is a multiple of 2^m, we obtain shifted versions of the same wavelet coefficients. However, for many applications such as pattern recognition or motion estimation in the wavelet domain it is desirable to achieve translation invariance. This problem can be solved by computing all values

$$
w_x(n, 2^m) = 2^{-\frac{m}{2}} \sum_k x(k) \, \psi^*(2^{-m}(k - n)).
\tag{8.206}
$$

In general, this is computationally very expensive, but when using the à trous algorithm outlined in the next section, the computation is as efficient as with the DWT.

8.8.1 The À Trous Algorithm

A direct evaluation of (8.204) and (8.206) is very costly if the values of the wavelet transform must be determined for several octaves because the number of filter coefficients roughly doubles from octave to octave. Here, the so-called *à trous algorithm* allows efficient evaluation with respect to computing effort. This algorithm has been proposed by Holschneider *et al.* [73] and Dutilleux [48]. The relationship between the à trous and the Mallat algorithm was derived by Shensa [132].

We start with dyadic sampling according to (8.204). The impulse response of the filter $H_1(z)$ is chosen to be

$$
h_1(n) = 2^{-\frac{1}{2}} \, \psi^*(-n/2).
\tag{8.207}
$$

With this filter the output values of the first stage of the filter bank in Figure 8.19 are equal to those according to (8.204), we have

$$
w_x(2n, 2) = \tilde{w}_x(2n, 2).
$$

The basic idea of the à trous algorithm is to evaluate equation (8.204) not exactly, but approximately. For this, we use an interpolation filter as
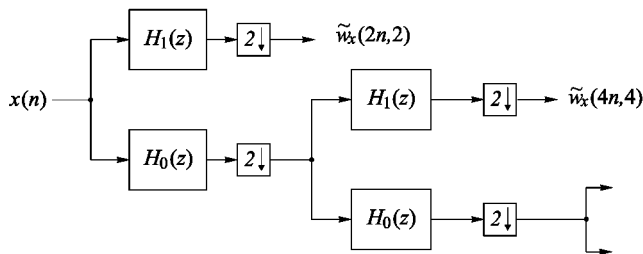
Figure 8.19. Analysis filter bank.
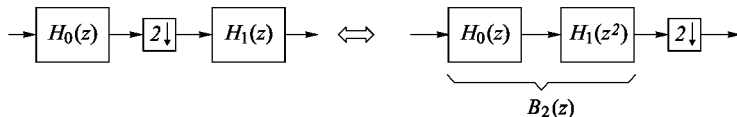
Figure 8.20. Equivalent arrangements.

the analysis lowpass $H_0(z)$.[4] This may for instance be a Lagrange halfband filter, but in principle any interpolation filter will do. In order to explain this approach in more detail let us take a look at the flow graphs shown in Figure 8.20, which both have the transfer function $\frac{1}{2} H_1(z^2) [H_0(z) + H_0(-z)]$. The transfer function $B_2(z)$ is

$$B_2(z) = H_0(z) \, H_1(z^2). \tag{8.208}$$

If $H_0(z)$ is an interpolation filter, (8.208) can be interpreted as follows: first we insert zeros into the impulse response $h_1(n)$. By convolving the upsampled impulse response $h_1'(2n) = h_1(n)$, $h_1'(2n + 1) = 0$ with the interpolation filter the values $h_1'(2n)$ remain unchanged, while the values $h_1'(2n + 1)$ are interpolated. Thus, the even numbered values of the impulse response $b_2(n) \longleftrightarrow B_2(z)$ are equal to the even numbered samples of $2^{-1}\psi^*(-n/4)$. The interpolated intermediate values are approximately the sample values of $2^{-1}\psi^*(-n/4)$ at the odd positions. Thus, we have

$$b_2(n) \approx 2^{-1} \, \psi^*(-n/4). \tag{8.209}$$

Iteration of this approach yields

$$B_m(z) = \begin{cases} H_1(z), & \text{for } m = 1, \\ H_1\left(z^{2^{m-1}}\right) \displaystyle\prod_{j=0}^{m-2} H_0\left(z^{2^j}\right), & \text{for } m > 1. \end{cases} \tag{8.210}$$

---

[4]The term "à trous" means "with gaps", which refers to the fact that an interpolation lowpass filter is used.
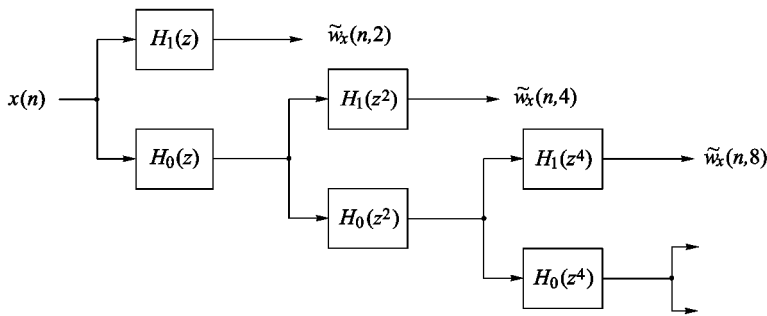
Figure 8.21. Filter bank for computing wavelet coefficients.

For the impulse responses $b_m(n) \longleftrightarrow B_m(z)$ we get

$$b_m(n) \approx 2^{-\frac{m}{2}}\, \psi^*(-2^{-m}n), \qquad m \geq 1. \tag{8.211}$$

The values $\tilde{w}_x(2^m n, 2^m)$ computed with the filter bank in Figure 8.19 are given by

$$\tilde{w}_x(2^m n, 2^m) \approx w_x(2^m n, 2^m). \tag{8.212}$$

Thus, the scheme in Figure 8.19 yields an approximate wavelet analysis.

Oversampled Wavelet Series. Although the coefficients of critically sampled representations contain all information on the analyzed signal, they suffer from the drawback that the analysis is not translation invariant. The aim is now to compute an approximation of

$$w_x(n, 2^m) = 2^{-\frac{m}{2}} \sum_k x(k)\, \psi^*(2^{-m}(k - n)) \tag{8.213}$$

by means of the filters $b_m(n) \longleftrightarrow B_m(z)$ according to (8.210):

$$\tilde{w}_x(n, 2^m) = 2^{-\frac{m}{2}} \sum_k x(k)\, b_m(n - k) \tag{8.214}$$

While the direct evaluation of these formulae means high computational cost, the values $\tilde{w}_x(n, 2^m)$ may be efficiently computed by use of the filter bank in Figure 8.21. The filters $H_0(z^{2^m})$ and $H_1(z^{2^m})$, $m > 1$, can be realized in polyphase structure. The number of operations that have to be carried out is very small so that such an evaluation is suitable for real-time applications also.

In many cases the frequency resolution of a pure octave-band analysis is not sufficient. An improved resolution can be obtained by implementing M

octave filter banks in parallel where each bank covers only an Mth part of the octaves. This concept has been discussed in Section 8.4.2 for the continuous-time case. The application to a discrete-time analysis based on the à trous algorithm is straightforward.

8.8.2   The Relationship between the Mallat and À Trous Algorithms

The discussion above has shown that the only formal difference between the filters used in the Mallat and à trous algorithms lies in the fact that in the Mallat algorithm the impulse response of the filter $H_1(z)$ does not, in general, consist of sample values of the continuous-time wavelet. However, both concepts can easily be reconciled. For this, let us consider a PR two-channel filter bank, where $H_0(z)$ is an interpolation filter and where $H_1(z)$ satisfies $H_1(1) = 0$. Based on the filter bank we can construct the associated continuous-time scaling functions and wavelets. Since $H_0(z)$ is supposed to be an interpolation filter, we have the following correspondence between the impulse response of the highpass filter, $h_1(n)$, and the sample values of the wavelet $\psi(t)$, which is iteratively determined from $h_0(n)$ and $h_1(n)$:

$$h_1(n) = 2^{-\frac{1}{2}} \, \psi^*(-n/2). \tag{8.215}$$

For the filters $B_m(z)$ defined in (8.210) we have

$$b_m(n) = 2^{-\frac{m}{2}} \, \psi^*(-2^{-m}n), \tag{8.216}$$

and we derive

$$\tilde{w}_x(2^m n, 2^m) = w_x(2^m n, 2^m). \tag{8.217}$$

This means that the à trous algorithm computes the wavelet transform exactly if $H_0(z)$ and $H_1(z)$ belong to a PR two-channel filter bank while $H_0(z)$ is an interpolation filter. Then, all computed wavelet coefficients $w_x(2^m n, 2^m)$, $m > 0$, can be interpreted as sample values of a continuous wavelet transform provided the demand for regularity is met: $w_x(2^m n, 2^m) = \mathcal{W}_x(2^m n, 2^m)$, $m > 0$.

In order to determine filters that yield perfect wavelet analyses of discrete-time signals with $\tilde{w}_x(2^m k, 2^m) = w_x(2^m n, 2^m)$ we may proceed as follows: we take an interpolation filter $H_0(z)$ and compute a filter $G_0(z)$ such that

$$\sum_n g_0(n) h_0(2\ell - n) = \delta_{\ell 0}. \tag{8.218}$$

Note that (8.218) is just an underdetermined linear set of equations. From $H_0(z)$ and $G_0(z)$ we can then calculate the filters $H_1(z)$ and $G_1(z)$ according to equation (6.22) and can construct the wavelet via iteration. The solution to (8.218) is not unique, so that one can choose a wavelet which has the desired properties.

Example. For the analysis lowpass we use a binary filter with 31 coefficients as given in (8.181). The length of the analysis highpass is restricted to 63 coefficients. The overall delay of the analysis-synthesis system is chosen such that a linear-phase highpass is yielded. Figures 8.22(a) and 8.22(b) show the respective scaling function, the wavelet, and the sample values $\phi(-n/2) = h_0(n)$ and $\psi(-n/2) = h_1(n)$. The frequency responses of $H_0(z)$ and $H_1(z)$ are pictured in Figure 8.22(c).

8.8.3   The Discrete-Time Morlet Wavelet

The Morlet wavelet was introduced in Section 8.2. In order to realize a wavelet analysis of discrete-time signals, the wavelet is sampled in such a way that

$$h_1(n) = b_1(n) = e^{j\omega_0 n} \; e^{-\beta^2 n^2/2}, \qquad (8.219)$$

where $b_1(n)$ is defined as in (8.210). In order to obtain a "practically" admissible and analytic wavelet we choose

$$2\pi\beta \le \omega_0 \le \pi/2. \qquad (8.220)$$

In the discrete-time case a further problem arises due to the periodicity of the spectra. In order to ensure that we achieve an analytic wavelet we have to demand that

$$\Psi(e^{j\omega}) = 0 \quad \text{for} \quad \pi < \omega \le 2\pi.$$

In order to guarantee this, at least approximately, the parameters ω_0 and β are chosen such that

$$\omega_0 \le \pi - \sqrt{2} \; \beta \qquad (8.221)$$

is also satisfied [132].
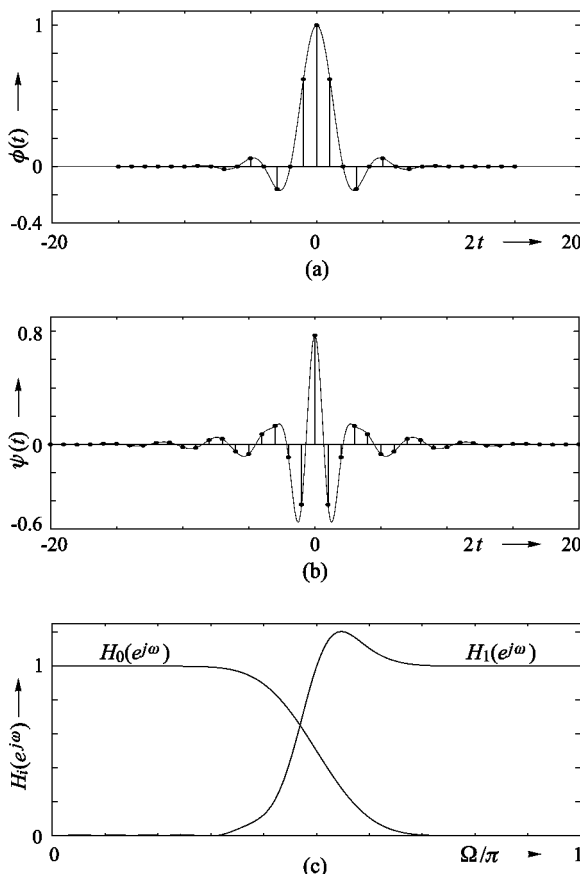
Figure 8.22. Example; (a) scaling function $\phi(t)$ and the sample values $\phi(-nT/2) = h_0(n)$; (b) wavelet $\psi(t)$ and the sample values $\psi(-nT/2) = h_1(n)$; (c) frequency responses of the analysis filters.

8.9 DWT-Based Image Compression

Image compression based on the DWT is essentially equivalent to compression based on octave-band filter banks as outlined in Section 6.8. The strategy is as follows: the image is first decomposed into a set of subband signals by using a separable[5] 2-D filter bank. Then, the subband samples are quantized and further compressed. The filters, however, satisfy certain conditions such as regularity and vanishing moments.

To give an example of the discrete wavelet transform of a 2-D signal,

---

[5]Non-separable 2-D wavelets and filter banks are not considered throughout this book.

(a)   (b)
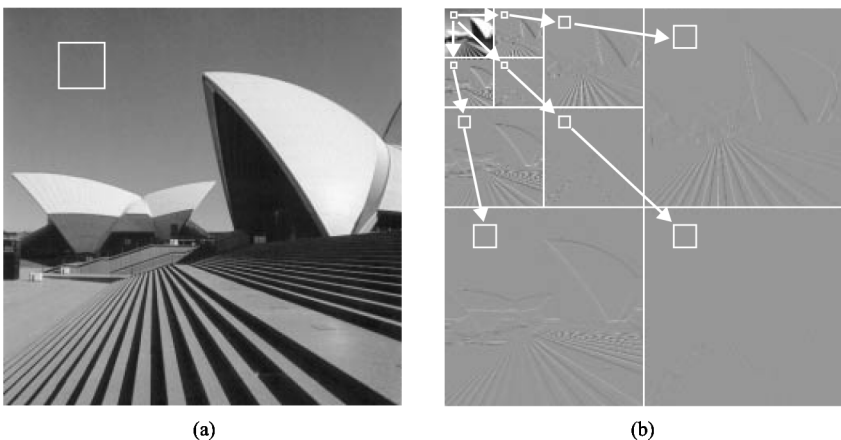
Figure 8.23. Separable 2-D discrete wavelet transform; (a) original; (b) DWT.

Figure 8.23(a) shows an original image and Figure 8.23(b) shows its 2-D wavelet transform. The squares in Figure 8.23(b) indicate spatial regions that belong to the same region in Figure 8.23(a). The arrows indicate parent-child relationships. An important observation can be made from Figure 8.23(b), which is true for most natural images: if there is little low-frequency informa-tion in a spatial region, then it is likely that there is also little high-frequency information in that region. Thus, if a parent pixel is small, then it is likely that the belonging children are also small. This relationship can be exploited in order to encode the subband pixels in an efficient way. The coding technique is known as *embedded zerotree wavelet coding* [131, 128].

We will not study the embedded zerotree coding here in great detail, but we will give a rough idea of how such a coder works. Most importantly, the quantization of the wavelet coefficients is carried out successively, using a bitplane technique. One starts with a coarse quantization and refines it in every subsequent step. Whenever a tree of zeros (pixels quantized to zero with respect to a given threshold) is identified, it will be coded as a so-called zerotree by using a single codeword. Starting with coarse quantization ensures that a high number of zerotrees can be identified at the beginning of the encod-ing process. During the refinement process, when the quantization step size is successively reduced, the number of zerotrees successively decreases. Overall one gets an embedded bitstream where the most important information (in terms of signal energy) is coded first. The refinement process can be continued until one reaches a desired precision. One of the most interesting features of this coding technique is that the bitstream can be truncated at any position, resulting in an almost optimal rate-distortion behavior for any bit rate.

8.10   Wavelet-Based Denoising

The aim of denoising is to remove the noise $w(n)$ from a signal

$$y(n) = x(n) + w(n). \tag{8.222}$$

For example, $w(n)$ may be a Gaussian white noise process, which is statistically independent of $x(n)$. One tries to remove the noise by applying a nonlinear operation to the wavelet representation of $y(n)$. The same problem has been addressed in Chapter 7.3 in the context of the STFT, where it was solved via spectral subtraction. In fact, wavelet-based denoising is closely related to spectral subtraction. The main difference between both approaches lies in the fact that the wavelets used for denoising are real-valued while the STFT is complex.
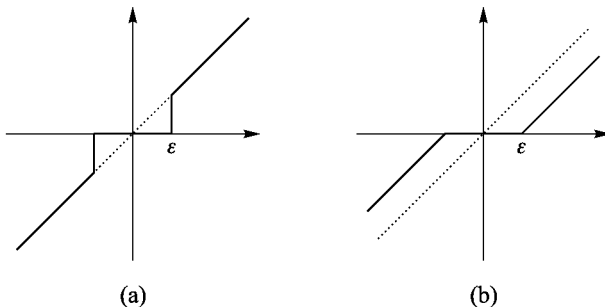
Figure 8.24. Thresholding techniques; (a) hard; (b) soft thresholding.

The denoising procedure is as follows. First, the signal $y(n)$ is decomposed using an octave-band filter bank, thus performing a discrete wavelet transform. Then, the wavelet coefficients are manipulated in order to remove the noise component. Two approaches known as *hard* and *soft thresholding* have been proposed for this purpose [43, 42]. They use the following non-linearities:

$$\hat{y}(n) = \begin{cases} y(n), & y(n) > \varepsilon \\ y(n), & y(n) < -\varepsilon \\ 0, & |y(n)| \le \varepsilon \end{cases} \quad \text{(hard)} \tag{8.223}$$

$$\hat{y}(n) = \begin{cases} y(n) - \varepsilon, & y(n) > \varepsilon \\ y(n) + \varepsilon, & y(n) < -\varepsilon \\ 0, & |y(n)| \le \varepsilon \end{cases} \quad \text{(soft)} \tag{8.224}$$

Figure 8.24 illustrates both techniques.

Basically, the idea of thresholding is that $x(n)$ can be represented via a few wavelet coefficients, while the noise has wideband characteristics and spreads out on all coefficients. For example, this holds true if $x(n)$ is a lowpass signal, while $w(n)$ is white noise. The thresholding procedure then sets the small wavelet coefficients representing $w(n)$ to zero, while the large coefficients due to $x(n)$ are only slightly affected. Thus, provided the threshold ε is chosen appropriately, the signal $\hat{y}(n)$ reconstructed from the manipulated wavelet coefficients will contain much less noise than $y(n)$ does. In practice, the problem is to choose ε, because the amount of noise is usually not known *a priori*. If ε is too small, the noise will not be efficiently removed. If it is too large, the signal will be distorted.

Chapter 9

Non-Linear Time-Frequency Distributions

In Chapters 7 and 8 two time-frequency distributions were discussed: the spectrogram and the scalogram. Both distributions are the result of linear filtering and subsequent forming of the squared magnitude. In this chapter time-frequency distributions derived in a different manner will be considered. Contrary to spectrograms and scalograms, their resolution is not restricted by the uncertainty principle. Although these methods do not yield positive distributions in all cases, they allow extremely good insight into signal properties within certain applications.

9.1   The Ambiguity Function

The goal of the following considerations is to describe the relationship between signals and their time as well as frequency-shifted versions. We start by looking at time and frequency shifts separately.

Time-Shifted Signals. The distance $d(x, x_\tau)$ between an energy signal $x(t)$ and its time-shifted version $x_\tau(t) = x(t + \tau)$ is related to the autocorrelation function $r_{xx}^E(\tau)$. Here the following holds (cf. (1.38)):

$$d(x_\tau, x)^2 = 2 \|x\|^2 - 2 \ \Re\{r_{xx}^E(\tau)\}, \qquad (9.1)$$

where

$$r_{xx}^E(\tau) = \langle \boldsymbol{x}_\tau, \boldsymbol{x} \rangle = \int_{-\infty}^{\infty} x^*(t) \, x(t+\tau) dt. \qquad (9.2)$$

As explained in Section 1.2, $r_{xx}^E(\tau)$ can also be understood as the inverse Fourier transform of the energy density spectrum $S_{xx}^E(\omega) = |X(\omega)|^2$:

$$
\begin{aligned}
r_{xx}^E(\tau) &= \frac{1}{2\pi} \int_{-\infty}^{\infty} S_{xx}^E(\omega) \, e^{j\omega\tau} \, d\omega \\
&= \frac{1}{2\pi} \int_{-\infty}^{\infty} X^*(\omega) \, X(\omega) \, e^{j\omega\tau} \, d\omega.
\end{aligned}
\qquad (9.3)
$$

In applications in which the signal $x(t)$ is transmitted and the time shift τ is to be estimated from the received signal $x(t+\tau)$, it is important that $x(t)$ and $x(t+\tau)$ are as dissimilar as possible for $\tau \neq 0$. That is, the transmitted signal $x(t)$ should have an autocorrelation function that is as Dirac-shaped as possible. In the frequency domain this means that the energy density spectrum should be as constant as possible.

Frequency-Shifted Signals. Frequency-shifted versions of a signal $x(t)$ are often produced due to the Doppler effect. If one wants to estimate such frequency shifts in order to determine the velocity of a moving object, the distance between a signal $x(t)$ and its frequency-shifted version $x_\nu(t) = x(t)e^{j\nu t}$ is of crucial importance. The distance is given by

$$d(\boldsymbol{x}, \boldsymbol{x}_\nu) = 2 \, \|\boldsymbol{x}\|^2 - 2 \, \Re\{\langle \boldsymbol{x}_\nu, \boldsymbol{x} \rangle\}. \qquad (9.4)$$

For the inner product $\langle \boldsymbol{x}_\nu, \boldsymbol{x} \rangle$ in (9.4) we will henceforth use the abbreviation $\rho_{xx}^E(\nu)$. We have

$$
\begin{aligned}
\rho_{xx}^E(\nu) &= \langle \boldsymbol{x}_\nu, \boldsymbol{x} \rangle \\
&= \int_{-\infty}^{\infty} x^*(t) \, x(t) \, e^{j\nu t} dt \\
&= \int_{-\infty}^{\infty} s_{xx}^E(t) \, e^{j\nu t} dt \qquad \text{with} \qquad s_{xx}^E(t) = |x(t)|^2,
\end{aligned}
\qquad (9.5)
$$

where $s_{xx}^E(t)$ can be viewed as the temporal energy density.[1] Comparing (9.5) with (9.3) shows a certain resemblance of the formulae for $r_{xx}^E(\tau)$ and $\rho_{xx}^E(\nu)$,

---

[1]In (9.5) we have an inverse Fourier transform in which the usual prefactor $1/2\pi$ does not occur because we integrate over t, not over ω. This peculiarity could be avoided if ν was replaced by $-\nu$ and (9.5) was interpreted as a forward Fourier transform. However, this would lead to other inconveniences in the remainder of this chapter.

however, with the time frequency domains being exchanged. This becomes even more obvious if $\rho_{xx}^E(\nu)$ is stated in the frequency domain:

$$\rho_{xx}^E(\nu) = \frac{1}{2\pi} \int_{-\infty}^{\infty} X(\omega) \, X^*(\omega + \nu) \, d\omega. \tag{9.6}$$

We see that $\rho_{xx}^E(\nu)$ can be seen as the autocorrelation function of $X(\omega)$.

Time and Frequency-Shifted Signals. Let us consider the signals

$$\begin{aligned} x_{-\frac{\tau}{2},-\frac{\nu}{2}}(t) &= x(t - \frac{\tau}{2}) e^{-j\nu t/2}, \\ x_{\frac{\tau}{2},\frac{\nu}{2}} &= x(t + \frac{\tau}{2}) e^{j\nu t/2}, \end{aligned} \tag{9.7}$$

which are time and frequency shifted versions of one another, centered around $x(t)$. With the abbreviation

$$A_{xx}(\nu,\tau) = \left\langle x_{\frac{\tau}{2},\frac{\nu}{2}}, \; x_{-\frac{\tau}{2},-\frac{\nu}{2}} \right\rangle \tag{9.8}$$

for the so-called *time-frequency autocorrelation function* or *ambiguity function*[2] we get

$$\begin{aligned} d(x_{-\frac{\tau}{2},-\frac{\nu}{2}}, \; x_{\frac{\tau}{2},\frac{\nu}{2}}) &= 2\,\|x\|^2 - 2\,\Re\{\langle x_{\frac{\tau}{2},\frac{\nu}{2}}, \; x_{-\frac{\tau}{2},-\frac{\nu}{2}} \rangle\} \\ &= 2\,\|x\|^2 - 2\,\Re\{A_{xx}(\nu,\tau)\}. \end{aligned} \tag{9.9}$$

Thus, the real part of $A_{xx}(\nu,\tau)$ is related to the distance between both signals.

In non-abbreviated form (9.8) is

$$A_{xx}(\nu,\tau) = \int_{-\infty}^{\infty} x^*(t - \frac{\tau}{2}) \, x(t + \frac{\tau}{2}) \, e^{j\nu t} \, dt. \tag{9.10}$$

Via Parseval's relation we obtain an expression for computing $A_{xx}(\nu,\tau)$ in the frequency domain

$$A_{xx}(\nu,\tau) = \frac{1}{2\pi} \int_{-\infty}^{\infty} X(\omega - \frac{\nu}{2}) \, X^*(\omega + \frac{\nu}{2}) \, e^{j\omega\tau} \, d\omega. \tag{9.11}$$

---

[2]We find different definitions of this term in the literature. Some authors also use it for the term $|A_{xx}(\nu,\tau)|^2$ [150].

Example. We consider the Gaussian signal

$$x(t) = \left(\frac{\alpha}{\pi}\right)^{\frac{1}{4}} e^{-\frac{1}{2}\alpha t^2}, \qquad (9.12)$$

which satisfies $\|x\| = 1$. Using the correspondence

$$e^{-\pi t^2} \longleftrightarrow e^{-\frac{1}{4\pi^2}\omega^2}, \qquad (9.13)$$

we obtain

$$A_{xx}(\nu, \tau) = e^{-\frac{\alpha}{4}\tau^2} e^{-\frac{1}{4\alpha}\nu^2}. \qquad (9.14)$$

Thus, the ambiguity function is a two-dimensional Gaussian function whose center is located at the origin of the τ-ν plane.

Properties of the Ambiguity Function.

1. A time shift of the input signal leads to a modulation of the ambiguity function with respect to the frequency shift ν:

$$\tilde{x}(t) = x(t - t_0) \quad \Rightarrow \quad A_{\tilde{x}\tilde{x}}(\nu, \tau) = e^{j\nu t_0} A_{xx}(\nu, \tau). \qquad (9.15)$$

   This relation can easily be derived from (9.11) by exploiting the fact that $\tilde{X}(\omega) = e^{-j\omega t_0} X(\omega)$.

2. A modulation of the input signal leads to a modulation of the ambiguity function with respect to τ:

$$\tilde{x}(t) = e^{j\omega_0 t} x(t) \quad \Rightarrow \quad A_{\tilde{x}\tilde{x}}(\nu, \tau) = e^{j\omega_0 \tau} A_{xx}(\nu, \tau). \qquad (9.16)$$

   This is directly derived from (9.10).

3. The ambiguity function has its maximum at the origin,

$$\max\{A_{xx}(\nu, \tau)\} = A_{xx}(0, 0) = E_x, \qquad (9.17)$$

   where E_x is the signal energy. A modulation and/or time shift of the signal $x(t)$ leads to a modulation of the ambiguity function, but the principal position in the τ-ν plane is not affected.

Radar Uncertainty Principle. The classical problem in radar is to find signals $x(t)$ that allow estimation of time and frequency shifts with high precision. Therefore, when designing an appropriate signal $x(t)$ the expression

$$|A_{xx}(\nu, \tau)|^2$$

is considered, which contains information on the possible resolution of a given $x(t)$ in the τ-ν plane. The ideal of having an impulse located at the origin of the τ-ν plane cannot be realized since we have [150]

$$\frac{1}{2\pi} \int_{-\infty}^{\infty} \int_{-\infty}^{\infty} |A_{xx}(\nu,\tau)|^2 \; d\tau \; d\nu = |A_{xx}(0,0)|^2 = E_x^2. \tag{9.18}$$

That is, if we achieve that $|A_{xx}(\nu,\tau)|^2$ takes on the form of an impulse at the origin, it necessarily has to grow in other regions of the τ-ν plane because of the limited maximal value $|A_{xx}(0,0)|^2 = E_x^2$. For this reason, (9.18) is also referred to as the *radar uncertainty principle*.

Cross Ambiguity Function. Finally we want to remark that, analogous to the cross correlation, so-called *cross ambiguity functions* are defined:

$$\begin{aligned} A_{yx}(\nu,\tau) &= \int_{-\infty}^{\infty} x(t + \tfrac{\tau}{2}) \, y^*(t - \tfrac{\tau}{2}) \, e^{j\nu t} \, dt \\ &= \frac{1}{2\pi} \int_{-\infty}^{\infty} X(\omega - \tfrac{\nu}{2}) \, Y^*(\omega + \tfrac{\nu}{2}) \, e^{j\omega\tau} \, d\omega. \end{aligned} \tag{9.19}$$

9.2   The Wigner Distribution

9.2.1   Definition and Properties

The Wigner distribution is a tool for time-frequency analysis, which has gained more and more importance owing to many extraordinary characteristics. In order to highlight the motivation for the definition of the Wigner distribution, we first look at the ambiguity function. From $A_{xx}(\nu,\tau)$ we obtain for $\nu = 0$ the temporal autocorrelation function

$$r_{xx}^E(\tau) = A_{xx}(0,\tau), \tag{9.20}$$

from which we derive the energy density spectrum by means of the Fourier transform:

$$\begin{aligned} S_{xx}^E(\omega) &= \int_{-\infty}^{\infty} r_{xx}^E(\tau) \, e^{-j\omega\tau} \, d\tau \\ &= \int_{-\infty}^{\infty} A_{xx}(0,\tau) \, e^{-j\omega\tau} \, d\tau. \end{aligned} \tag{9.21}$$

On the other hand, we get the autocorrelation function $\rho_{xx}^E(\nu)$ of the spectrum $X(\omega)$ from $A_{xx}(\nu, \tau)$ for $\tau = 0$:

$$\rho_{xx}^E(\nu) = A_{xx}(\nu, 0). \qquad (9.22)$$

The temporal energy density $s_{xx}^E(t)$ is the Fourier transform of $\rho_{xx}^E(\nu)$:

$$\begin{aligned} s_{xx}^E(t) &= \frac{1}{2\pi} \int_{-\infty}^{\infty} \rho_{xx}^E(\nu)\, e^{-j\nu t}\, d\nu \\[2mm] &= \frac{1}{2\pi} \int_{-\infty}^{\infty} A_{xx}(\nu, 0)\, e^{-j\nu t}\, d\nu. \end{aligned} \qquad (9.23)$$

These relationships suggest defining a two-dimensional *time-frequency distribution* $W_{xx}(t, \omega)$ as the two-dimensional Fourier transform of $A_{xx}(\nu, \tau)$:

$$W_{xx}(t, \omega) = \frac{1}{2\pi} \int_{-\infty}^{\infty} \int_{-\infty}^{\infty} A_{xx}(\nu, \tau) e^{-j\nu t} e^{-j\omega\tau}\, d\nu\, d\tau. \qquad (9.24)$$

The time-frequency distribution $W_{xx}(t, \omega)$ is known as the *Wigner distribution*.[3]

The two-dimensional Fourier transform in (9.24) can also be viewed as performing two subsequent one-dimensional Fourier transforms with respect to τ and ν. The transform with respect to ν yields the *temporal autocorrelation function*[4]

$$\begin{aligned} \phi_{xx}(t, \tau) &= \frac{1}{2\pi} \int_{-\infty}^{\infty} A_{xx}(\nu, \tau)\, e^{-j\nu t}\, d\nu \\[2mm] &= x^*(t - \tfrac{\tau}{2})\, x(t + \tfrac{\tau}{2}). \end{aligned} \qquad (9.25)$$

The Fourier transform of $A_{xx}(\nu, \tau)$ with respect to τ yields

$$\begin{aligned} \Phi_{xx}(\nu, \omega) &= \int_{-\infty}^{\infty} A_{xx}(\nu, \tau)\, e^{-j\omega\tau}\, d\tau \\[2mm] &= X(\omega - \tfrac{\nu}{2})\, X^*(\omega + \tfrac{\nu}{2}). \end{aligned} \qquad (9.26)$$

---

[3]Wigner used $W_{xx}(t, \omega)$ for describing phenomena of quantum mechanics [163], Ville introduced it for signal analysis later [156], so that one also speaks of the Wigner–Ville distribution.

[4]If $x(t)$ was assumed to be a random process, $E\{\phi_{xx}(t, \tau)\}$ would be the autocorrelation function of the process.
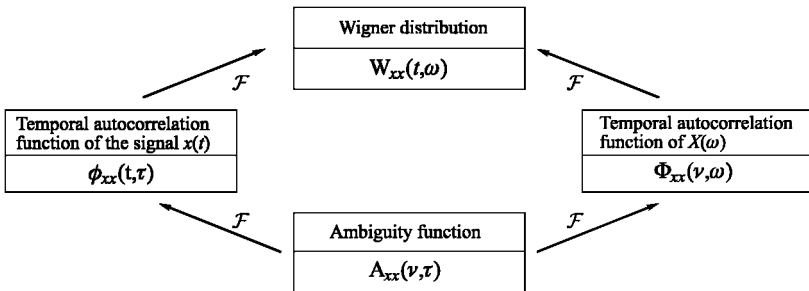
Figure 9.1. Relationship between ambiguity function and Wigner distribution.

The function $\Phi_{xx}(\nu, \omega)$ is so to say the *temporal autocorrelation function* of $X(\omega)$. Altogether we obtain

$$
\begin{aligned}
W_{xx}(t, \omega) &= \int_{-\infty}^{\infty} \phi_{xx}(t, \tau)\, e^{-j\omega\tau}\, d\tau \\
&= \frac{1}{2\pi} \int_{-\infty}^{\infty} \Phi_{xx}(\nu, \omega)\, e^{-j\nu t}\, d\nu
\end{aligned}
\tag{9.27}
$$

with $\phi_{xx}(t, \tau)$ according to (9.25) and $\Phi_{xx}(\nu, \omega)$ according to (9.26), in full:

$$
\begin{aligned}
W_{xx}(t, \omega) &= \int_{-\infty}^{\infty} x^*(t - \tfrac{\tau}{2})\, x(t + \tfrac{\tau}{2})\, e^{-j\omega\tau}\, d\tau \\
&= \frac{1}{2\pi} \int_{-\infty}^{\infty} X(\omega - \tfrac{\nu}{2})\, X^*(\omega + \tfrac{\nu}{2})\, e^{-j\nu t}\, d\nu.
\end{aligned}
\tag{9.28}
$$

Figure 9.1 pictures the relationships mentioned above.

We speak of $W_{xx}(t, \omega)$ as a distribution because it is supposed to reflect the distribution of the signal energy in the time-frequency plane. However, the Wigner distribution cannot be interpreted pointwise as a distribution of energy because it can also take on negative values. Apart from this restriction it has all the properties one would wish of a time-frequency distribution. The most important of these properties will be briefly listed. Since the proofs can be directly inferred from equation (9.28) by exploiting the characteristics of the Fourier transform, they are omitted.

Some Properties of the Wigner Distribution:

1. The Wigner distribution of an arbitrary signal $x(t)$ is always real,

$$W_{xx}(t,\omega) = W_{xx}^*(t,\omega) = \Re\{W_{xx}(t,\omega)\}. \qquad (9.29)$$

   If $x(t)$ is real itself, we conclude from (9.28), by observing the properties of the Fourier transform, that $W_{xx}(t,\omega)$ is an even function of ω, that is $W_{xx}(t,\omega) = W_{xx}(t,-\omega)$.

2. By integrating over ω we obtain the temporal energy density

$$s_{xx}^E(t) = \frac{1}{2\pi} \int_{-\infty}^{\infty} W_{xx}(t,\omega)\ d\omega = |x(t)|^2. \qquad (9.30)$$

3. By integrating over t we obtain the energy density spectrum

$$S_{xx}^E(\omega) = \int_{-\infty}^{\infty} W_{xx}(t,\omega)\ dt = |X(\omega)|^2. \qquad (9.31)$$

4. Integrating over time and frequency yields the signal energy:

$$\frac{1}{2\pi} \int_{-\infty}^{\infty}\int_{-\infty}^{\infty} W_{xx}(t,\omega)\ d\omega\ dt = \int_{-\infty}^{\infty} |x(t)|^2\ dt = E_x. \qquad (9.32)$$

5. If a signal $x(t)$ is non-zero in only a certain time interval, then the Wigner distribution is also restricted to this time interval:

$$
\begin{aligned}
x(t) &= 0 \ \ \text{for} \ \ t < t_1 \ \ \text{and/or} \ \ t > t_2 \\
&\Downarrow \\
W_{xx}(t,\omega) &= 0 \ \ \text{for} \ \ t < t_1 \ \ \text{and/or} \ \ t > t_2.
\end{aligned}
\qquad (9.33)
$$

   This property immediately follows from (9.28).

6. If $X(\omega)$ is non-zero only in a certain frequency region, then the Wigner distribution is also restricted to this frequency region:

$$
\begin{aligned}
X(\omega) &= 0 \ \ \text{for} \ \ \omega < \omega_1 \ \ \text{and/or} \ \ \omega > \omega_2 \\
&\Downarrow \\
W_{xx}(t,\omega) &= 0 \ \ \text{for} \ \ \omega < \omega_1 \ \ \text{and/or} \ \ \omega > \omega_2.
\end{aligned}
\qquad (9.34)
$$

7. A time shift of the signal leads to a time shift of the Wigner distribution (cf. (9.25) and (9.27)):

$$\tilde{x}(t) = x(t - t_0) \quad \Rightarrow \quad W_{\tilde{x}\tilde{x}}(t,\omega) = W_{xx}(t - t_0, \omega). \tag{9.35}$$

8. A modulation of the signal leads to a frequency shift of the Wigner distribution (cf. (9.26) and (9.27)):

$$\tilde{x}(t) = x(t)e^{j\omega_0 t} \quad \Rightarrow \quad W_{\tilde{x}\tilde{x}}(t,\omega) = W_{xx}(t, \omega - \omega_0). \tag{9.36}$$

9. A simultaneous time shift and modulation lead to a time and frequency shift of the Wigner distribution:

$$\tilde{x}(t) = x(t - t_0)e^{j\omega_0 t} \quad \Rightarrow \quad W_{\tilde{x}\tilde{x}}(t,\omega) = W_{xx}(t - t_0, \omega - \omega_0). \tag{9.37}$$

10. Time scaling leads to

$$\tilde{x}(t) = x(at) \quad \Rightarrow \quad W_{\tilde{x}\tilde{x}}(t,\omega) = \frac{1}{|a|} W_{xx}(at, \frac{\omega}{a}). \tag{9.38}$$

Signal Reconstruction. By an inverse Fourier transform of $W_{xx}(t,\omega)$ with respect to ω we obtain the function

$$\phi_{xx}(t,\tau) = x^*(t - \frac{\tau}{2}) \, x(t + \frac{\tau}{2}), \tag{9.39}$$

cf. (9.27). Along the line $t = \tau/2$ we get

$$\hat{x}(\tau) = \phi_{xx}(\frac{\tau}{2}, \tau) = x^*(0) \, x(\tau). \tag{9.40}$$

This means that any $x(t)$ can be perfectly reconstructed from its Wigner distribution except for the prefactor $x^*(0)$.

Similarly, we obtain for the spectrum

$$\hat{X}^*(\nu) = \Phi_{xx}(\frac{\nu}{2}, \nu) = X(0) \, X^*(\nu). \tag{9.41}$$

Moyal's Formula for Auto-Wigner Distributions. The squared magnitude of the inner product of two signals $x(t)$ and $y(t)$ is given by the inner product of their Wigner distributions [107], [18]:

$$\left| \int_{-\infty}^{\infty} x(t) \, y^*(t) \, dt \right|^2 = \frac{1}{2\pi} \iint W_{xx}(t,\omega) \, W_{yy}(t,\omega) \, dt \, d\omega. \tag{9.42}$$

9.2.2   Examples

Signals with Linear Time-Frequency Dependency. The prime example for demonstrating the excellent properties of the Wigner distribution in time-frequency analysis is the so-called chirp signal, a frequency modulated (FM) signal whose instantaneous frequency linearly changes with time:

$$x(t) = A \; e^{j\frac{1}{2}\beta t^2} \; e^{j\omega_0 t}. \tag{9.43}$$

We obtain

$$W_{xx}(t,\omega) = 2\pi \; |A|^2 \; \delta(\omega - \omega_0 - \beta t). \tag{9.44}$$

This means that the Wigner distribution of a linearly modulated FM signal shows the exact instantaneous frequency.

Gaussian Signal. We consider the signal

$$\tilde{x}(t) = e^{j\omega_0 t} \; x(t - t_0) \tag{9.45}$$

with

$$x(t) = \left(\frac{\alpha}{\pi}\right)^{\frac{1}{4}} \; e^{-\frac{1}{2}\alpha t^2}. \tag{9.46}$$

The Wigner distribution $W_{xx}(t,\omega)$ is

$$W_{xx}(t,\omega) = 2 \; e^{-\alpha t^2} \; e^{-\frac{1}{\alpha} \, \omega^2}, \tag{9.47}$$

and for $W_{\tilde{x}\tilde{x}}(t,\omega)$ we get

$$W_{\tilde{x}\tilde{x}}(t,\omega) = 2 \; e^{-\alpha(t - t_0)^2} \; e^{-\frac{1}{\alpha} \, [\omega - \omega_0]^2}. \tag{9.48}$$

Hence the Wigner distribution of a modulated Gaussian signal is a two-dimensional Gaussian whose center is located at $[t_0, \omega_0]$ whereas the ambiguity function is a modulated two-dimensional Gaussian signal whose center is located at the origin of the τ-ν plane (cf. (9.14), (9.15) and (9.16)).

Signals with Positive Wigner Distribution. Only signals of the form

$$x(t) = \left(\frac{\alpha}{\pi}\right)^{\frac{1}{4}} \; e^{-\frac{1}{2}\alpha t^2} \; e^{j\frac{1}{2}\beta t^2} \; e^{j\omega_0 t} \tag{9.49}$$

have a positive Wigner distribution [30]. The Gaussian signal and the chirp are to be regarded as special cases.

For the Wigner distribution of $x(t)$ according to (9.49) we get

$$W_{xx}(t,\omega) = 2 \; e^{-\alpha t^2} \; e^{-\frac{1}{\alpha} \, [\omega - \omega_0 - \beta t]^2} \tag{9.50}$$

with $W_{xx}(t,\omega) \geq 0 \; \forall \; t, \omega$.
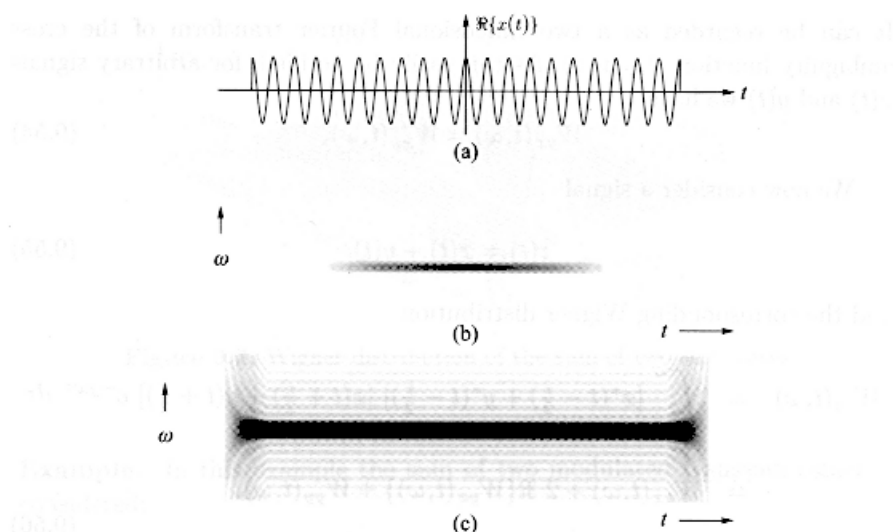
Figure 9.2. Time-limited exponential; (a) time signal; (b) Wigner distribution; (c) spectrogram.

Time-Limited Exponential. We consider an exponential limited to the interval $[-T, T]$:

$$x(t) = \begin{cases} e^{j\omega_0 t} & \text{for } |t| < T, \\ 0 & \text{otherwise.} \end{cases} \tag{9.51}$$

The Wigner distribution is

$$W_{xx}(t, \omega) = \begin{cases} \frac{2}{\omega - \omega_0} \sin(2(\omega - \omega_0)(T - |t|)) & \text{for } |t| < T, \\ 0 & \text{otherwise.} \end{cases} \tag{9.52}$$

Figure 9.2 shows an example of such an $x(t)$ and two gray-scale images picturing the Wigner distribution and the spectrogram. We observe that the spectrogram is not limited to $[-T, T]$. Furthermore, we notice clear differences in the interference geometries of the Wigner distribution and the spectrogram.

9.2.3 Cross-Terms and Cross Wigner Distributions

The *cross Wigner distribution* is defined as

$$\begin{aligned} W_{yx}(t, \omega) &= \int_{-\infty}^{\infty} y^*(t - \tfrac{\tau}{2})\, x(t + \tfrac{\tau}{2})\, e^{-j\omega\tau}\, d\tau \\ &= \frac{1}{2\pi} \int_{-\infty}^{\infty} X(\omega - \tfrac{\nu}{2})\, Y^*(\omega + \tfrac{\nu}{2})\, e^{-j\nu t}\, d\nu. \end{aligned} \tag{9.53}$$

It can be regarded as a two-dimensional Fourier transform of the cross ambiguity function $A_{yx}(\nu, \tau)$. As can easily be verified, for arbitrary signals $x(t)$ and $y(t)$ we have

$$W_{yx}(t, \omega) = W^*_{xy}(t, \omega). \tag{9.54}$$

We now consider a signal

$$z(t) = x(t) + y(t) \tag{9.55}$$

and the corresponding Wigner distribution

$$
\begin{aligned}
W_{zz}(t, \omega) &= \int_{-\infty}^{\infty} [x^*(t - \tfrac{\tau}{2}) + y^*(t - \tfrac{\tau}{2})] \, [x(t + \tfrac{\tau}{2}) + y(t + \tfrac{\tau}{2})] \, e^{-j\omega\tau} \, d\tau \\[2mm]
&= W_{xx}(t, \omega) + 2 \, \Re\{W_{yx}(t, \omega)\} + W_{yy}(t, \omega).
\end{aligned}
\tag{9.56}
$$

We see that the Wigner distribution of the sum of two signals does not equal the sum of their respective Wigner distributions. The occurrence of cross-terms $W_{yx}(t, \omega)$ complicates the interpretation of the Wigner distribution of real-world signals. Size and location of the interference terms are discussed in the following examples.

Moyal's Formula for Cross Wigner Distributions. For the inner product of two cross Wigner distributions we have [18]

$$\frac{1}{2\pi} \iint W_{x_1 y_1}(t, \omega) \, W_{x_2 y_2}(t, \omega) \, dt \, d\omega = \langle x_1, y_1 \rangle \, \langle x_2, y_2 \rangle \tag{9.57}$$

with $\langle x, y \rangle = \int x(t) \, y^*(t) \, dt$.

Example. We consider the sum of two complex exponentials

$$z(t) = \frac{A_1}{\sqrt{2\pi}} \, e^{j\omega_1 t} + \frac{A_2}{\sqrt{2\pi}} \, e^{j\omega_2 t}. \tag{9.58}$$

For $W_{zz}(t, \omega)$ we get

$$
\begin{aligned}
W_{zz}(t, \omega) &= A_1^2 \, \delta(\omega - \omega_1) + A_2^2 \, \delta(\omega - \omega_2) \\[2mm]
&\quad + 2A_1 A_2 \, \cos((\omega_2 - \omega_1)t) \, \delta(\omega - \tfrac{1}{2}(\omega_1 + \omega_2))
\end{aligned}
\tag{9.59}
$$

Figure 9.3 shows $W_{zz}(t, \omega)$ and illustrates the influence of the cross-term $2A_1 A_2 \, \cos((\omega_2 - \omega_1)t) \, \delta(\omega - \tfrac{1}{2}(\omega_1 + \omega_2))$.
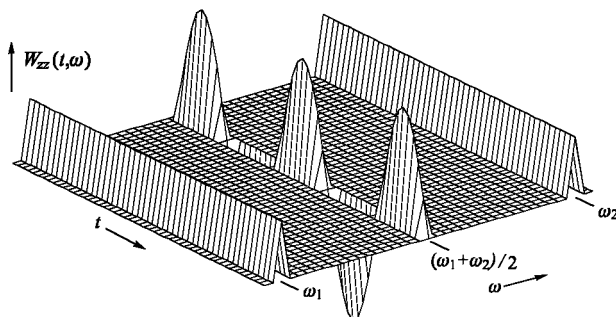
Figure 9.3. Wigner distribution of the sum of two sine waves.

Example. In this example the sum of two modulated Gaussian signals is considered:

$$z(t) = x(t) + y(t) \tag{9.60}$$

with

$$x(t) = e^{j\omega_1(t - t_1)} \, e^{-\frac{1}{2}\alpha(t - t_1)^2} \tag{9.61}$$

and

$$y(t) = e^{j\omega_2(t - t_2)} \, e^{-\frac{1}{2}\alpha(t - t_2)^2}. \tag{9.62}$$

Figures 9.4 and 9.5 show examples of the Wigner distribution. We see that the interference term lies between the two signal terms, and the modulation of the interference term takes place orthogonal to the line connecting the two signal terms. This is different for the ambiguity function, also shown in Figure 9.5. The center of the signal term is located at the origin, which results from the fact that the ambiguity function is a time-frequency autocorrelation function. The interference terms concentrate around

$$
\begin{aligned}
\tau_1 &= t_1 - (t_1 + t_2)/2, \\
\nu_1 &= \omega_2 - (\omega_1 + \omega_2)/2, \\
\tau_2 &= t_2 - (t_1 + t_2)/2, \\
\nu_2 &= \omega_1 - (\omega_1 + \omega_2)/2.
\end{aligned}
$$
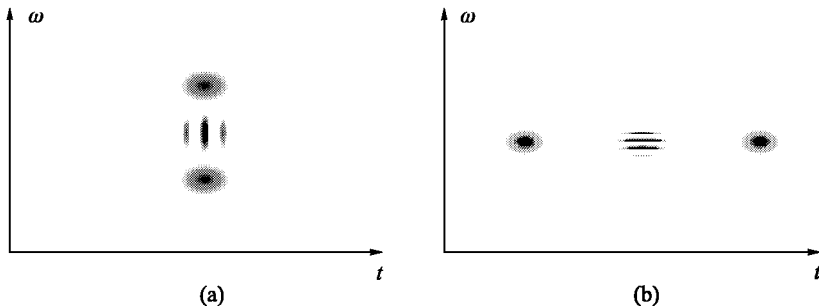
Figure 9.4. Wigner distribution of the sum of two modulated and time-shifted Gaussians; (a) $t_1 = t_2$, $\omega_1 \neq \omega_2$; (b) $t_1 \neq t_2$, $\omega_1 = \omega_2$.
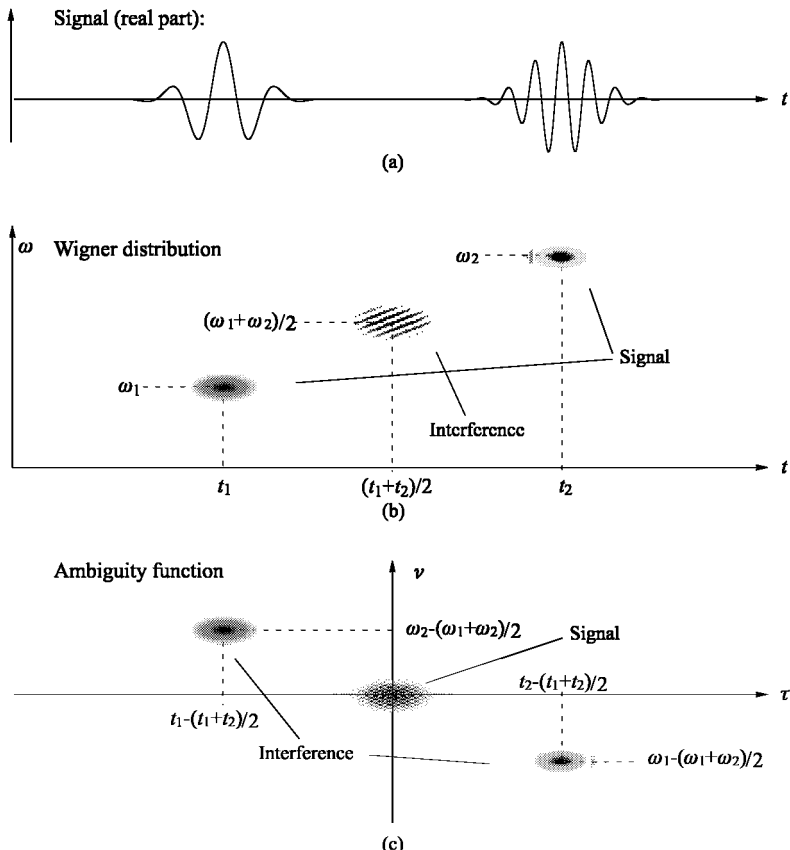
Figure 9.5. Wigner distribution and ambiguity function of the sum of two modulated and time-shifted Gaussians ($t_1 \neq t_2$, $\omega_1 \neq \omega_2$).

9.2.4 Linear Operations

Multiplication in the Time Domain. We consider the signal

$$\tilde{x}(t) = x(t)\ h(t). \tag{9.63}$$

For the Wigner distribution we get

$$W_{\tilde{x}\tilde{x}}(t,\omega) = \int_{-\infty}^{\infty} x^*(t - \tfrac{\tau}{2})\ x(t + \tfrac{\tau}{2})\ h^*(t - \tfrac{\tau}{2})\ h(t + \tfrac{\tau}{2})\ e^{-j\omega\tau}\ d\tau$$

$$= \int_{-\infty}^{\infty} \phi_{xx}(t,\tau)\ \phi_{hh}(t,\tau)\ e^{-j\omega\tau}\ d\tau. \tag{9.64}$$

The multiplication of $\phi_{xx}(t,\tau)$ and $\phi_{hh}(t,\tau)$ with respect to τ can be replaced by a convolution in the frequency domain:

$$W_{\tilde{x}\tilde{x}}(t,\omega) = \frac{1}{2\pi}\ W_{xx}(t,\omega) \overset{\omega}{*} W_{hh}(t,\omega)$$

$$= \frac{1}{2\pi} \int_{\omega'} W_{xx}(t,\omega')\ W_{hh}(t,\omega - \omega')\ d\omega'. \tag{9.65}$$

That is, a multiplication in the time domain is equivalent to a convolution of the Wigner distributions $W_{xx}(t,\omega)$ and $W_{hh}(t,\omega)$ with respect to ω.

Convolution in the Time Domain. Convolving $x(t)$ and $h(t)$, or equivalently, multiplying $X(\omega)$ and $H(\omega)$, leads to a convolution of the Wigner distributions $W_{xx}(t,\omega)$ and $W_{hh}(t,\omega)$ with respect to t. For

$$\tilde{x}(t) = x(t) * h(t) \tag{9.66}$$

we have

$$W_{\tilde{x}\tilde{x}}(t,\omega) = W_{xx}(t,\omega) \overset{t}{*} W_{hh}(t,\omega)$$

$$= \int_{t'} W_{xx}(t',\omega)\ W_{hh}(t - t',\omega)\ dt'. \tag{9.67}$$

Pseudo-Wigner Distribution. A practical problem one encounters when calculating the Wigner distribution of an arbitrary signal $x(t)$ is that (9.28) can only be evaluated for a time-limited $x(t)$. Therefore, the concept of windowing is introduced. For this, one usually does not apply a single window

$h(t)$ to $x(t)$, as in (9.65), but one centers $h(t)$ around the respective time of analysis:

$$W_{xx}^{(PW)}(t,\omega) := \int_{-\infty}^{\infty} x^*(t - \frac{\tau}{2})\ x(t + \frac{\tau}{2})\ h(\tau)\ e^{-j\omega\tau}\ d\tau. \qquad (9.68)$$

Of course, the time-frequency distribution according to (9.68) corresponds only approximately to the Wigner distribution of the original signal. Therefore one speaks of a *pseudo-Wigner distribution* [26].

Using the notation

$$W_{xx}^{(PW)}(t,\omega) = \int_{-\infty}^{\infty} h(\tau)\ \phi_{xx}(t,\tau)\ e^{-j\omega\tau}\ d\tau \qquad (9.69)$$

it is obvious that the pseudo-Wigner distribution can be calculated from $W_{xx}(t,\omega)$ as

$$\begin{aligned} W_{xx}^{(PW)}(t,\omega) &= \frac{1}{2\pi} W_{xx}(t,\omega) * H(\omega) \\[2ex] &= \frac{1}{2\pi} \int_{-\infty}^{\infty} W_{xx}(t,\omega')\ H(\omega - \omega')\ d\omega' \end{aligned} \qquad (9.70)$$

with $H(\omega) \longleftrightarrow h(t)$. This means that the pseudo-Wigner distribution is a smoothed version of the Wigner distribution.

9.3   General Time-Frequency Distributions

The previous section showed that the Wigner distribution is a perfect time-frequency analysis instrument as long as there is a linear relationship between instantaneous frequency and time. For general signals, the Wigner distribution takes on negative values as well and cannot be interpreted as a "true" density function. A remedy is the introduction of additional two-dimensional smoothing kernels, which guarantee for instance that the time-frequency distribution is positive for all signals. Unfortunately, depending on the smoothing kernel, other desired properties may get lost. To illustrate this, we will consider several shift-invariant and affine-invariant time-frequency distributions.

9.3.1 Shift-Invariant Time-Frequency Distributions

Cohen introduced a general class of time-frequency distributions of the form [29]

$$T_{xx}(t,\omega) = \frac{1}{2\pi} \iiint e^{j\nu(u-t)} \, g(\nu,\tau) \, x^*(u - \frac{\tau}{2}) \, x(u + \frac{\tau}{2}) \, e^{-j\omega\tau} \, d\nu \, du \, d\tau.$$

$$(9.71)$$

This class of distributions is also known as *Cohen's class*. Since the kernel $g(\nu,\tau)$ in (9.71) is independent of t and ω, all time-frequency distributions of Cohen's class are shift-invariant. That is,

$$\tilde{x}(t) = x(t - t_0) \quad \Rightarrow \quad T_{\tilde{x}\tilde{x}}(t,\omega) = T_{xx}(t - t_0, \omega),$$

$$(9.72)$$

$$\tilde{x}(t) = x(t)e^{j\omega_0 t} \quad \Rightarrow \quad T_{\tilde{x}\tilde{x}}(t,\omega) = T_{xx}(t, \omega - \omega_0).$$

By choosing $g(\nu,\tau)$ all possible shift-invariant time-frequency distributions can be generated. Depending on the application, one can choose a kernel that yields the required properties.

If we carry out the integration over u in (9.71), we get

$$T_{xx}(t,\omega) = \frac{1}{2\pi} \iint g(\nu,\tau) \, A_{xx}(\nu,\tau) \, e^{-j\nu t} \, e^{-j\omega\tau} \, d\nu \, d\tau. \qquad (9.73)$$

This means that the time-frequency distributions of Cohen's class are computed as two-dimensional Fourier transforms of two-dimensionally windowed ambiguity functions. From (9.73) we derive the Wigner distribution for $g(\nu,\tau) = 1$. For $g(\nu,\tau) = h(\tau)$ we obtain the pseudo-Wigner distribution. The product

$$M(\nu,\tau) = g(\nu,\tau) \, A_{xx}(\nu,\tau) \qquad (9.74)$$

is known as the *generalized ambiguity function*.

Multiplying $A_{xx}(\nu,\tau)$ with $g(\nu,\tau)$ in (9.73) can also be expressed as the convolution of $W_{xx}(t,\omega)$ with the Fourier transform of the kernel:

$$T_{xx}(t,\omega) \;=\; \frac{1}{2\pi} \, W_{xx}(t,\omega) * * \, G(t,\omega)$$

$$(9.75)$$

$$=\; \frac{1}{2\pi} \iint W_{xx}(t',\omega') \, G(t - t', \omega - \omega') \, dt' \, d\omega'$$

with

$$G(t,\omega) = \frac{1}{2\pi} \iint g(\nu,\tau) \, e^{-j\nu t} \, e^{-j\omega\tau} \, d\nu \, d\tau. \qquad (9.76)$$

That is, all time-frequency distributions of Cohen's class can be computed by means of a convolution of the Wigner distribution with a two-dimensional impulse response $G(t, \omega)$.

In general the purpose of the kernel $g(\nu, \tau)$ is to suppress the interference terms of the ambiguity function which are located far from the origin of the τ-ν plane (see Figure 9.5); this again leads to reduced interference terms in the time-frequency distribution $T_{xx}(t, \omega)$. Equation (9.75) shows that the reduction of the interference terms involves "smoothing" and thus results in a reduction of time-frequency resolution.

Depending on the type of kernel, some of the desired properties of the time-frequency distribution are preserved while others get lost. For example, if one wants to preserve the characteristic

$$\frac{1}{2\pi} \int_{-\infty}^{\infty} T_{xx}(t, \omega) \; d\omega = |x(t)|^2, \tag{9.77}$$

the kernel must satisfy the condition

$$g(\nu, 0) = 1. \tag{9.78}$$

We realize this by substituting (9.73) into (9.77) and integrating over $d\omega$, $d\tau$, $d\nu$. Correspondingly, the kernel must satisfy the condition

$$g(0, \tau) = 1 \tag{9.79}$$

in order to preserve the property

$$\int_{-\infty}^{\infty} T_{xx}(t, \omega) \; dt = |X(\omega)|^2. \tag{9.80}$$

A real distribution, that is

$$T_{xx}(t, \omega) = T_{xx}^*(t, \omega), \tag{9.81}$$

is obtained if the kernel satisfies the condition

$$g(\nu, \tau) = g^*(-\nu, -\tau). \tag{9.82}$$

Finally it shall be noted that although (9.73) gives a straightforward interpretation of Cohen's class, the implementation of (9.71) is more advantageous. For this, we first integrate over ν in (9.71). With

$$r(u, \tau) = \frac{1}{2\pi} \int_{-\infty}^{\infty} g(\nu, \tau) \; e^{j\nu u} \; d\nu \tag{9.83}$$
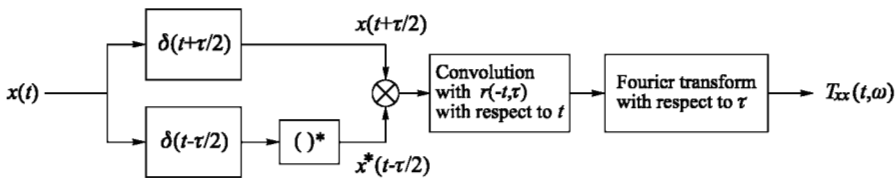
Figure 9.6. Generation of a general time-frequency distribution of Cohen's class.

we obtain

$$T_{xx}(t,\omega) = \iint r(u-t,\tau)\, x^*(u - \frac{\tau}{2})\, x(u + \frac{\tau}{2})\, e^{-j\omega\tau}\, du\, d\tau. \qquad (9.84)$$

Figure 9.6 shows the corresponding implementation.

9.3.2 Examples of Shift-Invariant Time-Frequency Distributions

Spectrogram. The best known example of a shift-invariant time-frequency distribution is the spectrogram, described in detail in Chapter 7. An interesting relationship between the spectrogram and the Wigner distribution can be established [26]. In order to explain this, the short-time Fourier transform is expressed in the form

$$\mathcal{F}_x(t,\omega) = \int_{-\infty}^{\infty} x(t')\, h^*(t-t')\, e^{-j\omega t'}\, dt'. \qquad (9.85)$$

Then the spectrogram is

$$S_x(t,\omega) = |\mathcal{F}_x(t,\omega)|^2 = \left| \int_{-\infty}^{\infty} x(t')\, h^*(t-t')\, e^{-j\omega t'}\, dt' \right|^2. \qquad (9.86)$$

Alternatively, with the abbreviation

$$x_t(t') = x(t')\, h^*(t-t'), \qquad (9.87)$$

(9.85) can be written as

$$S_{x_t}(\omega) = |X_t(\omega)|^2. \qquad (9.88)$$

Furthermore, the energy density $|X_t(\omega)|^2$ can be computed from the Wigner distribution $W_{x_t x_t}(t',\omega)$ according to (9.31):

$$|X_t(\omega)|^2 = \int_{-\infty}^{\infty} W_{x_t x_t}(t',\omega)\, dt' \qquad (9.89)$$

Observing (9.35) and (9.65), we finally obtain from (9.89):

$$
\begin{aligned}
S_x(t,\omega) &= \frac{1}{2\pi} \iint W_{xx}(t',\omega')\, W_{hh}(t-t',\omega-\omega')\, dt'\, d\omega' \\[2mm]
&= \frac{1}{2\pi} W_{xx}(t,\omega) \, **\, W_{hh}(t,\omega).
\end{aligned}
\tag{9.90}
$$

Thus the spectrogram results from the convolution of $W_{xx}(t,\omega)$ with the Wigner distribution of the impulse response $h(t)$. Therefore, the spectrogram belongs to Cohen's class. The kernel $g(\nu,\tau)$ in (9.73) is the ambiguity function of the impulse response $h(t)$ (cf. (9.75)):

$$
g(\nu,\tau) = A_{hh}(\nu,\tau) = \int_{-\infty}^{\infty} h^*(t-\frac{\tau}{2})\, h(t+\frac{\tau}{2})\, e^{j\nu t}\, dt.
\tag{9.91}
$$

Although the spectrogram has the properties (9.81) and (9.72), the resolution in the time-frequency plane is restricted in such a way (uncertainty principle) that (9.77) and (9.80) cannot be satisfied. This becomes immediately obvious when we think of the spectrogram of a time-limited signal (see also Figure 9.2).

Separable Smoothing Kernels. Using separable smoothing kernels

$$
g(\nu,\tau) = G_1(\nu)\, g_2(\tau),
\tag{9.92}
$$

means that smoothing along the time and frequency axis is carried out separately. This becomes obvious in (9.75), which becomes

$$
\begin{aligned}
T_{xx}(t,\omega) &= \frac{1}{2\pi} G(t,\omega) \, **\, W_{xx}(t,\omega) \\[2mm]
&= \frac{1}{2\pi} g_1(t) \, *\, [\, G_2(\omega) \, *\, W_{xx}(t,\omega)\,]
\end{aligned}
\tag{9.93}
$$

where

$$
G(t,\omega) = g_1(t)\, G_2(\omega), \qquad g_1(t) \longleftrightarrow G_1(\omega), \quad G_2(\omega) \longleftrightarrow g_2(t).
\tag{9.94}
$$

From (9.83) and (9.84) we derive the following formula for the time-frequency distribution, which can be implemented efficiently:

$$
T_{xx}(t,\omega) = \int \left[\iint x^*(u-\frac{\tau}{2})\, x(u+\frac{\tau}{2})\, g_1(u-t)\, du \right] g_2(\tau)\, e^{-j\omega\tau}\, d\tau.
\tag{9.95}
$$

Time-frequency distributions which are generated by means of a convolution of a Wigner distribution with separable impulse responses can also be understood as temporally smoothed pseudo-Wigner distributions. The window

$g_2(\tau)$ in (9.95) plays the role of $h(\tau)$ in (9.68). Temporal smoothing is achieved by filtering with $g_1(t)$.

An often used smoothing kernel (especially in speech analysis) is the Gaussian

$$g(\nu, \tau) = \frac{1}{2} e^{-\alpha^2 \nu^2 / 4} e^{-\beta^2 \tau^2 / 4}, \qquad \alpha, \beta \in \mathbb{R}, \ \alpha, \beta > 0. \tag{9.96}$$

Thus we derive the distribution

$$T_{xx}^{(\text{Gauss})}(t, \omega) =$$

$$\frac{1}{2\alpha\sqrt{\pi}} \int \int e^{-(u-t)^2/\alpha^2 - \frac{\beta^2}{4}\tau^2 - j\omega\tau} \, x^*\!\left(u - \frac{\tau}{2}\right) x\!\left(u + \frac{\tau}{2}\right) du \, d\tau. \tag{9.97}$$

For the two-dimensional impulse response $G(t, \omega)$ we have

$$G(t, \omega) = g_1(t) \, G_2(\omega) \tag{9.98}$$

with

$$g_1(t) = \frac{1}{\alpha} e^{-t^2/\alpha^2} \tag{9.99}$$

and

$$G_2(\omega) = \frac{1}{\beta} e^{-\omega^2/\beta^2}. \tag{9.100}$$

It can be shown that for arbitrary signals a positive distribution is obtained if [75]

$$\alpha\beta \geq 1. \tag{9.101}$$

For $\alpha\beta = 1$, $T_{xx}^{(\text{Gauss})}(t, \omega)$ is equivalent to a spectrogram with Gaussian window. For $\alpha\beta > 1$, $T_{xx}^{(\text{Gauss})}(t, \omega)$ is even more smoothed than a spectrogram.

Since $T_{xx}^{(\text{Gauss})}(t, \omega)$ for $\alpha\beta \geq 1$ can be computed much more easily and more efficiently via a spectrogram, computing with the smoothed pseudo-Wigner distribution is interesting only for the case

$$\alpha\beta < 1. \tag{9.102}$$

The choice of α and β is dependent on the signal in question. In order to give a hint, consider a signal $x(t)$ consisting of the sum of two modulated time-shifted Gaussians. It is obvious that smoothing should be carried out towards the direction of the modulation of the cross term (compare Figures 9.4 and 9.5). Although the modulation may occur in any direction, we look at

(a)

(b)
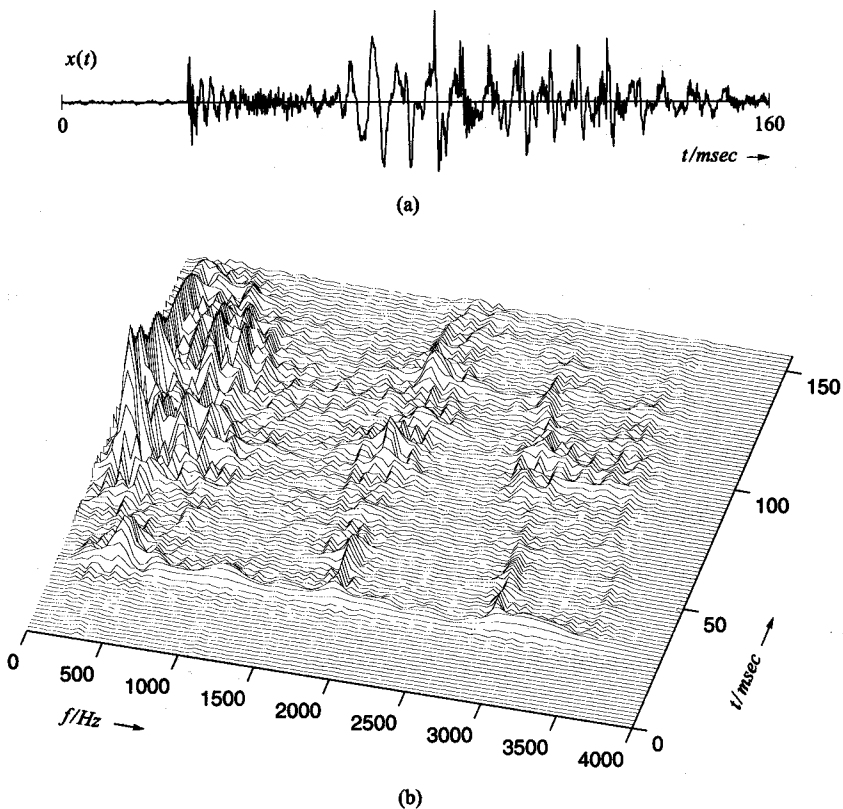
Figure 9.7. Time-frequency analysis of the word "taxi". The signal and the time-frequency distribution are shown up to the beginning of the "x"; (a) time signal; (b) smoothed pseudo-Wigner distribution.

time and frequency separately. For a signal $x(t) = x_0(t)e^{j\omega_1 t} + x_0(t)e^{j\omega_2 t}$ with $\omega_2 > \omega_1$, the cross-term is modulated along the time axis with frequency $\omega_2 - \omega_1$ (compare Figure 9.4(a)). Therefore one should choose $\alpha > 2\pi/(\omega_2 - \omega_1)$ in order to achieve efficient smoothing. The superposition of two signal components which are identical except for a time shift $x(t) = x_0(t - t_1) + x_0(t - t_2))$, leads to a cross-term that is modulated along the frequency axis (compare Figure 9.4(b)). Here, β must be chosen just large enough to achieve efficient smoothing of the oscillations along the frequency axis.

Figure 9.7 shows the smoothed pseudo-Wigner distribution of a speech signal, and Figure 9.8 shows two corresponding spectrograms. The time resolution in Figure 9.7 is the same as in Figure 9.8(a), while the frequency resolution in Figure 9.7 is the same as in Figure 9.8(b).
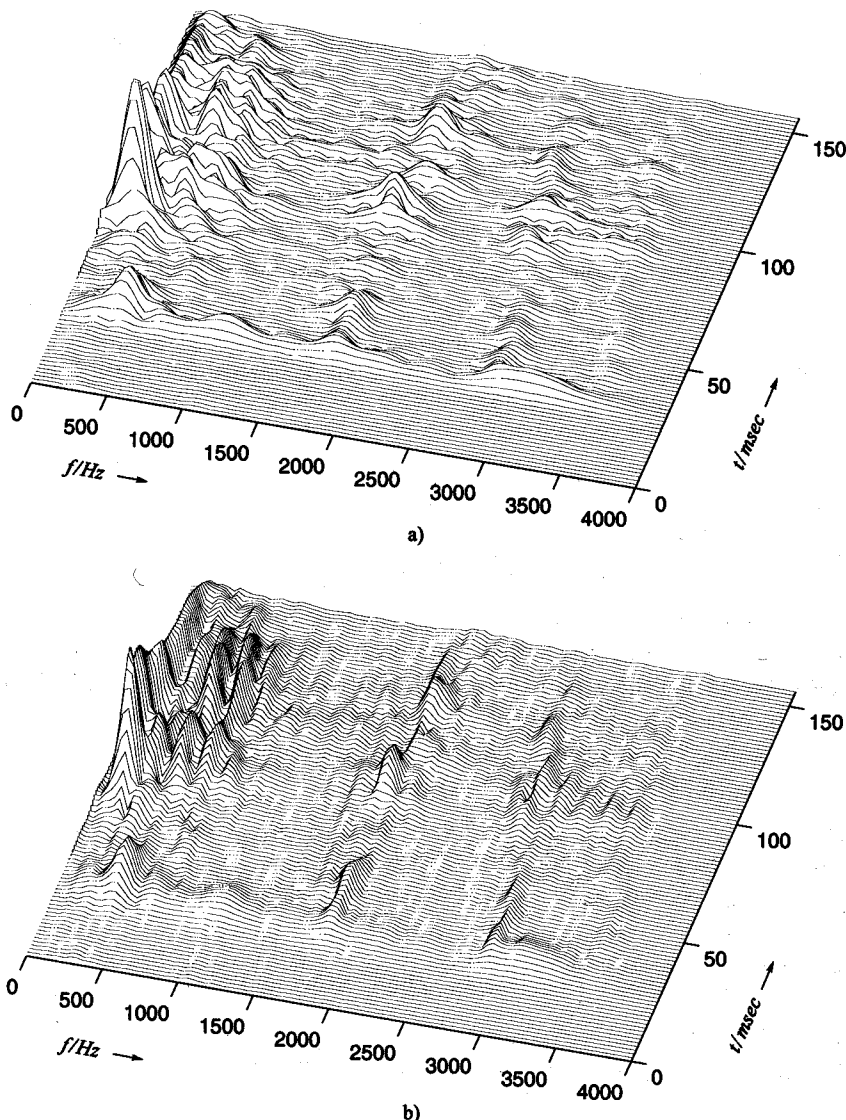
Figure 9.8. Spectrogram of the signal shown in Figure 9.7; (a) good time resolution; (b) good frequency resolution.

Examples of Time-Frequency Distributions of Cohen's Class. In the literature we find many proposals of shift-invariant time-frequency distributions. A survey is presented in [72] for instance. In the following, three examples will briefly be mentioned.

Rihaczek distribution. The Rihaczek distribution is defined as [124]

$$
\begin{aligned}
T_{xx}^{(R)}(t,\omega) &= \int x^*(t)\, x(t+\tau)\, e^{-j\omega\tau}\, d\tau \\[2mm]
&= x^*(t)\, X(\omega)\, e^{j\omega t}.
\end{aligned}
\tag{9.103}
$$

This type of distribution is of enticing simplicity, but it is not real-valued in general.

Choi–Williams Distribution. For the Choi–Williams distribution the following product kernel is used [24]:

$$
g(\nu,\tau) = e^{-\nu^2\tau^2/(4\pi^2\sigma)}, \quad \sigma > 0.
\tag{9.104}
$$

We see that $g(\nu,0) = 1$ and $g(0,\tau) = 1$ are satisfied so that the Choi–Williams distribution has the properties (9.77) and (9.80).

The quantity σ in (9.104) may be understood as a free parameter. If a small σ is chosen, the kernel concentrates around the origin of the τ-ν plane, except for the τ and the ν axis. Thus we get a generalized ambiguity function $M(\nu,\tau) = g(\nu,\tau)\, A_{xx}(\nu,\tau)$ with reduced interference terms, and the corresponding time-frequency distribution has reduced interference terms as well. From (9.71), (9.83), and (9.84) we get

$$
T_{xx}^{(CW)}(t,\omega) = \int_{-\infty}^{\infty}\int_{-\infty}^{\infty} \sqrt{\frac{\pi\sigma}{\tau^2}}\, e^{-\pi^2\sigma(u-t)^2/\tau^2}\, x^*\!\left(u - \frac{\tau}{2}\right) x\!\left(u + \frac{\tau}{2}\right) e^{-j\omega\tau}\, du\, d\tau.
\tag{9.105}
$$

Zhao–Atlas–Marks Distribution. Zhao, Atlas and Marks [168] suggested the kernel

$$
g(\nu,\tau) = g_1(\tau)\, \frac{2\sin(\nu|\tau|/a)}{\nu}.
\tag{9.106}
$$

This yields the distribution

$$
T_{xx}^{(ZAM)}(t,\omega) = \int_{-\infty}^{\infty} g_1(\tau)\, e^{-j\omega\tau} \int_{t-|\tau|/a}^{t+|\tau|/a} x^*\!\left(u - \frac{\tau}{2}\right) x\!\left(u + \frac{\tau}{2}\right) du\, d\tau.
\tag{9.107}
$$

9.3.3 Affine-Invariant Time-Frequency Distributions

Affine smoothing is an alternative to regular smoothing of the Wigner distribution (Cohen's class). A time-frequency distribution that belongs to the affine class is invariant with respect to time shift and scaling:

$$\tilde{x}(t) = \sqrt{|a|}\; x(a(t - t_0)) \quad \Rightarrow \quad T_{\tilde{x}\tilde{x}}(t,\omega) = T_{xx}(a(t - t_0), \omega/a). \quad (9.108)$$

Any time-frequency distribution that satisfies (9.108) can be computed from the Wigner distribution by means of an affine transform [54], [126]:

$$T_{xx}(t,\omega) = \frac{1}{2\pi} \iint K(\omega(t' - t), \omega'/\omega)\, W_{xx}(t',\omega')\, dt'\, d\omega'. \quad (9.109)$$

This can be understood as correlating the Wigner distribution with kernel K along the time axis. By varying ω the kernel is scaled.

Since (9.108) and (9.72) do not exclude each other, there exist other time-frequency distributions besides the Wigner distribution which belong to the shift-invariant Cohen class as well as to the affine class. These are, for instance, all time-frequency distributions that originate from a product kernel, such as the Choi–Williams distribution.

Scalogram. An example of the affine class is the scalogram, that is, the squared magnitude of the wavelet transform of a signal:

$$|\mathcal{W}_x(b,a)|^2 = \left| \int_{-\infty}^{\infty} x(t)\, \psi_{b,a}^*(t)\, dt \right|^2 \quad (9.110)$$

with

$$\psi_{b,a}(t) = |a|^{-\frac{1}{2}}\, \psi\left(\frac{t - b}{a}\right). \quad (9.111)$$

Moyal's formula (9.42) yields the relationship

$$|\mathcal{W}_x(b,a)|^2 = \frac{1}{2\pi} \iint W_{\psi_{b,a}, \psi_{b,a}}(t',\omega')\, W_{xx}(t',\omega')\, dt'\, d\omega', \quad (9.112)$$

where

$$W_{\psi_{b,a}, \psi_{b,a}}(t',\omega') = W_{\psi,\psi}\left(\frac{t' - b}{a}, a\omega'\right). \quad (9.113)$$

Thus, from (9.112) we derive

$$|\mathcal{W}_x(b,a)|^2 = \frac{1}{2\pi} \iint W_{\psi,\psi}\left(\frac{t' - b}{a}, a\omega'\right)\, W_{xx}(t',\omega')\, dt'\, d\omega'. \quad (9.114)$$

The substitutions $b = t$ and $a = \omega_0/\omega$ finally yield

$$
\begin{aligned}
T_{xx}(t,\omega) &= |\mathcal{W}_x(t,\omega_0/\omega)|^2 \\[6pt]
&= \frac{1}{2\pi} \iint W_{\psi,\psi}\left(\frac{\omega}{\omega_0}(t'-t), \frac{\omega_0}{\omega}\omega'\right) W_{xx}(t',\omega') \; dt' \; d\omega'.
\end{aligned}
\tag{9.115}
$$

The resolution of the scalogram is, just like that of the spectrogram, limited by the uncertainty principle.

9.3.4   Discrete-Time Calculation of Time-Frequency Distributions

If we wish to calculate the Wigner distribution or some other time-frequency distribution on a computer we are forced to sample our signal and the transform kernel and to replace all integrals by sums. If the signal and the kernel are bandlimited and if the sampling rate is far above the Nyquist rate for both signal and kernel, we do not face a substantial problem. However, in some cases, such as the Choi–Williams distribution, sampling the kernel already poses a problem. On the other hand, the test signal may be discrete-time right away, so that discrete-time definitions of time-frequency distributions are required in any case.

Discrete-Time Wigner Distribution [26]. The *discrete-time Wigner distribution* is defined as

$$
W_{xx}(n, e^{j\omega}) = 2 \sum_m x^*(n-m) \; x(n+m) \; e^{-j2\omega m}.
\tag{9.116}
$$

Here, equation (9.116) is the discrete version of equation (9.28), which, using the substitution $\tau' = \tau/2$, can be written as

$$
W_{xx}(t, \omega) = 2 \int_{-\infty}^{\infty} x^*(t-\tau') \; x(t+\tau') \; e^{-j2\omega\tau'} \; d\tau'.
\tag{9.117}
$$

As we know, discrete-time signals have a periodic spectrum, so that one could expect the Wigner distribution of a discrete-time signal to have a periodic spectrum also. We have the following property: while the signal $x(n)$ has a spectrum $X(e^{j\omega}) \longleftrightarrow x(n)$ with period 2π, the period of the discrete-time Wigner distribution is only π. Thus,

$$
W_{xx}(n, e^{j\omega}) = W_{xx}(n, e^{j\omega + k\pi}), \quad k \in \mathbb{Z}.
\tag{9.118}
$$

The reason for this is subsampling by the factor two with respect to τ. In order to avoid aliasing effects in the Wigner distribution, one has to take care that the bandlimited signal $x(t)$ is sampled with the rate

$$f_a \geq 4\ f_{max} \qquad (9.119)$$

and not with $f_a \geq 2\ f_{max}$, where

$$X(\omega) = 0 \quad \text{for} \quad |\omega| > 2\pi\ f_{max}. \qquad (9.120)$$

Because of the different periodicity of $X(e^{j\omega})$ and $W_{xx}(n, e^{j\omega})$ it is not possible to transfer all properties of the continuous-time Wigner distribution to the discrete-time Wigner distribution. A detailed discussion of the topic can be found in [26], Part II.

General Discrete-Time Time-Frequency Distributions. Analogous to (9.84) and (9.116), a general discrete-time time-frequency distribution of Cohen's class is defined as

$$T_{xx}(n, k) = 2 \sum_{m=-M}^{M} \sum_{\ell=-N}^{N} \rho(\ell, m)\ x^*(\ell + n - m)\ x(\ell + n + m)\ e^{-j4\pi km/L}.$$
$$(9.121)$$

Here we have already taken into account that in practical applications one would only consider discrete frequencies $2\pi k/L$, where L is the DFT length.

Basically we could imagine the term $\rho(\ell, m)$ in (9.121) to be a $2M + 1 \times 2N + 1$ matrix which contains sample values of the function $r(u, \tau)$ in (9.84). However, for kernels that are not bandlimited, sampling causes a problem. For example, for the discrete-time Choi–Williams distribution we therefore use the matrix

$$\rho^{(CW)}(n, m) = \begin{cases} \dfrac{1}{|m|\ \alpha_m}\ e^{-\sigma n^2/4m^2}, & m \neq 0, \\[2mm] \delta(n), & m = 0, \end{cases} \qquad (9.122)$$

with

$$\alpha_m = \sum_{k=-N}^{N} \frac{1}{|m|}\ e^{-\sigma k^2/4m^2}, \quad n = -N, \ldots, N, \quad m = -M, \ldots, M. \quad (9.123)$$

The normalization $\sum_n \rho(n, m) = 1$ in (9.122) is necessary in order to preserve the properties [11]

$$\sum_n T_{xx}^{(CW)}(n, k) = |X(k)|^2 = |X(e^{j\omega_k})|^2 \qquad (9.124)$$

and

$$\sum_k T_{xx}^{(CW)}(n,k) = |x(n)|^2. \tag{9.125}$$

9.4   The Wigner–Ville Spectrum

So far the signals analyzed have been regarded as deterministic. Contrary to the previous considerations, $x(t)$ is henceforth defined as a stochastic process. We may view the deterministic analyses considered so far as referring to single sample functions of a stochastic process. In order to gain information on the stochastic process we define the so-called *Wigner–Ville spectrum* as the expected value of the Wigner distribution:

$$\bar{W}_{xx}(t,\omega) = E\{W_{xx}(t,\omega)\} = \int_{-\infty}^{\infty} r_{xx}(t+\frac{\tau}{2},t-\frac{\tau}{2})\, e^{-j\omega\tau}\, d\tau \tag{9.126}$$

with

$$r_{xx}(t+\frac{\tau}{2},t-\frac{\tau}{2}) = E\{\phi_{xx}(t,\tau)\} = E\left\{x^*(t-\frac{\tau}{2})\, x(t+\frac{\tau}{2})\right\}. \tag{9.127}$$

This means that the temporal correlation function $\phi_{xx}(t,\tau)$ is replaced by its expected value, which is the autocorrelation function $r_{xx}(t+\frac{\tau}{2},t-\frac{\tau}{2})$ of the process $x(t)$.

The properties of the Wigner–Ville spectrum are basically the same as those of the Wigner distribution. But by forming the expected value it generally contains fewer negative values than the Wigner distribution of a single sample function.

The Wigner–Ville spectrum is of special interest when analyzing non-stationary or cyclo-stationary processes because here the usual terms, such as power spectral density, do not give any information on the temporal distribution of power or energy. In order to illustrate this, the Wigner–Ville spectrum will be discussed for various processes in connection with standard characterizations.

Stationary Processes. For stationary processes the autocorrelation function only depends on τ, and the Wigner–Ville spectrum becomes the power spectral density:

$$\bar{W}_{xx}(t,\omega) = S_{xx}(\omega) = \int_{-\infty}^{\infty} r_{xx}(\tau)\, e^{-j\omega\tau}\, d\tau \tag{9.128}$$

if $x(t)$ is stationary.

Processes with Finite Energy. If we assume that the process $x(t)$ has finite energy, an average energy density spectrum can be derived from the Wigner–Ville spectrum as

$$\bar{s}_{xx}(t) \;=\; E\left\{|x(t)|^2\right\} = \frac{1}{2\pi} \int_{-\infty}^{\infty} \bar{W}_{xx}(t,\omega) \; d\omega, \qquad (9.129)$$

$$\bar{S}_{xx}(\omega) \;=\; E\left\{|X(\omega)|^2\right\} = \int_{-\infty}^{\infty} \bar{W}_{xx}(t,\omega) \; dt. \qquad (9.130)$$

For the mean energy we then have

$$E_x = E\left\{\int_{-\infty}^{\infty} |x(t)|^2 \; dt\right\} = \frac{1}{2\pi} \int_{-\infty}^{\infty} \bar{W}_{xx}(t,\omega) \; d\omega \, dt. \qquad (9.131)$$

Non-Stationary Processes with Infinite Energy. For non-stationary processes with infinite energy the power spectral density is not defined. However, a mean power density is given by

$$\bar{S}_{xx}(\omega) = \lim_{T\to\infty} \frac{1}{T} \int_{-T/2}^{T/2} \bar{W}_{xx}(t,\omega) \; dt. \qquad (9.132)$$

Cyclo-Stationary Processes. For cyclo-stationary processes it is sufficient to integrate over one period T in order to derive the mean power density:

$$\bar{S}_{xx}(\omega) = \frac{1}{T} \int_{-T/2}^{T/2} \bar{W}_{xx}(t,\omega) \; dt. \qquad (9.133)$$

Example. As a simple example of a cyclo-stationary process, we consider the signal

$$x(t) = \sum_{i=-\infty}^{\infty} d(i) \; g(t - iT). \qquad (9.134)$$

Here, $g(t)$ is the impulse response of a filter that is excited with statistically independent data $d(i)$, $i \in \mathbb{Z}$. The process $d(i)$ is assumed to be zero-mean and stationary. The signal $x(t)$ can be viewed as the complex envelope of a real bandpass signal.

Now we consider the autocorrelation function of the process $x(t)$. We

obtain

$$
\begin{aligned}
r_{xx}(t+\tau,t) &= E\left\{x^*(t)x(t+\tau)\right\} \\[2mm]
&= \sum_{i=-\infty}^{\infty}\sum_{j=-\infty}^{\infty} E\left\{d^*(i)d(j)\right\}\, g^*(t-iT)\, g(t-jT+\tau) \\[2mm]
&= \sigma_d^2 \sum_{i=-\infty}^{\infty} g^*(t-iT)\, g(t-iT+\tau).
\end{aligned}
$$

$$(9.135)$$

As (9.135) shows, the autocorrelation function depends on t and τ, and in general the process $x(t)$ is not stationary. Nevertheless, it is cyclo-stationary, because the statistical properties repeat periodically:

$$
r_{xx}(t+\tau,t) = r_{xx}(t+\tau+\ell T, t+\ell T), \qquad \ell \in \mathbb{Z}. \tag{9.136}
$$

Typically, one chooses the filter $g(t)$ such that its autocorrelation function $r_{gg}^E(\tau)$ satisfies the first Nyquist condition:

$$
r_{gg}^E(mT) = \begin{cases} 1 & \text{for } m = 0, \\ 0 & \text{otherwise.} \end{cases} \tag{9.137}
$$

Commonly used filters are the so-called *raised cosine filters*, which are designed as follows. For the energy density $S_{gg}^E(\omega) \longleftrightarrow r_{gg}^E(t)$ we take

$$
S_{gg}^E(\omega) = \begin{cases} 1 & \text{for } |\omega T|/\pi \leq 1-r, \\[2mm] \tfrac{1}{2}[1+\cos[\tfrac{\pi}{2r}(\omega T/\pi - (1-r))]] & \text{for } 1-r \leq |\omega T|/\pi \leq 1+r, \\[2mm] 0 & \text{for } |\omega T|/\pi \geq 1+r. \end{cases}
$$

$$(9.138)$$

Here, r is known as the *roll-off factor*, which can be chosen in the region $0 \leq r \leq 1$. For $r = 0$ we get the ideal lowpass. For $r > 0$ the energy density decreases in cosine form.

From (9.138) we derive

$$
r_{gg}^E(t) = \frac{1}{T}\,\frac{\sin \pi t/T}{\pi t/T}\,\frac{\cos r\pi t/T}{1-(2rt/T)^2}. \tag{9.139}
$$

As we see, for $r > 0$, $r_{gg}^E(t)$ is a windowed version of the impulse response of the ideal lowpass. Because of the equidistant zeros of the si-function, condition (9.137) is satisfied for arbitrary roll-off factors.

With

$$G(\omega) = \sqrt{S_{gg}^E(\omega)}, \tag{9.140}$$

the required impulse response $g(t)$ can be derived from (9.138) by means of an inverse Fourier transform:

$$g(t) = \frac{(4rt/T)\ \cos(\pi t(1+r)/T) + \sin(\pi t(1-r)/T)}{\pi t\ [1 - (4rt/T)^2]} \tag{9.141}$$

where

$$
\begin{aligned}
g(0) &= \frac{1}{T}\left(1 + r(\frac{4}{\pi} - 1)\right), \\[2mm]
g(\pm\frac{T}{4r}) &= -\frac{r}{T}\left[\frac{2}{\pi}\cos\left(\frac{\pi(1+r)}{4r}\right) - \cos\left(\frac{\pi(1-r)}{4r}\right)\right].
\end{aligned}
\tag{9.142}
$$

Figure 9.9 shows three examples of autocorrelation functions with period T and the corresponding Wigner–Ville spectra. We observe that for large roll-off factors there are considerable fluctuations in power in the course of a period. When stating the mean power density in the classical way according to (9.133) these effects are not visible (cf. Figure 9.10).

As can be seen in Figure 9.9, the fluctuations of power decrease with vanishing roll-off factor. In the limit, the ideal lowpass is approached ($r = 0$), and the process $x(t)$ becomes wide-sense stationary. In order to show this, the autocorrelation function $r_{xx}(t+\tau, t)$ is written as the inverse Fourier transform of a convolution of $G^*(-\omega)$ and $G(\omega)$:

$$
\begin{aligned}
r_{xx}(t+\tau, t) = \ &\sigma_d^2 \sum_{k=-\infty}^{\infty} \frac{1}{4\pi^2} \int_{-\infty}^{\infty}\int_{-\infty}^{\infty} G^*(-\omega')\ G(\omega - \omega') \\
&e^{j(\omega-\omega')\tau - j\omega kT}\ d\omega'\ e^{j\omega t} d\omega.
\end{aligned}
\tag{9.143}
$$

Here the summation is to be performed over the complex exponentials only. Thus, by using

$$\sum_{k=-\infty}^{\infty} e^{-j\omega kT} = \frac{2\pi}{T} \sum_{k=-\infty}^{\infty} \delta(\omega - k\frac{2\pi}{T}), \tag{9.144}$$

we achieve

$$
\begin{aligned}
r_{xx}(t+\tau, t) = \ &\frac{\sigma_d^2}{2\pi T} \int_{-\infty}^{\infty}\int_{-\infty}^{\infty} G^*(-\omega')\ G(\omega-\omega')\ e^{-j\omega'\tau} \\
&e^{j\omega\tau}\ e^{j\omega t} \sum_{k=-\infty}^{\infty} \delta(\omega - k\frac{2\pi}{T})\ d\omega\ d\omega'.
\end{aligned}
\tag{9.145}
$$
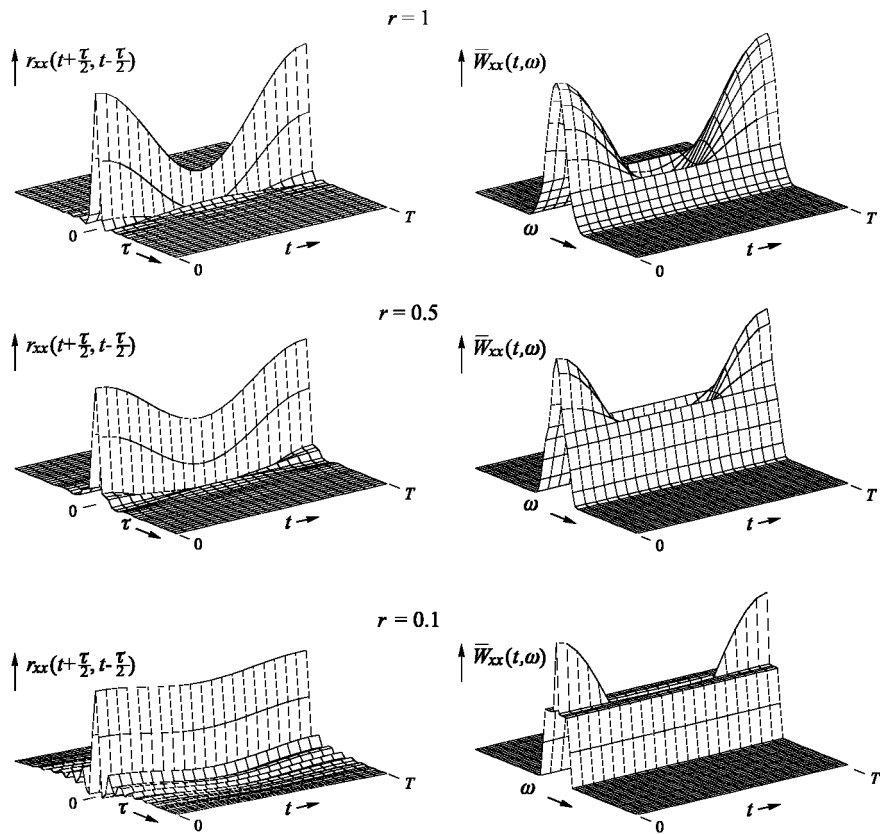
Figure 9.9. Periodic autocorrelation functions and Wigner–Ville spectra (raised cosine filter design with various roll-off factors r).

Integrating over ω yields

$$r_{xx}(t + \tau, t) =$$

$$\frac{\sigma_d^2}{2\pi T} \int_{-\infty}^{\infty} \sum_{k=-\infty}^{\infty} G^*(-\omega') \, G(k\frac{2\pi}{T} - \omega') \, e^{-j\omega'\tau} \, e^{jk\frac{2\pi}{T}\tau} \, e^{jk\frac{2\pi}{T}t} \, d\omega'.$$

$$(9.146)$$

If $G(\omega)$ is bandlimited to π/T, only the term for $k = 0$ remains, and the
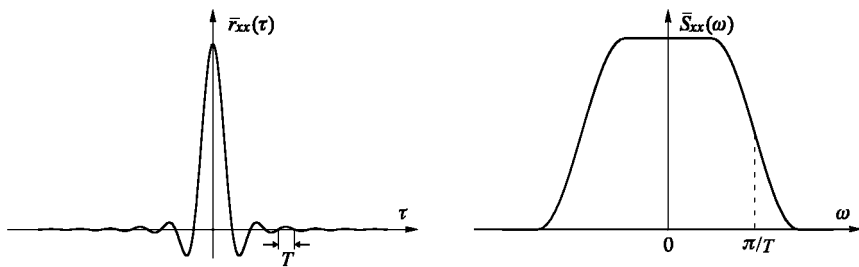
Figure 9.10. Mean autocorrelation functions $\bar{r}_{xx}(\tau) = \frac{1}{T}\int_0^T r_{x'x'}(t+\tau,t)dt$ and mean power spectral density ($r = 0.5$).

autocorrelation function depends on τ only:

$$
\begin{aligned}
r_{xx}(t+\tau,t) &= \sigma_d^2 \, \frac{1}{2\pi T} \int_{-\infty}^{\infty} G^*(-\omega') \, G(-\omega') \, e^{-j\omega'\tau} \, d\omega' \\[2mm]
&= \sigma_d^2 \, \frac{1}{2\pi T} \int_{-\infty}^{\infty} S_{gg}^E(\omega') \, e^{j\omega'\tau} \, d\omega' \qquad (9.147) \\[2mm]
&= \sigma_d^2 \, \frac{1}{T} \, r_{gg}^E(\tau).
\end{aligned}
$$

This shows that choosing $g(t)$ to be the ideal lowpass with bandwidth π/T yields a Nyquist system in which $x(t)$ is a wide-sense stationary process. However, if we consider realizable systems we must assume a cyclo-stationary process.

Stationarity within a realizable framework can be obtained by introducing a delay of half a sampling period for the imaginary part of the signal. An example of such a modulation scheme is the well-known offset phase shift keying. The modified signal reads

$$
x'(t) = \sum_{i=-\infty}^{\infty} \Re\{d(i)\} \, g(t-iT) \, + \, j\Im\{d(i)\} \, g(t-iT-T/2). \qquad (9.148)
$$

Assuming that

$$
\begin{aligned}
E\{\Re\{d(i)\}\Re\{d(j)\}\} &= \tfrac{1}{2}\,\sigma_d^2\,\delta_{ij}, \\[2mm]
E\{\Im\{d(i)\}\Im\{d(j)\}\} &= \tfrac{1}{2}\,\sigma_d^2\,\delta_{ij}, \qquad (9.149) \\[2mm]
E\{\Re\{d(i)\}\Im\{d(j)\}\} &= 0, \quad i,j \in \mathbb{Z},
\end{aligned}
$$

we have

$$
\begin{aligned}
r_{x'x'}(t+\tau,t) \;=\;\; & \frac{1}{2}\sigma_d^2 \sum_{i=-\infty}^{\infty} g^*(t-iT)\,g(t-iT+\tau) \\[2mm]
+\;\; & \frac{1}{2}\sigma_d^2 \sum_{i=-\infty}^{\infty} g^*(t-iT-\frac{T}{2})\,g(t-iT+\tau-\frac{T}{2}) \\[2mm]
=\;\; & \frac{1}{2}\sigma_d^2 \sum_{i=-\infty}^{\infty} g^*(t-i\frac{T}{2})\,g(t+\tau-i\frac{T}{2})
\end{aligned}
$$

$$(9.150)$$

for the autocorrelation function. According to (9.146) this can be written as

$$
r_{x'x'}(t+\tau,t) =
$$

$$
\frac{\sigma_d^2}{2\pi T}\int_{-\infty}^{\infty}\sum_{k=-\infty}^{\infty} G^*(-\omega')\,G(k\frac{4\pi}{T}-\omega')e^{-j\omega'\tau}e^{jk\frac{4\pi}{T}\tau}e^{jk\frac{4\pi}{T}t}d\omega'.
$$

$$(9.151)$$

We see that only the term for $k=0$ remains if $G(\omega)$ is bandlimited to $2\pi/T$, which is the case for the raised cosine filters. The autocorrelation function then is

$$
r_{x'x'}(t+\tau,t) = \sigma_d^2\,\frac{1}{T}\,r_{gg}^E(\tau). \tag{9.152}
$$

Hence the autocorrelation function $r_{x'x'}(t+\tau,t)$ and the mean autocorrelation function are identical. Correspondingly, the Wigner–Ville spectrum equals the mean power spectral density.

If we regard $x'(t)$ as the complex envelope of a real bandpass process $x_{\mathrm{BP}}(t)$, then we cannot conclude from the wide-sense stationarity of $x'(t)$ the stationarity of $x_{\mathrm{BP}}(t)$: for this to be true, the autocorrelation functions $r_{x_R x_R}(t+\tau,t)$ and $r_{x_I x_I}(t+\tau,t)$ would have to be identical and would have to be dependent only on τ (cf. Section 2.5).

Bibliography

[1] A.N. Akansu and R.A. Haddad. *Multiresolution Signal Decomposition.* Academic Press, New York, 1992.

[2] A.N. Akansu and F.E. Wadas. On lapped orthogonal transforms. *IEEE Trans. Signal Processing,* 40(2):439–443, Feb 1992.

[3] A. Albert. *Regression and the Moore–Penrose Pseudoinverse.* Academic Press, New York, 1972.

[4] J.B. Allen and L.R. Rabiner. A unified approach to STFT analysis and synthesis. *Proceedings of the IEEE,* 65:1558 – 1564, November 1977.

[5] M. Antonini, M. Barlaud, P. Mathieu, and I. Daubechies. Image coding using wavelet transform. *IEEE Trans. Image Processing,* 1(2):205–220, April 1992.

[6] H.J. Barnard, J.H. Weber, and J. Biemond. Efficient signal extension for subband/wavelet decomposition of arbitrary length signals. In *Proc. SPIE, VCIP,* volume 2094, pages 966–975, November 1993.

[7] R. Bellman. *Introduction to Matrix Analysis.* McGraw-Hill, New York, 1960.

[8] R.B. Blackman and J.W. Tukey. *The Measurement of Power Spectra* Dover, New York, 1958.

[9] R.E. Blahut. *Fast Algorithms for Digital Signal Processing* Addison Wesley, Reading, MA, 1995.

[10] L. Bluestein. A linear filtering approach to the computation of the discrete Fourier transform. *IEEE Trans. Audio and Electroacoustics,* 18:451–455, 1970.

[11] B. Boashash and A. Riley. Algorithms for time-frequency signal analysis. In *Time-Frequency Signal Analysis,* B. Boashash (ed.). Longman, Cheshire, 1992.

[12] S. Boll. Suppression of acoustic noise in speech using spectral subtraction. *IEEE Trans. Acoust., Speech, Signal Processing,* 27(2):113–120, April 1979.

[13] R.N. Bracewell. The discrete Hartley transform. *J. Opt. Soc. America,* 73:1832–1835, December 1983.

[14] R.N. Bracewell. The fast Hartley transform. *Proc. IEEE,* 72:1010–1018, 1984.

[15] R.N. Bracewell. *The Hartley Transform.* Oxford University Press, Oxford, UK, 1985.

[16] J.N. Bradley, C.M. Brislawn, and V. Faber. Reflected boundary conditions for multirate filter banks. In *Proc. Int. Symp. Time-Frequency and Time-Scale Analysis*, pages 307–310, Canada, 1992.

[17] K. Brandenburg, G. Stoll, F. Dehery, and J.D. Johnston. The ISO-MPEG-1 audio: A generic standard for coding of high-quality digital audio. *Journal of the Audio Engineering Society*, 42(10):780–792, October 1994.

[18] N.G. De Bruijn. A theory of generalized functions, with applications to Wigner distribution and Weyl correspondence. *Nieuw Archief voor Wiskunde (3)*, XXI:205–280, 1980.

[19] J.P. Burg. Maximum entropy spectral analysis. In *Proc. 37th Meeting Society of Exploration Geophysicists, Oklahoma City, October 1967. Reprint in Modern Spectrum Analysis, Selected Reprint Papers*, D.G. Childers (ed.), IEEE Press, New York, 1978.

[20] C.S. Burrus and P. Eschenbacher. An in-place in-order prime factor FFT algorithm. *IEEE Trans. Acoust., Speech, Signal Processing*, 29:806–817, 1981.

[21] P.M. Cassereau, D.H. Staelin, and G. de Jager. Encoding of images based on a lapped orthogonal transform. *IEEE Trans. on Communications*, 37(2):189–193, February 1989.

[22] D.C. Champeney. *A Handbook of Fourier Theorems.* Cambridge University Press, New York, 1987.

[23] L. Chen, T. Nguyen, and K.P. Chan. Symmetric extension methods for M-channel PR LP FIR analysis/synthesis systems. In *Proc. IEEE Int. Symp. Circuits and Systems*, pages 2.273 – 2.276, London, June 1994.

[24] H.I. Choi and W.J. Williams. Improved time-frequency representation on multicomponent signals using exponential kernels. *IEEE Trans. Acoust., Speech, Signal Processing*, 37(6):862–871, 1989.

[25] C.K. Chui. *An Introduction to Wavelets.* Academic Press, New York, 1992.

[26] T.A.C.M. Claasen and W.F.G. Mecklenbräuker. The wigner distribution - a tool for time-frequency signal analysis - parts I-III. *Philips J. Res.*, 35: 217–250, 276–300, 372–389, 1980.

[27] M. Coffrey. Boundary compensated wavelet bases. In *Proc. IEEE Int. Conf. Acoust., Speech, Signal Processing*, pages 2129–2132, München,

May 1997.

[28] A. Cohen, I. Daubechies, and J.C. Feauveau. Biorthogonal bases of compactly supported wavelets. *Comm. Pure and Appl. Math.*, XLV:485–560, 1992.

[29] L. Cohen. Generalized phase-space distribution functions. *J. of Math. Phys*, 7:781–786, 1966.

[30] L. Cohen. Introduction: A primer on time-frequency analysis. In *Time-Frequency Signal Analysis*, B. Boashash (ed.). Longman, Cheshire, 1992.

[31] J. Cooley and J. Tukey. An algorithm for machine calculation of complex Fourier series. *Math. Comp.*, 19:297–301, 1965.

[32] R.E. Crochiere and L.R. Rabiner. *Multirate Digital Signal Processing.* Prentice-Hall, Englewood Cliffs, NJ, 1983.

[33] G. Cvetković and M. Vetterli. Oversampled filter banks. *IEEE Trans. Signal Processing*, 46(5):1245–1255, May 1998.

[34] I. Daubechies. Orthonormal bases of compactly supported wavelets. *Comm. Pure and Appl. Math.*, 41:909–996, 1988.

[35] I. Daubechies. The wavelet transform, time-frequency localization and signal analysis. *IEEE Trans. on Inf. Theory*, 36(5):961–1005, September 1990.

[36] I. Daubechies. *Ten Lectures on Wavelets*. SIAM, 1992.

[37] I. Daubechies and W. Sweldens. Factoring wavelet transforms into lifting steps. *J. Fourier Anal. Appl.*, 4(3):245–267, 1998.

[38] W.B. Davenport and W.L. Root. *Random Signals and Noise*. McGraw-Hill, New York, 1958.

[39] R.L. de Queiroz. Subband processing of finite length signals without border distortions. In *Proc. IEEE Int. Conf. Acoust., Speech, Signal Processing*, volume IV, pages 613 – 616, San Francisco, USA, March 1992.

[40] R.L. de Queiroz and K.R. Rao. Optimal orthogonal boundary filter banks. In *Proc. IEEE Int. Conf. Acoust., Speech, Signal Processing*, volume II, pages 1296 – 1299, Detroit, USA, May 1995.

[41] Z. Doganata, P.P. Vaidyanathan, and T.Q. Nguyen. General synthesis procedures for FIR lossless transfer matrices, for perfect reconstruction multirate filter bank applications. *IEEE Trans. Acoust., Speech, Signal Processing*, 36(10):1561–1574, October 1988.

[42] D.L. Donoho. De-noising by soft-thresholding. *IEEE Trans. on Inf.*

Theory, 41(3):613–627, May 1995.

[43] D.L. Donoho and I.M. Johnstone. Ideal spatial adaptation via wavelet shrinkage. *Biometrika*, 81:425–455, 1994.

[44] R.O. Duda and P.E. Hart. *Pattern Classification and Scene Analysis*. Wiley, New York, 1973.

[45] P. Duhamel. Implementation of the split-radix FFT algorithms for complex, real, and real-symmetric data. *IEEE Trans. Acoust., Speech, Signal Processing*, 34:285–295, 1986.

[46] P. Duhamel and H. Hollmann. Split radix FFT algorithms. *Electron. Letters*, 20:14–16, 1984.

[47] J. Durbin. Efficient estimation of parameters in moving average models. *Biometrica*, 46:306–316, 1959.

[48] P. Dutilleux. An implementation of the algorithm à trous to compute the wavelet transform. In *Wavelets: Time-Frequency Methods and Phase Space, IPTI*, pages 289–304. Springer, New York, 1989.

[49] Y. Ephraim. Statistical-model-based speech enhancement systems. *Proceedings of the IEEE*, 80(10):1526–1555, October 1992.

[50] Y. Ephraim and D. Malah. Speech enhancement using a minimum mean-square error short-time spectral amplitude estimator. *IEEE Trans. Acoust., Speech, Signal Processing*, 32(6):1109–1121, December 1984.

[51] Y. Ephraim and D. Malah. Speech enhancement using a minimum mean-square log-spectral amplitude estimator. *IEEE Trans. Acoust., Speech, Signal Processing*, 33(2):443–445, April 1985.

[52] D. Esteban and C. Galand. Application of quadrature mirror filters to split band voice coding schemes. In *Proc. IEEE Int. Conf. Acoust., Speech, Signal Processing*, pages 191–195, May 1977.

[53] A. Fettweis, J.A. Nossek, and K. Meerkötter. Reconstruction of signals after filtering and sampling rate reduction. *IEEE Trans. Acoust., Speech, Signal Processing*, 33(4):893–901, August 1985.

[54] P. Flandrin and O. Rioul. Affine smoothing of the Wigner–Ville distribution. In *Proc. IEEE Int. Conf. Acoust., Speech, Signal Processing*, pages 2455–2458, Albuquerque, NM, April 1990.

[55] N.J. Fliege. *Multirate Digital Signal Processing*. John Wiley and Sons, Chichester, UK, 1994.

[56] C. Fogg, D.J. LeGall, J.L. Mitchell, and W.B. Pennebaker. *MPEG Video*

Compression Standard. Chapman & Hall, New York, NY, 1996.

[57] L.E. Francks. *Signal Theory*. Prentice-Hall, Englewood Cliffs, NJ, 1969.

[58] K.S. Fu. *Digital Pattern Recognition*. Springer, New York, 1980.

[59] K. Fukunaga. *Introduction to Statistical Pattern Recognition*. Academic Press, New York, 1972.

[60] S. Furui and M.M. Sondhi. *Advances in Speech Signal Processing*. Marcel Dekker, New York, 1991.

[61] D. Gabor. Theory of communication. *Journal of the Institute for Electrical Engineers*, 93:429–439, 1946.

[62] X. Gao, Z. He, and X.G. Xia. A new implementation of arbitrary-length cosine-modulated filter bank. In *Proc. IEEE Int. Conf. Acoust., Speech, Signal Processing*, volume 3, pages 1465–1468, Seattle, May 1998.

[63] A. Gersho and R.M. Gray. *Vector Quantization and Signal Compression*. Kluwer Academic Publishers, Boston, 1991.

[64] I. Good. The interaction algorithm and practical Fourier analysis. *J. Royal Stat. Soc. Series B*, 20:361–372, 1958.

[65] A. Grossmann, R. Kronland-Martinet, and J. Morlet. Reading and understanding continuous wavelet transforms. In *Time-Frequency Methods and Phase Space, IPTI*, pages 2–20. Springer, New York, 1989.

[66] H. Harmuth. *Transmission of Information by Orthogonal Functions*. Springer, New York, 1972.

[67] R.V.L Hartley. A more symmetrical Fourier analysis applied to transmission problems. *Proc. of the Inst. Radio Eng.*, 30:144–150, March 1942.

[68] P.N. Heller, T. Karp, and T.Q. Nguyen. A formulation of modulated filter banks. Submitted to IEEE Trans. on Signal Processing, 1996.

[69] C. Herley. Boundary filters for finite-length signals and time-varying filter banks. *IEEE Trans. Circuits and Systems II*, 42(2):102–114, February 1995.

[70] C. Herley, J. Kovačević, K. Ramachandran, and M. Vetterli. Tilings of the time-frequency plane: construction of arbitrary orthogonal bases and fast tiling algorithms. *IEEE Trans. Signal Processing*, 41(12):3341–3359, December 1993.

[71] C. Herley and M. Vetterli. Wavelets and recursive filter banks. *IEEE Trans. Signal Processing*, 41(8):2536–2556, August 1993.

[72] F. Hlawatsch and G.F. Boudreaux-Bartels. Linear and quadratic time-frequency signal representations. *IEEE Signal Processing Magazine*, 9(2):21–67, April 1992.

[73] M. Holschneider, R. Kronland-Martinet, J. Morlet, and Ph. Tchamitchian. A real-time algorithm for signal analysis with the help of the wavelet transform. In *Time-Frequency Methods and Phase Space, IPTI*, pages 286–297. Springer, New York, 1989.

[74] J.H. Husøy and T.A. Ramstad. Application of an efficient parallel IIR filter bank to image subband coding. *Signal Processing*, 20:279–292, 1990.

[75] A.J.E.M. Janssen. Positivity of time-frequency distribution functions. *Signal Processing*, 14:243–252, 1988.

[76] N.S. Jayant and P. Noll. *Digital Coding of Waveforms*. Prentice-Hall, Englewood Cliffs, NJ, 1984.

[77] G.M. Jenkins and D.G. Watts. *Spectral Analysis and its Applications*. Holden Day, San Francisco, CA, 1968.

[78] J.D. Johnston. A filter family designed for use in quadrature mirror filter banks. In *Proc. IEEE Int. Conf. Acoust., Speech, Signal Processing*, pages 291–294, 1980.

[79] Joint photographic experts group. JPEG technical specification: Revision (DRAFT). *ISO/IEC JTC1/SC2/WG8, CCITT SGVIII*, August 1990.

[80] E.I. Jury. *Theory and Application of the z-Transform Method*. Wiley, New York, 1964.

[81] K. Karhunen. über lineare methoden in der wahrscheinlichkeitsrechnung. *Ann. Acad. Sci. Fenn. Ser. A.I.37 Math. Phys., Helsinki*, 1947.

[82] T. Karp and N. Fliege. Mdft filter banks with perfect reconstruction. In *Proc. IEEE Int. Symp. Circuits and Systems*, pages 744–747, Seattle, May 1995.

[83] T. Karp, A. Mertins, and G. Schuller. Recent trends in the design of biorthogonal modulated filter banks. In *Proc. Workshop On Transforms and Filter Banks '98*, Tampere, Finland, February 1998.

[84] S.M. Kay. *Modern Spectral Estimation*. Prentice-Hall, Englewood Cliffs, NJ, 1987.

[85] J. Kliewer and A. Mertins. Design of paraunitary oversampled cosine-modulated filter banks. In *Proc. IEEE Int. Conf. Acoust., Speech, Signal*

Processing, volume 3, pages 2073–2076, Munich, Germany, April 1997.

[86] J. Kliewer and A. Mertins. Oversampled cosine-modulated filter banks with low system delay. *IEEE Trans. Signal Processing*, 46(4):941–955, April 1998.

[87] R.D. Koilpillai and P.P. Vaidyanathan. Cosine-modulated FIR filter banks satisfying perfect reconstruction. *IEEE Trans. Signal Processing*, 40:770–783, April 1992.

[88] D. Kolba and T. Parks. A prime factor FFT algorithm using high speed convolution. *IEEE Trans. Acoust., Speech, Signal Processing*, 25:281–294, 1977.

[89] N. Levinson. The Wiener RMS error criterion in filter design and prediction. *J. Math. Phys.*, 25:261–278, 1947.

[90] S. Mallat. Multifrequency channel decomposition of images and wavelet models. *IEEE Trans. Acoust., Speech, Signal Processing*, 37:2091–2110, December 1989.

[91] S. Mallat. A theory for multiresolution signal decomposition: The wavelet representation. *IEEE Trans. on Patt. Anal. and Mach. Intell.*, 11(7):674–693, July 1989.

[92] S. Mallat. *A Wavelet Tour of Signal Processing*. Academic Press, San Diego, CA, 1997.

[93] H.S. Malvar. The LOT: A link between transform coding and multirate filter banks. In *Proc. IEEE Int. Symp. Circuits and Systems*, pages 835–838, 1988.

[94] H.S. Malvar. Extended lapped transforms: Fast algorithms and applications. *IEEE Trans. Signal Processing*, 40, November 1992.

[95] H.S. Malvar. *Signal Processing with Lapped Transforms*. Artech House, Norwood, MA, 1992.

[96] H.S. Malvar. Lapped biorthogonal transforms for transform coding with reduced blocking and ringing artifacts. In *Proc. IEEE Int. Conf. Acoust., Speech, Signal Processing*, volume 3, pages 2421–2424, München, Germany, April 1997.

[97] H.S. Malvar and D.H. Staelin. Reduction of blocking effects in image coding with a lapped-orthogonal transform. In *Proc. IEEE Int. Conf. Acoust., Speech, Signal Processing*, pages 781–784, 1988.

[98] H.S. Malvar and D.H. Staelin. The LOT: Transform coding without blocking effects. *IEEE Trans. Acoust., Speech, Signal Processing*,

37(4):553–559, April 1989.

[99] S.L. Marple Jr. *Digital Spectral Analysis with Applications.* Prentice-Hall, Englewood Cliffs, NJ, 1987.

[100] J. Mau. Perfect reconstruction modulated filter banks, fast algorithms and attractive new properties. In *Proc. IEEE Int. Conf. Acoust., Speech, Signal Processing*, pages III.225–III.228, Minneapolis, MN, USA, April 1993.

[101] A. Mertins. Time-varying and support preservative filter banks: Design of optimal transition and boundary filters via SVD. In *Proc. IEEE Int. Conf. Acoust., Speech, Signal Processing*, pages 1316–1319, Detroit, May 1995.

[102] A. Mertins. Optimized biorthogonal shape adaptive wavelets. In *Proc. ICIP'98*, Chicago, October 1998.

[103] A. Mertins. Subspace approach for the design of cosine-modulated filter banks with linear-phase prototype filter. *IEEE Trans. Signal Processing*, 46(10):2812–2818, October 1998.

[104] Y. Meyer. Ondelettes et fonction splines. *Séminare EDP, École Polytechnique, Paris*, December 1986.

[105] J. Morlet. Sampling theory and wave propagation. In *NATO ASI series, Issues in acoustic signal/image processing and recognition*, volume 1, pages 233–261. Springer, New York, 1983.

[106] J. Morlet, G. Arens, I. Fourgeau, and D. Giard. Wave propagation and sampling theory. *Geophysics*, 47:203–236, 1982.

[107] J.E. Moyal. Quantum mechanics as a statistical theory. *Camb. Phil. Soc.*, 45:99–124, 1949.

[108] MPEG-2 Video Compression Standard. Generic Coding of Moving Pictures and Associated Audio, ISO/IEC CD 13818-2, 1993.

[109] MPEG-4 Video Verification Model, Version 11. Generic Coding of Moving Pictures and Associated Audio, ISO/IEC JTC1/SC 29/WG 11, 1998.

[110] K. Nayebi, T.P. Barnwell III, and M.J.T. Smith. Low delay FIR filter banks: Design and evaluation. *IEEE Trans. Signal Processing*, SP-42:24–31, January 1994.

[111] T.Q. Nguyen. Digital filter bank design quadratic constraint formulation. *IEEE Trans. Signal Processing*, 43:2103–2108, September 1995.

[112] T.Q. Nguyen and P.N. Heller. Biorthogonal cosine-modulated filter

banks. In *Proc. IEEE Int. Conf. Acoust., Speech, Signal Processing*, Atlanta, USA, May 1996.

[113] A.V. Oppenheim and R.W. Schafer. *Digital Signal Processing*. Prentice-Hall, Englewood Cliffs, NJ, 1975.

[114] A. Papoulis. *The Fourier Integral and its Applications*. McGraw-Hill, New York, 1962.

[115] A. Papoulis. *Signal Analysis*. McGraw-Hill, New York, 1977.

[116] J.P. Princen and A.B. Bradley. Analysis / synthesis filter bank design based on time domain aliasing cancellation. *IEEE Trans. Acoust., Speech, Signal Processing*, 34:1153–1161, October 1986.

[117] J.G. Proakis, C.M. Rader, F. Ling, and C.L. Nikias. *Advanced Digital Signal Processing*. Macmillan, New York, 1992.

[118] R.L. de Queiroz, T.Q. Nguyen, and K.R. Rao. The GenLOT: Generalized linear-phase lapped orthogonal transform. *IEEE Trans. Signal Processing*, 44(3):497–507, March 1996.

[119] L.R. Rabiner and R.W. Schafer. *Digital Processing of Speech Signals*. Prentice-Hall, Englewood Cliffs, NJ, 1978.

[120] C. Rader. Discrete Fourier transform when the number of data samples is prime. *Proc. IEEE*, 5:1107–1108, 1968.

[121] T.A. Ramstad and J.P. Tanem. Cosine modulated analysis-synthesis filter bank with critical sampling and perfect reconstruction. In *Proc. IEEE Int. Conf. Acoust., Speech, Signal Processing*, pages 1789–1792, Toronto, Ont., Canada, May 1991.

[122] K.R. Rao and P. Yip. *Discrete Cosine Transform*. Academic Press, New York, 1990.

[123] W.D. Ray and R.M. Driver. Further decomposition of the karhunen loéve series representation of a stationary random process. *IEEE Trans. on Inf. Theory*, IT-16:663–668, November 1970.

[124] A.W. Rihaczek. Signal energy distribution in time and frequency. *IEEE Trans. on Inf. Theory*, 14(3):369–374, 1968.

[125] O. Rioul. Simply regularity criteria for subdivision schemes. *SIAM J. Math. Anal.*, 23:1544–1576, 1992.

[126] O. Rioul and P. Flandrin. Time-scale energy distributions: A general class extending wavelet transforms. *IEEE Trans. Signal Processing*, July 1992.

[127] J.H. Rothweiler. Polyphase quadrature filters - a new subband coding

technique. In *Proc. IEEE Int. Conf. Acoust., Speech, Signal Processing,* pages 1280–1283, 1983.

[128] A. Said and W.A. Pearlman. A new fast and efficient image codec based on set partitioning in hierarchical trees. *IEEE Trans. Circ. and Syst. for Video Technology,* 6(3):243–250, June 1996.

[129] G.D.T. Schuller and M.J.T. Smith. A new framework for modulated perfect reconstruction filter banks. *IEEE Trans. Signal Processing,* 44(8):1941–1954, August 1996.

[130] I. Schur. On power series which are bounded in the interior of the unit circle. (in German). *J. Reine u. Angew. Math.,* 147:205–232, 1917.

[131] J.M. Shapiro. Embedded image coding using zerotrees of wavelet coefficients. *IEEE Trans. Signal Processing,* 41(12):3445–3462, December 1993.

[132] M.J. Shensa. The discrete wavelet transform: Wedding the à trous and Mallat algorithms. *IEEE Trans. Signal Processing,* 40(10):2464–2482, October 1992.

[133] F. Shum, A. Elliot, and W. Brown. Speech processing with Walsh–Hadamard transforms. *IEEE Trans. on Audio and Electroacoustics,* pages 174–179, June 1973.

[134] E.A.B. da Silva and M. Ghanbari. On the performance of linear phase wavelet transforms in low bit-rate image coding. *IEEE Trans. Image Processing,* 5(5):689–704, May 1996.

[135] M.J.T. Smith and T.P. Barnwell III. Exact reconstruction for tree-structured subband coders. *IEEE Trans. Acoust., Speech, Signal Processing,* 34:434–441, June 1986.

[136] M.J.T. Smith and S.L. Eddins. Analysis/synthesis techniques for subband coding. *IEEE Trans. Acoust., Speech, Signal Processing,* pages 1446–1456, Aug 1990.

[137] A.K. Soman, P.P. Vaidyanathan, and T.Q. Nguyen. Linear phase paraunitary filter banks: Theory, factorizations and applications. *IEEE Trans. Signal Processing,* 41(12):3480–3496, May 1993.

[138] H. Sorensen, M. Heidemann, and C.S. Burrus. On calculation the split-radix FFT. *IEEE Trans. Acoust., Speech, Signal Processing,* 34:152–156, 1986.

[139] H.V. Sorensen, D.L. Jones, C.S. Burrus, and M.T. Heidemann. On computing the discrete Hartley transform. *IEEE Trans. Acoust., Speech, Signal Processing,* 33:1231–1238, October 1985.

[140] G. Strang and T. Nguyen. *Wavelets and Filter Banks*. Wellesley–Cambridge Press, Wellesley, MA, 1996.

[141] W. Sweldens. The lifting scheme: A custom design construction of biorthogonal wavelets. *Journal of Appl. and Comput. Harmonic Analysis*, 3(2):186–200, 1996.

[142] C. Temperton. Self-sorting in-place fast Fourier transforms. *SIAM J. Sci. Comput.*, 12:808–823, 1991.

[143] L. Thomas. Using a computer to solve problems in physics. In *Applications of Digital Computers, Ginn, Boston, MA*, 1963.

[144] T.D. Tran, R.L. de Queiroz, and T.Q. Nguyen. The generalized lapped biorthogonal transform. In *Proc. IEEE Int. Conf. Acoust., Speech, Signal Processing*, volume 3, pages 1441–2424, Seattle, USA, May 1998.

[145] P.P. Vaidyanathan. On power-complementary FIR filters. *IEEE Trans. Circuits and Systems*, 32:1308–1310, December 1985.

[146] P.P. Vaidyanathan. *Multirate Systems and Filter Banks*. Prentice-Hall, Englewood Cliffs, NJ, 1993.

[147] P.P. Vaidyanathan and P.Q. Hoang. Lattice structures for optimal design and robust implementation of two-band perfect reconstruction QMF banks. *IEEE Trans. Acoust., Speech, Signal Processing*, 36:81–95, 1988.

[148] P.P. Vaidyanathan, T.Q. Nguyen, Z. Doganata, and T. Saramäki. Improved technique for design of perfect reconstruction FIR QMF banks with lossless polyphase matrices. *IEEE Trans. Acoust., Speech, Signal Processing*, 37(7):1042–1056, July 1989.

[149] H.L. Van Trees. *Detection, Estimation, and Modulation Theory, Part I*. Wiley, New York, 1968.

[150] H.L. Van Trees. *Detection, Estimation, and Modulation Theory, Part III*. Wiley, New York, 1971.

[151] M. Vetterli. Perfect transmultiplexers. In *Proc. IEEE Int. Conf. Acoustics, Speech, and Signal Processing*, pages 48.9.1–48.9.4, Tokyo, April 1986.

[152] M. Vetterli and P. Duhamel. Split radix algorithms for length p^m dfts. *IEEE Trans. Acoust., Speech, Signal Processing*, 34:57–64, 1989.

[153] M. Vetterli and C. Herley. Wavelets and filter banks: Theory and design. *IEEE Trans. Acoust., Speech, Signal Processing*, 40(9):2207–2232, September 1992.

[154] M. Vetterli and J. Kovačević. *Wavelets and Subband Coding.* Prentice-Hall, Englewood Cliffs, NJ, 1995.

[155] J.D. Villasenor, B. Belzer, and J. Liao. Wavelet filter evaluation for image compression. *IEEE Trans. Image Processing,* 4(8):1053–1060, August 1995.

[156] J. Ville. Theorie et applications de la notion de signal analytique. *Cables et Transmission, 2 A,* pages 61–74, 1948.

[157] G.K. Wallace. The JPEG still picture compression standard. *Communications of the ACM,* 34:31–44, April 1991.

[158] Z. Wang. Harmonic analysis with a real frequency function—I. Aperiodic case. *Appl. Math. and Comput.,* 9:53–73, 1981.

[159] Z. Wang. Harmonic analysis with a real frequency function—II. Periodic and bounded case. *Appl. Math. and Comput.,* 9:153–163, 1981.

[160] Z. Wang. Harmonic analysis with a real frequency function—III. Data sequence. *Appl. Math. and Comput.,* 9:245–255, 1981.

[161] Z. Wang. Fast algorithms for the discrete W transfom and for the discrete Fourier transform. *IEEE Trans. Acoust., Speech, Signal Processing,* 21:803–816, August 1984.

[162] P.D. Welch. The use of the fast Fourier transform for the estimation of power spectra: A method based on time averaging over short modified periodograms. *IEEE Trans. Audio and Electroacoustics,* 15:70–73, 1967.

[163] E.P. Wigner. On the quantum correction for thermodynamic equilibrium. *Physical Review,* 40:749–759, 1932.

[164] S. Winograd. On computing the discrete Fourier transform. *Math. Comp.,* 32:175–199, 1978.

[165] J. Woods and S. O'Neil. Subband coding of images. *IEEE Trans. Acoust., Speech, Signal Processing,* 34(5):1278–1288, May 1986.

[166] H. Xu, W.-S. Lu, and A. Antoniou. Efficient iterative design method for cosine-modulated QMF banks. *IEEE Trans. Signal Processing,* 44(7):1657–1668, July 1996.

[167] T.Y. Young and T.W. Calvert. *Classification, Estimation and Pattern Recognition.* Elsevier, New York, 1974.

[168] Y. Zhao, L.E. Atlas, and R.J. Marks II. The use of cone-shaped kernels for generalized time-frequency representations of non-stationary signals. *IEEE Trans. Acoust., Speech, Signal Processing,* 38(7):1084–1091, 1990.

Signal Analysis

Signal Analysis
Wavelets, Filter Banks,
Time-Frequency Transforms and Applications

Alfred Mertins
University of Wollongong, Australia

Contents

Preface

A central goal in signal analysis is to extract information from signals that are related to real-world phenomena. Examples are the analysis of speech, images, and signals in medical or geophysical applications. One reason for analyzing such signals is to achieve better understanding of the underlying physical phenomena. Another is to find compact representations of signals which allow compact storage or efficient transmission of signals through real-world environments. The methods of analyzing signals are wide spread and range from classical Fourier analysis to various types of linear time-frequency transforms and model-based and non-linear approaches. This book concentrates on transforms, but also gives a brief introduction to linear estimation theory and related signal analysis methods. The text is self-contained for readers with some background in system theory and digital signal processing, as typically gained in undergraduate courses in electrical and computer engineering.

The first five chapters of this book cover the classical concepts of signal representation, including integral and discrete transforms. Chapter 1 contains an introduction to signals and signal spaces. It explains the basic tools for classifying signals and describing their properties. Chapter 2 gives an introduction to integral signal representation. Examples are the Fourier, Hartley and Hilbert transforms. Chapter 3 discusses the concepts and tools for discrete signal representation. Examples of discrete transforms are given in Chapter 4. Some of the latter are studied comprehensively, while others are only briefly introduced, to a level required in the later chapters. Chapter 5 is dedicated to the processing of stochastic processes using discrete transforms and model-based approaches. It explains the Karhunen–Loève transform and the whitening transform, gives an introduction to linear estimation theory and optimal filtering, and discusses methods of estimating autocorrelation sequences and power spectra.

The final four chapters of this book are dedicated to transforms that provide time-frequency signal representations. In Chapter 6, multirate filter banks are considered. They form the discrete-time variant of time-frequency transforms. The chapter gives an introduction to the field and provides an overview of filter design methods. The classical method of time-frequency analysis is the short-time Fourier transform, which is discussed in Chapter 7. This transform was introduced by Gabor in 1946 and is used in many applications, especially in the form of spectrograms. The most prominent example of linear transforms with time-frequency localization is the wavelet transform. This transform attracts researchers from almost any field of science, because

it has many useful features: a time-frequency resolution that is matched to many real-world phenomena, a multiscale representation, and a very efficient implementation based on multirate filter banks. Chapter 8 discusses the continuous wavelet transform, the discrete wavelet transform, and the wavelet transform of discrete-time signals. Finally, Chapter 9 is dedicated to quadratic time-frequency analysis tools like the Wigner distribution, the distributions of Cohen's class, and the Wigner–Ville spectrum.

The history of this book is relatively long. It started in 1992 when I produced the first lecture notes for courses on signal theory and linear time-frequency analysis at the Hamburg University of Technology, Germany. Parts of the material were included in a thesis ("Habilitationsschrift") that I submitted in 1994. In 1996, the text was published as a textbook on Signal Theory in German. This book appeared in a series on Information Technology, edited by Prof. Norbert J. Fliege and published by B.G. Teubner, Stuttgart, Germany. It was Professor Fliege who encouraged me to write the book, and I would like to thank him for that and for his support throughout many years. The present book is mainly a translation of the original German. However, I have rearranged some parts, expanded some of the chapters, and shortened others in order to obtain a more homogeneous and self-contained text. During the various stages, from the first lecture notes, over the German manuscript to the present book, many people helped me by proofreading and commenting on the text. Marcus Benthin, Georg Dickmann, Frank Filbir, Sabine Hohmann, Martin Schönle, Frank Seide, Ursula Seifert, and Jens Wohlers read portions of the German manuscript. Their feedback significantly enhanced the quality of the manuscript. My sister, Inge Mertins–Obbelode, translated the text from German into English and also proofread the new material that was not included in the German book. Tanja Karp and Jörg Kliewer went through the chapters on filter banks and wavelets, respectively, in the English manuscript and made many helpful suggestions. Ian Burnett went through a complete draft of the present text and made many suggestions that helped to improve the presentation. I would like to thank them all. Without their effort and enthusiasm this project would not have been realizable.

Alfred Mertins
Wollongong, December 1998

Index